Fragment-based Discovery of Modulators of the Aurora-A Kinase

Christopher James Arter

Submitted in accordance with the requirements for the degree of

Doctor of Philosophy

The University of Leeds

School of Chemistry

and

Astbury Centre for Structural Molecular Biology

December 2021

The candidate confirms that the work submitted is his own, except where work which has formed part of jointly authored publications has been included. The contribution of the candidate and the other authors toward this work has been described below. The candidate confirms appropriate credit has been given within the thesis where reference has been made toward the work of others.

A section of the work presented in Chapter 2 has appeared in the following publication:

"Efficient Approaches for the Synthesis of Diverse α-Diazo Amides", S. Chow, A. I. Green, **C. Arter**, S. Liver, A. Leggott, L. Trask, G. Karageorgis, S. Warriner, and A. Nelson, Synthesis, 2020, **52**(11), 1695-1706.

From the work contained in this publication, the candidate developed methods and expanded substrate scope for the synthesis of α-diazo amide containing compounds (Method B1) and synthesised six compounds. Synthetic methods were also developed by SC and AIG (A, B, and C). Synthesis was also performed by SC, AIG, SL, AL, LT, and GK. The project was supervised by AN, and conceived by AN and SW. The manuscript was written by AN, and the supporting information written by the candidate and SL.

Other contributions:

Dr Mohd Syed Ahanger (Post-doctoral Research Fellow, University of Leeds) provided crystal structures for compounds **F1**, **F2**, and **F3** in Chapter 2. Mathilde Suarez (Research Internship, University of Leeds/SIGMA Clermont Graduate School of Engineering, France) performed the analysis of Aurora-A PDB structures to determine kinase activation state and druggability scores of Y-pocket, which were used in Chapter 3 to select appropriate PDB structures for use in further docking studies.

Acknowledgements

First and foremost, I would like to extend my sincere thanks to both of my supervisors for their excellent support during my PhD studies, I feel incredibly lucky to have received supervision that is second-to-none. I would like to thank Prof. Adam Nelson for his continuous support and willingness to tailor his supervision style to meet my sometimes-frenetic method of working, especially when it comes to writing. I genuinely believe my thesis wouldn't have made it this far without his guidance and generosity with his time. I'm also indebted to Prof. Richard Bayliss for his support with everything biology related and his phenomenal ability to collaborate with other scientists. Knowing I could rely on him to pull a miracle out of thin air when it comes to working elsewhere to obtain biological data at the last minute has been a huge help.

Secondly, I would like to extend my thanks to all the past and present members of G56 and in the wider chemistry department I've had the pleasure of working, and drinking, with. Luke, Hai Bro! It's been a real honour working with you, through all the nonsense since our MSc, thanks for letting me ride your coattails along the way when I needed to, and for being a generally top bloke. Dan, Kyle, you know why you're on here. Cheers for all the banter along the way, I can't wait to laud about being plebian Drs with you both for years to come, just with more money. And to everyone else in G56 - thanks for putting up with my sometimes-banal questions about chemistry, hopefully some of your knowledge has sunk in. Special thanks go to Dr Sam Liver for letting me mess about on the robotics while they were here in Leeds to support my work.

I'd like to thank my family for their unwavering support over the last few years, for the inherent curiosity in trying to understand how things tick that has propelled me to pursue scientific research, and for patiently listening when I try to explain my work to you. Last, but certainly not least, huge thanks go to my wonderful partner Magda for her love and support during my time in academia. You took a huge leap moving up to Leeds to be with me while I've been underpaid and over-stressed, but we've made it work and I can't wait to move on to the next stage of our life together.

Cheers.

Abstract

Allosteric inhibition of kinases presents an innovative and potentially selective method of targeting these enzymes for bioactive small molecule development. Contrary to the orthosteric inhibition of highly conserved and defined binding sites, allosteric inhibitors are challenging to develop due to the shallow and flat nature of their binding pockets yet present a desirable target for medicinal chemistry. This thesis focuses on the development of allosteric Aurora-A inhibitors, exploiting standard medicinal chemistry techniques as well as implementing a development workflow that focuses exclusively on productively elaborated fragments from high-throughput microscale arrays.

Chapter 1 gives an overview of Aurora-A kinase structure and function and introduces existing small molecule inhibitors in various stages of development, including allosteric inhibitors and those targeting the Aurora-A/TPX2 protein-protein interaction. Chapter 1 also outlines modern drug discovery practices and focuses on recent methods for the high-throughput and integrated discovery and development of biologically active small molecules.

Chapter 2 describes the design and implementation of three microscale reaction arrays for the activity-directed elaboration of allosteric inhibitors of Aurora-A kinase. Two dirhodium(II) carbenoid reaction arrays were performed, totalling 504 reactions, followed by high-throughput LC-MS analysis of reaction array 1 and purification of productive reactions. The identification of improved bioactive compounds guided the design of the third reaction array, exploiting amide bond formations.

Chapter 3 describes the development of a series of fragments based on known allosteric inhibitors of Aurora-A kinase through design and synthesis of a library of fragments. The SAR landscape was initially explored through generation and biological screening of a small library, which was then supplemented with an *in silico* docking campaign. The combined SAR and docking results were used to design further analogues of elaborated fragments for synthesis and biological screening. Overall, this medicinal chemistry strategy resulted in the expansion of the SAR for the fragment series and led to an increase in biological potency against Aurora-A kinase.

List of Abbreviations

Abl	abelson tyrosine kinase
ADP	adenosine diphosphate
ADS	activity-directed synthesis
AI	artifical intelligence
AR	androgen receptor
ASMS	affinity-selection mass-spectrometry
ATP	adenosine triphosphate
AURKAIP1	aurora kinase a interacting protein 1
CADD	computer-aided drug-design
Cdk	cyclin-dependent kinase
CHK1	checkpoint kinase 1
CML	chronic myeloid leukaemia
DMFDA	*N-N*-dimethylformamide dimethyl acetal
ELS	evaporative light scattering
ERK2	extracellular signal-regulated kinase 2
FA	fluorescence anisotropy
FBDD	fragment-based drug-discovery
FDA	federal drug administration
FRET	fluorescence resonance energy transfer
HPLC	high-performance liquid chromatography
HTS	high-throughput screening
ITC	isothermal titration calorimetry
LC-MS	liquid-chromatography mass-spectrometry
LE	ligand efficiency

MD	molecular dynamics
MK2	mitogen-activated protein 2
MW	molecular weight
Nek6	NIMA related kinase 6
Nek7	NIMA related kinase 7
NMR	nuclear magnetic resonance
PAINS	pan-assay interference compounds
PDB	protein data bank
PDK1	pyruvate dehydrogenase lipoamide kinase isozyme 1
PIF	PDK1-interacting fragment
PKC	protein kinase C
Plk1	polo-like kinase 1
PLKs	polo-like kinases
PPI	protein-protein interaction
PTM	post-translational modification
SAR	structure-activity relationship
SBDD	structure-based drug design
SH2	src-homology 2 domain
SH3	src-homology 3 domain
SPR	surface plasmon resonance
TPX2	targeting protein for Xklp2
TR-FRET	time-resolved fluorescence resonance energy transfer
TSA	thermal shift assay
UPLC	ultra-high performance liquid chromatography
XRD	X-ray diffraction

1   Introduction

1.1   Protein Kinases & General Structure

Post-translational modifications (PTMs) are a key regulatory mechanism employed for cell signalling, providing a reversible and dynamic cellular system for interpreting and responding to extracellular stimuli, and instigating intercellular downstream signalling.[1] Proteomic analysis has identified over 200 PTMs, with acetylation, amidation, and glycosylation amongst the more common types.[2] However, the most common experimentally-found PTM is phosphorylation[3], indicating the importance of this particular modification. Performed by the kinase superfamily of proteins, phosphorylation in eukaryotes is the transfer of the *γ*-phosphate of adenosine triphosphate (ATP) to a substrate, usually a partner protein.

The human kinome consists of 518 known kinases[4], able to be roughly grouped by the residue of the substrate that undergoes phosphorylation: serine/threonine- or tyrosine-kinases. Despite being an extensive family of enzymes, there are structural motifs conserved across all kinases, consisting of a strictly organised internal structure in an otherwise highly diverse and dynamic group of proteins.[5] The conserved catalytic domain is divided in to the *N*-terminal and *C*-terminal lobes separated by a hinge region, with the *N*-lobe typically formed of a single β-sheet of five antiparallel *β*-strands and a helical subdomain comprised of a small number of *α*-helices. Conversely, the *C*-lobe is mostly formed of *α*-helices and contains the catalytically significant "activation loop". The active site is formed by a cleft between the two lobes, in which ATP binds and ADP is released due to transfer of the *γ*-phosphate from ATP to the bound substrate.

The mechanism of kinase activation resulting in phosphorylation of an associated substrate has been closely scrutinised. This has shown these protein kinases can exist in a range of conformations from fully inactive to fully active[6], dependant on a number of highly conserved structural features; the activation loop, the Asp-Phe-Gly (DFG) and His-Arg-Asp (HRD) motifs, the glycine-rich loop, a group of hydrophobic residues forming a regulatory spine (the "R-spine"), and a lysine-glutamic acid salt bridge, shown in Fig. **1.1**.
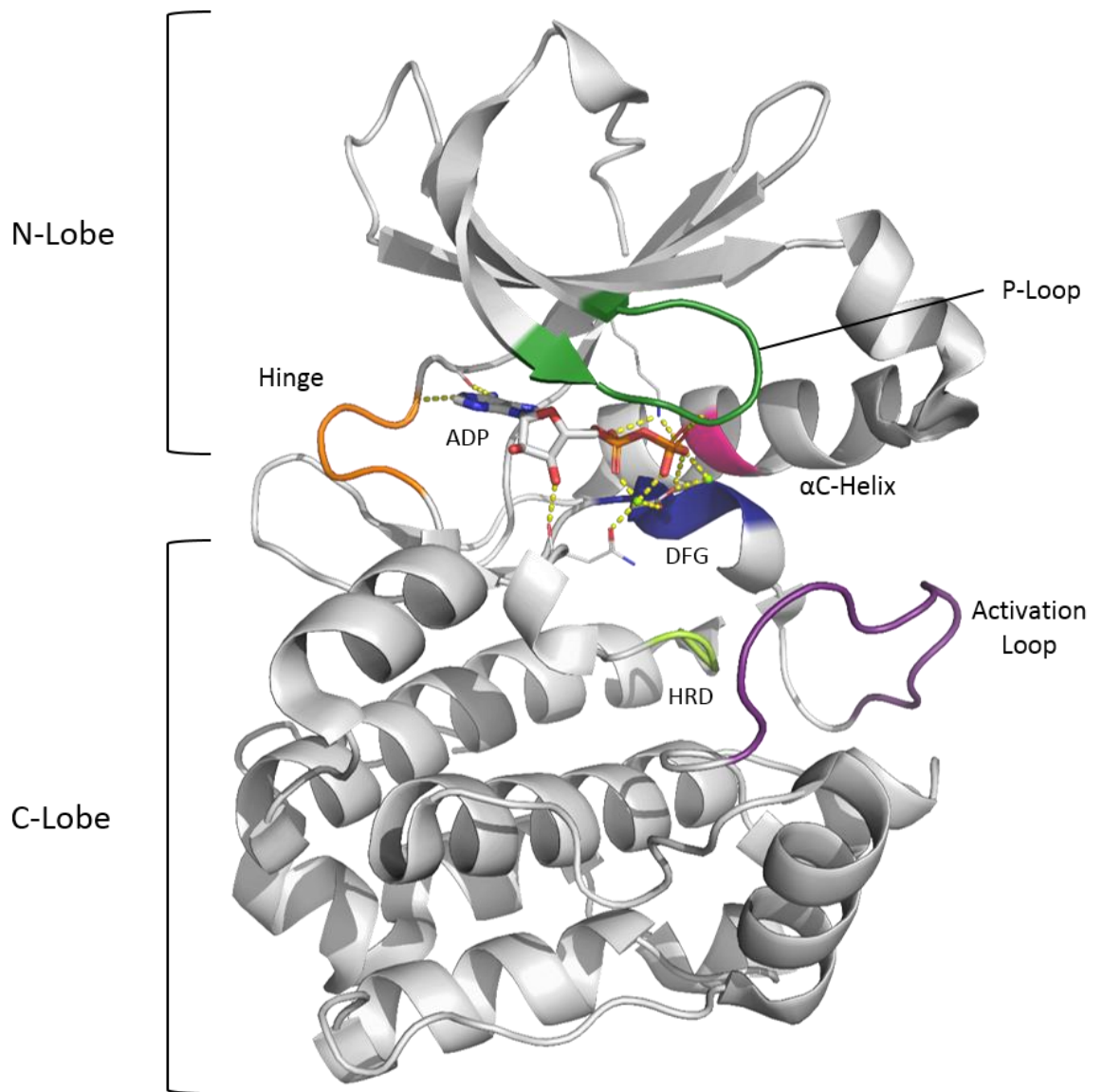
Figure **1.1**. X-ray crystal structure of Aurora-A in complex with ADP (PDB: 4DEE). Highlighted are important structures used to define an active kinase conformation. Not shown is the Lys-Glu salt bridge, or the aligned residues of the R-spine.

The activation loop is perhaps one of the most crucial components in regulating kinase activity, as the region that contains residues able to be phosphorylated, through autophosphorylation or as the substrate for a partner kinase. Upon phosphorylation, this flexible loop region can coordinate with a group of basic residues nearby. This has the effect of stabilising the loop in a less disordered conformation and constraining its mobility, forming the binding site for the various substrates of the kinase.[7]

The DFG and HRD motifs form crucial catalytic regions that assist in the transfer of the γ-phosphate of ATP to the associated substrate. Situated immediately before the activation

loop, the DFG motif coordinates the Mg^{2+} ions via an aspartic acid residue and forms polar interactions with the phosphate groups of ATP.[7] This motif exists in two orientations, 'DFG-in' and 'DFG-out', that denote the positioning of the aspartate residue important for catalytic activity. The difference between the two is controlled by the neighbouring phenylalanine residue, where in the 'DFG-in' conformation the Phe sidechain points toward the α-helix of the *N*-lobe forming hydrophobic interactions that serve to stabilise the conformation. This orients the Asp residue toward the active site, allowing the interactions with Mg^{2+} and ATP. The 'DFG-out' conformation displays the Phe residue facing the opposite direction, therefore moving the Asp residue away from the active site resulting in an inactive conformation.[8]

Less strictly conserved than the DFG motif, the HRD motif nonetheless remains a crucial region for kinase activation.[9] The first His residue interacts with the DFG motif and assists in stabilising the activate kinase conformation. The second residue, Arg, is the least conserved member of the motif, despite forming a salt-bridge with the phosphorylated residue on the activation loop when present.[10] However, the absence of this Arg provides an indication of a kinase's lack of regulation through phosphorylation of the activation loop. Finally, the highly conserved Asp residue acts as a base to deprotonate the acceptor hydroxyl-containing residue of the substrate, in anticipation of the subsequent phosphorylation.[11]

In a similar role to the DFG motif, the glycine-rich loop (often named the "P-loop") interacts with the γ-phosphate of ATP. Situated within the *N*-lobe, this loop forms the top of the active site and positions ATP for more efficient transfer of the phosphate to the substrate.

The R-spine is a region of four hydrophobic residues that links the *N*-lobe β-sheet and *C*α-helix to a central, buried α-helix in the *C*-lobe. Through organisation of the sidechains of these four residues in to a linear arrangement, a framework is formed around which the remainder of the active site is organised in active kinases.[8] An inactive kinase lacks this linear organisation of the sidechains, allowing the kinase to adopt an inactive conformation.[8] In an active kinase, a Lys-Glu salt-bridge is present and serves to associate a central β-strand and the *C*α-helix within the *N*-lobe with one another. The Phe residue of the DFG-in conformation kinase also interacts with the *C*α-helix and stabilises the arrangement of the salt bridge with the Lys residue.

Collectively, the outlined structures form the hallmarks of an active kinase conformation based on structural determination of over 100 kinases and comparison of the catalytic centres.[7] Through this understanding, the activation state of a kinase when involved in a protein-protein interaction (PPI), bound to a small molecule modulator, or in different states of phosphorylation

can be outlined to provide mechanistic understanding of the effects of these external influences on overall kinase catalytic centre structure.

1.1.1   Mitotic Kinases

The cell cycle, the mechanisms by which a cell replicates its genetic material and forms two new daughter cells containing copies, is one of the fundamental and most important functions in life. Eukaryotic cells display three stages during this cycle; interphase, mitosis, and cytokinesis. Here we focus on mitosis, the crucial process of separation of replicated centrosomes and chromosomes to opposite ends of the dividing cell.

High levels of control are present throughout mitosis and PTMs perform the direct regulation of these events. Phosphorylation and ubiquitination are commonly found throughout this process[12], regulating progression through mitosis and directing proteolysis, respectively. The complex interplay between phosphorylation and proteolysis is apparent through observation of control of proteolytic machinery *via* phosphorylation, as well as downregulation of mitotic kinases through degradation by said machinery.[12] Phosphorylation acts as an activator, phosphorylating substrates of the protein kinases, therefore progressing the cell through the mitotic stage. The importance of this process is also reflected through the functional opposite of kinases, phosphatases, which de-phosphorylate their substrates, and have been shown to play a crucial role in mitotic regulation and exit.[13] Consequently, with a variety of crucial roles throughout mitosis, it stands to reason that dysregulation of mitotic protein kinases will impact the cells ability to undergo healthy division and proliferation.

Several kinase families have been identified that have roles in both the regulation of mitosis and the onset of cancer when displaying aberrant behaviour. The most extensively researched family is the cyclin-dependant kinase (Cdk) family, with activated Cdks for example phosphorylating nuclear lamins, microtubule-binding proteins and condensins.[12] The polo-like kinases (Plks) are also well-studied, with an established role in centrosome separation and mitotic exit.[14] The Aurora family of kinases has three members in human cells, with each being involved in various regulatory events in mitosis, including mitotic spindle assembly, microtubule localisation, and centrosome separation.[15]

With a range of mitotic protein kinases well known and characterised with potential as anti-cancer therapeutics, fully realising the development of development of a drug targeting these kinases requires not only an understanding of small molecule kinase inhibition, but a

deeper understanding of the cellular mechanism of each individual protein. These factors govern whether targeting a kinase will cause apoptosis, or cell necrosis or quiescence – both undesirable outcomes for cancer therapeutics. However, research continues toward effective therapeutics due to the potential presented by these targets.[16]

1.1.1.1   Aurora Kinases

The Aurora Kinases are a small family of serine/threonine kinases, conserved across yeast, *Drosophila*, and mammalian cells.[17,18] All three members regulate mitotic events, with Aurora-A and -B the most well studied, showing similar sequence homology but vastly different temporal and physical localisation during mitosis. Aurora-A has been shown to assist in regulating mitotic spindle assembly, centrosome separation, and chromosome segregation during early mitosis.[19] Later in mitosis, Aurora-B localises to microtubules near kinetochores, connecting the mitotic spindle to the centromere.[15] Aurora-C is the least studied member of the family but it is involved in spermatogenesis and adopts similar roles to Aurora-B in cells lacking the latter.[20]

Overall sequence homology between the members of the Aurora Kinase family is around 60%[21], outlined in Fig. **1.2**, with the active domains highlighted in green flanked by short C-terminal domains (15 -20 residues) and variable length *N*-terminal domains (39-129 residues). Sequence homology between these *N*-terminal domains is much less conserved than the catalytic region homology of around 71% between Aurora-A and -B, and is potentially responsible for the selectivity of each isoform for its partners in PPIs.
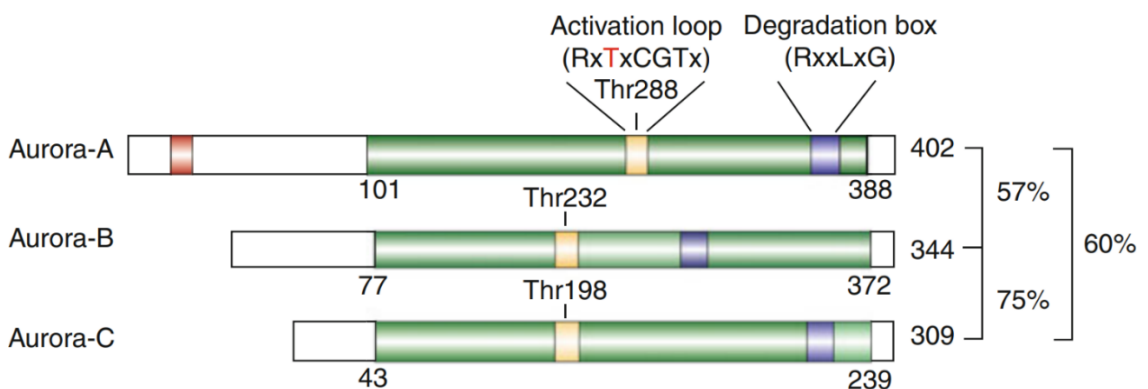
Figure **1.2**. Diagrammatic representation of the Aurora-A family member domain structure. Percentages indicate sequence identity between Aurora-A, -B, and -C. Shown are the kinase/catalytic domain (green), degradation motifs (blue), activation loops (yellow), and the A-box (red). Figure adapted from [21].

Functional differences between the Aurora kinase family and their clinical relevance are also apparent in their localisation on the chromosomes. *aurora-a* is located on chromosome 20q13.2, a region commonly amplified in tumours, implicating Aurora-A as a possible driver of cancer formation. Conversely, *aurora-b* is located on 17p13.1, a region not commonly associated with amplification in human malignancies. However, despite this lack of gene amplification of *aurora-b*, increased levels of Aurora-B mRNA and protein are frequently found in human tumours.[21]

1.1.1.2 Aurora-A Kinase Function

As the most studied member of the Aurora family Aurora-A has been shown to be a critical regulator of multiple events during mitosis. Expression and activity levels of Aurora-A peak during G2 phase and early mitosis in the cell cycle, in tandem with localisation at the centrosomes and spindle poles. Progression to cytokinesis sees Aurora-A undergoing degradation by the Anaphase-promoting complex/cyclosome (APC/C) and levels remain relatively low throughout the G1 and S phases, shown in Fig **1.3.**[21]
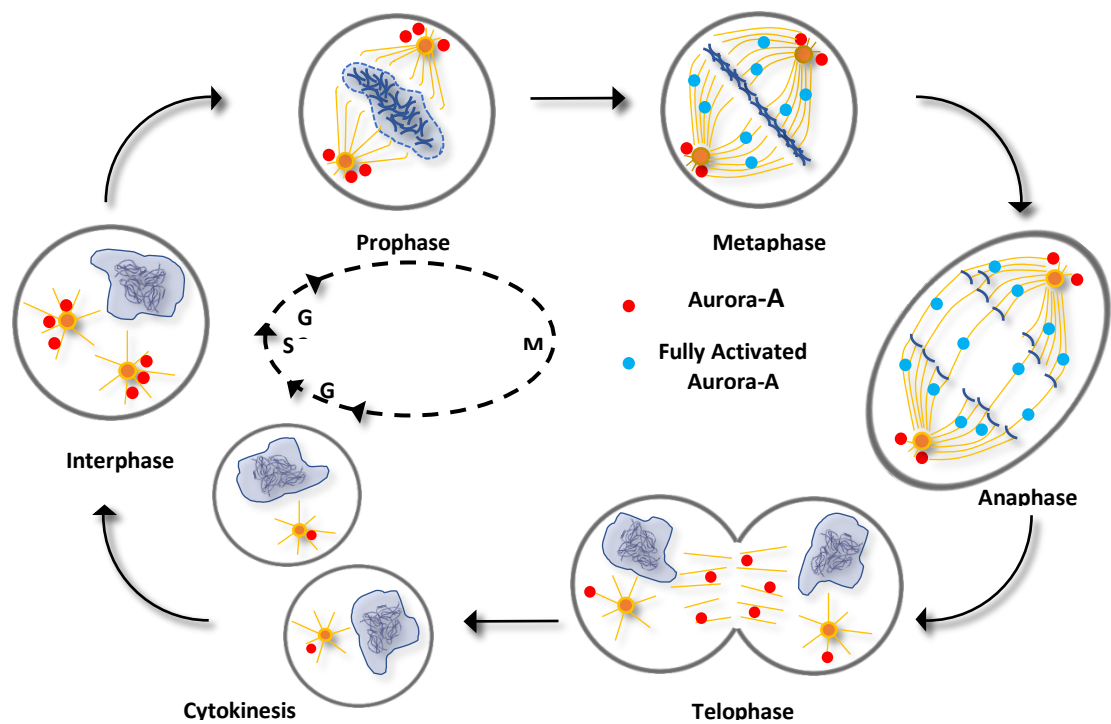
Figure **1.3**. Overview of Aurora-A localisation and function during Mitosis. Figure adapted from [22].

Aurora-A assists in the regulation of centrosome separation, chromosome segregation, and mitotic spindle assembly *via* phosphorylation of its many substrates, interactions with a wide variety of binding partners, and through activation of a number of downstream regulators such as Nek6, Nek7, and Plk1.[17,19] Able to be broadly divided in to three categories; activators, inhibitors, and substrates, these binding partners of Aurora-A closely regulate its localisation and activity during mitosis. A snapshot of a small number of these partners are shown in Fig. **1.4**, and while this is by no means an exhaustive list it is intended to indicate how even a small portion of the Aurora-A interactome is highly complex, highlighting the central role it plays in mitosis.
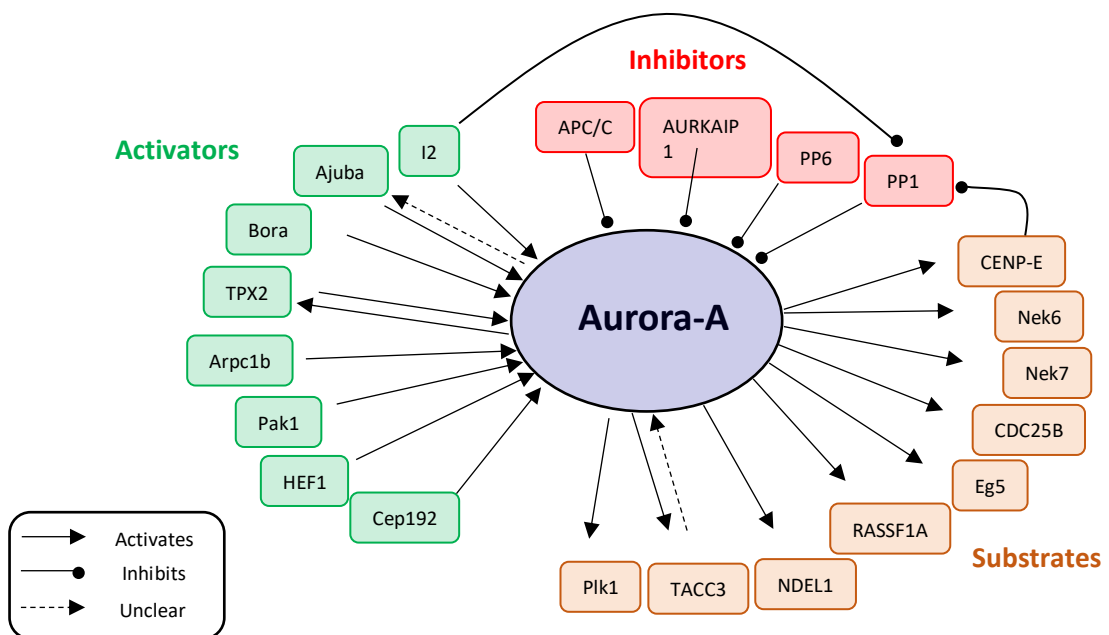
Figure **1.4**. Diagram showing a small cohort of Aurora-A binding partners, regulators of function, and substrates. Figure adapted from [22].

The level of kinase activity of Aurora-A is directly linked to its own activation state, which itself is determined by several factors. The phosphorylation state of Aurora-A is directly linked to activity. Upon phosphorylation at Thr287 and Thr288 on the activation loop, the kinase enters a more active state, with dephosphorylation by phosphatases such as PP1 and PP6 down-regulating activity.[22] Proteolytic degradation has a role in attenuation of Aurora-A activity, reducing the levels of kinase present.[23] Binding with other proteins plays a major role in the activity and degradation profile of Aurora-A, with the most active state apparent upon association with targeting protein for xenopus-kinesin-like-protein 2 (TPX2)[24], and proteins such as Aurora kinase A interacting protein (AURKAIP1) acting as a down-regulator.[25]

Activators of Aurora-A operate *via* a number of mechanisms, with proteins such as Ajuba promoting autophosphorylation of Aurora-A alongside undergoing phosphorylation itself[26], recruitment and formation of an increased activity Aurora-A homodimer by Cep192[27], direct phosphorylation of catalytically important Aurora-A residues such as Thr288 by partner kinases[28], or through down-regulation of phosphatase activity upon Aurora-A via a number of mechanisms including shielding of the activation loop from phosphatase activity by TPX2, for example.[29,30]

Under the assumption that dephosphorylated Aurora-A is no longer active in a regulatory role during mitosis, a majority of the work has focused on the function of Aurora-A in this state. However, research upon the *C. elegans* orthologue, AIR-1, has established it is localised to the microtubules by the associated TPX2 analogue, TPXL-1.[31] This, combined with evidence showing dephosphorylated Aurora-A still retains significant activity when associated with TPX2[22], shows the potential for a kinase-independent role during mitosis in an 'inactive' state alongside kinase activity when un-phosphorylated.

Considering the central position Aurora-A takes within mitosis, it is perhaps unsurprising that dysfunctional expression and regulation of Aurora-A has been linked to tumorigenesis and development of cancers. The location of the *aurora-a* gene at chromosome site 20q13.2 resides in an area frequently found amplified in tumours, indicating a possible connection that overexpression of Aurora-A may drive the development of cancers. It has been found overexpressed or amplified in a variety of cancer types, including colorectal[32], breast[33], head and neck[34], lymphoma[35], lung[36], and pancreatic[37], amongst others.[38] Overexpression of Aurora-A has shown malignant transformation potential in focus formation and xenograft assays, cooperation with oncogenic RAS during tumour development, and hyperplasia in mammary glands.[38] Overall, the association between aberrant Aurora-A behaviour and malignant phenotypes has identified *aurora-a* as a *bona fide* oncogene.

The presentation of aneuploidy associated with overexpression of Aurora-A has been associated with centrosome amplification, failure of cytokinesis and mitotic abnormalities. This aneuploid phenotype has been associated with simultaneous chromosomal instability, with both recognised as tumour drivers.[38] The induction of aneuploidy in Aurora-A over-expressed cells has been observed as p53-dependent, a critical tumour suppressor protein, suggesting Aurora-A overexpression leads to p53 degradation. This process eliminates checkpoints during mitosis that prevent the development of polyploid and aneuploid phenotypes, with the resulting cells predisposed to malignant transformation. Several binding partners of Aurora-A are also

overexpressed in cancers, with perhaps the most important within the current scope of research being TPX2.[39] The Aurora-A/TPX2 interaction was identified as a potential oncogenic holoenzyme, whereby the capacity to drive tumour formation is greater when both proteins are overexpressed in tandem, and will be covered in further detail in Section **1.2.1**.[40]

1.1.2 Small Molecule Regulation of Kinases

As outlined above, aberrant mitotic kinase behaviour has the potential to lead to severe mitotic defects and hinder the normal progression of the cell cycle. Overexpression or dysregulation of kinase function is therefore intrinsically linked to the proliferation of tumour cells as a precursor to cancer.[41] As such, down-regulating kinase function through removal of the ability to bind ATP by competing for the active site would effectively starve the enzyme of the source of phosphate and formed the strategy for development of initial kinase inhibitors around thirty years ago.[42]

Early uncertainty surrounding the use of ATP-competitive kinase inhibitors was focused on the structural similarity within the kinase superfamily, as well as the variety in the various substrates, leading to doubt around the selectivity of any inhibitors developed.[43] Other doubts highlighted the high cellular ATP concentration (*ca* 5 mM)[44] as a potential roadblock to effective small molecule inhibition of kinases. However, the discovery and subsequent FDA approval of imatinib[45], a selective, ATP-competitive inhibitor of the tyrosine kinase bcr-abl, was a seminal study in the treatment of chronic myelogenous leukaemia (CML) *via* protein kinase inhibition. To date, >90 protein kinase inhibitors have received FDA approval[46,47], the majority of which are ATP-competitive. Regardless of the kinase targeted, inhibitors are grouped by the binding mode displayed during inhibition. As previously discussed, a kinase active site has several conformations dependent on the activation state, and inhibitors belonging to the different groups will selectively bind these different conformations, outlined in Table **1.1**.

Class of Inhibitor	Mechanism of Action	Examples (target)
Type I	Competes for the substrate and binds to ATP pocket of active conformation kinase	Bosutinib (**BCR-ABL**) Cabozantinib (**c-Met**)
Type II	Binds to ATP pocket of inactive conformation kinases, with DFG-out structure	Imatinib (**BCR-ABL**) Sorafenib (**VEGFR**)
Type III	Exclusively occupy site adjacent to ATP-binding pocket, so that small molecule and ATP bind simultaneously	Trametinib (**MEK1/2**)
Type IV	Binds to remote (allosteric) regions outside of the ATP pocket, blocking interactions with partner proteins	ONO12380 (**BCR-ABL**)
Type V	Covalently bound (irreversible) inhibitors	Afatinib (**Her2**) Ibrutinib (**BTK**)

Table **1.1**. Overview of Kinase inhibitor classes, their mechanism of action, and example therapeutic targets.

1.1.2.1 Type IV Allosteric Kinase Inhibitors

Type IV kinase inhibitors are defined as inhibitors that bind to pockets on the kinase catalytic domain remote from the ATP-binding site[48]. These sites tend to be broader, shallower, more solvent-exposed and less well-defined than the ATP-binding site, therefore targeting these sites presents a potentially greater challenge. This is offset, however, by the potential for achieving exquisite small-molecule selectivity targeting these pockets due to the lack of sequence similarity compared to closely related kinases, unlike the highly conserved ATP-binding site.

This approach is exemplified by the discovery and development of asciminib (ABL001)[49], the first Type IV inhibitor of BCR-ABL1 to enter clinical trials. Asciminib also recently gained FDA approval for the treatment of chronic myelogenous leukaemia (CML)[50,51] in two separate indications – accelerated approval for treatment of Philadelphia chromosome positive CML (Ph+ CML-CP) in chronic phase in adults who have been treated with two or more tyrosine kinase inhibitors (TKIs); and full approval for Ph+ CML-CP with T315I gatekeeper mutation in adults. The development of asciminib began with GNF-2 and GNF-5, the first well characterised allosteric inhibitors of BCR-ABL1, shown to inhibit kinase activity through an allosteric mechanism upon binding to the C-terminal myristate pocket of Abl kinase[52]. Binding modes of GNF-2 and -5 to the

myristate pocket centre on a trifluoromethoxy group extending deep into a hydrophobic pocket, with an amide extending out of the pocket toward the solvent exposed region, shown in Fig. **1.5**. Important water-mediated H-bonding interactions between a pyrimidine and Tyr454, and an amine with Ala452, were also exploited to confer excellent selectivity between the GNF compounds and Abl over related myristate-binding proteins[53]. The binding of the GNF compounds to Abl was found to cause a significant structural change, resulting in inhibition of kinase activity. Upon GNF-2 and GNF-5 binding, a C-terminal helix local to the myristate binding site is shifted, resulting in the overlap of the SH2 and SH3 domains with the ATP-binding site. This allosteric mechanism of inhibition mimics natural autoinhibition lost in the BCR-ABL1 fusion protein, and was characterised with an NMR assay to enable further biophysical screening against this allosteric mechanism for small molecule discovery and development[54].
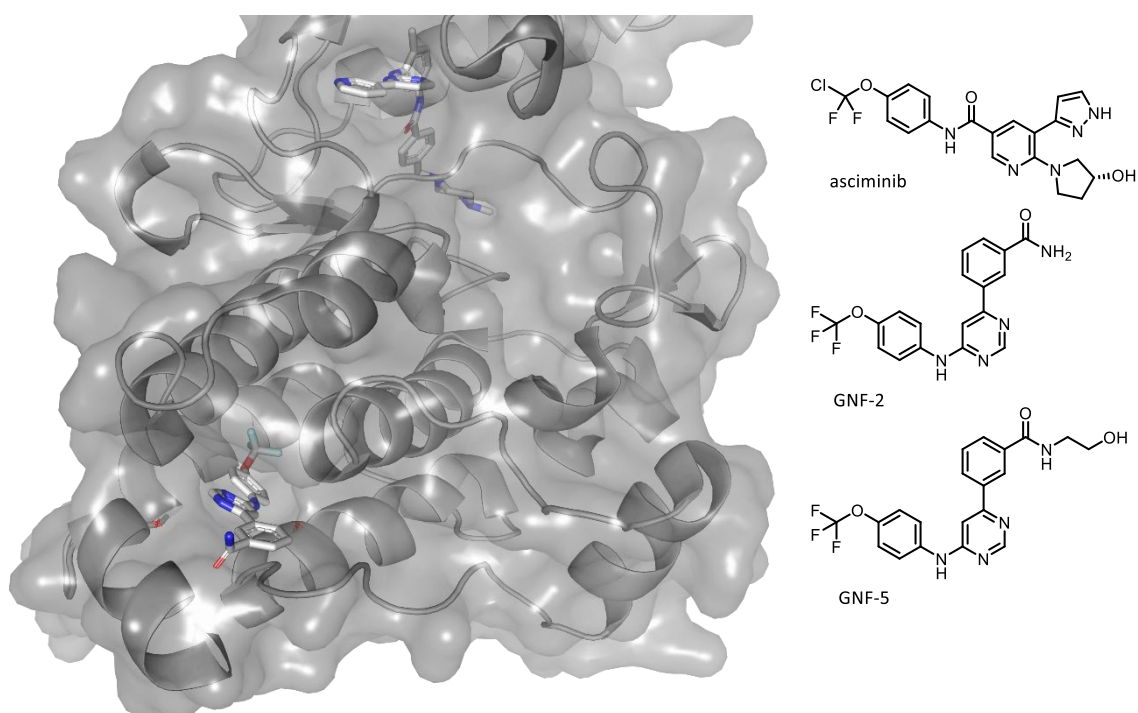
Figure **1.5**. Abl kinase in complex with Imatinib (top) and GNF-2 (bottom) (PDB: 3K5V). Imatinib occupies the ATP-binding site, GNF-2 occupies allosteric myristoyl-binding pocket, with important water molecules included. Surface/ribbon overlay highlights the trifluoromethoxy group of GNF-2 bound within a deep hydrophobic pocket.

GNF-2 and GNF-5, shown in Fig. **1.5**, while selective and potent against wt-BCR-ABL1, were found to have reduced efficacy against BCR-ABL1 mutants, with the gatekeeper residue T135I mutant severely attenuating potency (IC$_{50}$: >10 µM) of these compounds. A fragment screen was performed using the NMR conformational assay[54] to generate early SAR, followed by extensive medicinal chemistry efforts and structure-based design resulting in asciminib[49].

While binding in a similar manner to the myristate pocket as GNF-2 and GNF-5, asciminib retains inhibitory potential against all ATP-binding site mutations of BCR-ABL1 including the T135I mutant, a major advance over the previous compounds. Additionally, when combined with BCR-ABL1 ATP-competitive inhibitors asciminib has been shown to overcome acquired resistance mutations from either of the compounds in isolation[55]. This orthogonal and complementary mode of inhibition between asciminib and ATP-competitive inhibitors has led to evaluation of asciminib in >15 planned or ongoing clinical trials[56], both as a single treatment agent and as combined therapies, highlighting the potential of advanced Type IV inhibitors in the current treatment landscape.

Allosteric pockets on other kinases are often not so well-defined as the myristoyl-binding site of Abl but can still be targeted with Type IV inhibitors. For example, phosphoinositide-dependent protein kinase 1 (PDK1) is a major regulator of the AGC kinase family, with at least 23 downstream kinases dependent on PDK1 activation[57]. The PDK1 Interacting Fragment (PIF) pocket is a pocket remote to the ATP-binding site crucial for both the recruitment of downstream proteins and stimulating the activity of PDK1 itself, presenting this site as an attractive target for the discovery and development of allosteric PDK1 inhibitors[58,59]. Additionally, this pocket is located on the N-lobe of the kinase domain between the C-helix and ꞵ4 strand, a critical region for kinase regulation *via* protein-protein interactions (PPIs) that presents a potential opportunity for modulating kinase activity[60]. Conventional medicinal chemistry, *in silico* docking, and high-throughput crystallography have been employed in the discovery and development of allosteric inhibitors for equivalent pockets on PKC[61,62] and Aurora-A[63,64], respectively. Additionally, understanding of the bi-directional structural communication between active site inhibition and partner protein binding modulation has been elucidated for Aurora-A and PDK1[65,66]. Limited examples of Type IV kinase inhibitors, despite the tools to develop them, mean only a limited theory of design is applicable for ongoing development. Their design is still exploratory and when combined with the highly diverse structures of potential allosteric pockets to exploit, this challenge is multiplied. The understanding of regulatory mechanisms within kinase biology are also incomplete in even the most highly studied kinases, meaning the knowledge in this field often progresses parallel to inhibitor development rather than before it.

1.1.2.2 Inhibitors of Aurora-A

Currently no Aurora-A inhibitors have obtained FDA approval, despite several having entered clinical trials for a variety of cancer-types.[67] With sequence homology within the Aurora-A family being high, there are small molecule inhibitors that modulate the activity of all three isoforms – the so-called pan-Aurora inhibitors.[68–70] While some of these present certain advantages, such as treatment of taxane-resistant cancer cell lines[68], others were withdrawn from clinical trials due to concerns with toxicity.[70] More specific dual-Aurora inhibitors have been developed, targeting only the Aurora-A and -B isoforms.[71–73] Interestingly, while displaying good affinity of 3 nM toward both Aurora-A and -B isoforms, AT9283 displayed a phenotype typical of Aurora-B inhibition in HCT116 cancer cells, as well as inhibiting several other kinases – JAK2 and a imatinib-resistant bcr-abl mutant.[73] Other clinically advanced dual-Aurora inhibitors such as PF-03814375 have also displayed evidence of an Aurora-B inhibition phenotype, indicating a mechanism of action achieving Aurora-A inhibition was still not obtained, despite low nanomolar affinities.[72]

However, inhibitors selective for Aurora-A over the -B and -C isoforms have been described in the literature as well as undergoing clinical trials. Shown in Fig. **1.6**, several clinically advanced inhibitors (alisertib, MLN8054, MK-8745, MK-5108) have been developed and display a phenotype indicative of Aurora-A inhibition; accumulation of cells paused in G2/M phase, defective mitotic spindle formation, and inhibition of cell proliferation.[74–76] TC-A2317 exhibits reduced tumour growth in mouse-human xenograft studies, a promising result.[77] Conversely, while the Genentech Aurora-A Inhibitor 1 displayed good inhibition of Aurora-A with an IC_{50} of 3.4 nM, off-target effects were evidenced by high toxicity in multiple cell lines.[78]
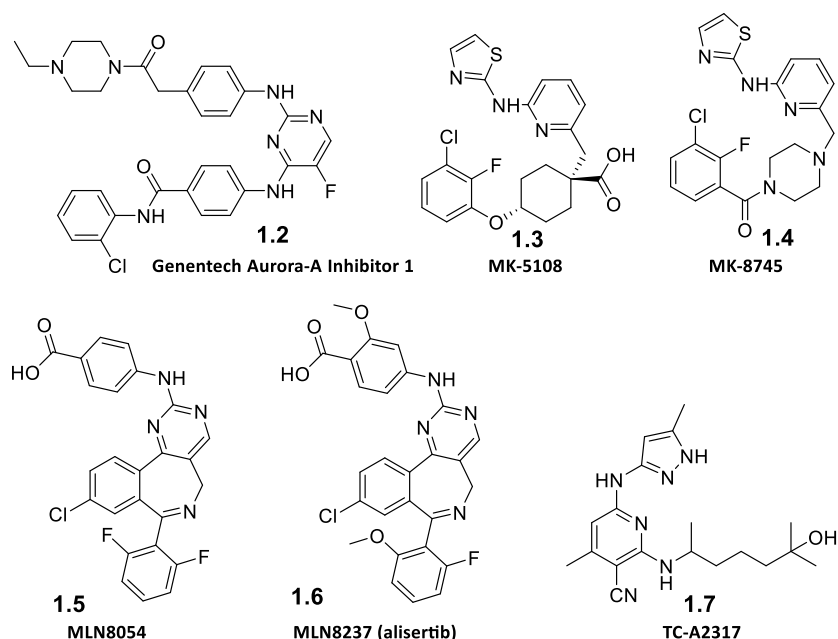
Figure **1.6**. Structures of clinically advanced selective Aurora-A inhibitors.

As the active site of kinases is the most highly conserved region in all kinases, Type I bioactive small molecules are unsurprisingly prone to high levels of promiscuity across both the Aurora kinases and the kinase superfamily, increasing the chance of undesirable off-target effects and toxicity, and therefore potentially fail before reaching either clinical trials or FDA approval. In an attempt to sidestep the potential selectivity issues present with Type I/II modulators of Aurora-A, an alternative approach to modulate activity would be to target an allosteric site using a Type IV inhibitor. Through inhibition of Aurora-A or the association between Aurora-A and a partner protein, modulation of activity may be able to be achieved *via* this mechanism. Targeting the PPI with an activator of Aurora-A such as TPX2 would provide an alternative mechanism of Aurora-A downregulation compared to ATP competition, but would require experimental validation to assess the feasibility of this method. To date, no allosteric inhibitors of Aurora-A have been described in the literature outside those that target the Aurora-A/TPX2 interaction, the detail of which will be covered in the following section.

1.1.2.2.1 Type IV Allosteric Inhibitors of Aurora-A

TPX2 is a large (85.6 kDa) protein that acts as a regulator during mitosis in the nucleation and assembly of the mitotic spindle *via* interaction with a wide variety of partners, including Aurora-A. Under normal cellular conditions TPX2 binds to Aurora-A at the centrosome and

localises it to the poles of the mitotic spindle.[79] TPX2 also stabilises and regulates Aurora-A levels and kinase activity, with evidence showing protection of Aurora-A against proteolytic activity[24] and an increase of up to seven-fold in kinase activity[80] upon TPX2 binding. This highlights TPX2 as a crucial partner for the localisation, stabilisation and regulation of Aurora-A activity, and has been highlighted as a target for the development of anti-cancer therapeutics.[40] TPX2 binds Aurora-A at two separate sites on the kinase connected by a flexible linker region evidenced by a lack of electron density in X-ray crystal structures.[22] The interaction is characterised by three hot-spots, shown in Fig. **1.7**, identified as the Y-, F-, and W-pockets based on the identity of the TPX2 residues that occupy each pocket upon formation of the Aurora-A/TPX2 complex.[64]
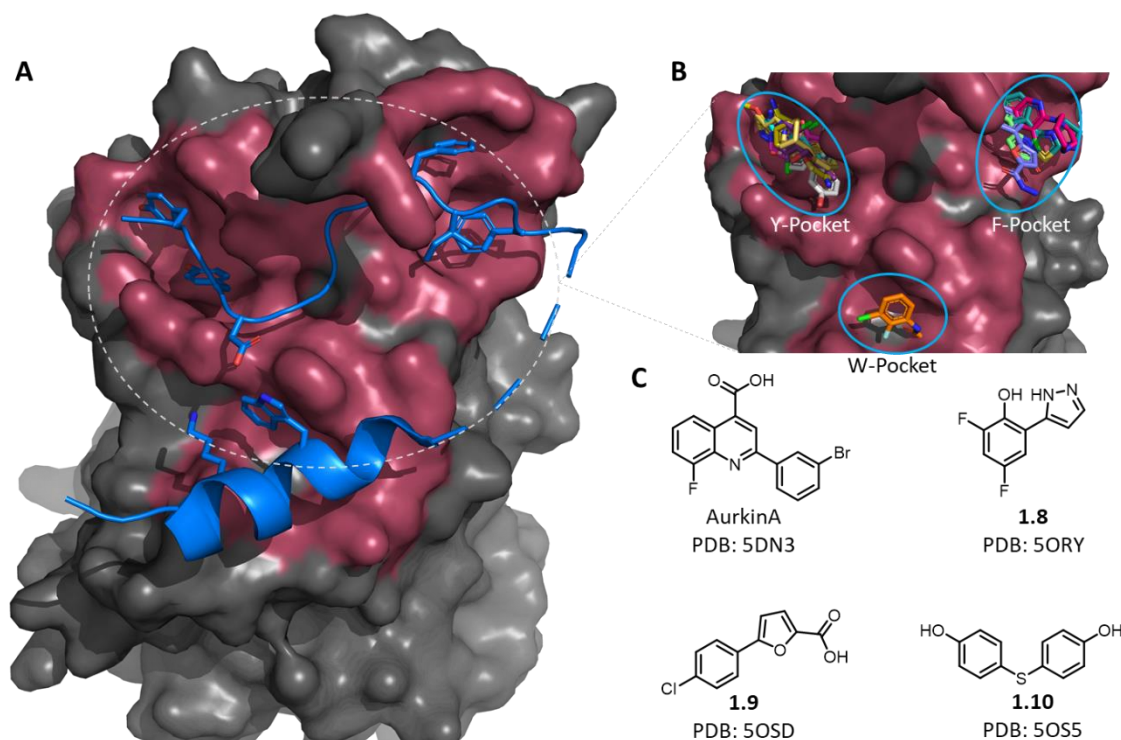
Figure **1.7**. Aurora-A/TPX Interaction and Small Molecule Allosteric Inhibitors. Panel **A** shows the Aurora-A(grey)/TPX2(blue ribbon) interaction, with the binding interface highlighted in purple. Panel **B** shows location of a subset of small molecules found to bind to the Aurora-A/TPX2 binding interface, overlaid on PDB: 1OL5 with TPX2 removed.[63,64] Panel **C** shows example allosteric inhibitor structures, AurkinA[63] and **1.8**-**1.10**.[64]

A high-throughput, fluorescence anisotropy (FA) screen was performed that probed the displacement of TPX2 from Aurora-A[63], in which a library of 17,000 targeted small molecules were screened. This HTS resulted in 15 potential inhibitors of the PPI and following a small SAR campaign, the authors were successful in identifying a small molecule (AurkinA, structure shown in Fig. **1.7**) that binds to the Y-pocket and competes with TPX2. AurkinA was also found to inhibit kinase activity in a non-ATP-competitive manner and mis-localises Aurora-A from the mitotic

spindle in a cellular assay. Interestingly, AurkinA also inhibits activation of Aurora-A by phosphorylation *in vitro* despite only small changes observed in the N-lobe in the crystal structure, mainly around the Y-pocket to accommodate ligand binding. Phosphorylated Aurora-A has been shown to be highly dynamic[81,82], more so than the un-phosphorylated species, and a plausible alternative mechanism of inhibition is that AurkinA binding restricts catalytically significant movement.

A different study first identified three hotspots on the Aurora-A/TPX2 interface using a co-precipitation assay and ITC, and subsequently used the X-Chem high-throughput crystallography platform at Diamond Light Source to screen a library of 1255 fragments to identify binders to Aurora-A[64], resulting in identification of >50 ligands that bind specifically to the identified Y-, F-, and W-pockets. Binding and inhibition assays revealed many of the fragments attenuate TPX2 binding and associated activation of Aurora-A, confirming the allosteric mode of inhibition and validating the strategy of targeting the Aurora-A/TPX2 interaction. Several of the compounds were found to inhibit the activity of phosphorylated Aurora-A in isolation, in a similar manner to AurkinA, confirming biochemically as well as structurally that the ligands bind to an allosteric site when modulating kinase activity. Interestingly, some compounds from this study were found to increase the rate of Aurora-A autophosphorylation, indicating allosteric regulation may be either positive or negative depending on the ligand itself.

These small molecule-led studies suggest the Aurora-A/TPX2 interaction is remarkably druggable and that binding to an allosteric site has the potential to both downregulate Aurora-A activity and localisation through perturbation of the PPI, as well as a direct modulation of phosphorylated Aurora-A in the absence of TPX2. However, the allosteric ligands described so far show that modulation distant from the ATP-binding site is not a guarantee that the ligand in question will not also block activation of Aurora-A by phosphorylation, with further probe molecules required to fully understand how targeting the TPX2 binding sites affect the structure and dynamics of this region and therefore guide therapeutic development.

1.1.3 Future Perspectives on Allosteric Inhibitors of Aurora-A

A wide range of studies in to the structural and mechanistic underpinnings of the Aurora-A/TPX2 interaction have been performed, as well the effects of both inhibition and mis-localisation of Aurora-A function and the role of TPX2 upon all the above. This PPI complex may

form the basis of healthy progression through mitotic spindle assembly during mitosis, and the consequences of overexpression (or downregulation) of either or both critical components has been indicated.

However, there is a link between the interaction and cancer-like phenotypes observed when either constituent is overexpressed. The combination of both proteins being overexpressed in cancer as an oncogenic holoenzyme has led to early-stage but in-depth and ongoing study on how to effectively inhibit the formation of the Aurora-A/TPX2 complex and target Aurora-A in an allosteric manner as a potential anti-cancer therapeutic. Initial steps have been taken through the development and characterisation of a variety of small molecule inhibitors, with promising outcomes. It is expected this work will continue based on the chemical diversity of effective hits, which would allow a variety of medicinal chemistry strategies, as well as the potential to reveal the implications of the interaction as a true cancer-driver.

1.2 Bioactive Small Molecule Discovery

Drug discovery programmes typically follow a set procedure of initial identification and validation of a suitable biological target that demonstrates the desired therapeutic effect when either inhibited or activated in a diseased state.[83] This is followed by hit identification, in which libraries of compounds are screened with the aim of discovering a hit molecule capable of the desired target modulation. Hits are then characterised by intense SAR studies to improve target selectivity and potency, as well as increase ligand efficiency and improve the pharmacokinetic properties. These so-called lead compounds will then undergo further optimisation of the pharmacokinetic properties and toxicity screening to reduce rates of failure in pre-clinical studies.[83] Careful tuning of solubility, polarity, polar surface area, and MW, for example, can be performed to improve cell permeability, solubility, reduce hERG inhibition, increase penetration through the blood-brain barrier, and reduce metabolic liabilities, therefore increasing the chances of the chosen hit series progressing onward through the drug development pipeline.

Historically, common practice for hit identification has been high-throughput screening (HTS), in which vast compound libraries would be screened against the target of interest.[84] However, with the introduction and industry acceptance of the "rule of five" guidelines by Lipinski *et. al.* in 2001[85] (≤5 H-bond donors, ≤10 H-bond acceptors, MW <500, and log*P* <5), the number of small molecules that meet these criteria is estimated at 10^{33}, meaning even a library of hundreds of millions of compounds would inefficiently sample this vast chemical space.[86] By

reducing the size of the molecules, the corresponding chemical space is reduced in size, with compounds restricted to twelve heavy atoms (non-hydrogen atoms) producing a data set of around 100 million compounds.[87] While this is not an inconsequential number, it narrows the field considerably compared to 10^{33} compounds of MW <500 Da, allowing for more efficient sampling of chemical space by these smaller fragment compounds. This forms the basis of fragment-based drug discovery (FBDD).

1.2.1   Fragment-based Drug Discovery

Contrary to HTS, FBDD approaches bioactive small molecule discovery through screening of libraries of several thousand compounds against a validated target, with lower molecular weight and binding affinity but incorporating tight regulation on molecular properties. Fragment hits are then identified with biophysical or biochemical methods, before strategies are devised on elaboration *via* fragment growing, linking, or merging to yield potent bioactive compounds.[88]

With a lower MW compared to HTS compounds, the rule-of-five guidelines are no longer appropriate, and as such early fragment libraries generally followed the rule-of-three; MW <300 Da, fewer than three H-bond donors/acceptors, fewer than three rotatable bonds, and a clogP of less than three.[88] As FBDD became more widespread, fragment libraries became more specialised and employed stricter guidelines for molecular properties; MW of 10-15 heavy atoms, logP (-1 to 3), complexity *via* 3D shape and *sp³* character, removal of PAINS, and solubility.[89] The use of targeted fragment libraries against particular protein families is also becoming more commonplace, with libraries targeting kinases, metalloproteinases, and oxacillinases, amongst many others.[90–93] Through analysis of chemotypes known to bind a particular target, incorporation of similar motifs or scaffold hopping increases the chances of discovering a bioactive modulator, streamlining the fragment hit identification workflow.[92]

With fragments forming low affinity interactions with protein binding sites compared to larger HTS compounds, it has been necessary to change tactics when characterising and scrutinising any potential hits. Sensitive biophysical methods may be required for binding affinity from 1-10 mM, and traditionally these have included X-ray crystallography, NMR, SPR, FRET/TR-FRET assays, and ITC.[94] More recent techniques include cell-based assays, microfluidic electrophoresis, and thermal shift assays.[88] Ligand efficiency (LE)[95] has also been utilised as an

aid to quantify high quality hits, outlined below, with hits displaying an LE of 0.3 or higher generally considered appropriate for further elaboration.[96]

$$Ligand\ Efficiency\ (LE) = \frac{\Delta G^{\theta}}{Heavy\ Atom\ Count\ (HA)} \approx \frac{1.37}{HA} \times pIC_{50}$$

Equation **1**. Equation for Ligand Efficiency, used to quantify the efficiency of binding interactions

The seminal paper by Fesik *et. al.* utilised NMR spectroscopy to screen fragments against a protein followed by optimisation and linking of fragment hits, coined SAR by NMR.[97] This study offered proof-of-concept work in which multiple low-affinity fragments were linked and thereby produce a higher-affinity ligand, the K_d of which was equal or greater than the fragments individually. More recent strategies exploit structural information on fragment-protein binding to inform further fragment elaboration, structure-based drug design (SBDD).[88] This structural information has proven critical in efficient fragment elaboration, with optimal linking or growing of fragments yielding compounds with higher potency than the original fragments combined.

An exemplary use of FBDD in combination with SBDD is found in the discovery and development of vemurafenib, evidenced by this being the first FDA-approved drug resulting from this method.[98,99] In this example a library of 20,000 fragments was screened against several protein kinase targets, at 200 μM. From this initial screen, 238 hits were selected for co-crystallisation studies resulting in 100 solved structures. The Pim-1 protein system constituted 16 of the 100 structures, one of which was the initial fragment hit, shown in Fig. **11**, seen binding at the ATP active site of the kinase. Analogues of this initial fragment were co-crystallised with FGFR kinase in an SAR-like study, to identify key binding motifs followed by further SAR that indicated the difluoro-phenylsulfonamide as having the greatest increase in potency, with analogues synthesised and screened through co-crystallisation with oncogenic Braf-V600E.[98] Crucially, vemurafenib was shown to have selectivity for the oncogenic Braf-V600E mutant over WT-Braf, with IC_{50} values of 13 nM and 160 nM respectively.
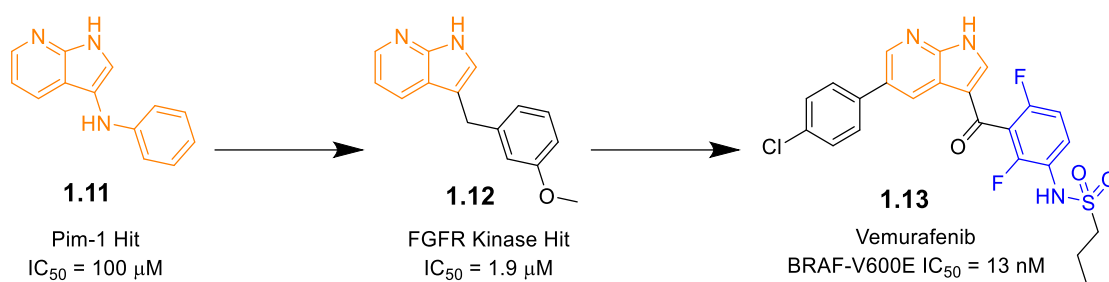
Figure **1.8**. Development of Vemurafenib. Initial fragment hit is highlighted in orange throughout development. Blue indicates key SAR optimisation along productive growth vector.

1.2.2 Computer-aided Drug Design and Ensemble Docking in Drug Discovery

Traditionally, *in silico* docking techniques were performed with static target crystal structures, docking libraries of compounds against the target protein in three dimensions and ranking the results. Early studies were successful in validating this technique, discovering antiviral compounds against HIV and influenza[100,101]. Understanding of ligand binding thermodynamics and methods of modelling, simulating and generating protein structures has unsurprisingly progressed since these seminal studies. With advances in cheminformatics, machine-learning, and widely available increases in computing power, computer-aided drug design (CADD) is now commonplace and examples include use of artificial neural networks or artificial intelligence (AI)[102,103], covalent inhibitor docking[104], and cover a wide range of protein targets[105].

Ensemble docking describes the generation of an "ensemble" of drug target conformations for use in computational and structure-based drug discovery, often obtained by molecular dynamics (MD) simulation, to which ligands are docked. This docking strategy samples multiple conformations of the target protein rather than a singular static structure, introduced in a seminal paper against the catalytic domain of HIV integrase[106]. Here the authors showed that consensus pharmacophore models based on multiple MD or crystallographic structures were more successful than models based on single conformations in predicting binding, resulting in a docking study leading to the discovery of new HIV-1 integrase inhibitors[107]. Sampling the inherent flexibility of proteins and their ligand binding sites through ensemble docking allows for a potentially more accurate model in which to dock desired ligands, compared to singular static crystal structures. More recent advances in ensemble docking have been fuelled by the large number of available and derivable target structures, large advances in readily available computational power, machine-learning, and improved methodologies[108,109],

and have tended to explore MD-derived structures and improving aggregation of docking scores, rather than ensembles of crystal structures.

1.2.3 Integrated Methods in High-throughput Chemistry for Drug Discovery

Integrated methods are frequently employed in molecular discovery, conferring several advantages over HTS and FBDD approaches. By typically conducting chemical synthesis directly prior to biological screening, the purchase and maintenance of a large screening library and associated costs can be avoided when employing an integrated approach. While HTS libraries typically costing between $400 million and $2 billion, an integrated approach can be implemented for a small fraction of this cost (<0.1%)[110]. Similarly, chemical diversity within an HTS library cannot be easily altered to target a specific protein meaning relevant chemical matter may not be included when screening against challenging protein targets[84]. Highly optimised and efficient processes are employed to create libraries of compounds poised for on-demand biological screening. The libraries may consist of pure compounds, mixtures of compounds with individual tags containing information on the compounds in question, or crude reaction mixtures[111–117]. Reactions are performed on the micro- or nano-scale and require milligrams, or even micrograms, of starting materials mean the use of expensive building blocks can be routine.

1.2.3.1 Small Molecule Discovery by Integrating Chemical Synthesis and Screening

Miniaturisation of chemistry to the micro- or nano-scale enables hundreds or thousands of reactions to be run in parallel[111–114,118–123]. Investigation of both the reactivity and biological activity of large libraries of building blocks is enabled through use of small amounts of material, usually <1 mg, and has led to the rapid optimisation of challenging reactions in the discovery and development of drugs[122]. Similarly, the combination of microscale synthesis and biological screening has broadened the chemical space tested against a target[111,123]. These integrated microscale approaches typically exploit plate-format batch chemistry and screen crude reaction mixtures, although some workflows incorporate in-line purification or flow chemistry as an alternative approach[111,112,114,115,119,124,125].

Nanoscale synthesis with affinity ranking (NanoSAR) is an example of this approach, where reaction arrays were performed on the nanoscale using micrograms of material in each reaction (between 50 and 5 μg)[111]. Over 1700 reactions were performed to sample both reaction

space and biological activity space in the discovery of novel and potent inhibitors for Extracellular Signal-Regulated kinase 2 (ERK2), Checkpoint Kinase 1 (CHK1), and Mitogen-Activated Protein Kinase 2 (MK2). The crude reaction mixtures were subject to affinity-selection mass-spectrometry (ASMS) to identify active compounds. The reactions exploited to generate the library were based on commonly used transformations in small molecule discovery, including Suzuki-Miyaura cross-couplings, Buchwald-Hartwig cross-couplings, and amidation[126,127]. An initial investigation to identify productive reaction conditions for each transformation was performed, totalling over 1500 reactions, where each reaction was analysed by UPLC-MS to identify reactions producing the desired product and estimation of the yield.
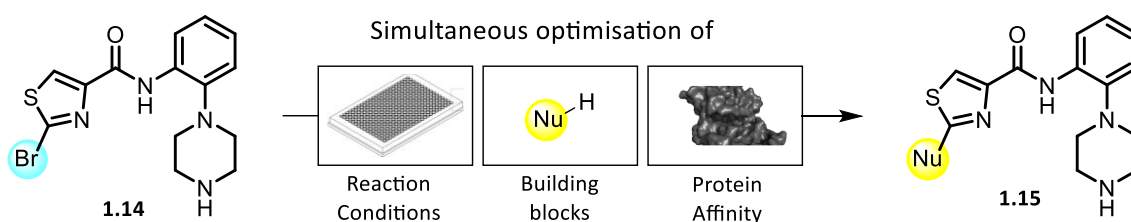
Figure **1.9**. Workflow of the simultaneous synthesis, optimisation, and biological screening of kinase inhibitors in NanoSAR. Reactions were performed in 384-well plates, at 1.2 µL final reaction volume dispensed by microfluidic handling robotics. Products were subject to affinity-selection mass-spectrometry to identify hit compounds.

The kinase targets were each assigned a different central scaffold, which was elaborated by one or more of the chemistries employed. A diverse set of coupling partners were used with each reaction type to decorate these scaffolds, along with a broad range of coupling conditions. Totalling 435 building blocks across all three targets, UPLC-MS analysis identified 396 of the scaffold-building block combinations that furnished the desired product, from a total of over 1700 individual reactions. These libraries were then screened for affinity to either ERK2, CHK1, or MK2, dictated by the central scaffold, and several hits were identified. By reducing the concentration of protein in the ASMS assay each reaction well was subject to multiple protein concentrations, allowing estimation of the binding affinity of the reaction product. The products acting as protein ligands were identified from analysis of the protein-bound fraction at these differing protein concentrations. Selectivity was also scrutinised through inclusion of a fixed concentration of competitor protein. Hit compounds were resynthesized on a 20 mg scale and re-screened in the ASMS assay, as well as a biochemical assay measuring kinase activity, to confirm the nanoscale results were validated with pure compounds.

Had the library generation been performed under a single set of reaction conditions, only a small proportion of the available chemical space would have been explored. 24 C-N cross-coupling reaction conditions were explored with five amine building blocks, identifying four reaction conditions deemed robust enough for use with the 96 amines exploited in the NanoSAR library. The resulting nanoscale C-N cross-coupling reactions were successful in synthesising 92 of 96 possible products as part of the library, highlighting the importance of chemical
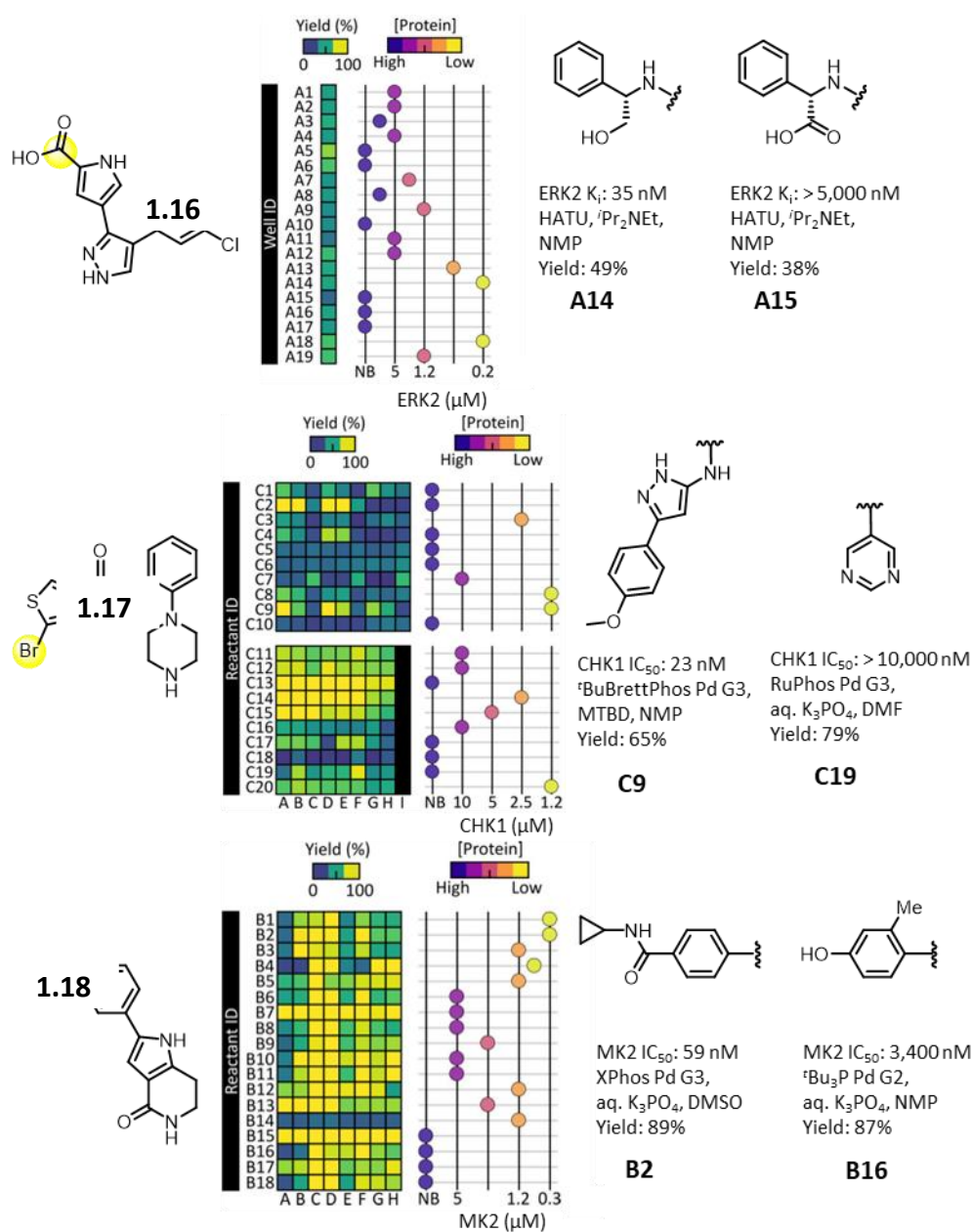
Figure **1.10**. Representative results of NanoSAR libraries screened against ERK2, CHK1, and MK2, utilising amidation, Buchwald-Hartwig C-N cross-coupling, and Suzuki-Miyaura cross-coupling reactions, respectively. Hit compounds identified by detectable binding in ASMS assay at lowest protein concentrations. Figure adapted from [112].

optimisation in the efficient exploration of biologically relevant chemical space. The diversification and optimisation of the typically exploited chemistry toolkit in the drug discovery

workflow may therefore be enabled by NanoSAR, simultaneous to the discovery of novel bioactive small molecules.

1.2.3.2 Activity-directed Synthesis

Traditionally, natural products or their derivatives have been very successfully exploited in the pursuit of bioactive small molecules, with around one-third of FDA-approved drugs between 1981 and 2010 from this source.[128] These natural products arise as a result of the evolution of biosynthetic pathways in the host organism, inferring a competitive advantage to the host. These pathways are structure-blind, function-driven – a principle that has been directly translated to activity-directed synthesis (ADS). Drawing inspiration from natural product pathways, ADS applies this concept to the identification of small molecule modulators of biological targets. Synthetic routes arise simultaneously with active products, and subsequent rounds of ADS are designed based on the prior round of synthesis that afforded active products in an attempt to increase product potency and/or yield of product from the reaction array. In addition, the chemistry employed can be less established within the traditional medicinal chemistry toolkit, due to the low demand within the workflow for characterisation and purification. This allows for more interesting chemistries with multiple potential outcomes in any one reaction to be utilised.
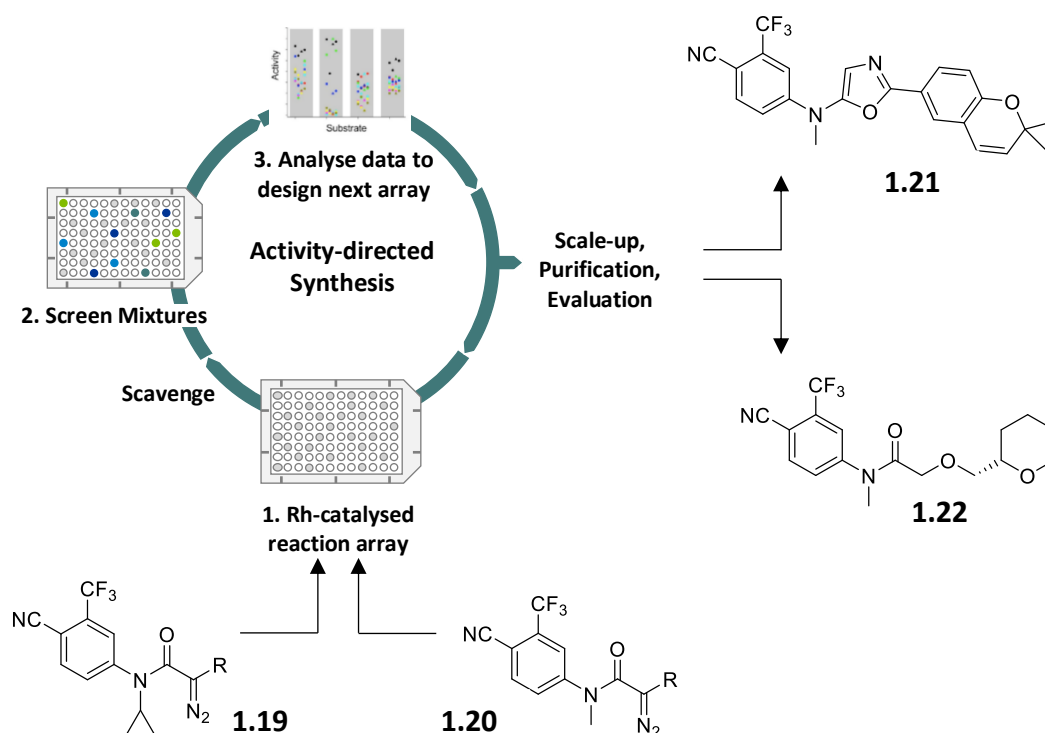
Figure **1.11** ADS workflow utilised in the discovery of novel bioactive ligands against the AR. Starting materials enter the cycle at the bottom, followed by iterative rounds of synthesis, evaluation, and re-design of reaction conditions to yield potent compounds **1.21** and **1.22**.

ADS has been shown to be viable for the discovery of novel bioactive small molecules against a range of targets.[112–115] Two related publications exemplified the use of α-diazo amides with transition metal catalysts for the discovery of novel ligands for the androgen receptor (AR).[114,115] The highly reactive and promiscuous nature of metal catalysed carbenes was chosen to intentionally exploit the potential to form multiple products within each reaction mixture. Reaction arrays were performed in 96-well plates on 100 µL scale under ambient conditions and were screened against the AR using a time-resolved fluorescence resonance energy transfer (TR-FRET) assay following the scavenging of metal catalysts. This assay data was then analysed to identify biologically active reaction mixtures, which formed the basis upon which subsequent arrays were designed. By reducing the screening concentration of reaction mixtures in successive rounds, selection pressure was applied to the outcomes, optimising both biological activity of products and reaction yields.

Initial ADS experiments were performed with 16 α-diazo amides containing an AR-binding 4-cyano-3-trifluoromethylphenyl motif combined with several transition metal catalysts to harness intramolecular reactions.[114] An initial round one combined 12 α-diazo amides, **1.23**-

1.34, three catalysts and one solvent, with the products screened at 10 µM resulting in identification of four α-diazo amides yielding active products: **1.24**, **1.25**, **1.28**, and **1.30**. Round two was designed based on these four diazo substrates, and consisted of six α-diazo amides **1.24**, **1.25**, **1.28**, **1.30**, **1.33** and **1.34**, eight catalysts, and four solvents. These 192 reaction mixtures were screened at 1 µM, with diazo substrates **1.23** and **1.27** resulting in the most active mixtures. These two substrates, along with related analogues **1.35**-**1.38**, formed the basis of round three, in combination with six catalysts and three solvents. 108 reaction mixtures were screened at 100 nM total product concentration and eight reactions were found to have produced promising biologically active products and were therefore scaled-up to obtain pure products for analysis. Three active compounds were identified that displayed sub-micromolar activity, **1.39**-**1.41**. These results highlight the ability of intramolecular ADS to discover novel and potent scaffolds alongside simultaneous optimisation of reaction yields.
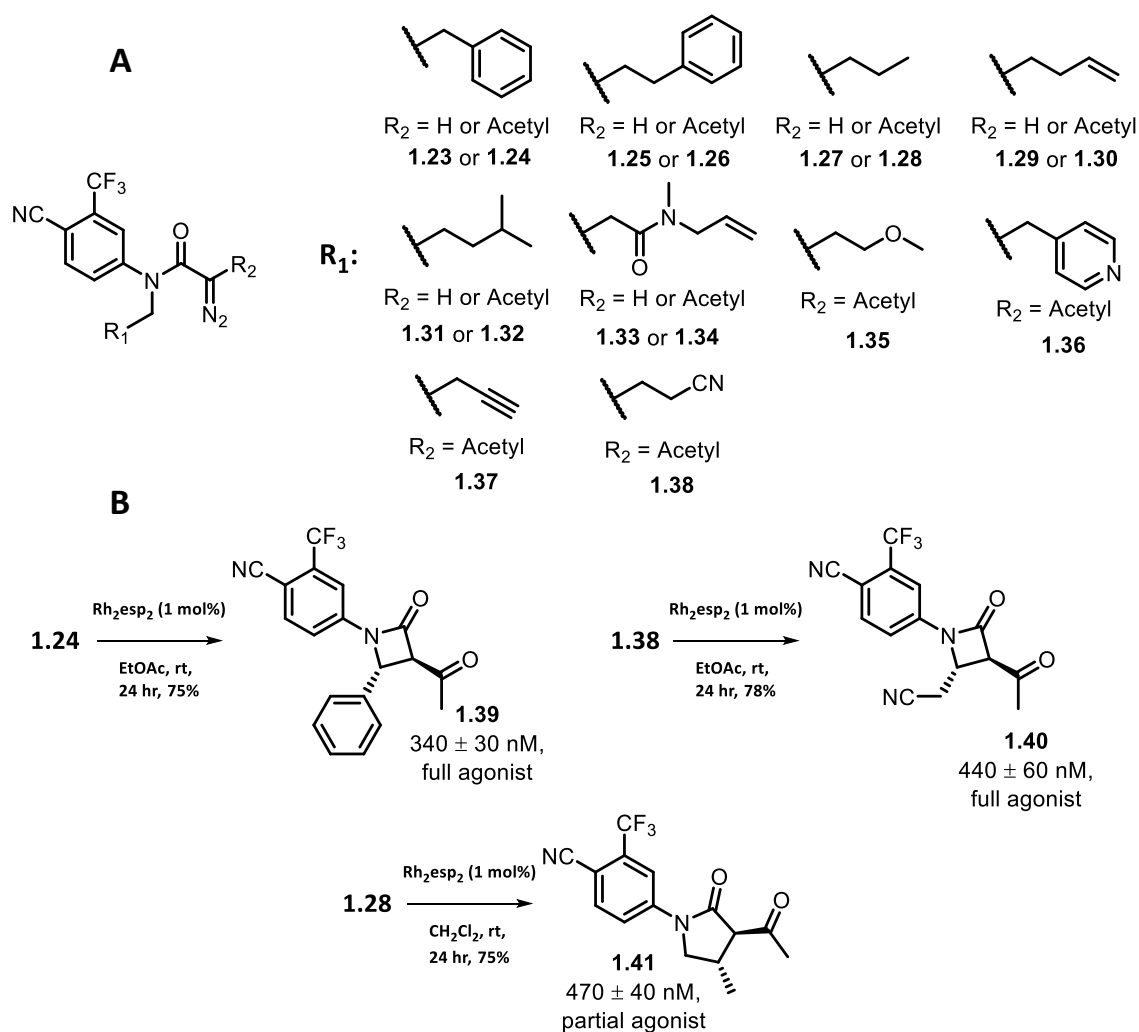
Figure **1.12**. Intramolecular ADS Reactions for AR agonist discovery. Panel **A**: Diazo substrates used in reaction arrays. Panel **B**: Biologically active products identified following scale-up, purification, and characterisation of active reaction mixtures.

A second ADS series was performed, this time to investigate intermolecular reactions for the discovery of AR ligands[115]. A set of co-substrates with diverse structure and reactivity were selected to enable activity-directed fragment growth from an α-diazo amide binding fragment N-[4-cyano-3-(trifluoromethyl)phenyl]-N-methylacetamide, with an existing IC_{50} of 92 µM, exploiting metal-catalysed carbene chemistry. Three iterative rounds of ADS were performed in a non-exhaustive manner, totalling 326 from a possible 888 reactions, with the reactions in rounds one and two selected at random from the designed set. Much like the intramolecular experiments, selection pressure was applied between successive reaction arrays through the reduction of screening concentration of the reaction mixtures. Round one was screened at 10 µM and rounds two and three at 5 µM and 1 µM, respectively. Unlike the intramolecular reactions, however, diversity and design between rounds was explored through the co-substrates $i.e.$, round one co-substrates yielding active reaction mixtures formed the basis of round two co-substrate selection.
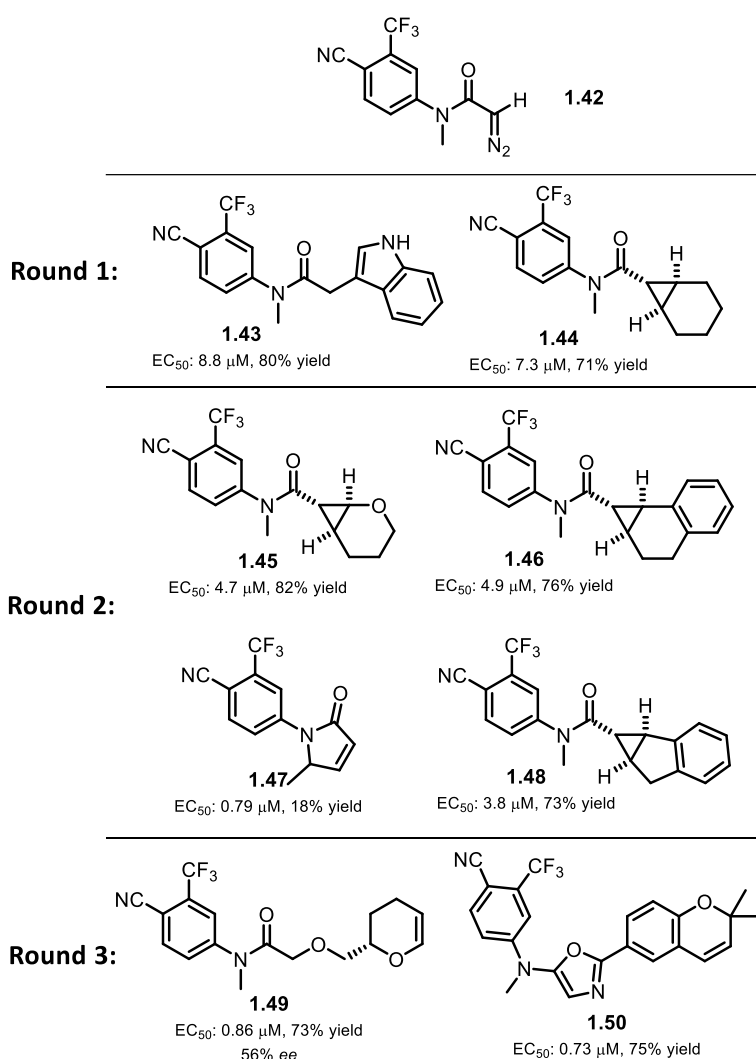
Figure **1.13**. Intermolecular ADS Products for AR agonist discovery

Following identification and scale-up of the most active reaction mixtures, active compounds were purified and characterised (Fig. **1.13**). The active components from round one are **1.43** and **1.44**, the product of a C-H insertion to the C3 position of indole and cyclopropanation of cyclohexene, respectively. Round two introduced various co-substrates to expand on the cyclopropanation to identify alternative compounds. Round three introduced new functionality to the co-substrates, including alcohols and nitrile groups, resulting in unexpected reactions forming products **1.49** and **1.50**. The product **1.49** was formed by a previously unknown enantioselective O-H insertion reaction, meaning this product was unlikely to have been predicted. Intermolecular ADS has therefore been able to identify novel transformations in the process of bioactive compound discovery.

ADS has also been employed in the determination of SAR of a series of anti-bacterial compounds against *S. aureus*.[112] Through use of several Pd-catalysed reaction types in microscale array format, the SAR landscape of a series of quinazolinones was expanded following crude reaction mixture screening. Identification of active reaction mixtures and subsequent purification and characterisation led to the discovery of compounds **1.51** and **1.52**, products of a Pd-catalysed carbonylation/cyclisation cascade reaction. Through purification and characterisation of both active and relatively inactive compounds, ADS enabled the SAR of this series to be expanded following screening of the pure compounds. Interestingly, this was able to be performed on relatively low yielding reactions, positioning ADS as a method of exploration of chemical space that may have otherwise been ignored.

1.51
ATCC29213 MIC: 0.016 μg/mL,
4% yield

1.52
ATCC29213 MIC: 0.5 μg/mL,
14% yield
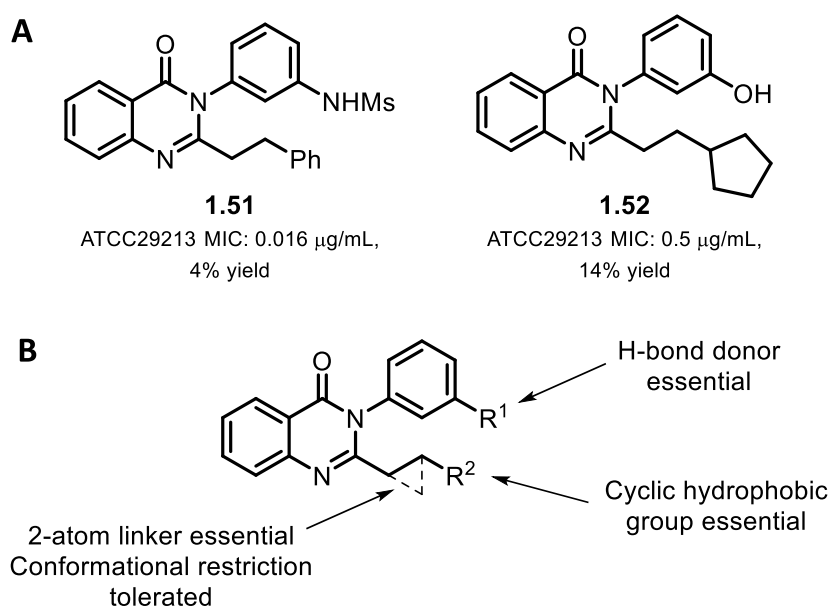
Figure **1.14**. Pd-catalysed ADS Products for the discovery of novel anti-bacterials. Panel **A**: Biologically active products identified following scale-up, purification, and characterisation. Panel **B**: Expanded SAR of quinazolinones through use of ADS.

Finally, ADS has been harnessed for the discovery of distinct and novel series of inhibitors against the p53/*h*DM2 PPI.[113] The design centred on a set of diazo-containing substrates and a set of co-substrates with at least one functional group with precedented reactivity for the metal carbenoid chemistry employed. Many of the diazo substrates and co-substrates also included motifs with the potential to mimic p52 hotspot residues, including phenyl, chlorophenyl, and cyclic, branched, and fluorinated alkyl groups. Two iterative rounds of ADS were performed, totalling 346 microscale reactions comprised of 10 diazo substrates, 21 co-substrates, and two catalysts. Biological screening was performed using a fluorescence anisotropy (FA) competition assay at 20 μM total product concentration and identified six reaction conditions producing active products.
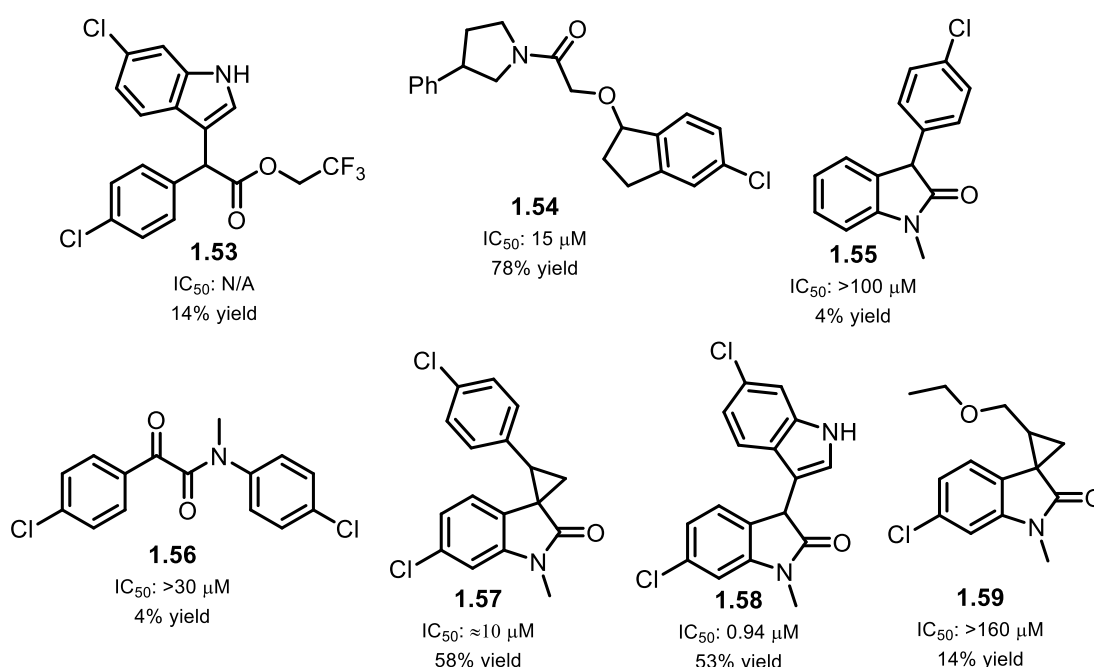
Figure **1.15**. Purified ADS reaction products in the discovery of p53/*h*DM2 ligands.

Following scale-up, purification, and characterisation of the active reaction mixture products, four products (**1.54**, **1.56**-**1.58**) were found to displace the peptide tracer in the FA competition assay, indicating significant protein-ligand interaction. Interestingly, all four binding ligands were subject to *in silico* docking studies which suggested the aromatic substituents bind to the same *h*DM2 subpockets as those in optimised inhibitors. This positions ADS as a potential strategy for experimentally determined scaffold-hopping, enabling ligand discovery containing common pharmacophores with alternative central scaffolds. Additionally, ADS has facilitated

ligand discovery against a PPI lacking a well-defined small-molecule binding site, a strategy generally considered to be a more challenging target than an ATP-binding site, for example.

ADS has been validated as a complementary method for the medicinal chemistry toolkit for molecular discovery and could be integrated with existing drug discovery strategies. Scaffold discovery[114], fragment growth[115], SAR expansion[112], and scaffold hopping[113] have been demonstrated, covering key challenges in medicinal chemistry and drug discovery. ADS has also shown efficacy with multiple biological targets, covering typical small-molecule binding sites[112,114,115] and less well-defined PPI binding sites[113], indicating applicability against both traditional and non-traditional drug targets.

1.3 Project Outline

Activity-directed synthesis is a powerful method for the discovery of chemical matter for various protein targets, including those with well-defined small molecule binding sites and for shallower, less well-defined PPI binding sites. A key aim of the project is to expand upon the existing repertoire of challenging biological targets for ADS by targeting shallow, allosteric binding sites potentially amenable to the activity-directed discovery of novel chemical matter. Allosteric pockets, such as the Y-, F-, and W-pockets of Aurora-A provide an ideal challenge for further validation of ADS as a tool against under-explored and challenging targets to develop potent allosteric inhibitors. Additionally, the medicinal chemistry and SAR landscape of allosteric inhibitors of Aurora-A is relatively unexplored. A second aim of the project is to further expand upon this SAR, therefore enabling the discovery of more potent allosteric Aurora-A inhibitors. More traditional medicinal chemistry strategies can be utilised to broaden this landscape, validating structure-based drug design and *in silico* techniques for the development of allosteric small molecules against Aurora-A.

1.3.1 Activity-Directed Discovery of Allosteric Aurora-A Inhibitors

Aurora-A has been shown to have three shallow, undefined ligand binding sites that form the interaction surface for TPX2 binding, meaning the development of hit compounds to improve potency can be very challenging. It was proposed ADS could be employed to directly elaborate upon analogues of existing fragments targeting these pockets to discover novel allosteric inhibitors with structures unlikely to be exploited in a traditional medicinal chemistry

campaign at this stage. Microscale reaction arrays would be designed to exploit close analogues of known fragment-sized allosteric inhibitors with multiple sites of reactivity, in combination with rhodium(II)-carbene chemistry, to identify new ligands that target the allosteric binding pockets. The successful application of ADS for this purpose would demonstrate the method can be employed against challenging targets without large investments in chemical synthesis. This work is described in Chapter 2, and discusses the implementation of two ADS reaction arrays, the purification of one reaction array and biological screening of purified products, followed by a third reaction array to further develop potency.

1.3.2 Development of SAR of Allosteric Inhibitors of Aurora-A

SAR of existing fragment series targeting allosteric pockets of Aurora-A is relatively limited, and combined with the challenging nature of shallow, undefined binding sites means further development is potentially challenging. It was proposed that the SAR of the most encouraging fragment series would be expanded through the design and biological testing of a library of fragments targeting the Y-pocket of Aurora-A. An initial library would be designed, synthesised and assayed, with the SAR experimentally determined from this library to be combined with an ensemble docking study against various Aurora-A crystal structures. These combined results would then be used to guide further fragment elaboration, library design and synthesis, and biological screening. Successful application of this strategy would broaden the SAR of allosteric Y-pocket inhibitors and potentially provide potent probe compounds to further understand the dynamics of allosteric Aurora-A inhibition. This work is described in Chapter 3, and discusses the design, synthesis and biological screening of two fragment libraries and the ensemble docking study used to guide design of the second library.

2 Activity-Directed Fragment-based Discovery of Allosteric Aurora-A Inhibitors

In this Chapter the use of activity-directed fragment-based discovery as a method of fragment elaboration of known fragments capable of allosterically inhibiting the Aurora-A enzyme was investigated. The aim was to use these known fragments as the basis of direct fragment elaboration, to improve biological potency by directly growing the fragment. These fragments would be reacted in combination with diazo substrates in microscale parallel arrays, harnessing transition metal catalysis to form highly reactive metal-carbenoid species capable of various distinct transformations. The crude reaction products would then be screened to identify fragments that had been productively grown. Subsequent isolation and characterisation of only the most potent novel compounds would be carried out following iterative rounds of ADS. This method allowed for novel allosteric fragment-based discovery in the absence of structural guidance, through the inherent structural diversity and reactive promiscuity of the array.

Figure **2.1** shows hypothetical examples of fragment elaboration of known fragment inhibitors of Aurora-A, **2.1** and **2.2**, within the chemical context of established activity-directed synthesis chemistry. The fragments have multiple opportunities to react with metal carbenoids - ring-expansion from the isoxazole-based inhibitor to give the 2H-1,3-oxazine **P1** or the phenolic O-H insertion product **P2** shown in Figure **2.1-A** are both potential outcomes of the reaction described, resulting in structurally diverse elaborated fragments. Similarly, the C-H insertion product **P3** or O-H insertion product **P4** in Scheme **2.1-B** are possible outcomes with significantly different structure. Through similar transformations, the aim was to elaborate fragments and identify productive yet structurally diverse outcomes *via* biological screening, enabling fragment-based ligand discovery while precluding the need for structure-guided ligand design.
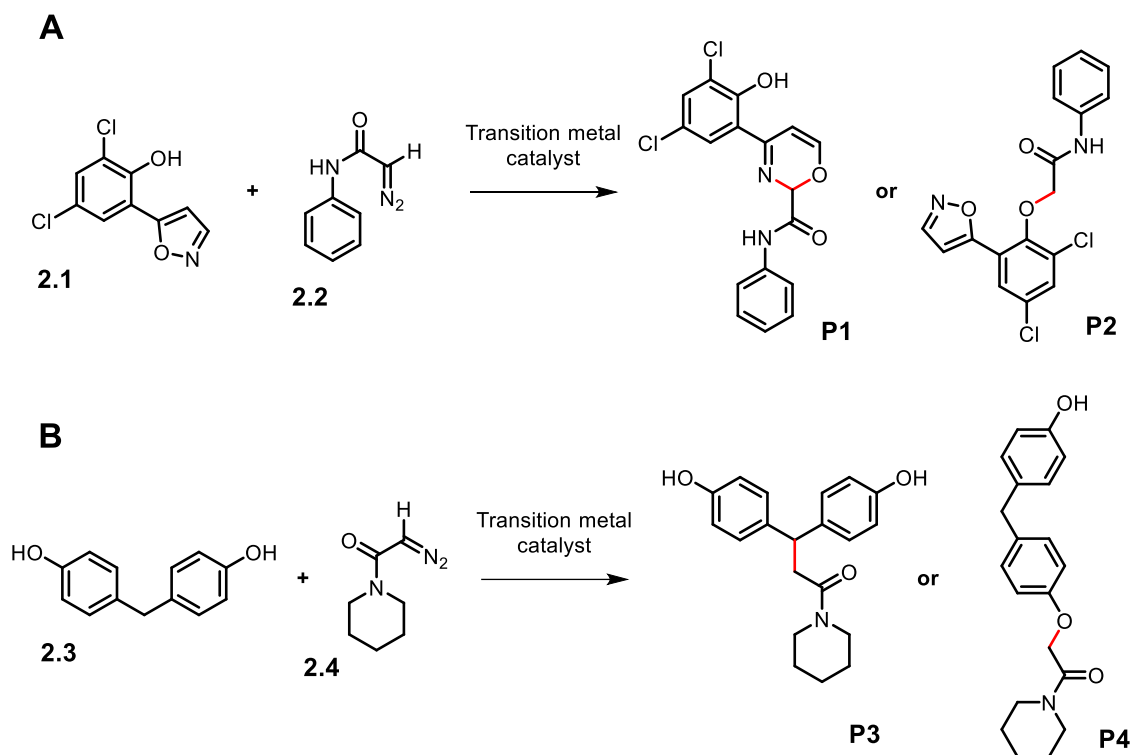
Figure **2.1**. Hypothetical reaction outcomes based on known allosteric inhibitors of Aurora-A. Reaction of fragments **2.1** and **2.3** with diazos **2.2** and **2.4** *via* metal carbenoid chemistry is expected to enable fragment growth to yield products such as **P1-4**. It was anticipated that biological evaluation of crude reaction mixtures would be employed to enable identification of any potential productively grown fragments.

2.1 Known Allosteric Fragment Inhibitors of Aurora-A

The selection of fragments for activity-direct elaboration was informed by known allosteric fragment inhibitors of Aurora-A. Specifically, those shown to both inhibit Aurora-A in isolation and to perturb the Aurora-A/TPX2 PPI. Prior work by Patrick McIntyre had identified six allosteric inhibitors of Aurora-A *via* a high-throughput crystallographic screen of 1255 fragments, followed by triage of the 59 structural hits to six promising fragments following orthogonal biophysical assays to determine binding affinity and perturbation of the Aurora-A/TPX2 PPI.[64] These six hits were then subject to a limited SAR study using commercially available compounds[129], resulting in the fragments shown in Fig. **2.2**. These six fragment hits were utilised as the basis of the work described in this Chapter. The absence of crystal structures of some of these fragment hits bound to Aurora-A positions ADS as a potentially useful strategy for the elaboration of these compounds in a structure-blind manner.
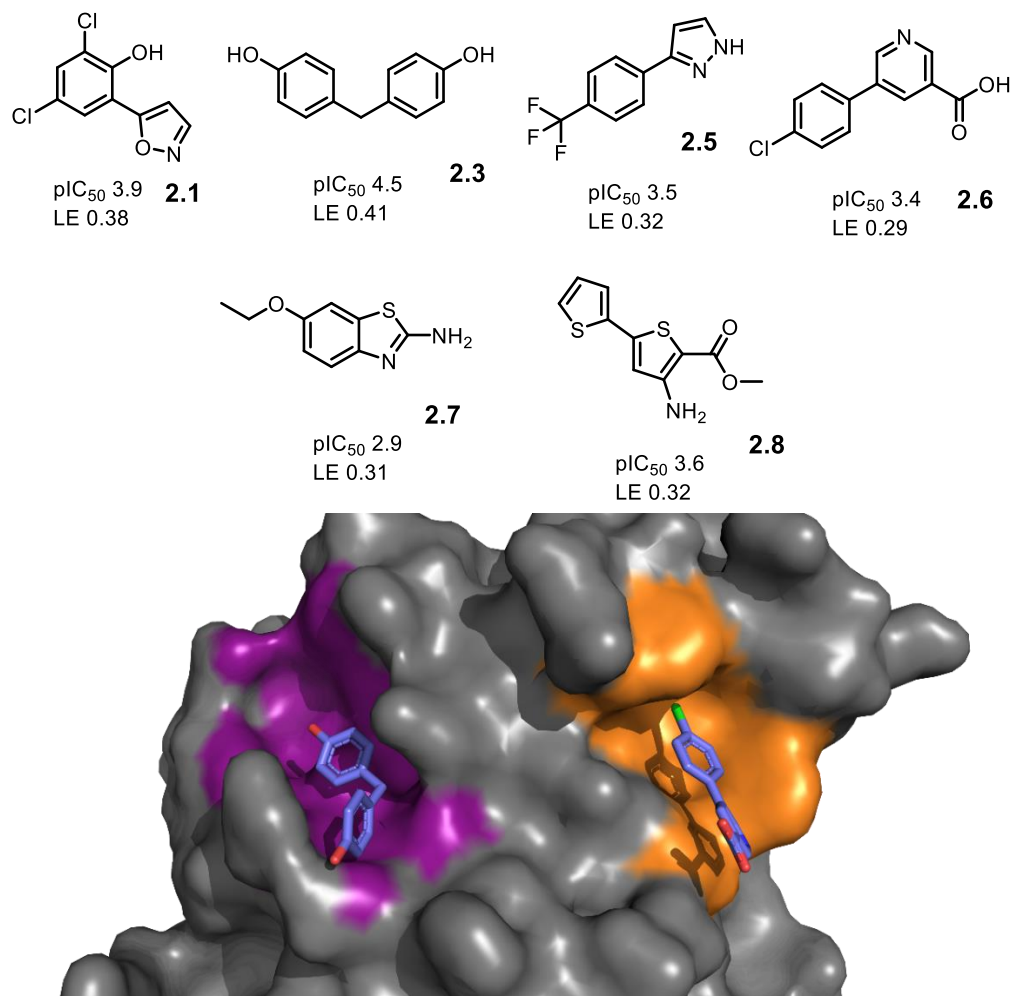
Figure **2.2**. Allosteric fragment hits that informed reaction array design. Panel **A**: Fragment structures, LE values, and pIC$_{50}$ values (determined *via* ADP-Quest biochemical assay)[129]. Panel **B**: An overlay of fragment **2.3** bound to the Y-pocket (purple) and fragment **2.6** bound to the F-pocket of Aurora-A[129]. Compounds bound to both pockets were shown to inhibit Aurora-A, as well as perturb the Aurora-A/TPX2 interaction.

2.2 Results and Discussion

2.2.1 Design of Reaction Array 1

Initially, a reaction array was designed that was informed by known allosteric fragment inhibitors of Aurora-A. Nine close analogues of the original fragment substrates (**F1-9**), eight diazo substrates (**D1-8**), and four catalysts (**C1-4**) were designed and selected. These components were combined exhaustively for a reaction array totalling 288 reactions. A combination of existing fragment hits and close analogues were designed and synthesised for

use as substrates within the reaction array. The fragment analogues were designed to be plausible substrates for the metal carbenoid chemistry utilised in the array, with multiple sites of reactivity to promote numerous possible reaction outcomes with the diazo substrates and result in novel bioactive compounds.

The design of the fragments and analogues selected for the array is summarised in Fig **2.3**. Panel **A** shows fragment **F2** (**2.5**) and close analogue **F1**, both of which were used in the reaction array, while Panel **B** shows how the design and selection of additional substrates was informed by other fragment hits. Fragments that inspired analogue design but were not used in the array are shown in orange, with the analogues in black chosen to take forward in the reaction array. Their design was intended to provide potential reactive sites with the metal carbenoids, highlighted in green, while maintaining structural similarity to avoid reducing potency. Notable examples include the trifluoromethyl-containing pyrazole species **F2**, where the analogue **F1** includes a methyl substituent instead. While **F1** lacks the electron-withdrawing effect of the trifluoromethyl group on the aromatic ring, it may retain the same structural characteristics and binding mode to the Y-pocket on Aurora-A in a similar manner to **F2** and offers the possibility of insertion into this methyl group. Similar principles were applied to the design of fragments **F6** and **F9**, with inclusion of a benzylic methyl group as a potential site for C-H insertion. Similarly, utilising -OH and -NH groups (fragments **F3**-**F9**) as potentially reactive handles, or inclusion of alternative functional groups such as the cyano group (fragment **F5**) incorporate multiple reactive sites while maintaining similarity to the fragment hits.
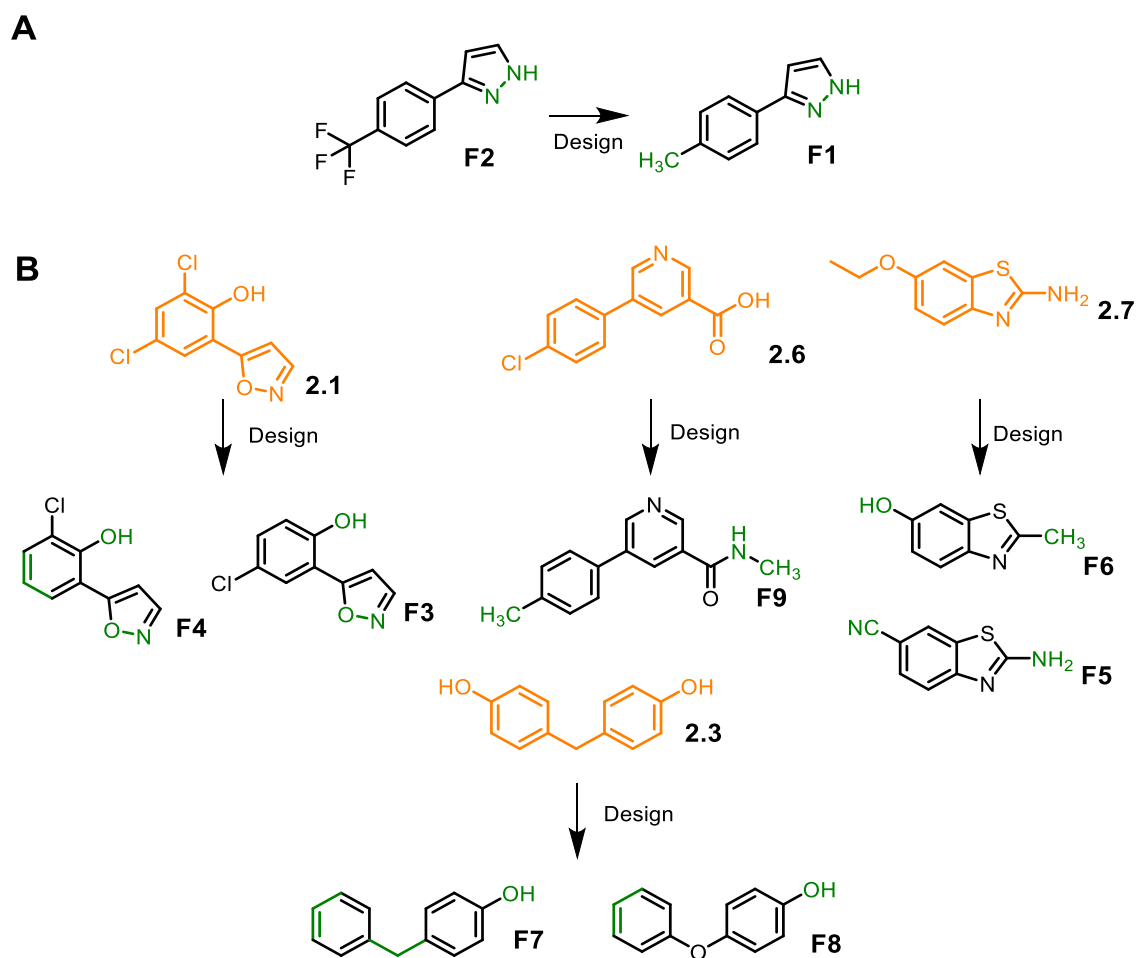
Figure **2.3**. Selection of substrates (black) based on fragment hits (orange) for the initial reaction array in which potentially reactive groups are highlighted (green). Panel **A**: Example of fragment (**F2**) that was exploited directly as a substrate and informed design of **F1**. Panel **B**: Fragment hits (orange) that informed the design of close analogues exploited in the initial reaction array but were not directly used in the array. Green indicates site of potential reactivity with metal carbenoid chemistry.

Next, eight α-diazo amide co-substrates with specific properties were selected from a library previously described within the group. These were chosen largely on the following chemical properties: a heavy atom count of 10-16 (excluding the diazo group) and cLogP of -2 to 1. Additional criteria were the structural diversity and synthetic tractability of the compounds. It was envisaged that these selected substrates would efficiently react with the functionalised fragment set while elaborating in a productive manner for activity against Aurora-A.

Prior work within the group by Adam Green also allowed for an informed choice of catalyst. The properties of numerous dirhodium catalysts were plotted for comparison and allowed visual selection of three dirhodium(II)catalysts based on diversity in structure, electronics, and reactivity, as well as catalytic competency for the desired reactions. As the

ligand has a critical effect on reaction outcome, the three dirhodium(II) catalysts covered a variety of ligand structure and electronics: **C1** [Rh$_2$(cap)$_4$] contains carboxamide ligands, **C2** [Rh$_2$(pfb)$_4$] contains electron-poor carboxylate ligands, while **C3** [Rh$_2$((*S*)-DOSP)$_4$] includes chiral carboxylate ligands. Additionally, a gold(I) catalyst, **C4**, was included as it offered complementary reactivity to that of the dirhodium catalysts, while still amenable to the reaction array conditions. The initial reaction array was performed exhaustively totalling 288 reactions and the final design is shown in Fig **2.4**. This enabled a high degree of diversity in reactants and catalysts for the first round, from which reactions giving rise to bioactive products can be selected to guide the design of subsequent reaction arrays.

Fragments

Diazo Substrates

Catalysts

C1 [Rh$_2$(cap)$_4$]
C2 [Rh$_2$(pfb)$_4$]
C3 [Rh$_2$((*S*)-DOSP)$_4$]
C4 (2,4-di^{t}BuPhO)$_3$PAuCl.SbF$_3$
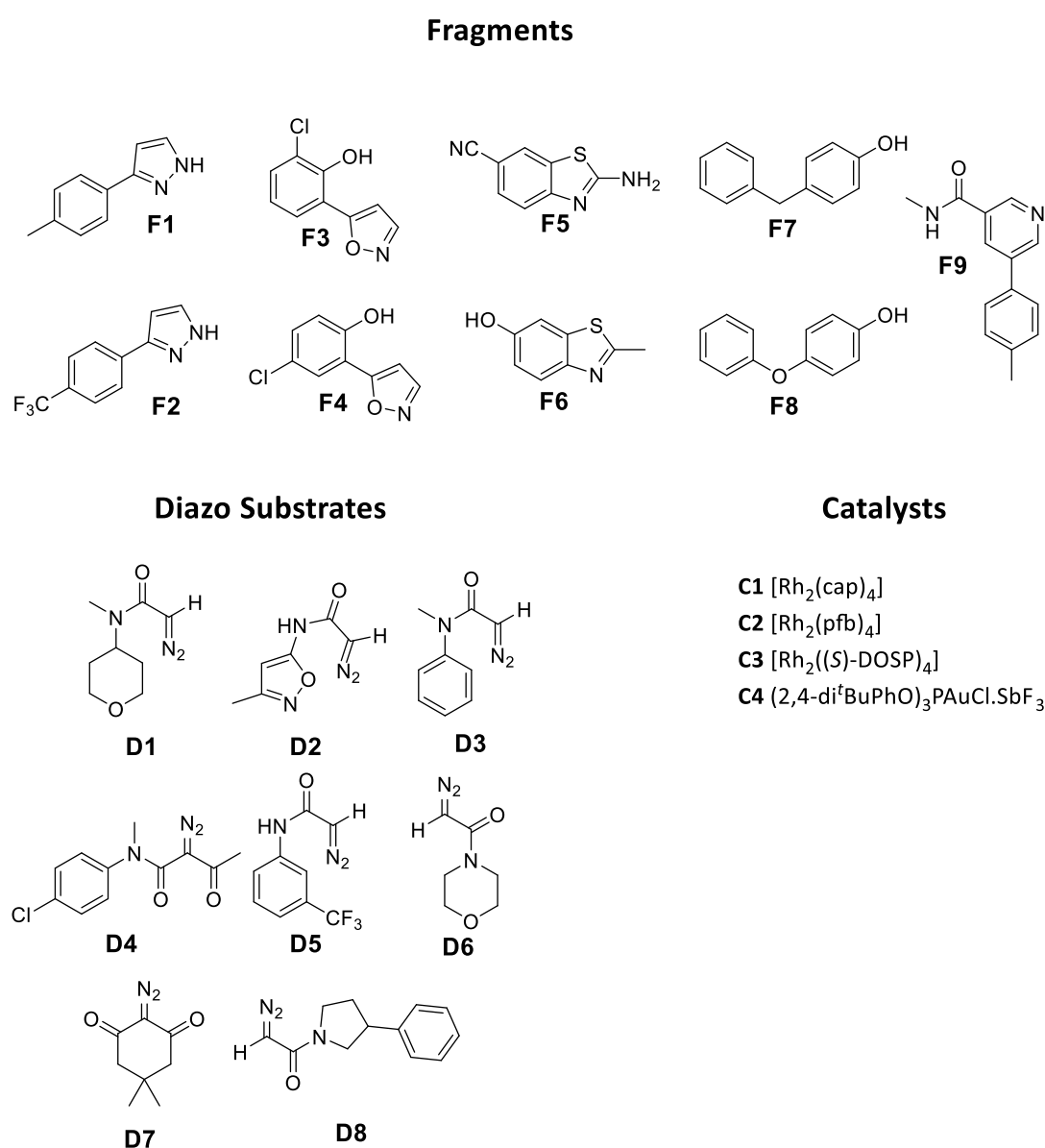
Figure **2.4**. Design of Reaction Array 1. Top panel shows selected fragments, bottom left shows selected diazo substrates, and bottom right describes selected catalysts. All possible combinations of reactants were explored *via* 288 total reactions.

Overall, careful selection and design of fragments and analogues, diazo substrates, and catalysts enabled a structurally diverse reaction array to be performed with a similarly diverse panel of catalyst reactivity. It was envisioned the reaction array would produce a diverse and novel set of elaborated fragments potentially capable of improved inhibition of Aurora-A, the most potent of which would then be identified through biological screening of the crude reaction mixtures for further iterative round/s of activity-directed fragment discovery.

2.2.2 Substrate Synthesis for the Initial Reaction Array

2.2.2.1 Fragment Synthesis
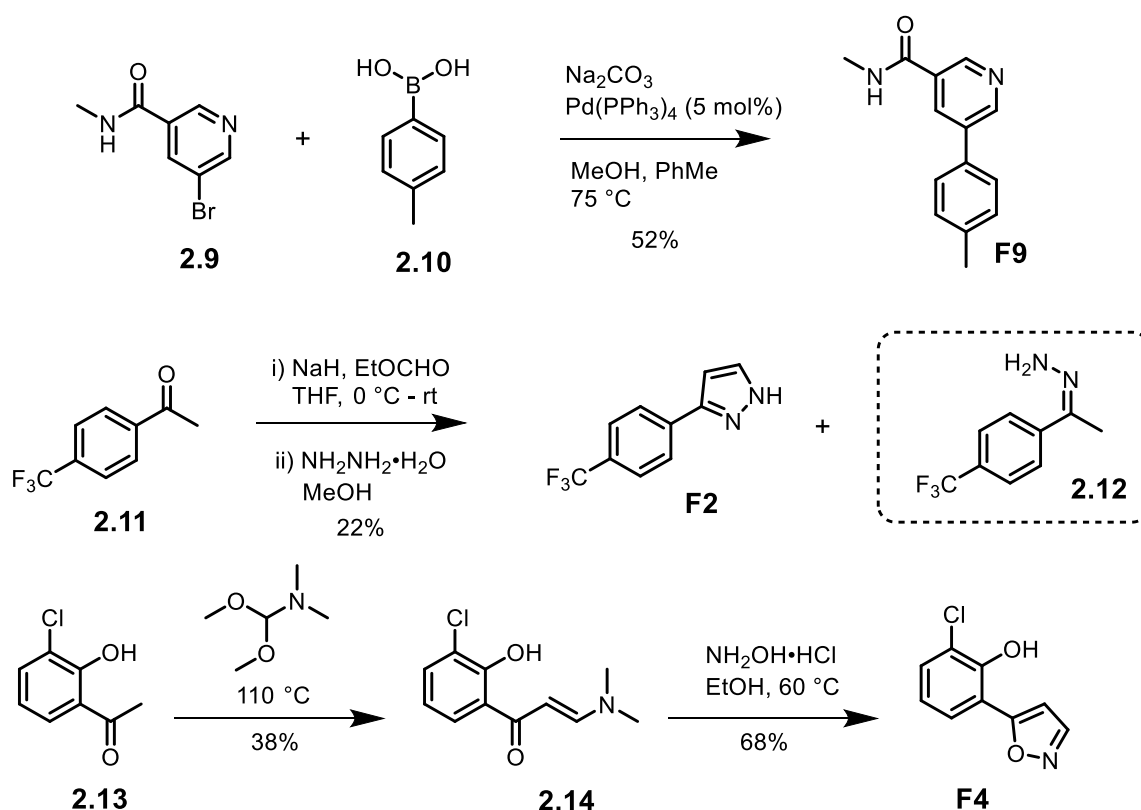
Scheme **2.1** Synthesis of substrates for the initial reaction array.

The synthesis of the three substrates *N*-methyl-5-(4-methylphenyl)pyridine-3-carboxamide **F9**, 3-(4-(trifluoromethyl)phenyl)-1*H*-pyrazole **F2**, and 2-chloro-6-(1,2-oxazol-5-yl)phenol **F4** is described in Scheme **2.1**. Synthesis of **F9** was achieved using adapted Suzuki coupling conditions as outlined in Scheme **2.1-A**. 5 mol% Pd(PPh₃)₄ was added to a solution of

5-bromo-*N*-methylnicotinamide, **2.9**, *p*-tolylboronic acid, **2.10**, and Na$_2$CO$_3$ in 15 ml toluene:MeOH (4:1) and stirred for 2 h to yield fragment **F9** in a 52% yield following purification. Synthesis of fragment **F2** proceeded from the commercially available 4'-(trifluoromethyl)acetophenone **2.11** treated with NaH and ethyl formate in THF; the resulting keto-aldehyde intermediate was immediately treated with hydrazine monohydrate in MeOH to yield the pyrazole **F2** in 22% yield following purification. While care was taken to ensure the majority of the acetophenone was converted into the corresponding keto-aldehyde intermediate prior to hydrazine addition, the mass of the hydrazone **2.12** was observed *via* LC-MS suggesting that some starting material remained when the hydrazine was added. Compound **F4** was synthesised from **t**he commercially available 1-(3-chloro-2-hydroxyphenyl)ethanone **2.13** undergoing reflux in the presence of *N*,*N*-dimethylformamide dimethyl acetal (DMFDA) to yield the enaminone compound **2.14**, in 38% yield following purification by crystallisation. The enaminone **2.14** was then subjected to heating in the presence of hydroxylamine hydrochloride in EtOH to yield fragment **F4** in 68% isolated yield. This reaction yielded only the 1,2-oxazol-5-yl phenol regioisomer, determined by 2D HMBC and HSQC NMR experiments observing coupling between 4-H and 5-C, in line with literature precedent. In retrospect, this chemistry may also have been suitable for the synthesis of fragment **F2** and would avoid the formation of the undesirable side product **2.12**.

The remaining fragments **F1**, **F3**, **F5**, **F6**, **F7**, and **F8** were commercially available, and with the entire fragment series in-hand they were subject to determination of biological activity against Aurora-A as a guide for the eventual reaction array screening concentrations.

2.2.2.1.1   Determination of Fragment Biological Activity against Aurora-A

Prior to the execution and screening of the reaction array, the fragments to be utilised were assessed for their biological activity against Aurora-A. This allowed for not only determination of IC$_{50}$ values of the novel fragment analogues to contribute to the SAR landscape of allosteric Aurora-A inhibitors, but also provided a baseline biological activity against which the reaction mixtures from the array were compared. From the IC$_{50}$ values an appropriate concentration of fragment to be utilised in the reaction array was also able to be determined, allowing identification of any significant increase in biological activity while reducing background activity from residual fragment in the reaction mixture.

The Aurora-A^{CM} complex was selected as the working enzyme for the array due to the increased stability compared to wt-Aurora-A under assay conditions. However, all fragments and analogues for the reaction array were evaluated against both wt-Aurora-A and Aurora-A^{CM}, the results shown in Fig. **2.5**. This evaluation was performed using the Caliper mobility-shift assay, as discussed in Experimental Section **4.4.1.1**, in kinetic mode, monitoring time-dependent phosphorylation of a fluorescent peptide substrate by Aurora-A (both wt-Aurora-A and Aurora-A^{CM} individually) in the presence of varying concentrations of inhibitor (3 mM – 152 nM) by performing a 10-point, 3-fold serial dilution of each inhibitor.
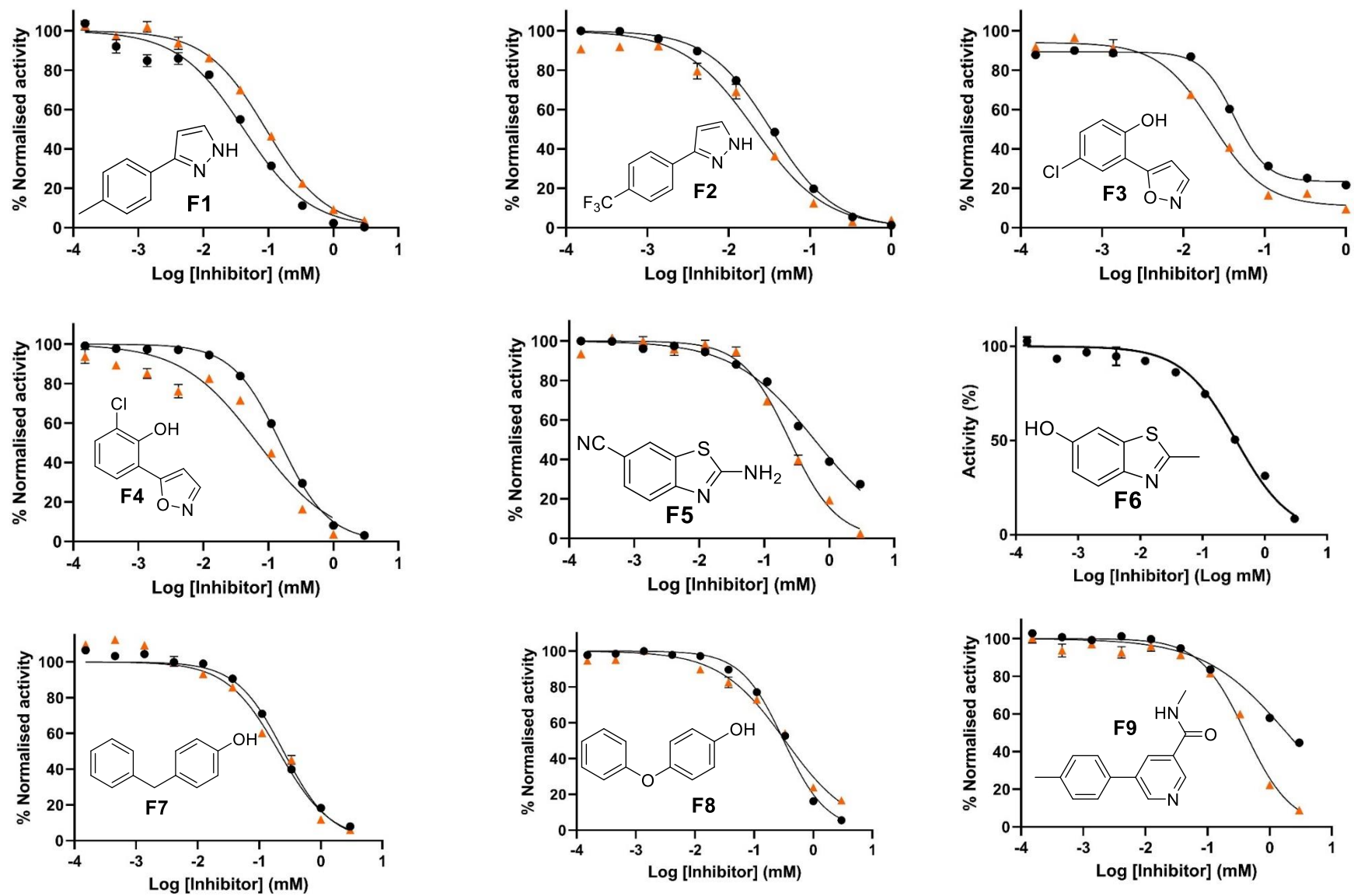
Figure **2.5**. IC$_{50}$ curves of reaction array fragments against wt-Aurora-A (orange) and Aurora-A^{CM} (black). Data obtained with the Caliper mobility-shift assay, with 12.5 nM wt-Aurora-A or 25 nM Aurora-A^{CM} with 2.5% final DMSO conc.

Points represent a 3-fold, 10-point serial dilution fragment titration from 3 mM to 152 nM, except fragments **3** and **8** due to insolubility at 3 mM. Error bars shown where larger than icons.

The results from the fragment IC_{50} determination are shown below in Fig. **2.6-A**. Interestingly, all fragments except **F1** appear to inhibit the wt-Aurora-A complex more strongly than Aurora-A^{CM}. While in some instances this increase in potency is marginal, fragments **F3**, **F4**, **F5**, and **F9** show significant increases in potency against the wt-Aurora-A, from roughly 2-fold for **F3**, **F4**, and **F5**, to around 4.5-fold more potent in the case of fragment **F9**.

Fragment	IC_{50} (µM)		$LE^{\dagger}$	Likely Binding Pocket
	wt-Aurora-A	Aurora-A^{CM}		
F1	90 ± 10	40 ± 10	0.51	Y*
F2/2.5	20 ± 6	33 ± 3	0.42	Y*
F3	20 ± 6	42 ± 11	0.47	Y*
F4	70 ± 20	153 ± 2	0.41	Y
F5	250 ± 50	600 ± 90	0.38	Y
F6	N/A	320 ± 50	0.44	Y
F7	200 ± 70	250 ± 30	0.36	Y
F8	320 ± 40	330 ± 80	0.35	Y
F9	400 ± 60	2000 ± 500	0.22	F
2.1	N/A	113‡	0.39	Y‡
2.3	N/A	34‡	0.42	Y‡
2.6	N/A	473‡	0.33	F‡
2.7	N/A	1021‡	0.32	Y‡
2.8	N/A	245‡	0.34	Y‡
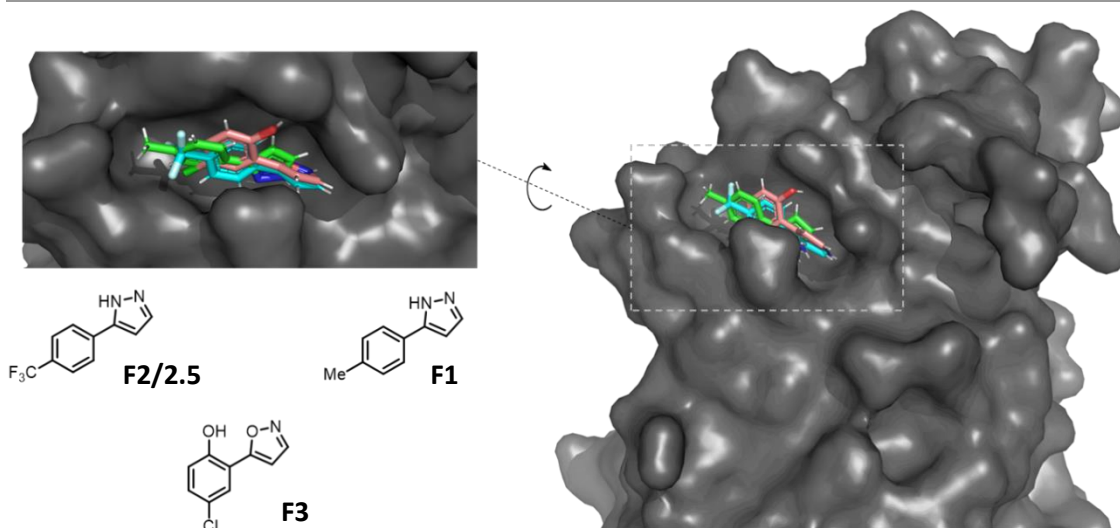
Figure **2.6**. IC_{50} values of fragments against Aurora-A. Likely binding pocket indicates the pocket of Aurora-A in which the fragments are speculated to bind, based on initial fragment hits binding to indicated pocket. * denotes direct structural evidence of binding mode for compounds **3, 7**, and **8**. † denotes LE values calculated based on Aurora-A^{CM} IC_{50} values. ‡ denotes IC_{50} value and crystal structures from [129].

Crystal structures of fragments **F1**, **F2**, and **F3** were able to be obtained by Mohd Syed Ahanger in the Bayliss group, and can be seen in Fig. **2.6-B**. All three fragments were shown to bind to the Y-pocket in a similar manner, with the 5-membered heterocycles in the same

orientation and occupying a hydrophobic region of the pocket and the methyl and CF_3 groups of **F1** and **F2** extending upwards toward the solvent exposed region at the top of the pocket. While ADS is intended as a structure-blind method of fragment elaboration, these structures may prove useful for ongoing work and for determining the structure of any productively elaborated fragments.

While interesting as stand-alone data in expanding the SAR of allosteric inhibitors, these IC_{50} values were used in the screening of the reaction array to guide the concentration at which the crude reaction mixtures would be assayed. Screening fragments **F1**-**F3** at 10 µM, 3- to 4-fold lower than the IC_{50} against Aurora-A^{CM}, was considered to provide suitable dynamic range in the assay conditions to allow identification of significant increases in potency from elaborated fragments while reducing residual fragment activity observed. Similarly, screening the remaining fragments at 100 µM, 1.5-10-fold lower than their associated IC_{50} values, was thought to do the same while applying increased selection pressure on the less potent fragments.

These IC_{50} results against Aurora-A^{CM}, therefore, guided the decision-making process in selecting a sensible screening concentration for the reaction array and controls, ensuring any interesting screening results were due to novel bioactive compounds rather than residual, un-reacted fragment activity. Simultaneously, a limited SAR landscape was obtained through analogue screening, as well as elucidating the mode of binding from crystal structures.

2.2.2.2 α-Diazo Amide Synthesis

The synthesis of diazo substrates **D1**, **D2**, and **D3** was performed *via* the same general synthetic route shown in Scheme **2.1**, under previously published conditions[130,131]. A stock of the hydrazone intermediate **2.15** was readily available in the group, prepared by Shiao Chow and Abbie Leggott. This hydrazone was heated in the presence of thionyl chloride in toluene to generate the corresponding acid chloride, which was then reacted with the appropriate amine; finally, decomposition of the resulting tosyl-hydrazone by treatment with triethylamine yielded the α-diazo amide products **D1**, **D3** and **D6** following purification. The remaining diazo substrates were prepared by Luke Trask and Adam Green from the Nelson group.
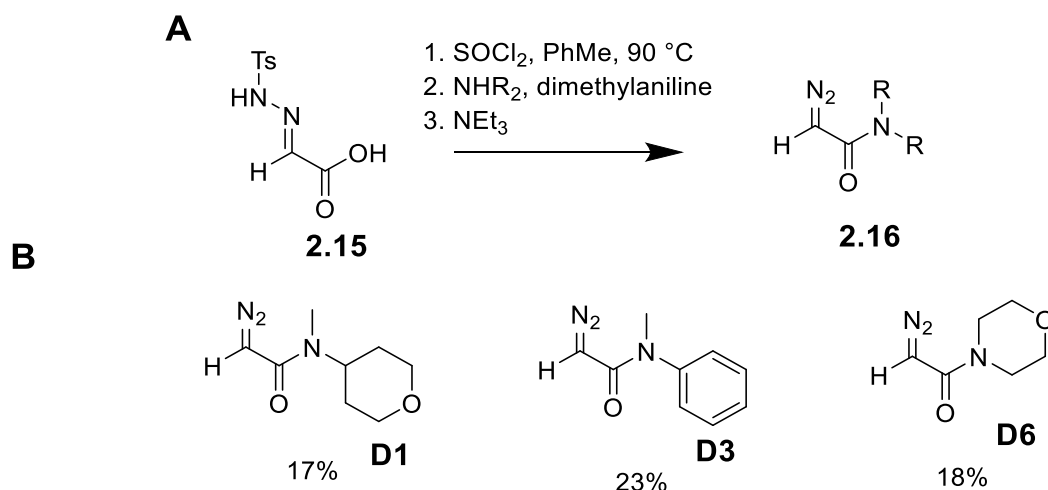
Scheme **2.1**. Synthesis of diazo substrates **D1**, **D3**, and **D6**. Panel **A)** General scheme and reaction conditions. Panel **B)** Structure and isolated yields of diazo substrates **D1**, **D3**, and **D6**.

2.2.3 Execution of the Initial Reaction Array

With the fragments and α-diazo amide co-substrates prepared, the parallel reaction array was performed in which all possible combinations of nine fragment substrates (**F1-9**), eight co-substrates (**D1-8**), and four catalysts (**C1-4**) in one solvent (DCM), totalling 288 reactions as seen in Fig **2.4**. Simultaneously, a separate control mock reaction array was performed following a closely related protocol by omitting the fragment substrate from the reaction mixtures, as a control to determine whether the diazo substrates reacted intramolecularly to yield bioactive products. All reactions were performed in blocks of 96 borosilicate glass vials in a final volume of 50 μL, (final concentrations: fragments 100 mM; diazo substrates 110 mM; catalyst 1 mM). Fragment substrates (25 μL of 200 mM stock solution in DCM, where applicable) and diazo substrates (25 μL of 220 mM stock solution in DCM) were added to the glass vials, and the solvent allowed to evaporate while open to atmosphere. Finally, 50 μL of 1 mM of appropriate catalyst in DCM was added to the vial and sealed. This method allowed for ease of handling with sensible volumes of solvent by multi-channel pipette, meant the reactions commenced at a similar time, and ensured solubility of reaction components. Reaction blocks with the glass vials were shaken 24 h into the reaction and following 48 h total reaction time *ca.* 30 mg QuadraPure TU thiourea resin was added to all crude reaction mixtures and controls, re-sealed, and allowed to sit for 24 h to remove metal catalysts. The resin was then filtered off, residual DCM allowed to evaporate followed by 24 h under vacuum to ensure all DCM was removed, and the reaction

mixtures and controls were re-dissolved in 50 µL DMSO to a final concentration of 100 mM relative to the fragment, in preparation for biological screening against Aurora-A.

2.2.3.1   Biological Screening of Control Array

The control array of mock reactions and pure starting materials was screened prior to the full reaction array. The fragments in isolation were screened at two different concentrations guided by prior IC_{50} determination: i) the more potent fragments **F1**-**F3** were screened at 10 µM, ii) less potent fragments **F4**-**F9** at 100 µM, to ensure the biological activity of any unreacted fragment would not be seen in the full array screening results. Catalysts were screened separately at 1 µM, the maximum they could be found in any crude reaction mixture if scavenging was ineffective. Having shown individual components were inactive against Aurora-A the exhaustive control array of mock reactions consisting of each catalyst with each diazo substrate having undergone the ADS workflow was screened at a total product concentration of 110 µM (1 µM catalyst), representative of the highest concentration any potential intramolecular product could be found in the reaction mixtures. This was to ensure any activity observed in the reaction array screen would not be from individual reaction components or intramolecular reactions of the diazo substrates forming a bioactive compound.

Figure **2.7**. – Control Array Screening Results. Screened against Aurora-A^{CM} (25 nM) using Ez-Reader mobility-shift assay. Screening concentration labelled underneath components in isolation, at maximum total product concentration each component would be found in reaction array. Fragments and catalysts (first, second and third groups from the left) screened in isolation. Mock reactions of each catalyst with each diazo substrate following reaction array workflow screened as intramolecular control at total product concentration of 110 µM diazo and 1 µM catalyst. Data normalised to controls: Red) 0% activity (no protein), Black square) 100% activity (no inhibitor).

The results shown in Fig. **2.7** show clearly that none of the fragments or catalysts screened in isolation inhibit Aurora-A kinase activity. Similarly, the diazo substrates having undergone the reaction array workflow in combination with the catalysts show no significant biological activity. Therefore, the reaction array was performed, confident that any biological activity identified from the evaluation of the complete reaction array would be from the formation of a novel bioactive compound rather than the individual fragments, catalysts, or a potential intramolecular reaction product of a diazo substrate.

2.2.3.2   Biological Screening of Initial Reaction Array

The crude reaction mixtures were subject to determination of biological activity against Aurora-A activity, the results of which are shown in Fig. **2.8**. The crude reaction mixtures were assayed at a total product concentration of either 10 µM for fragments **F1**-**F3** or 100 µM for fragments **F4**-**F9**. These screening concentrations allow both identification and selection of reaction mixtures with a potentially significant increase in biological activity over the parent fragment, as well as a more straightforward workflow when performing the biological assay.

Interestingly, three reaction mixtures resulted in clear inhibition of Aurora-A, summarised in Table **2**. In the preliminary screen, these crude reaction mixtures inhibited Aurora-A^{CM} by approximately 30-35% and above 2 s.d from the mean, therefore were identified as potential hit reaction mixtures. Validation of these hits is described in Section **2.2.3.3**. Similarly, a crude reaction mixture of fragment **F5** with co-substrate **D3** and the gold(I) catalyst showed 15% activation of Aurora-A relative to the control and was also considered a hit worth further investigation.
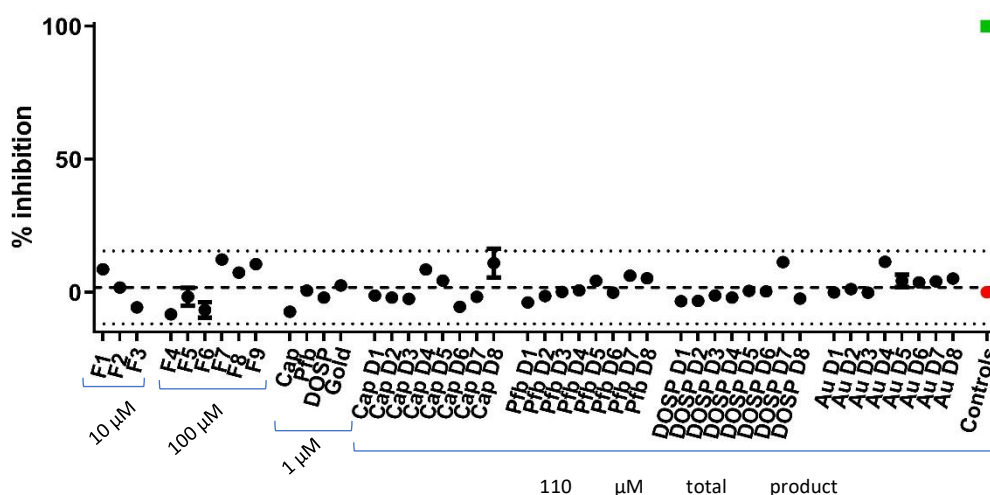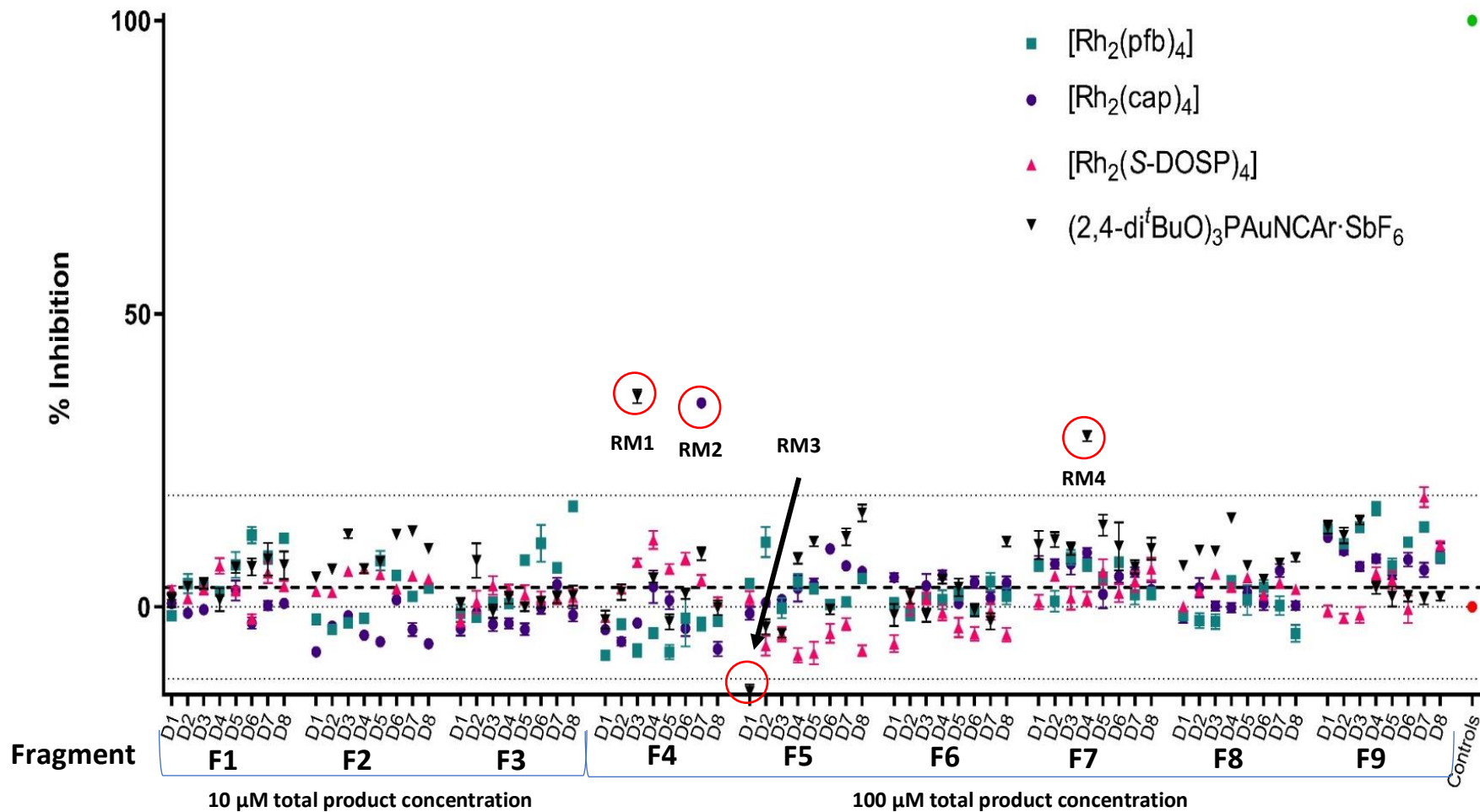
Figure **2.8**. Reaction Array 1 Screening Results. Screened against Aurora-A^{CM} (25 nM) using the Caliper mobility-shift assay. Final screening concentration is relative to fragment starting material, and labelled underneath fragment number. Icon shape and colour indicate catalyst; green circles = [Rh$_2$(cap)$_4$] (**C1**), purple squares = [Rh$_2$(pfb)$_4$] (**C2**), blue triangles = [Rh$_2$(S-DOSP)$_4$] (**C3**), orange inverted triangles = (2,4-di^{t}BuPhO)$_3$PAuCNAr·SbF$_6$ (**C4**). Thick dashed line represents mean of all data points, upper and lower dotted lines indicate 2 s.d from mean, central dotted line indicates 0 % enzyme inhibition. Data normalised to controls; upper green circle = 100% inhibition (no protein), lower red circle = 0% inhibition (no inhibitor). Hit reactions (more than 2 s.d. from mean of data set) highlighted with red circles and labelled **RM1-4**.

Figure **2.9** Hit reaction mixtures from reaction array 1. Structures are shown in panel **A**, tabulated inhibition data shown in panel **B**. Validation by scale-up chemistry and repeat of biological screening of crude reaction mixture, described in section **2.2.3.3**.

Four hit reaction mixtures were identified from the reaction array with biological activity significantly above or below (activation) that of the remainder of the reactions, shown in Fig. **2.9**. Additionally, the lack of observable or significant biological activity from the control array provided confidence that these hit reaction mixtures were not due to residual activity from individual reaction components. Therefore, these reaction conditions based on three different fragments (**F4**, **F5**, and **F7**) in combination with four diazo substrates and catalysed by either **C1** [Rh$_2$(cap)$_4$] or **C4** (2,4di^{t}BuO)$_3$PAuNCAr·SbF$_6$ were selected for further chemical and biological validation prior to the design of a subsequent reaction array.

2.2.3.3 Validation of Reaction Array 1 Hits

The hit reactions **RM1-4** were subject to further validation prior to designing the second reaction array. These reactions were repeated in an identical fashion to the initial reaction array outlined in section **2.2.3**, both with and without scavenging resin, as well as on a 50-fold larger scale-up format from the same stock solutions. These experiments were design with multiple outcomes in mind; i) the repeat reactions would form the same bioactive products identified in the first reaction array screen, therefore validating the chemistry, and ii) these bioactive compounds would inhibit Aurora-A^{CM} to a similar degree when assayed, validating the initial screening results.
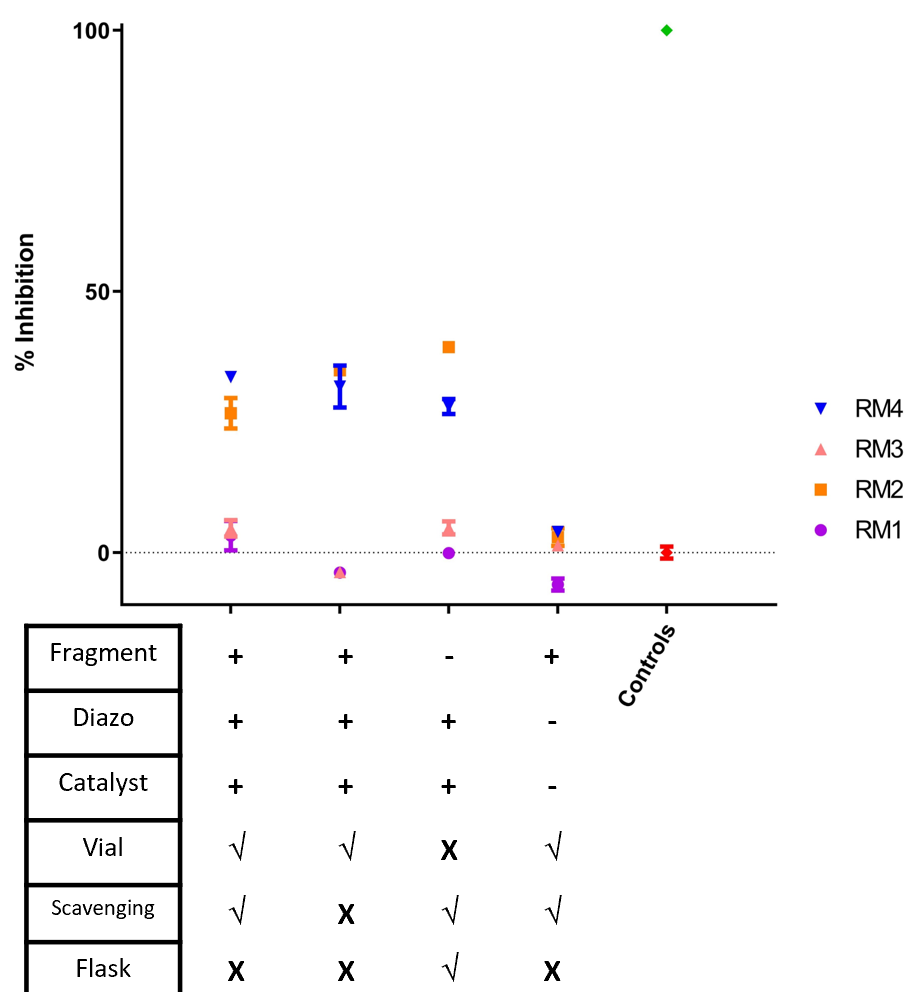
Figure **2.10**. Validation reaction screening results. Screened against Aurora-A^{CM} (25 nM) using the Caliper mobility-shift assay. Final screening concentrations of all components was 100 μM relative to associated fragment. Icon shape and colour indicate reaction mixture or diazo control/associated fragment; purple circles = **RM1**, orange squares = **RM2**, pink triangles = **RM3**, blue inverted triangles = **RM4**. Data normalised to Controls; green square = 100% inhibition (no protein), red circle = 0% inhibition (no inhibitor).

The selected fragments (**F4**, **F5**, and **F7**), diazos (**D3**, **D4**, **D6** and **D7**) and catalysts (**C1** and **C4**) were subject to identical conditions as the initial reaction array described in section **2.2.3**. Intramolecular diazo control reactions were also run, analogous to that found in the control array described in section **2.2.3.1**, by simply forgoing addition of the fragment stock solution during preparation of the appropriate reaction vials. Additionally, these stock solutions were used in parallel to repeat **RM1-4** at a 50-fold larger scale in round-bottom flasks with stirring. Following the completion of the ADS workflow, each reaction mixture was dissolved in DMSO to result in a concentration 100 mM relative to the fragment starting material ready for biological screening.

These crude reaction mixtures were then assayed, the results of which are shown in Fig. **2.10**. In line with the corresponding high-throughput screens, all crude reactions were screened at 100 µM total product concentration alongside fragments in isolation to ensure no residual activity. Pleasingly, **RM2** and **RM4**, showed levels of Aurora-A inhibition across all reaction conditions comparable to that of the initial screen in both the array-scale and 50-fold scale-up reaction mixtures, validating the initial hit reactions and suggesting the same bioactive compounds had been formed. Similarly, the repeated diazo intramolecular reaction controls and fragments in isolation showed no biological activity at 100 µM. **RM1** and **RM3**, however, showed no inhibition or activation of Aurora-A^{CM} contrary to the initial screening results, indicating the preliminary results were likely statistical outliers rather than reaction mixtures with productive outcomes.

Both crude reaction mixtures **RM2** and **RM4** had validated successfully in the biological assay upon repeating the array-scale reaction and performing a 50-fold scale-up. This success suggested the reaction outcome was a productively grown fragment with improved biological activity in sufficient yield to induce an observable biological response upon Aurora-A^{CM}. As **RM1** and **RM3** did not display this repeated biological activity, they were discarded as potential reaction conditions for ongoing development. Therefore, only **RM2** and **RM4**, shown in Fig. **2.9**, were chosen to form the design basis of the subsequent reaction array.

2.2.4   Reaction Array 2 Design

Reaction array 2 was designed around the bioactive results from the first array and in total consisted of 216 reactions, the design of which is shown in Fig. **2.11**, and appropriate controls of fragments in isolation and a full mock reaction array format similar to Control Reaction Array 1, see appendix. The fragments **F10**-**F13** were related to **F3** and **F7** were designed to probe the SAR of these compounds in a limited fashion while increasing structural diversity and providing additional sites of reactivity. Similarly, the diazo-containing substrates utilised were structurally similar to **D4** and **D7**. The combination of these changes was intended to optimise the bioactive compounds produced in the search for novel scaffolds and increase biological potency. Additionally, it was envisaged judicious catalyst selection may optimise the reaction conditions thereby increasing yield of the biologically active product. Rhodium catalyst choice was based on Adam Green's work(ref), selecting **C5** Rh_2pyr_4 for similar yet distinct ligand structure and reactivity. iPrAuCl **C6** was exploited as a complementary catalyst to **C4**, displaying orthogonal reactivity while still competent for relevant transformations.
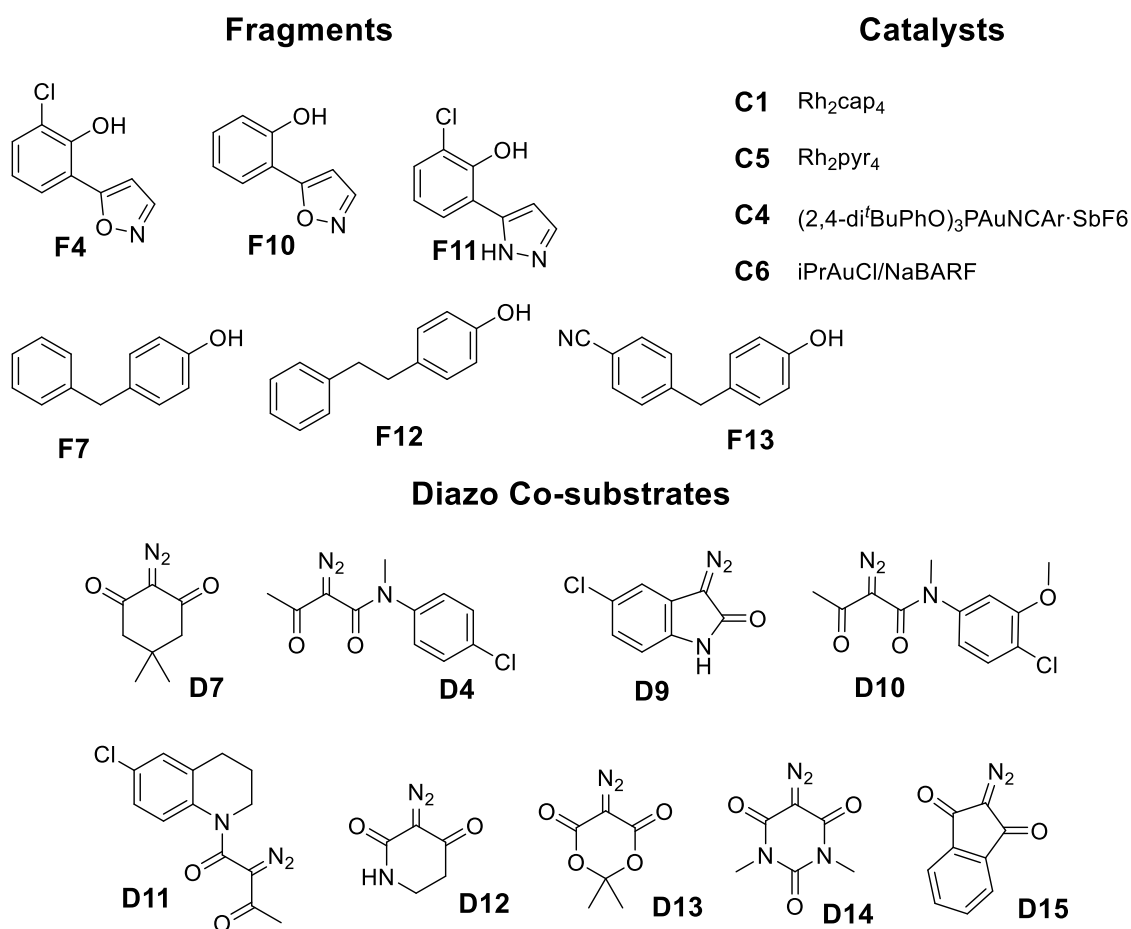
Figure **2.11**. Design of second reaction array.

2.2.4.1 Substrate Synthesis for Reaction Array 2

Fragments **F4** and **F7** were available from the previous reaction array and with fragment **F10** commercially available, fragments **F11**, **F12**, and **F13** required synthesis. The synthesis of 4-[(4-Hydroxyphenyl)methyl]benzonitrile **F13** is shown in Scheme **2.2**-**A**, where commercially available benzyl chloride **2.17** and boronic acid **2.18** were subject to Suzuki coupling conditions and stirred at 90 °C for 2 h to yield intermediate 4-(4-methoxyphenylmethyl)benzonitrile **2.19** in good yield following purification. This was followed by a boron tribromide mediated de-methylation in DCM and stirred for 6 h, which proceeded with excellent yield to result in fragment **F13** following purification.

Scheme **2.2**. Synthesis of Fragments for Reaction Array 2.
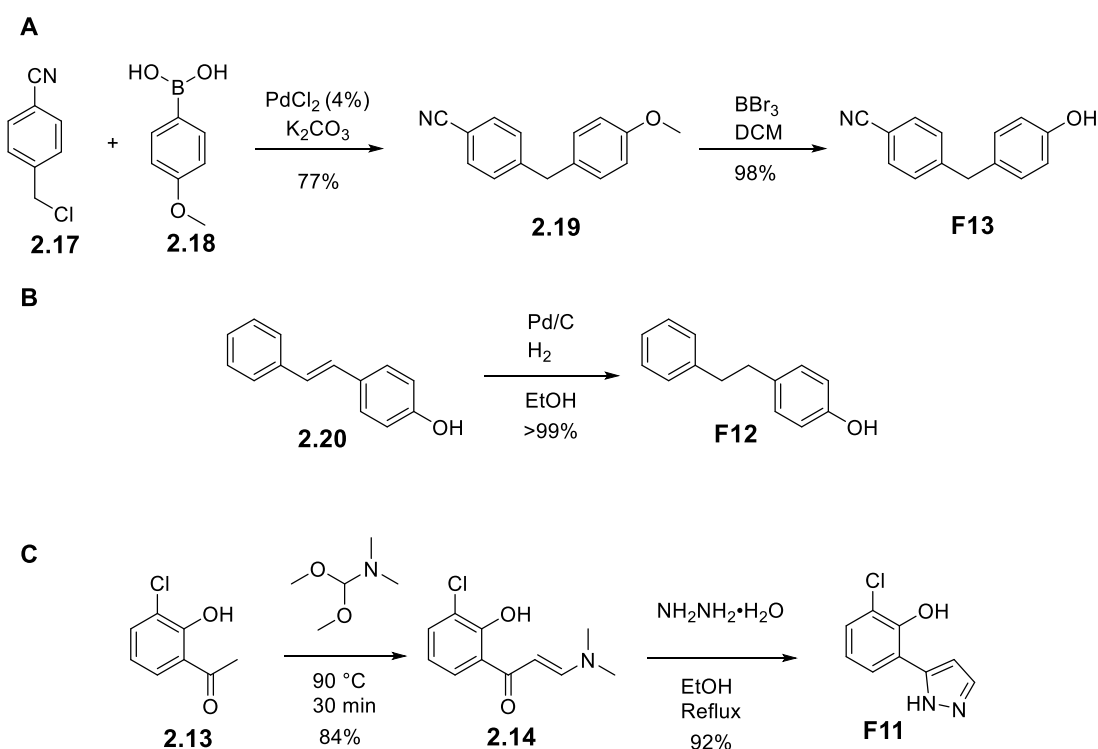
The commercially available *trans*-4-hydroxystilbene **2.20** underwent a facile Pd/C catalysed reduction, stirred for 24 h shown in Scheme **2.2**-**B** and filtered through a celite plug to yield 4-(2-phenylethyl)phenol **F12** in quantitative yield. Synthesis of fragment **F1** proceeded with 1-(3-chloro-2-hydroxyphenyl)ethanone **2.13** subjected to reflux in neat DMFDA to yield (*E*)-1-(3-chloro-2-hydroxyphenyl)-3-(dimethylamino)prop-2-en-1-one **2.14** which, following purification, was stirred and refluxed with hydrazine monohydrate in EtOH for 3 h to yield 2-

chloro-6-(1*H*-pyrazol-5-yl)phenol **F11** in excellent yield following column chromatography. During this synthesis it was noted the formation of the enaminone was accompanied with a distinct colour change from off-white to a deep green within 30 min. Halting the reaction at this stage significantly increased the isolated yield, likely due to the speed of formation of the enaminone and reducing any potential undesired side-product formed.

With most α-diazo amides utilised in the second reaction array previously prepared within the group or commercially available, only *N*-(4-chlorophenyl)-2-diazo-*N*-methyl-3-oxobutanamide **D4** required preparation for the array, described in Experimental Section **4.2.2**.

2.2.5 Execution of Reaction Array 2

With the fragments and α-diazo amide co-substrates prepared and in hand, the second reaction array was performed in an exhaustive manner as previously described in section **2.2.3** and appendix. All possible combinations of the six fragments (**F4**, **F7**, **F10**-**F13**), nine diazo co-substrates (**D4**, **D7**, **D9**-**D15**), and four catalysts (**C1**, **C4**, **C5**, **C6**) totalled 216 reactions, with controls performed simultaneously under the same conditions. As detailed for Reaction Array 1 in Section **2.2.3**, a control array of isolated fragments and mock reactions was performed alongside Reaction Array 2. The control array showed no significant biological activity and ensured any hit reactions from Reaction Array 2 were likely the result of a biologically active intermolecular product.

2.2.5.1 Biological Screening of Reaction Array 2

Following the biological screening of isolated fragments and mock reaction control array, the full reaction array was assayed against Aurora-A, results shown in Fig. **2.12**. Crude reaction mixtures with fragments **F4**, **F10**, and **F11** were screened at 1 µM total product concentration and fragments **F7**, **F12**, and **F13** at 100 µM total product concentration.

Fragments **F4**, **F10**, and **F11** were screened at 10-fold lower total product concentration in this array compared to the previous, to apply selection pressure on the reaction outcomes and focus on finding highly potent reaction mixtures and products rather than marginal improvements over the first round of results. Conversely, fragments **F7**, **F12**, and **F13** were screened at 100 µM total product concentration, as the parent compound was in the first reaction array assay. This is apparent in the general increase in biological activity seen across

53

the screening results. The results of Reaction Array 2 were compared with the validated hit reaction mixtures from Reaction Array 1, shown in Fig. **2.12** by markers at 35 and 29% inhibition. Disappointingly, no crude reaction mixtures from this array resulted in a significant improvement in potency over Reaction Array 1 hits, indicating that while products may have been formed, they were no more potent than prospective products formed in the preceding reaction array 1.
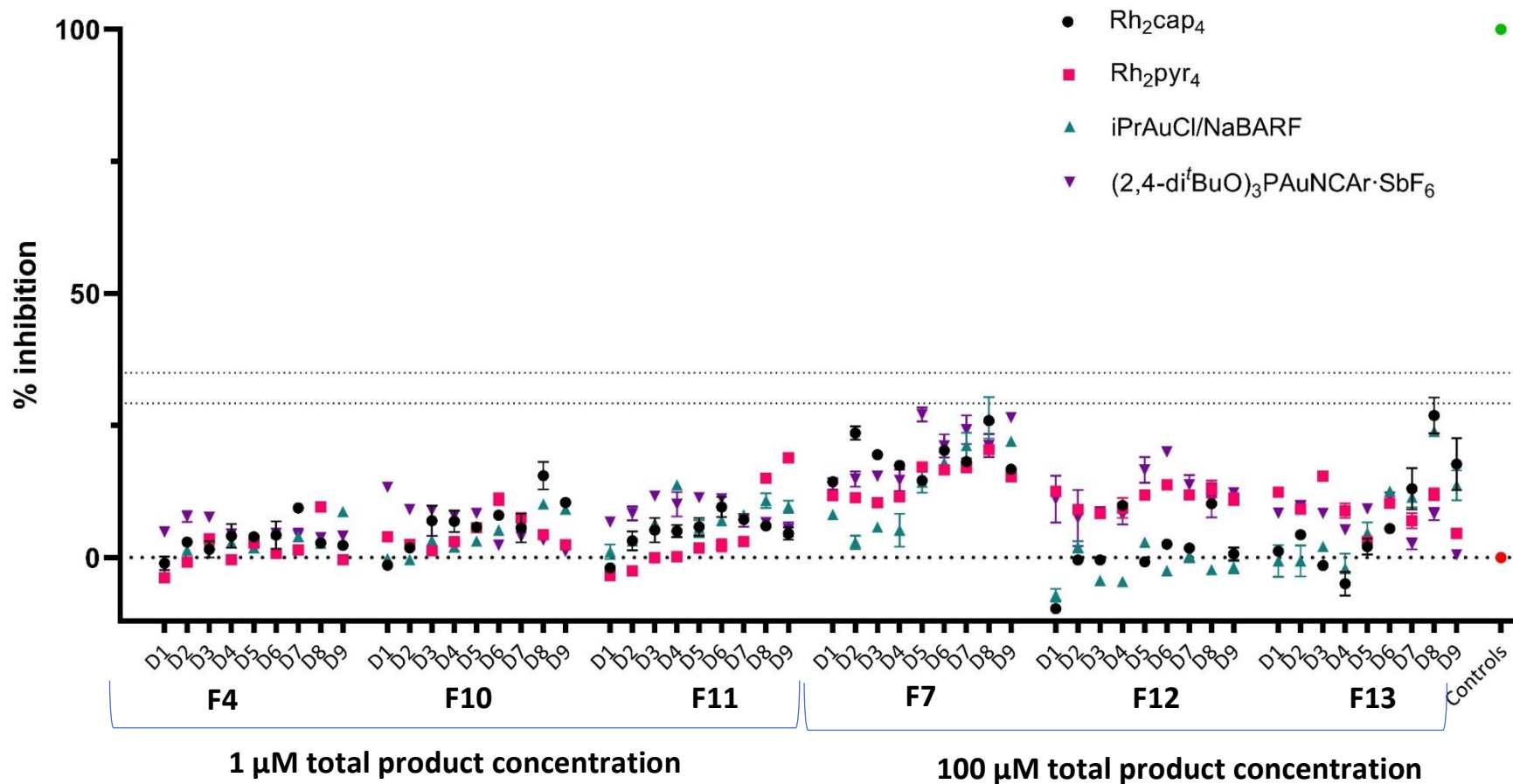
Figure **2.12**. Reaction Array 2 Screening Results. Screened against Aurora-A^{CM} (25 nm) using the Caliper mobility-shift assay. Final screening concentration is total product concentration, and labelled underneath fragment number. Icon shape and colour indicate catalyst; black circles = [Rh$_2$(cap)$_4$] (**C1**), pink squares = [Rh$_2$(pyr)$_4$] (**C5**), teal triangles = iPrAuCl (**C6**), purple inverted triangles = (2,4-di^{t}BuPhO)$_3$PAuCNAr·SbF$_6$ (**C4**). Thin dotted lines represent **RM2** and **RM4** activity from Reaction Array 1, central dotted line indicates 0 % enzyme inhibition. Data normalised to controls; upper green circle = 100% inhibition (no protein), lower red circle = 0% inhibition (no inhibitor).

2.2.6 High-throughput Analysis, Purification and Screen of Array 1 products

Typically hit reaction mixtures from an ADS campaign would be scaled-up, isolated and characterised to ascertain the structure of any productively grown fragment. In this instance, however, the failure to improve the apparent activity of hit reaction mixtures from Reaction Array 1 prompted investigation into the productivity of the chemistry for direct fragment elaboration. It was envisaged that high-throughput UPLC analysis of the reaction outcomes of Reaction Array 1 would allow identification of chemically productive reactions from a structurally diverse array design and enable selective purification and biological screening of the isolated products from the best performing reaction conditions.

While diverging from the original ethos of ADS through reaction analysis, purification, and biological screening of isolated products, it was envisioned the purification of these products would be performed on only the sufficiently high-yielding reactions followed by structural elucidation of only the biologically active components that outperform the parent fragment. This would allow direct fragment elaboration to be performed in a structure-blind manner, while expending the least amount of effort on unproductive reactions and elaborated but not active fragments.

2.2.6.1 High-throughput UPLC Analysis and Purification

The product mixtures from Reaction Array 1 were analysed by high-throughput UPLC, following dilution of crude reaction mixtures from 100 mM to 5 mM. Here, productive reactions were identified through observation of the formation of products with the mass expected for an intermolecular reaction. The results of the analysis in Fig. **2.14** allow for identification of patterns of reactivity or productivity in the array through colour-coding based on each of the reaction outcomes determined by LC-MS, UV, and with yields determined using an evaporative light scattering (ELS) assay previously developed by Sam Liver, RFI.

Surprisingly, **D4** and **D7** show no significant formation of the expected intermolecular product, regardless of fragment or catalyst, contrary to the hit reaction conditions identified in the biological screen in section **2.2.3.2**. **D4** has the potential to form an intramolecular product **2.15** proposed in Fig. **2.13**, with this reaction expected to proceed more rapidly upon formation of the metal carbenoid than any potential intermolecular reaction and represents the entropically favourable outcome, thereby depleting the available diazo for reaction with the fragment. The MW of this product (223) was observed during analysis by LC-MS, and prior work

within the group by Adam Green has observed and exploited this reaction type with structurally similar diazo-containing compounds as MDM2/P53 PPI inhibitors.
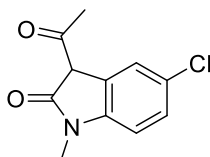
2.15

Figure **11**. Proposed intramolecular cyclisation product of **D4**

Fragments **F3**, **F4**, **F5** and **F9** also showed poor conversion to product, with only diazo **D3** reacting productively with all four fragments and fragment reacting productively with only three diazos (**D2**, **D3**, and **D8**) overall. Conversely, fragments **F1**, **F2**, **F6**, **F7**, and **F8** reacted well with most diazo substrates across the majority of catalytic conditions. With multiple sites of reactivity inherent in each fragment, this analysis identified multiple products in reactions with fragments **F1** and **F2**, with significantly different retention time to indicate different products formed. While interesting chemically, this would only be investigated further if one or both observed products has been elaborated productively, showing greater biological potency than the parent fragment.

Overall, the productive reactions highlighted with green icons constitute 34 unique combinations of fragment and diazo, representing 47% of the total possible substrate combinations. Of these 34, analysis of the ELS data identified 16 fragment-diazo combinations with sufficient intermolecular product (>0.15 mg) for purification, representing 22% of all fragment-diazo combinations and totalling 30 individual reactions. These 30 productive reactions are all from fragments **F1**, **F2**, **F7**, and **F8**, combined with diazos **D1**, **D2**, **D5**, **D6**, and **D8**, with all catalysts in various combinations.
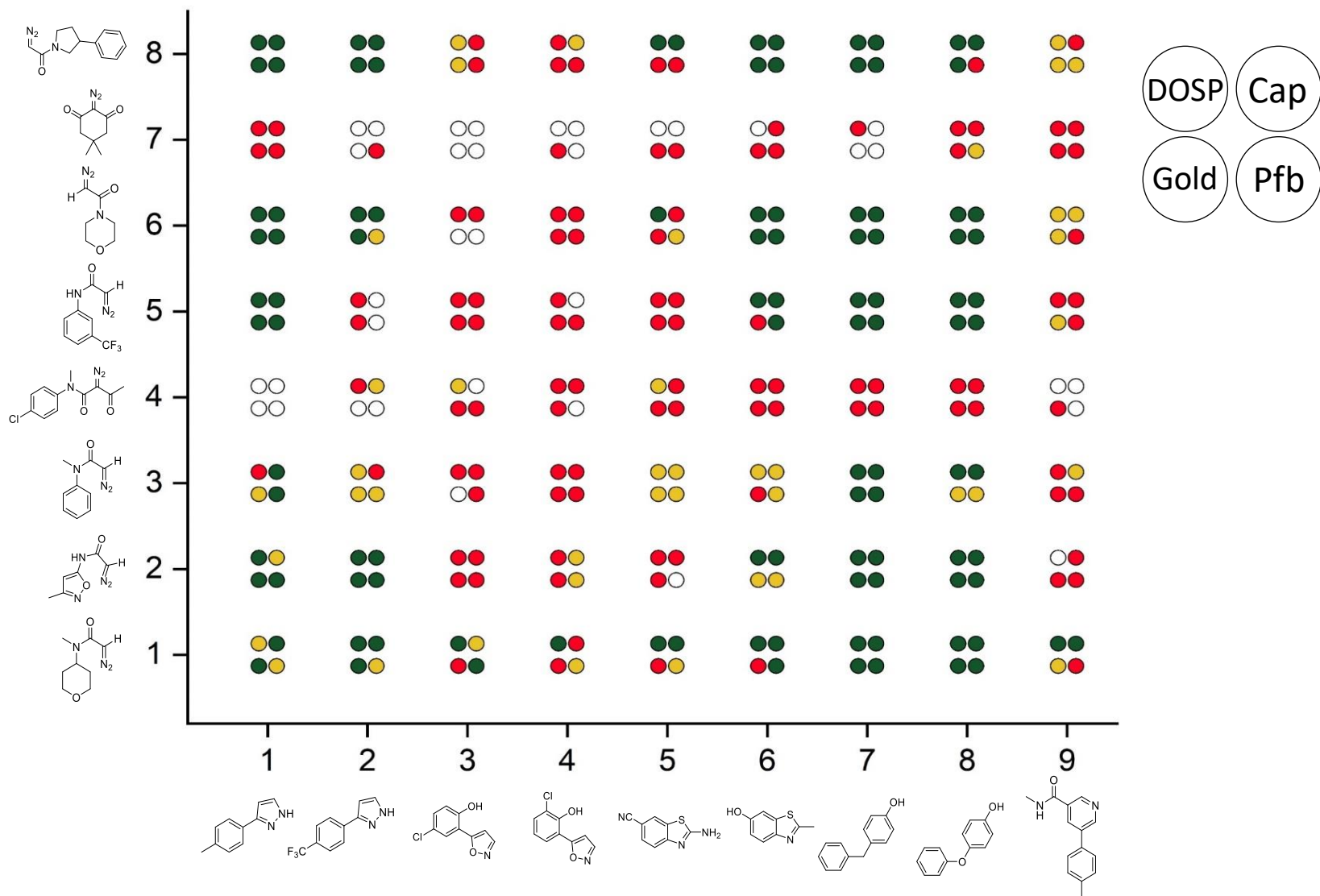
Figure **2.14**. Analytical UPLC Results of Reaction Array 1. Fragments are shown on X-axis, diazo substrates on Y-axis, with dot icon at which they intercept representing the results of each fragment-diazo combination. Location of dot in group of 4 represents catalyst used, outlined in Figure **12** legend, top right. Traffic light system denotes reaction outcome: Green – Intermolecular product mass observed in LC-MS, UV and ELS trace, Yellow – Product mass observed in LC-MS, UV, but trace ELS signal, Red – No ELS signal, only LC-MS or UV trace apparent, Empty – No intermolecular mass observed in analysis.

Reaction Mixture	Product 1			Product 2			Total Yield (%)
	(µg)	(% yield)	(mM)	(µg)	(% yield)	(mM)	
F1-D1-C4	26	0.8	4.1	44	1.4	7.1	2.2
F1-D2-C4	36	1.2	6.1	49	1.6	8.2	2.9
F1-D5-C4	42	1.2	5.8	133	3.7	19.1	4.9
F1-D5-C2	151	4.2	21		N/A		4.2
F1-D6-C1	12	0.4	2.2	18	0.6	3.1	1.0
F1-D6-C3	4	0.1	0.6	4	0.1	0.7	0.3
F1-D6-C4	31	1.1	5.5	106	3.7	18.5	4.8
F1-D6-C2	2	0.1	0.4	77	2.7	13.4	2.8
F1-D8-C4	80	2.3	11.6	93	2.7	13.5	5.0
F2-D1-C1	32	0.9	4.3	9	0.2	1.2	1.1
F2-D1-C3	65	1.8	8.8	1	0.03	0.1	1.8
F2-D6-C3	42	1.2	6.1		N/A		1.2
F2-D6-C4	48	1.4	7.0	47	1.4	7.0	2.8
F7-D2-C1	49	1.5	7.5		N/A		1.5
F7-D5-C1	73	1.9	9.5		N/A		1.9
F7-D5-C2	99	2.6	12.9		N/A		2.3
F7-D5-C3	90	2.3	11.6		N/A		2.6
F7-D6-C1	37	1.2	6.0		N/A		1.2
F7-D6-C2	33	1.1	5.3		N/A		1.6
F7-D6-C3	48	1.6	7.8		N/A		1.1
F7-D8-C3	133	3.6	18		N/A		3.6
F8-D1-C1	41	1.2	6.0		N/A		1.2
F8-D2-C1	122	3.7	18.7		N/A		3.7
F8-D2-C3	66	2.0	10.2		N/A		2.0
F8-D5-C1	60	1.5	7.7		N/A		1.5
F8-D5-C3	86	2.2	11.1		N/A		2.2
F8-D6-C2	33	1.1	5.3		N/A		1.1
F8-D8-C1	86	2.3	11.5		N/A		2.3
F8-D8-C3	5	2.0	10.1		N/A		2.0

Table **2.1**. Quantity, yield, and concentration of purified Reaction Array 1 products. (µg) denotes quantity of product in 20 µl DMSO stock, determined *via* UPLC-ELS assay, (%) denotes isolated yield, (mM) denotes concentration of product in 20 µl DMSO stock. Red or blue labels denote purified products with comparable or improved potency with parent fragment, respectively, see Section **2.2.7.2** and Fig. **2.13**.

The preparative UPLC solvent gradient required for purification of each compound was determined during the UPLC analysis, assigned based on the retention time observed *via* ELS and based on a previously determined calibration. In each case, the solvent gradient was selected to maximise separation of the product peaks with the observed analytical retention times. The selected reactions were purified by preparative mass-directed UPLC, collecting the expected mass of the expected intermolecular product. Following removal of solvent after purification, each purified product was re-dissolved in a fixed volume of DMSO (20 µl) for determination of concentration and subsequent biochemical screening. Following dissolution,

concentrations of purified products were determined using the UPLC-ELS assay, ranging from 100 µM to 21 mM. This analysis also provided the means to calculate final yield for each isolated product/s, shown in Table **2.1**, through determination of quantity of each product loaded on to the analytical column. Isolated yields range from 0.3 to 5% for the reactions identified as containing sufficient material to purify, indicating the chemistry generally performed poorly. Only through use of the analytical ELS assay to determine the UPLC column loading of each compound, therefore the concentration of each DMSO stock, was further biological screening enabled, as isolating <1 mg and accurately weighing such a small quantity is impractical. Observed conversion and isolated yields of the intermolecular reactions were generally low, indicating the reaction conditions were less than ideal and contributed to the relatively small number of compounds with sufficient quantity to be isolated. Efficient exploration of chemical space would only be possible through similarly efficient reactions, suggesting some optimisation would be needed if further rhodium(II)-carbene reaction arrays were to be performed. The implications of these poor conversions and yields on microscale chemistry in the overall ADS strategy are discussed in Section **2.3**.

2.2.6.2   Biological Screening of Array 1 Products

Each isolated compound was screened at a single concentration, defined by the mass obtained from purification at a fixed 5% final DMSO in assay buffer, providing final screening concentrations of 19 µM to 1.64 mM. These samples assayed individually against Aurora-A in kinetic mode, measuring the effect on kinase activity over time. The results from this screen can be seen in Fig. **2.15**, where purified products are plotted as single points, shown in black, blue, and red, against the dose-response of the parent fragment from which they are derived, shown as grey points with the IC_{50} curve.
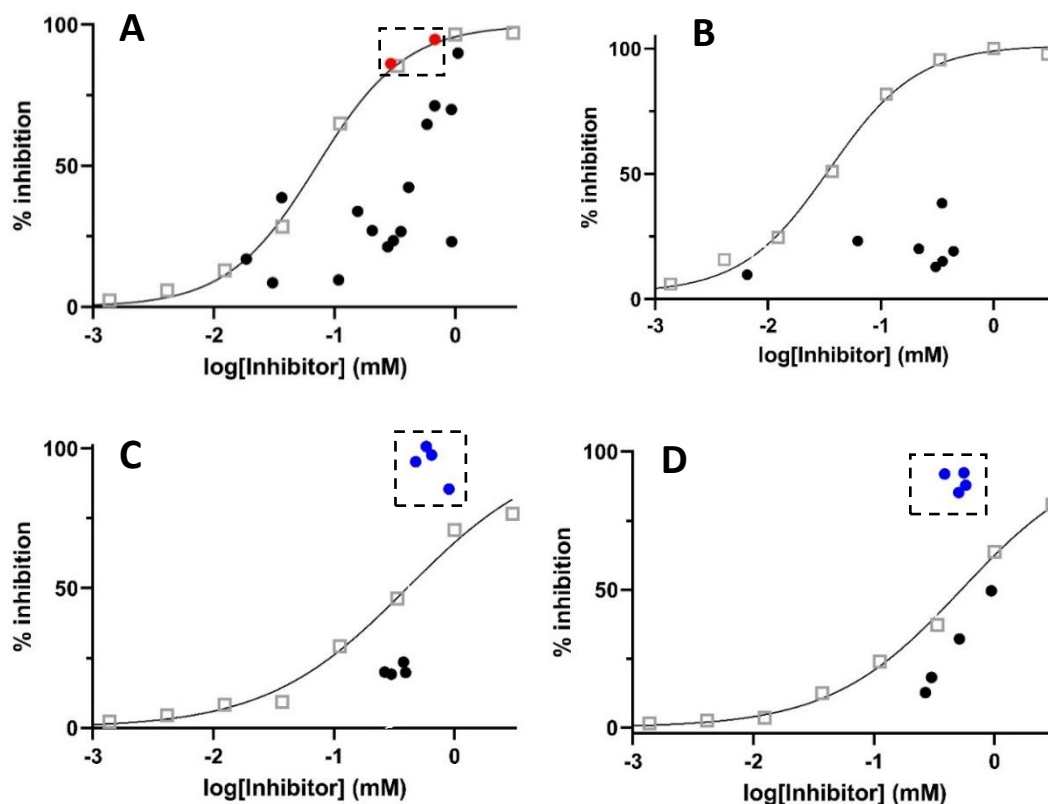
Figure **2.15**. Overlay of single-point purified products (circular spots) and parent fragment IC_{50} curve (grey boxes). Panel **A**) Fragment **F1.** Panel **B**) Fragment **F2**. Panel **C**) Fragment **F7**. Panel **D**) Fragment **F8**. Red icons indicate purified reaction products that were followed up with further biochemical validation, with comparable activity to the parent fragment at the same concentration. Blue icons indicate purified reaction products that were followed up with further biochemical validation due to improved potency over the parent fragment at the same concentration.

Products based on fragment **F1**, shown in Fig. **2.15**-**A**, fall mainly below the plot of the IC_{50} curve, indicating that at the single-point concentration previously determined these compounds are less potent than the starting fragment. The products that show comparable activity to the starting fragment, shown in close proximity to the plotted curve and highlighted in red were investigated further *via* dose response to ascertain how compounds only marginally different from the parent IC_{50} curve inhibit Aurora-A. Products derived from fragment **F2**, in Fig. **2.15**-**B** are likely to be similar to those based on fragment **F1**, where all the compounds fall underneath the IC_{50} curve indicating products are less potent than the starting fragment. None of these compounds were followed up any further as while the direct elaboration of the fragment was productive, the fragment growing had a detrimental effect on biological potency.

Reaction products based on fragments **F7** and **F8** were more successful. In both cases, clusters of compounds can be seen above the IC_{50} curve, highlighted in Fig **2.15-C** and **2.15-D**,

indicating these compounds are more effectively inhibiting kinase activity at their respective concentrations compared to the parent fragments. These eight products represent four different combinations of fragment and diazo, shown in Fig. **2.16**, from three different dirhodium(II) catalysts.
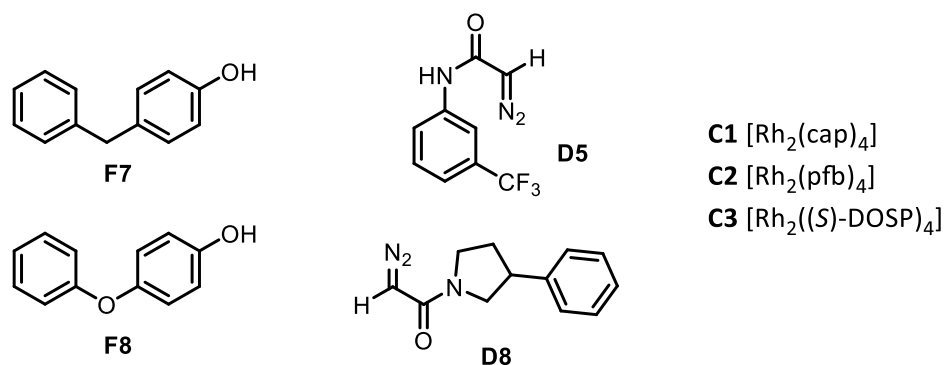

Figure **2.16**. Combinations of fragment, diazo and catalyst in productive reactions.

Several of these compounds were further investigated biochemically to determine the IC_{50} values, enabling a direct comparison against the parent fragments. Each was run as a 3-fold, 10-point serial dilution from the highest concentration available against Aurora-A kinase activity, shown in Fig. **2.17**. These comparisons show that products derived from fragment **F7** displayed a 3-to-5-fold increase in potency when reacted with **D5**, seen in Fig. **2.17**. Derivatives of fragment **F8** reacted with **D5** and **D8** show between a 3- and 10-fold increase in potency, from 549 to 56 μM for the most potent product in Fig **2.17**. While only relatively modest increases in potency, these results show that the workflow enabled direct fragment elaboration and discovery of compounds that were more active than the parent fragment. The varying increases in potency between identical combinations of fragment and diazo may be due to different catalysts producing different products, based on the reactivity profiles and propensity of each catalyst for O-H or C-H insertions, for example. It may, however, also be due to inherent error in determination of concentration by ELS following dilution of purified array products. As these initial results were encouraging, all the reaction conditions were selected for scale-up to enable full dose-response to be determined and full structural elucidation of the formed product.
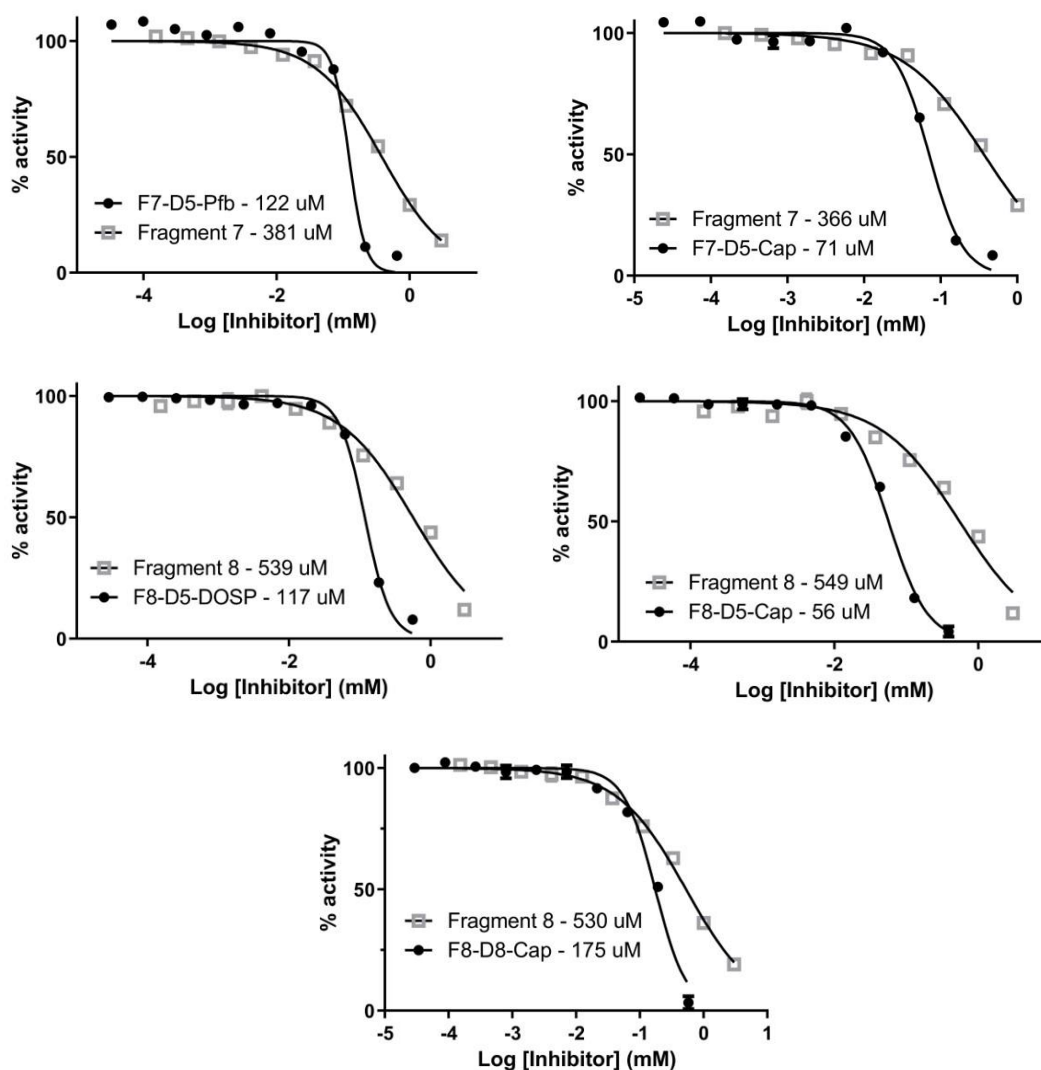
Figure **2.17**. Comparison of parent fragment and purified array product IC$_{50}$ curves. Parent fragment IC$_{50}$ shown in grey squares, elaborated product in black dots, with the conditions of each reaction mixture from which the product was purified outlined adjacent to the observed IC$_{50}$ value.

2.2.6.3 ^{1}H-NMR Spectroscopic Determination of Hit Structures

Prior to further fragment elaboration, the structure of the hit products was established *via* 500 MHz ^{1}H-NMR spectroscopy to allow comparison of structures and their potential effect on IC$_{50}$ values, as well as guide design of an additional reaction array to further expand upon the hits. ^{1}H-NMR spectra of these purified products from Reaction Array 1 shows all hit compounds derived from fragment **F7** and **F8** are O-H insertion, see Fig. **2.18**, regardless of catalyst. These compounds, **2.16**-**2.19**, indicate that the catalysts employed preferentially result in O-H insertion, even when additional sites of potential reactivity are present – methylene linker in

2.16 and **2.18**, or the *para* C-H of the phenoxyphenol derived compounds **2.17** and **2.19**. Confirmation of the structure of these reaction products enabled further hit expansion to take place, whether using transition metal catalysis as employed in Reaction Array 1 or exploiting an alternative chemistry amenable to the microscale parallel reaction format. Prior to further hit expansion based on the identified products, the compounds were re-synthesised at a larger scale for full structural characterisation and IC$_{50}$ validation with a full dose-response curve.
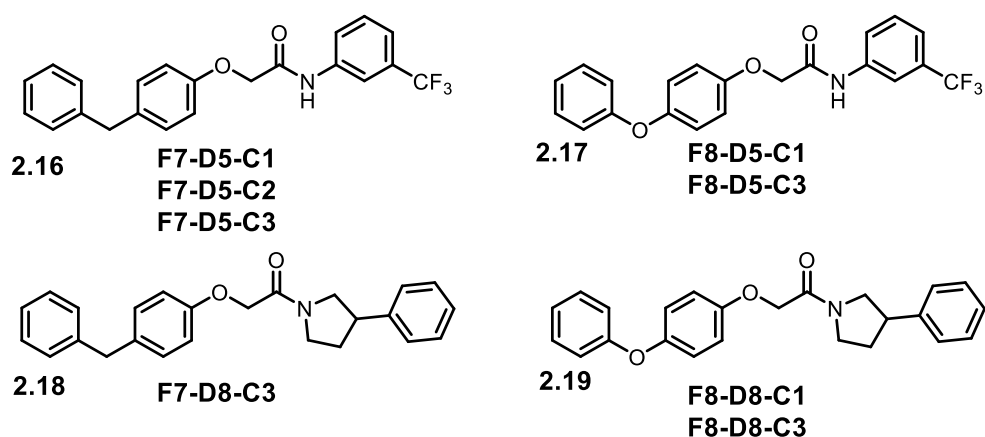

Figure **2.18**. ^{1}H-NMR determined structure of hit compounds. Reaction conditions that resulted in each structure are labelled below the identified compound.

2.2.6.4 Scale-up and Validation of Array 1 Hits

Scale-up synthesis of **2.16**-**2.19** was undertaken to obtain full structural and IC$_{50}$ data to inform selection of an appropriate screening concentration for single-point assays of subsequent array chemistry based on structurally validated hits. The synthesis was undertaken *via* two distinct routes to validate the transition metal catalysis on scale, enable attempts at chemical optimisation, and to obtain sufficient quantity of relevant intermediates for further microscale parallel array format chemistry exploiting an amide bond formation, detailed in Section **2.2.8**. Biological screening of the scaled-up compounds was then performed in a dose-response manner to validate prior biochemical screening results and inform further array design.

2.2.6.4.1 Scale-up Synthesis of Array 1 Hits

Hit compounds **2.18** and **2.19** were synthesised by the same metal carbenoid chemistry employed in the reaction array, from the diazo **D8** and fragments **F7** and **F8**. The original reaction conditions were repeated and scaled-up and -out to provide enough material for full characterisation even if similar yields were obtained to the original array (*c.a.* 5%). Each reaction was scaled-out 10-fold (repeating reaction 10 times in parallel and pooling crude material prior to purification) alongside an increase to 200 µl reaction volume at 100 mM concentration of fragment, resulting in a 20-fold scale-up over the original microscale array.

Brief attempts at optimisation of the chemistry were performed alongside the scale-up. Prior work in the group had shown that altering the stoichiometry of the reaction and changing the solvent had provided an increase in yield of the expected intermolecular product. Following removal of solvent *in vacuo* the reaction mixtures were combined and products were purified by preparative HPLC. The reaction conditions and isolated yields are shown in Scheme **2.3**.
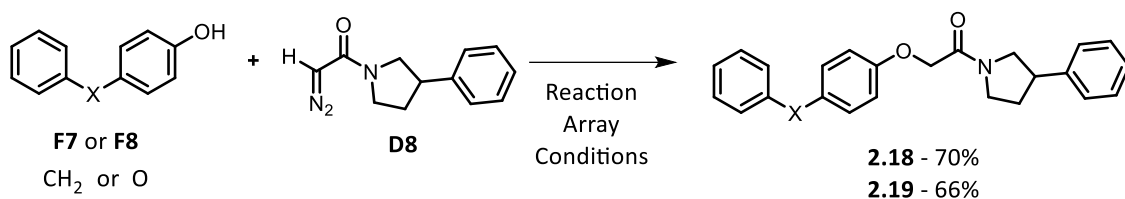

Scheme **2.3**. Scale-up and -out synthesis of **2.18** and **2.19**.

Changing the reaction conditions in this instance had little-to-no effect on the yield, with the original reaction conditions at 2-fold scale-up and 10-fold scale-out producing a satisfactory 70% isolated yield. While counterintuitive, scale-up of these transition metal catalysed reactions to obtain the desired product, rather than easily implemented amide couplings, indicates that future array format chemistry and bioactive compound discovery is supported by the ability to scale-up and -out to obtain identical products. This is crucially important in instances where said products may only be accessible *via* this route.

Hit compounds **2.16** and **2.17** based on 3-trifluoromethyl aniline were scaled-up *via* amide bond formation, shown in Scheme **2.4**. The preparation of these elaborated fragments was performed on a gram scale, to enable straightforward execution of any subsequent array with any number of desired amines and immediate scale-up of any hit products for structural characterisation. Benzylphenol **F7** and phenoxyphenol **F8** were each stirred overnight in the presence of ethyl bromoacetate and potassium carbonate in acetone to yield their respective

alkylated ester products **2.21** and **2.22** in excellent yield following purification. These esters were then hydrolysed to yield both carboxylic acids in good yield. Carboxylic acids **2.23** and **2.24** were subjected to amide coupling conditions, generating the activated ester with HATU followed by addition of 3-trifluromethyl aniline **2.25** to yield products **2.17** and **2.18** in good yield following purification.
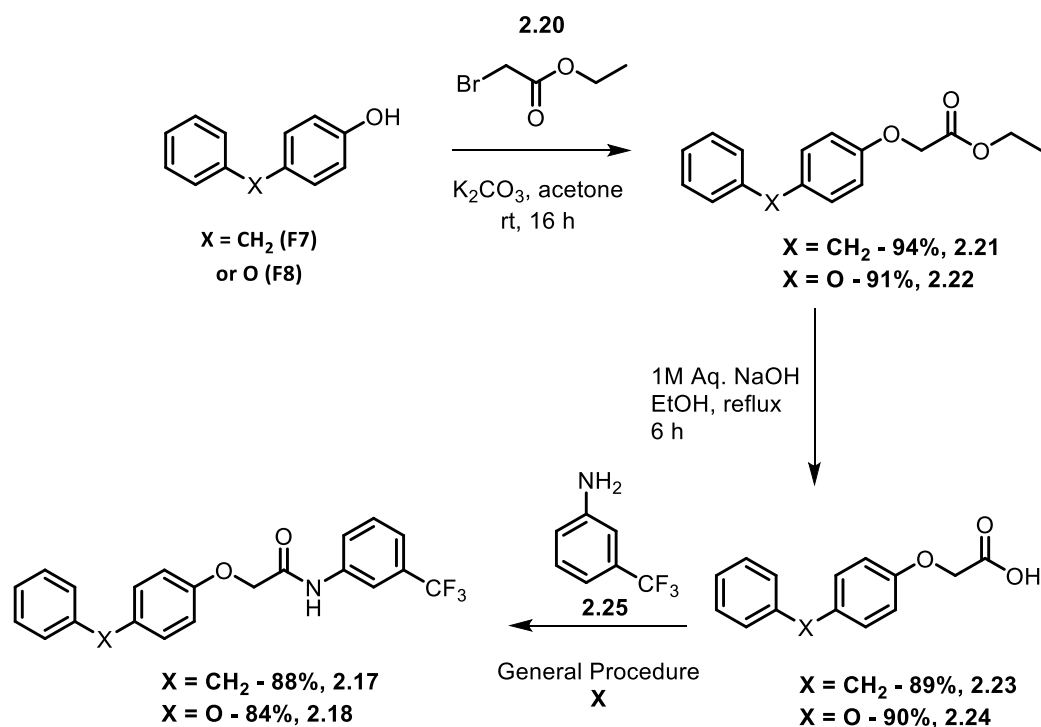
Scheme **2.4**. Scale-up synthesis of **P1** and **P3** by amide bond formation.

Following synthesis and purification of the scale-up products, the structure and identify of the original hit compounds were confirmed through comparison of HPLC retention time and ¹H-NMR spectra of the purified array products and the scale-up products. With purified products in hand, the biological screening of these scaled-up products was performed.

2.2.6.4.2 Biochemical Validation of Array 1 Hits

Following scale-up and purification of **2.16**-**2.19**, each compound was assayed against Aurora-A kinase to determine the biological activity with a full dose-response curve. A ten-point, 3-fold serial dilution of each compound was performed and screened against Aurora-A activity, shown in Fig. **2.19**, and directly compared alongside the parent fragments **F7** and **F8**, shown in grey icons.

Hit compounds **2.17** and **2.18** showed poor inhibition of Aurora-A, contradicting previous results from the purified microscale array products shown in Section **2.2.7.2**. Upon further investigation of prior results, re-screening all compounds, and increasing the final DMSO concentration to 10% to increase the solubility of the compounds in reaction buffer, no significant biological activity was observed for these compounds, with IC_{50} values >3 mM. It was noted that the previous results stem from poor solubility of the compounds in question. The steep IC_{50} slope, seen in Fig. **2.17** in Section **2.2.7.2**, is indicative of poor solubility of the compound, where the compound is crashing out of solution at higher concentrations which may impact on the solubility of the protein, resulting in the appearance of attenuated kinase activity.
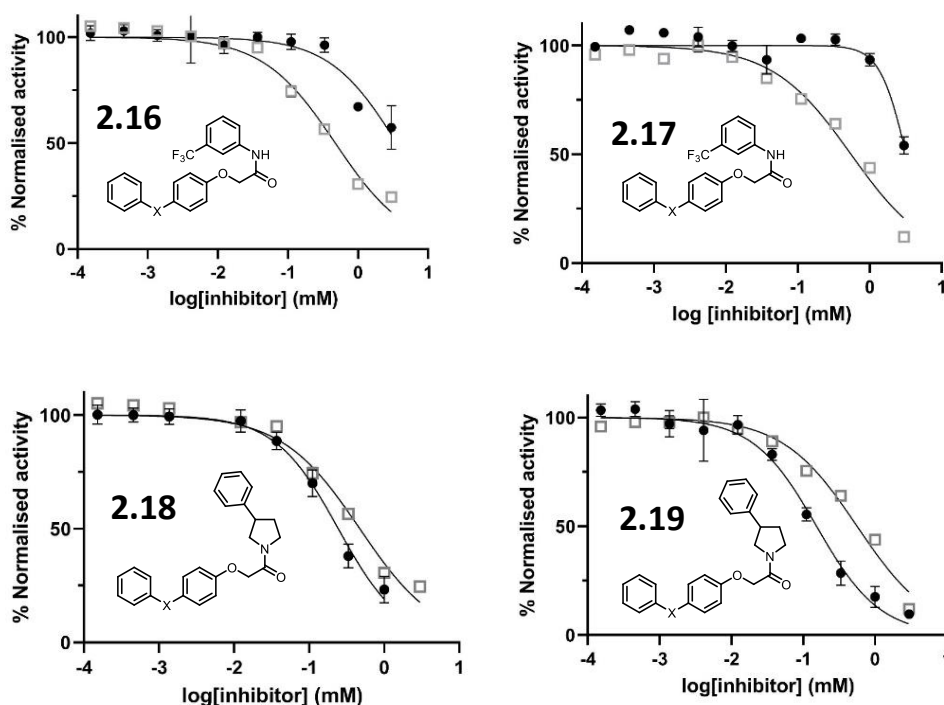

Figure **2.19**. IC_{50} curve comparison between parent fragments and scaled-up hit products. Parent fragment shown in grey boxes, hit products in black dots.

Considering this lack of potency under close scrutiny, hit reaction products **2.16** and **2.17** were no longer deemed worthy of further investigation as the elaboration completely abolished the biological activity of the fragment. Reaction products **2.18** and **2.19**, however, showed improved potency against Aurora-A compared to the parent fragment. Direct comparison of **2.18** to fragment **F7** shows a small increase in biological potency, improving the IC_{50} from **X** to **X** µM. **2.19** showed a greater increase in potency, with a roughly 3-fold improvement of IC_{50} value from 549 µM to 175 µM. While only a modest increase in potency, this improvement was

sufficient justification for the design and execution of a follow up microscale reaction array to expand upon the SAR around the 3-phenylpyrrolidine component of **2.18** and **2.19**.

While the transition metal catalysed Reaction Array 1 performed poorly, with low yields exacerbated by the microscale resulting in small amounts of elaborated fragment product, the overall workflow has proven viable in the direct elaboration of fragments to improve biological potency. Through UPLC analysis of reaction outcomes, selection of productive reactions for purification and subsequent biological screening to determine activity, hit compounds **2.18** and **2.19** were discovered. This activity was retained following scale-up and validation, therefore **2.18** and **2.19** formed the basis for further expansion of these hits *via* microscale reaction array.

2.2.7 Hit Expansion by Amide Array

With biochemically validated and structurally determined products **2.18** and **2.18**, attention was turned to designing and executing a small reaction array that would expand upon the SAR already determined and enable further improvements in biological potency over these products. While possible to perform a microscale parallel array using the transition metal catalysis previously employed in Reaction Arrays 1 and 2, a structurally diverse array based on only two parent fragments would require synthesis of a large number of amine/aniline-based analogues as their respective diazo carbonyl compounds – a route that has proven potentially synthetically challenging in substrate scope, long-term stability, and ease of purification. As described in Section **2.2.7.4**, a facile O-alkylation and ester hydrolysis was performed on gram scale with fragment **F7** and **F8**, providing sufficient material for a microscale parallel array of amide bond formations. This offered the advantages of reducing the number of synthetic steps per final product, removing the potentially troublesome diazo synthesis, and could be performed with cheap and readily available starting materials.

As a commonly utilised and robust chemistry, amide bond formation is ideally suited to the microscale array format – insensitive to air and moisture, robust and easy to handle, generally producing high yields, and with many suitable amines commercially available. Through design and execution of a small, focused microscale reaction array, it was envisaged that selection of amine analogues would allow exploration of relevant chemical space related to the elaborated fragments **2.18** and **2.19** to further improve biological potency.
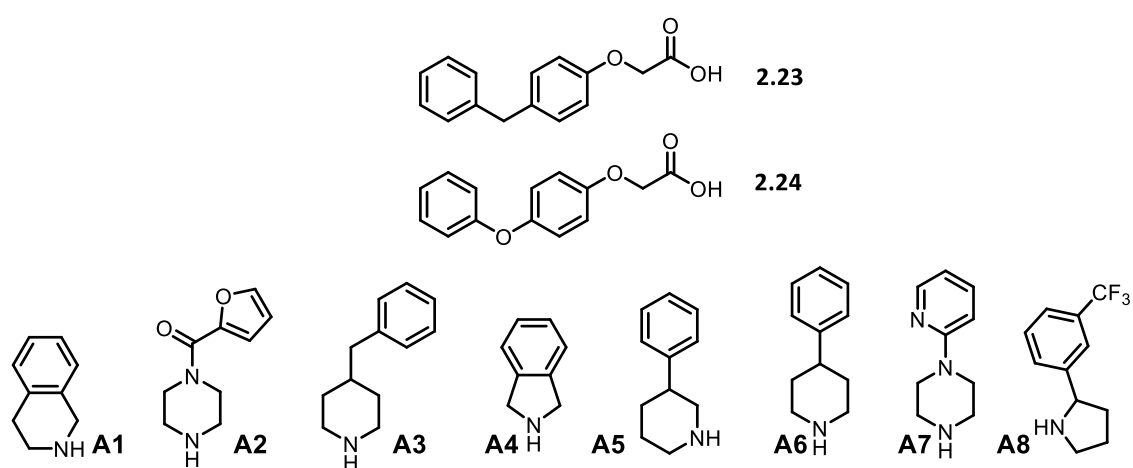
2.2.7.1   Amide Array Design

The Amide Array was designed upon the improved fragment products **2.18** and **2.19** from Reaction Array 1. Analogues of 3-phenyl pyrrolidine were selected based on availability, structural similarity, HA count of between 9 and 14, and inclusion of additional heterocycles. The design of this small array can be seen in Fig. **2.20**. At this stage the aniline-based products **2.16** and **2.17** were yet to be "de"-validated, as described in Section **2.2.7.4.2**, therefore the array included 14 anilines in addition to the cyclic secondary amines. Structures, reaction yields and assay results for these anilines are included in Appendix C.

2.2.7.2   Execution of the Amide Array

The reaction array was performed on a 200 µl scale with final concentrations of 100 mM carboxylic acid and 120 mM amine. A 200 mM stock solution of each acid was stirred for 30 min with HATU to form the activated ester then 100 µl added to designated vials *via* multi-channel pipette. 100 µl of 240 mM amine solution in DMF was then added, the vials were capped and stirred overnight. Following the designated reaction time, the solvent removed *in vacuo* and the crude mixture re-dissolved in DMSO prior to analysis and purification. Analytical UPLC was used to determine the reaction outcomes, with all the reactions showing good conversion determined by consumption of starting material. The successful reactions were then purified by mass-directed preparative HPLC into pre-weighed vials, HPLC solvent removed *in vacuo*, and the vials then re-weighed to allow calculation of yield, shown in Fig **2.20**.

This microscale array worked well with isolated yields ranging from 48 to 82%, providing an excess of product required for screening and in sufficient quantity to obtain full structural characterisation. These yields indicate that these reactions may be amenable to further reduction in scale, moving from the micro- to the nano-scale, while still producing sufficient quantity of product for isolation and biological screening. Prior to biological screening, each weighed product was dissolved in DMSO to 120 mM, allowing re-formatting to 96-well plate utilising liquid handling robotics (Hamilton).

Figure **2.20**. Design, yields, and assay results of amide bond array. Panel **A**) Carboxylic acid-containing fragments and cyclic secondary amines used in the Amide Array. Panel **B**) Tabulated results of reaction array and biological assays. Yield (%) represents isolated yield of Amide Array products. Inhibition (%) is percentage inhibition of Aurora-A[CM] at 100 µM product concentration, with sd of duplicates in parentheses. ΔTm (°C) is the effect on Tm of Aurora-A[CM] at 100 µM compared to a DMSO control, with s.d of duplicates in parentheses. Amide coupling conditions: i) Carboxylic acid (1 eq.), HATU (1.2 eq.) DIPEA (1.1 eq.) in DMF (0.1 M); ii) (1.25 eq.) and DIPEA (2.5 eq.) in DMF (0.1 M).

Compound No.	Amine	Acid	Yield (%)	Aurora-A Inhibition (%)	ΔTm (°C)
2.25	A1	2.23	81	-6 (3)	-0.37 (0.07)
2.26		2.24	80	14 (5)	-0.27 (0.08)
2.27	A2	2.23	78	5 (3)	0.29 (0.01)
2.28		2.24	76	4 (2)	-0.08 (0.02
2.29	A3	2.23	82	14 (2)	0.22 (0)
2.30		2.24	68	3 (1)	-0.1 (0.01)
2.31	A4	2.23	56	12 (2)	-0.04 (0.14)
2.32		2.24	54	15 (7)	0.12 (0.1
2.33	A5	2.23	80	8 (3)	0.07 (0.22)
2.34		2.24	77	4 (3)	-0.13 (0.03)
2.35	A6	2.23	83	15 (2)	-0.01 (0.02)
2.36		2.24	81	0 (1)	-0.12 (0.06)
2.37	A7	2.23	51	14 (2)	-1.39 (1.40)
2.38		2.24	48	10 (4)	0.17 (0.11)
2.39	A8	2.23	76	5 (5)	-0.09 (0.11)
2.40		2.24	70	2 (3)	-0.15 (0.23)

2.2.7.3 Biological Screening of Amide Array

Utilising the IC$_{50}$ determination of **2.18** and **2.19** from Section **2.2.7.4.2**, the full Amide Array was assayed at 100 µM product against Aurora-A, results shown in Fig. **2.20**. All compounds were screened at a 5% final DMSO concentration, with 100 µM screening concentration applying selection pressure to observe only compounds with a significant increase

in biological potency over the prior hit compounds. 2σ from the mean of data was used as an arbitrary cut off point by which to determine a "hit" compound from the overall dataset, equating to inhibition >21%, and as discussed in Section **2.2.3.2** for Reaction Array 1. Directly compared to products **2.18** and **2.19**, Amide Array products would need to exhibit inhibition of >30% and >45% at 100 µM, respectively, to have improved upon these previously identified hits. Disappointingly, no products from the amide array further improve on the potency of **2.18** and **2.19**, indicating the fragment expansion strategy was unsuccessful with the amines utilised, resulting in less potent compounds.

A Thermal Shift Assay (TSA) was utilised as an orthogonal assay, measuring the Tm of Aurora-A^{CM} in the presence or absence of 100 µM of the purified Amide Array products at 5% final DMSO. These Tm values were compared to 5% DMSO control, with shifts of ±>1.5 °C from the control considered significantly large enough to warrant further investigation. None of the purified amides resulted in a significant ΔTm value, see Fig. **2.20**. When compared to the parent fragments **F7** and **F8** and Reaction Array 1 products **2.18** and **2.19**, see Appendix, none of the compounds from the series had a significant effect on Aurora-A Tm at 100 µM, suggesting the binding affinity of these compounds is simply not high enough to detect *via* this method. This small array, when considering the effort expended following falsely positive results from initial screening of **2.16** and **2.17**, samples a narrower portion of biologically relevant chemical space than initially intended.

2.3   Conclusions and Future Perspectives

Two dirhodium(II)-carbene based arrays, Array 1 and Array 2, were performed on close analogues of allosteric Aurora-A inhibitors in an attempt to improve biological potency *via* ADS, totalling 504 reactions. Initially, an array of 288 reactions was performed that each involved a fragment hit (or close analogue thereof), a diazo co-substrate, and a catalyst. The crude products were directly screened for inhibition of Aurora-A kinase, and the identified hit reactions informed the design of a second reaction array. The second reaction array comprised 216 reactions that each involved a fragment, diazo, and a catalyst, each based on Array 1 results; unfortunately, after the biological screening of this second array, no further reaction hits were identified. At this stage, high-throughput UPLC analysis was performed to investigate the productivity and chemical outcomes of the first reaction array. Although the observed yields of intermolecular reaction products were generally poor, this analysis informed selection and

purification of the best yielding intermolecular reaction products, 40 of which were subsequently screened against Aurora-A. Two compounds showed mildly improved potency, upon which a small third reaction array was based exploiting amide bond formation. Following purification and biological screening, this array was found to have failed to improve further upon the biological activity against Aurora-A.

In contrast to prior successes with intermolecular ADS[112,113,115], described in Section **1.2.3.2**, it is interesting to compare the methodology by which novel compounds were discovered *via* the first two reaction arrays. Rather than building the reactive diazo handle in to an existing binding motif to react with a broad selection of simple co-substrates in excess, the strategy employed here was to directly elaborate upon known inhibitor fragments, or close analogues thereof. A challenge for this strategy was to design substrates that had the potential to react with metal carbenoids whilst remaining structurally similar to fragment hits. Reaction conditions *i.e.,* stoichiometry, were also different to prior ADS campaigns. A 30-fold excess of co-substrate to diazo was utilised previously[115], shown to have negligible biological activity in the crude mixtures, while here a 1.1-fold excess of diazo to fragment was employed. Any excess fragment would make identification of productively elaborated and biologically active compounds impossible by simple screening of the crude reaction mixtures – only residual fragment activity would be observable in the assay output. From a chemical perspective, the conditions employed in Reaction Arrays 1 and 2 may have contributed to the poor conversion to the desired intermolecular products, reducing the likelihood of identifying productive outcomes from the ADS workflow. Compounds formed in ≤5% yield would require a significant jump in biological activity >20-fold to stand out from the crude reaction mixtures that may still contain unreacted fragments, more than an order of magnitude greater. Incorporation of the reactive diazo handle to an existing binder may be a more feasible strategy, providing a potential increase in reaction yields and therefore increasing the likelihood of identifying productively elaborated and novel fragments.

A workflow of high-throughput UPLC analysis, purification and biological screening was successfully established and allowed identification of productively grown fragments from Reaction Array 1. This approach still retained the potential for unexpected reaction products to be formed but ensured that their activity did not need to be determined within a crude reaction mixture. This workflow allowed analysis and purification of microscale reactions to obtain products on µg scale in a suitable format for biological screening, despite the poor conversions observed in Reaction Array 1. Despite the small quantities (tens of micrograms) of these products obtained, the identification of small improvements in potency compared to the parent

fragment validates the efficacy of this workflow when compared with ADS. Additionally, identification and isolation of multiple products from the same reaction mixture provides a facile way to increase the diversity of products obtained from an array without increasing the number of reactions performed.

This workflow enabled a reaction type to be harnessed from outside the standard medicinal chemistry toolkit, and such reactions have the potential to enable exploration of distinctive regions of chemical space. Here, metal carbenoid chemistry enabled multiple fragment series to be developed in parallel through formation of different types of bonds (C-N, C-O, and C-C) and validated the approach through identification of productive vectors for direct fragment elaboration. Combined with parallel optimisation of reaction conditions, the overall approach may facilitate drug discovery to directly elaborate upon existing fragments and hit molecules, rather than *de novo* route design to reach similarly elaborated products.

3 Development of Structure-Activity Relationships of Allosteric Inhibitors of Aurora-A Kinase

In this Chapter the structure-activity relationships for a series of allosteric Aurora-A inhibitors were developed. This series was based on the 2-hetaryl phenol inhibitors (e.g. compound **F4**) that were introduced in Section **2.2.1**. The aim was to design and synthesise a library of analogues of these previously characterised inhibitors to improve the biological potency through rational design of compounds as well as compound design guided by *in silico* docking studies. Iterative changes would be made to the compound series based on synthetic tractability and availability of starting materials to build a landscape of SAR for the series following biological screening. *In silico* studies would then guide design and synthesis of further analogues based on collated docking results against a number of Aurora-A crystal structures. This strategy allowed novel design of allosteric Aurora-A inhibitors, through rational library design and guided by a novel docking strategy, resulting in improved inhibitors of Aurora-A. It was envisaged this strategy of fragment growth would provide elaboration on biologically active structures with a commensurate increase in potency, maintaining the ligand efficiency (LE) of the productively elaborated structures.

3.1 Structural and Biochemical Rationale for selection of 2-hetaryl Phenol Series

The selection of the 2-(1,2-oxazol-5-yl)phenol fragment series for SAR studies was informed by experimentally determined biochemical evidence and a limited exploration of SAR previously performed for ADS, shown in Section **2.1**. One of six hits identified by Patrick McIntyre[64], 2,4-difluoro-6-(1*H*-pyrazol-5-yl)phenol **3.1** (**1.8**), had been subject to a small SAR study of commercially available fragments[129], resulting in 2,4-dichloro-6-(1,2-oxazol-5-yl)phenol **3.2** (**2.1**) with an IC_{50} of 113 µM. Close analogues of this fragment, **3.3**-**3.6** (**F3**, **F4**, **F10** and **F11** in Chapter **2**) were prepared as substrates for ADS in Reaction Array 1 and 2, see Section **2.2.1**, and had been shown to have improved activity compared to the parent fragments.
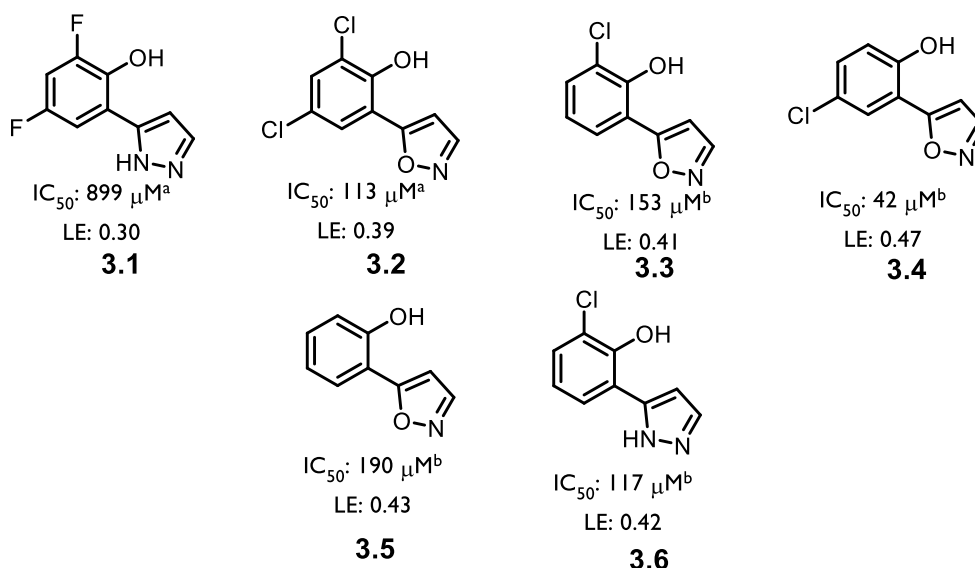

Figure **3.1**. 2-Hetaryl phenol-based Aurora-A inhibitors. [a] denotes IC_{50} determined by ADP-Quest assay[129], [b] denotes IC_{50} determined by Caliper mobility-shift.

Minor changes to the substitution around the phenol ring have previously shown significant effects on IC_{50} value, with removal of the 6-chloro from **3.2** to give **3.4** showing a roughly 3-fold improvement in biological potency and increasing LE from 0.39 to 0.47. Removal of the di-chloro groups had the opposite effect, reducing the potency roughly 2-fold compared to **3.2**. It is worth noting, however, that these compounds were assessed *via* different biological assay, with **3.1** and **3.2** assessed by ADP-Quest™[129] and **3.3**-**3.6** by Caliper mobility-shift. It was therefore important to reassess the biological potency of compounds assayed previously to

provide a valid point of reference for ongoing assays. As it had not been possible to further improve the potency of this series using ADS, a more traditional SAR study was envisaged to achieve this aim.

3.1.1 X-Ray Crystallography Structures of Known 2-hetaryl Phenol-based Inhibitors

Prior to synthesis of the series of analogues, existing crystal structures of compounds from the series were scrutinised to guide rational molecular design. The binding mode of fragments **3.1** and **3.4** are shown in Fig. **3.2-A**. The crystal structures shown indicate it may be possible to grow productively from multiple vectors of the fragment, highlighted in Fig. **3.2-B**, toward the more buried region of the pocket as well as toward Lys166 and a solvent exposed region. Additional growth extending "down" and out from the pocket may also be favourable, although a flat, solvent exposed and relatively featureless region. Initially, it was envisaged that simple substitution around the phenol ring would be explored to build a broader picture of the SAR, followed by further elaboration of the 2-hetaryl ring combined with productive substitution patterns discovered around the phenol.
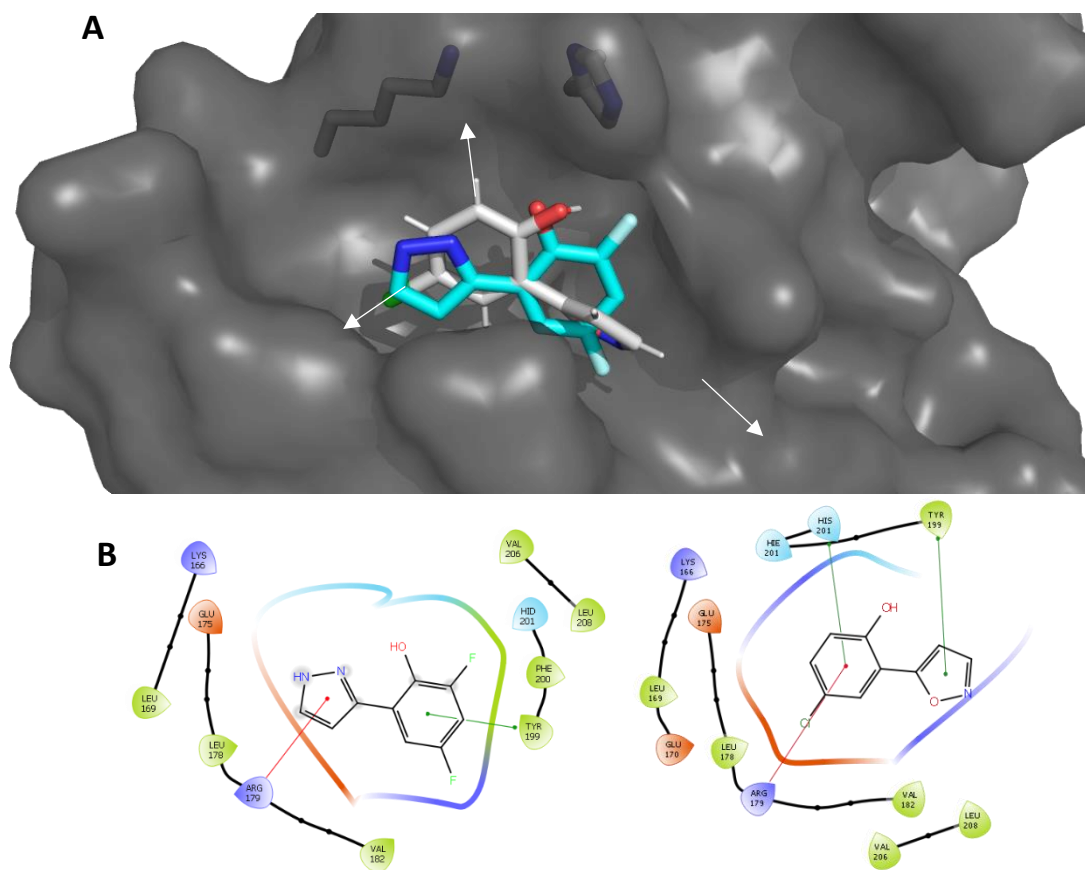
Figure **3.2**. Overlay of **3.1** (cyan, PDB: 5ORY) and **3.4** (grey, See Section **2.2.1.1**). Panel **A**: White arrows indicate vectors along which potential fragment growth may be productive. Highlighted are Lys166 and His201 side chains. Panel **B**: Ligand interaction diagrams of fragments **3.1** and **3.4**. Highlighted are π-π stacking (green lines) and cation-π (red lines) interactions. Borders indicate negatively charged (red), positively charged (blue), polar (cyan), and hydrophobic (green) regions.

3.2 Results and Discussion

3.2.1 Biological Evaluation of known analogues

The biological potency and ATP-competition profile of the known fragment inhibitors from the 2-hetaryl phenol series was determined, as a point of comparison for further analogues following synthesis and to confirm the mode of inhibition of Aurora-A. Additionally, determination of the IC_{50} values for compounds **3.1** and **3.2** *via* mobility-shift assay would provide a fair comparison to be drawn between prior work and subsequent IC_{50} values determined in this Chapter.

As the Y-pocket is sufficiently distant from the active site of Aurora-A, it was considered unlikely inhibitors bound to this pocket, such as **3.1** and **3.4**, would directly compete with ATP when attenuating kinase activity. Similarly, previous discussion of the remarkably dynamic structure of phosphorylated Aurora-A indicates it may be amenable to allosteric inhibition through ligand binding to the Y-pocket. ATP-competition experiments were performed to ascertain the likely mode of inhibition, prior to further analogue design and synthesis.

3.2.1.1 Synthesis of Known Aurora-A Inhibitors

Prior to determination of IC$_{50}$ values and ATP-competition data, fragments **3.1** and **3.2** were prepared (Scheme **3.1**). Briefly, the relevant hydroxyacetophenones **3.6** and **3.8** were stirred and heated in the presence of *N*,*N*-dimethylformamide dimethyl acetal (DMFDA) to afford enaminones **3.7** and **3.9** in good yield. These intermediates were then stirred and heated in EtOH with hydroxylamine hydrochloride or hydrazine monohydrate resulting in fragments **3.1** and **3.2**, respectively, in good yield following purification.
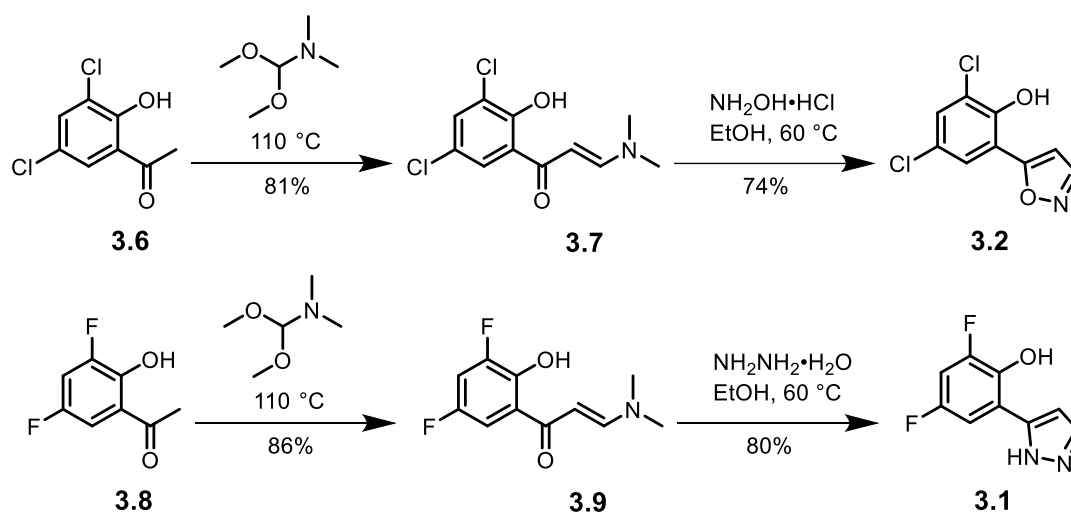
Scheme **3.1**. Synthesis of fragments **1** and **4**.

3.2.1.2 Determination of the Activity of Known 2-hetaryl Phenol Inhibitors

Following synthesis of compounds **3.1** and **3.2**, these compounds were assayed by Caliper mobility-shift against Aurora-A to determine their biological activity with a full dose-response curve. A ten-point, 3-fold serial dilution of each compound was performed resulting in a range of concentrations from 3 mM to 15 nM, the results of which are shown in Table **3.1**. Fragments **3.1** and **3.2** had IC$_{50}$ values of 765 ± 51 μM and 121 ± 11 μM, respectively, comparable

to the previous ADP-Quest assay results obtained by Patrick McIntyre of 113 and 899 µM, respectively. With the IC$_{50}$ values for compounds **3.1**-**3.6** determined, these were used to inform compound concentration in the determination of the ATP-competition profile for these fragments.

3.2.1.2.1 ATP-Competition Profile of 2-hetaryl phenol analogues

To complement structural studies of **1** and **4** indicating binding to the Y-pocket of Aurora-A, it was decided to perform a preliminary investigation into the mode of inhibition. Three alternative modes of inhibition are summarised in Fig. **3.3**: competitive, uncompetitive, and non-competitive, along with Equation **3.1** describing mixed-mode inhibition. It was anticipated that a more complex mode of inhibition would be observed for an allosteric inhibitor than an inhibitor that directly binds to the ATP-binding site, so was considered important to ascertain if only as an initial study.

Competitive Inhibtion

$$K_m^{obs}=K_m*(1+[I]/K_i)$$
$$Y=V_{max}*X/(K_m^{obs}+X)$$

Uncompetitive Inhibtion

$$V_{max}^{app}=V_{max}/(1+I/\alpha K_i)$$
$$K_m^{app}=K_m/(1+I/\alpha K_i)$$
$$Y=V_{max}^{app}*X/(K_m^{app}+X)$$

Non-competitive Inhibtion

$$V_{max}^{inh}=V_{max}/(1+I/K_i)$$
$$Y=V_{max}^{inh}*X/(K_m+X)$$

Mixed Inhibition

$$V_{max}^{app}= V_{max}/(1+I/(\alpha*K_i))$$
$$K_m^{app}= K_m*(1+I/K_i)/(1+I/(\alpha*K_i))$$
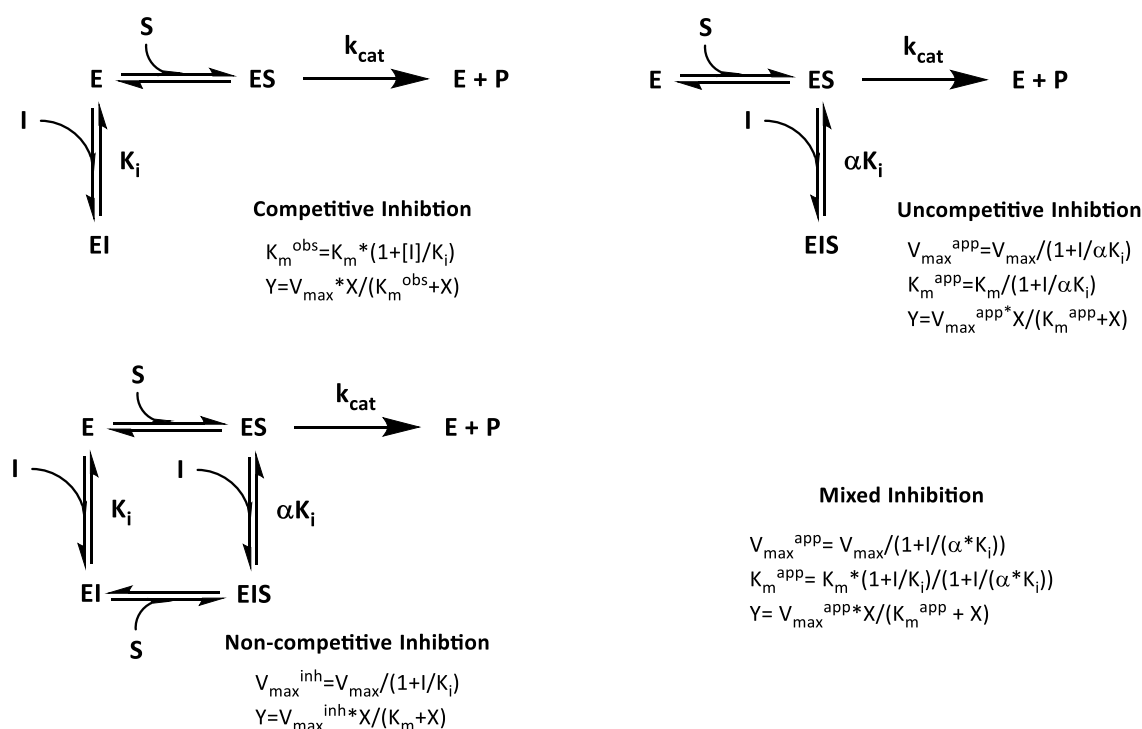$$Y= V_{max}^{app}*X/(K_m^{app} + X)$$

Figure **3.3**. Models of enzyme inhibition and associated equations. Panel **A** shows competitive inhibition, where inhibitor (I) directly competes with substrate (S) to reversibly bind to the enzyme (E). Panel **B** shows uncompetitive inhibition, where I reversibly binds solely to the enzyme-substrate complex (ES). Panel **C** shows non-competitive inhibition, where I reversibly binds both E and ES. Panel **D** shows the Equation **X** for mixed inhibition, a general equation that encompasses the 3 previously described types of inhibition as special cases and includes the parameter α as a descriptor for mechanism of inhibition.

ATP-competition assays for each fragment were performed in the presence of a 6-point, 3-fold serial dilution of ATP from 3 mM to 4 µM, at three different concentrations of each fragment determined by the IC_{50} value, at 0.5-, 1-, and 1.5-fold the IC_{50} of each fragment. Each data set was then plotted, and a non-linear regression analysis was performed. This non-linear regression was fit to differing models of inhibition, described in Fig. **3.3**, and each fit was then compared with one another to determine the statistically favourable model, results shown in Table **3.1**.

Compound	IC_{50} (µM)	LE	Preferred Model of Inhibition	α value
3.2	121	0.39	Mixed	5.3
3.3	153	0.41	Mixed	7.3
3.4	42	0.47	Mixed	5.7
3.5	190	0.43	Mixed	3.4
3.6	117	0.42	Mixed	2.5

Table **3.1**. IC_{50} and Mode of Inhibition of Known 2-hetaryl phenol Aurora-A Inhibitors. Preferred Model of Inhibition determined by comparison of inhibition models fit to biological data and compared. α value determined by fit of Equation **3.1** (Fig. **3.3**) to data in GraphPad Prism. See Appendix A for further data.

The preferred mixed-model inhibition observed suggests that each compound inhibits Aurora-A in a non-exclusively ATP-dependent manner. α here describes the affinity with which the inhibitor binds to both the free enzyme (E) and enzyme-substrate (ES) complexes, where when α > 1 the inhibitor preferentially binds the free enzyme, and when α < 1 the inhibitor binds with greater affinity to the ES complex or subsequent species. For purely competitive inhibitors α will tend toward infinity, therefore these inhibitors with relatively low α values suggest a non-competitive mode of inhibition whereby the inhibitors have similar affinity for the (E) and (ES) complexes[132]. This would indicate that the compound neither exclusively competes with ATP, nor does it inhibit in an exclusively un-competitive manner and confirms a mode of inhibition for the series that it was envisaged would be retained across subsequent close analogues. These preliminary results are consistent with previously determined allosteric inhibition and inhibiting Aurora-A through an allosteric mechanism, however further experiments would need to be performed to fully ascertain this mode of action.

3.2.2   Design and Synthesis of a Library of 2-hetaryl Phenols

A targeted library of 2-hetaryl phenol analogues was designed based on the compounds discussed in Sections **2.1** and **2.2**. Around 20 analogues were envisaged to explore SAR around the phenol ring, while leaving the phenol and heterocyclic motifs intact. When considering the simple change from fragment **3.2** to **3.4** by removal of a chlorine, and the significant impact this had on IC_{50} value, a small library mainly exploring mono- and di-halogenated 2-hetaryl phenols was envisaged. This library would explore and extend the existing SAR of the series of fragments, while remaining relatively small in size (≤14 HA).

In addition to envisaged substitution patterns, these analogues were designed based on the formation of an enaminone intermediate from hydroxyacetophenone starting materials and subsequent cyclisation to afford the desired heterocycle. These hydroxyacetophenones were also desirable due to their commercial availability and an envisaged modular synthesis where each starting material enabled the synthesis of multiple final products.

This design would enable straightforward synthesis of multiple 5-membered heterocycles, through cyclisation with hydroxylamine or hydrazine to afford the isoxazole or pyrazole, respectively. Subsequently, functionalisation of these 5-membered ring systems could be performed through formation of substituted chromen-4-ones from the same hydroxyacetophenone starting materials, furnished with a range of biologically or chemically relevant functional groups for immediate biological screening or further chemical functionalisation, following cyclisation to the desired heterocycle.

3.2.2.1   Design of 2-hetaryl Phenol Analogue Library

The design of the small library is summarised in Fig. **3.4** and was intended to explore singly and doubly substituted phenols with a range of halogens, alkyl substituents, amines and methoxy groups. Phenols with single and doubly substituted halogens formed the majority of the library, comprising 17 of the 26 total analogues. Notable analogues include compound **3.8**, containing a methoxy group in place of the phenolic OH to probe effect of substitution, **3.9**, containing a 4-methyl group on the isoxazole to probe the tolerance for functionalisation at this position, and **3.28**, containing a primary amine. Electron-withdrawing groups were included, as well as electron-rich groups in **3.22** and **3.28**.
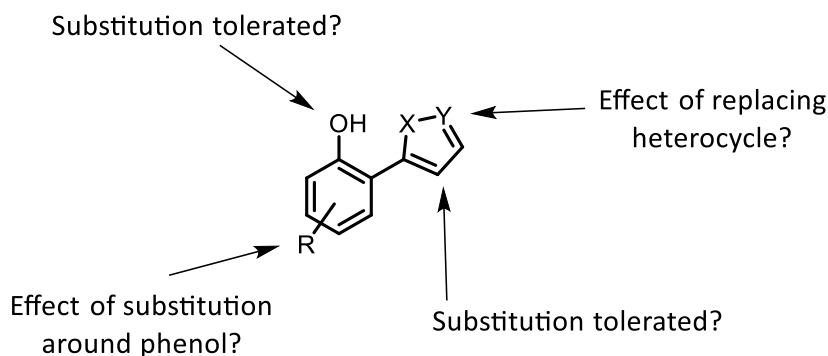
Figure **3.4**. SAR Considerations for 2-hetaryl Phenol Library Design.

Overall, careful design of a small library of compounds enabled exploration of the SAR of the fragment series. It was envisioned this library and subsequent biological screening would provide a baseline of activity with which the best performing analogues would inform design and synthesis of further analogues, *i.e.*, 5-membered heterocycles containing a variety of substitutions to exploit further interactions within the Y-pocket and improve biological potency.

3.2.2.2   Synthesis of 2-hetaryl Phenol Analogue Library

The synthesis of the library is shown in Fig. **3.5**. The synthesis of the enaminone intermediates was performed *via* 2 general protocols. General Procedure **C** was followed where the associated hydroxyacetophenone was dissolved in *N,N*-dimethylformamide dimethylacetal (DMFDA) as solvent and reactant and heated to 90 °C until consumption of starting material was observed by TLC. The solvent was removed *in vacuo* to yield enaminone intermediates in good yield as coloured crystalline solids. General Procedure **D** was followed where the associated hydroxyacetophenone was first dissolved in toluene and heated to 90 °C followed by addition of DMFDA portion-wise and stirred until the reaction was complete, observed by TLC. Removal of the solvent and DMFDA *in vacuo* afforded intermediates in generally good yield.

The enaminone intermediates were then subject to General Procedure **G** or **H** to afford the 5-membered heterocycles. The enaminone intermediates were dissolved in ethanol and subject to heating in the presence of hydroxylamine hydrochloride (General Procedure **G**) or hydrazine monohydrate (General Procedure **H**) to yield their respective isoxazole or pyrazole products in good yields following purification. Alternatively, a telescoped procedure **I** was used with hydroxylamine or hydrazine to yield the isoxazole or pyrazole compound, respectively.
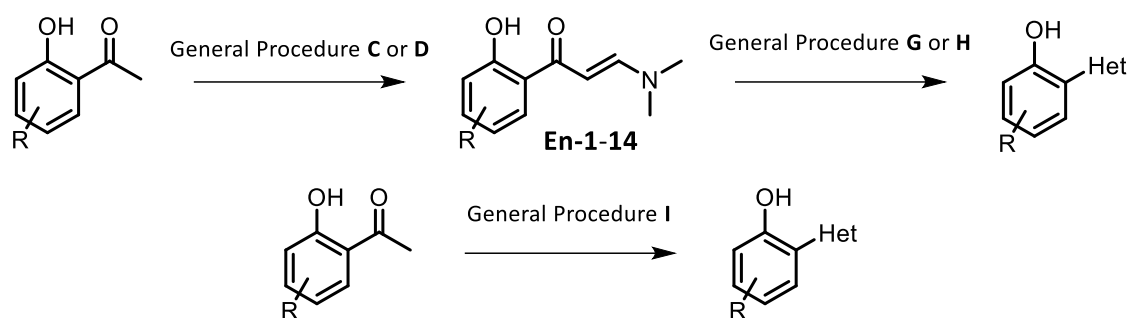
Compound	Phenol Substitution	OH Substitution	Heterocycle	Procedure (Yield)
3.7	3-chloro	N/A	Isoxazol-5-yl	C, G (76%)
3.8[a]	4-chloro	OMe	Isoxazol-5-yl	I (72%)
3.9	4-chloro	N/A	4-methyl Isoxazol-5-yl	I[b] (64%)
3.10	5-chloro	N/A	Isoxazol-5-yl	C, G (68%)
3.11	4,6-chloro	N/A	Pyrazol-5-yl	C, H (81%)
3.12	3-fluoro	N/A	Isoxazol-5-yl	I (77%)
3.13	4-fluoro	N/A	Isoxazol-5-yl	C, G (61%)
3.14	5-fluoro	N/A	Isoxazol-5-yl	I (63%)
3.15	6-fluoro	N/A	Isoxazol-5-yl	D, H (64%)
3.16	4,6-fluoro	N/A	Isoxazol-5-yl	I (73%)
3.17	4-bromo	N/A	Isoxazol-5-yl	C, G (51%)
3.18	5-bromo	N/A	Isoxazol-5-yl	C, G (61%)
3.19	6-bromo	N/A	Isoxazol-5-yl	D, G (63%)
3.20	4,6-bromo	N/A	Isoxazol-5-yl	D, G (63%)
3.21	4,6-bromo	N/A	Pyrazol-5-yl	D, H (77%)
3.22	4-ethyl	N/A	Isoxazol-5-yl	D, H (70%)
3.23	4-chloro,5-methyl	N/A	Isoxazol-5-yl	D, H (66%)
3.24	4-CF3	N/A	Isoxazol-5-yl	C, H (46%)
3.25[a]	4-CF3	OMe	Isoxazol-5-yl	I (55%)
3.26	5-CF3	N/A	Isoxazol-5-yl	D, H (60%)
3.27	4-NH2	N/A	Isoxazol-5-yl	D, H (38%)
3.28	4-OMe	N/A	Isoxazol-5-yl	D, H (56%)

Figure **3.5**. Synthesis and Yields of 2-hetaryl Phenol Library. [a] denotes methylether containing compound was used in reaction, [b] denotes 4-methyl isoxazol-5-yl was prepared from corresponding 1-(5-chloro-2-hydroxyphenyl)propan-1-one. General Procedure **C**: Hydroxyacetphenone (1 eq.), DMFDA, 90 °C. General Procedure **D**: Hydroxyacetophenone (1 eq.) DMFDA (2 eq.), toluene, 90 °C. General Procedure **G**: Enaminone (1 eq.), hydroxylamine hydrochloride (2.5 eq.), EtOH, 85 °C. General Procedure **H**: Enaminone (1 eq.), hydrazine monohydrate (2.5 eq.), EtOH, 85 °C. General Procedure **I**: i) Hydroxyacetophenone (1 eq.), DMFDA (2 eq.), toluene (0.5 M), 90 °C, ii) hydroxylamine hydrochloride (1.5 eq.) **or** hydrazine monohydrate (5 eq.), EtOH, 85 °C.

3.2.3 Biological and SAR Evaluation of 2-hetaryl Phenol Analogue Library

With the library of fragments in hand, biological screening was undertaken against Aurora-A kinase activity to provide biological data for determination of the SAR of the allosteric inhibitor series. A dose-response for each fragment was performed using the Caliper mobility-shift assay in kinetic mode to observe inhibition of Aurora-A, as discussed in Section **3.2.1.2**. A 10-point, 3-fold serial dilution of each fragment was utilised, resulting in a range of concentrations (3 mM – 152 nM). Additionally, each compound was subject to TSA assay, previously described in Section **2.2.8.3**, at 100 µM to observe the effect on thermal stabilisation, therefore ligand binding, of Aurora-A. The results of these assays can be seen in Table **3.2** and are summarised in Fig. **3.6**.

Methylation of the phenolic OH, seen in compounds **3.8** and **3.25**, resulted in a significant decrease in biological potency of between 6- to 20-fold when compared to the free hydroxyl counterparts **3.4** and **3.24**, indicating this OH is important for the biological activity of the series. The crystal structures of **3.1** and **3.2**, see Fig. **3.2**, show this OH occupying the same location within the Y-pocket despite the different binding poses observed between the two, indicating that this is likely important for binding. Precluding this binding through methylation of this position is therefore detrimental to the inhibition potential of the compound series.

Similarly, when substituting the 5-membered heterocycle at the 4-position, as seen in compound **3.9**, the potency of the compound was reduced by roughly 10-fold compared to compound **3.4**. This indicated the addition of groups in this position would likely be detrimental to the potency. Comparison of the ligand poses seen in Fig. **3.2** shows compounds **3.1** and **3.2** are relatively planar when bound, allowing the OH to occupy the top of the pocket. Compound **3.9** however, would likely adopt a more twisted confirmation due to the steric clash between the phenol ring and methyl group and this change in conformation may account for the reduction in observed potency by forcing an unfavourable ligand binding pose.

Compound	Phenol Substitution	OH Substitution	Heterocycle	IC$_{50}$ (uM)	Ligand Efficiency (LE)	ΔTm (°C)
3.7	3-chloro	N/A	Isoxazol-5-yl	366	0.37	0.99
3.4	4-chloro	N/A	Isoxazol-5-yl	42	0.47	2.01
3.8	4-chloro	OMe	Isoxazol-5-yl	>1000	0.32	1.54
3.9	4-chloro	N/A	4-methyl Isoxazol-5-yl	395	0.34	0.77
3.10	5-chloro	N/A	Isoxazol-5-yl	430	0.36	1.53
3.3	6-chloro	N/A	Isoxazol-5-yl	153	0.41	0.72
3.6	6-chloro	N/A	Pyrazol-5-yl	118	0.42	1.45
3.2	4,6-chloro	N/A	Isoxazol-5-yl	121	0.39	1.38
3.11	4,6-chloro	N/A	Pyrazol-5-yl	528	0.33	2.98
3.12	3-fluoro	N/A	Isoxazol-5-yl	401	0.37	0.67
3.13	4-fluoro	N/A	Isoxazol-5-yl	128	0.42	1.60
3.14	5-fluoro	N/A	Isoxazol-5-yl	247	0.39	0.74
3.15	6-fluoro	N/A	Isoxazol-5-yl	212	0.40	0.48
3.16	4,6-fluoro	N/A	Isoxazol-5-yl	231	0.36	0.63
3.1	4,6-fluoro	N/A	Pyrazol-5-yl	765	0.31	N/A
3.17	4-bromo	N/A	Isoxazol-5-yl	74	0.44	4.67
3.18	5-bromo	N/A	Isoxazol-5-yl	>1000	0.32	1.71
3.19	6-bromo	N/A	Isoxazol-5-yl	113	0.43	0.65
3.20	4,6-bromo	N/A	Isoxazol-5-yl	23	0.46	2.49
3.21	4,6-bromo	N/A	Pyrazol-5-yl	510	0.33	4.42
3.29	4-methyl	N/A	Isoxazol-5-yl	97	0.43	1.46
3.22	4-ethyl	N/A	Isoxazol-5-yl	85	0.41	1.45
3.23	4-chloro,5-methyl	N/A	Isoxazol-5-yl	>1000	0.30	2.18
3.24	4-CF$_3$	N/A	Isoxazol-5-yl	90	0.35	N/A
3.25	4-CF$_3$	OMe	Isoxazol-5-yl	565	0.28	1.05
3.26	5-CF$_3$	N/A	Isoxazol-5-yl	>1000	0.26	0.53
3.28	4-NH$_2$	N/A	Isoxazol-5-yl	385	0.37	N/A*
3.29	4-Me	N/A	Isoxazol-5-yl	110	0.40	1.46
3.5	N/A	N/A	Isoxazol-5-yl	190	0.43	N/A

Table **3.2**. Biological Screening Results of 2-hetaryl Phenol Library. IC$_{50}$ values determined by mobility-shift assay against Aurora-A activity, at 25 nM Aurora-A^{CM}, 2.5% final DMSO concentration and a 3-fold, 10-point serial dilution of fragment from 3 mM to 152 nM. ΔTm values determined by DSF assay in the presence of 100 μM fragment. IC$_{50}$ values in green indicate improved potency over previous best-in-class (42 μM). ΔTm values in green indicate value ≥1.5 °C, considered significant. * Compound **3.28** was darkly coloured and interfered with assay, therefore was omitted.

Brief exploration of the SAR of the 5-membered heterocycle was also performed, exemplified in compounds **3.6**, **3.11** and **3.21** containing pyrazole rings. Compound **3.6** showed a small increase in potency over the isoxazole counterpart; however, this was not significantly large enough to warrant further investigation. Additionally, compounds **3.11** and **3.21** showed

large decreases in potency of roughly 5- to 20-fold, respectively, over the isoxazole-based compounds. This indicates that the isoxazole is the favourable heterocycle for this series over pyrazoles. Interestingly, these compounds showed significant ΔTm suggesting that, while poor inhibitors of Aurora-A, they were able to bind and stabilise quite effectively.

Finally, the SAR of the phenol ring substitutions was determined. Substitutions at the 3-position were shown to be unfavourable, with compounds **3.7** and **3.12** (3-chloro and 3-fluoro, respectively) displaying a decrease in potency of 4- to 10-fold compared to analogues similarly substituted at the 4- and 6-positions. Substitution at the 5-position was similarly detrimental, with compounds **3.10**, **3.14**, **3.18**, and **3.26** all showing poor biological activity when compared to identical groups substituted at the majority of different positions around the ring.
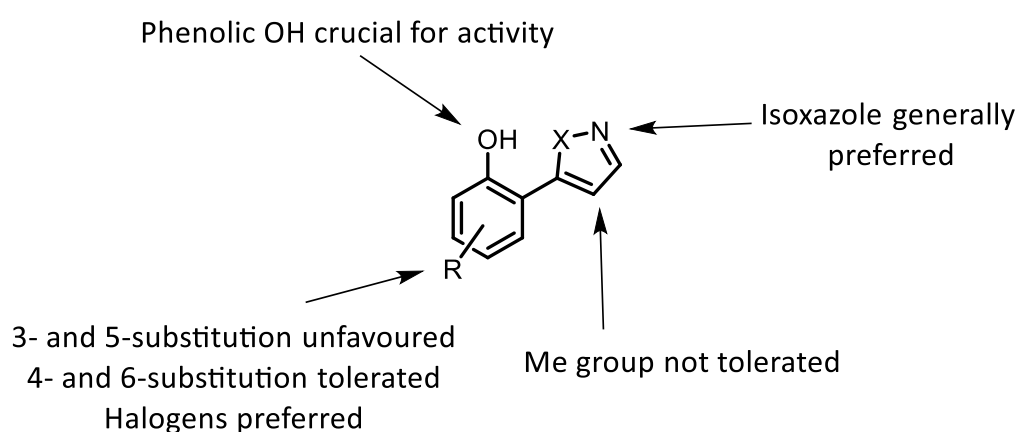
Figure **3.6**. Summary of SAR for 2-hetaryl Phenol Library.

Substitution at the 6-position of the ring was tolerated, with chloro- and bromo-substituted compounds **3.15** and **3.19** showing only small decreases in potency compared to more detrimental substitution. Substitution at the 4-position, however, appeared to be more beneficial. Singly substituted analogues were all more potent when substituted at the 4-position when compared to a different position, *e.g.*, the 4-chloro substituted compound **3.4** was more potent than the closely related 3-, 5-, or 6-chloro substituted analogues. Several different groups in this position were also tolerated, encompassing a fairly diverse range of substituents without large detrimental effects on potency. Additionally, ΔTm values were significant with compounds **3.4**, **3.13**, and **3.17**, indicating single substitutions at this position are beneficial for binding and stabilisation of Aurora-A. The greatest overall increase in potency was observed with 4,6-dibromo compound **3.20**, however, showing a 2-fold increase in potency over the previously most potent compound **3.4** from 42 to 23 μM, and ΔTm of 2.49 °C.

Having identified productive substitution and generated SAR around the 2-hetaryl phenol series, it was envisaged that a docking study could be performed to guide rational design of further analogues. Substitution from the 3-position of the 5-membered heterocycle had so far been unexplored experimentally, therefore an *in silico* approach exploring different substitutions with varying structural and electronic motifs would be employed to focus further synthetic efforts. These docking results would be combined with the best performing compounds identified through the SAR study and be used to guide further elaboration.

3.2.4   *In silico* docking of 2-hetaryl Phenol Series to Aurora-A

Following the limited SAR determined, described in Section **3.2.2** through synthesis and biological evaluation of a series of fragments, it was sought to complement this study through *in silico* docking of a much larger virtual library of analogues to inform further molecular design and synthesis. Typically docking studies will utilise very large *in silico* libraries (>1 million) of fragments/medicinally relevant compounds and dock these to a single crystal structure or receptor for the generation of hit matter. The highest scoring compounds are then either subject to further *in silico* studies or synthesised and tested against the target of interest. Similarly, docking can be used to guide rational design when optimising a series of hit compounds *in lieu* of other structural information such as a co-crystal structure.

Ensemble docking strategies have been employed as a way of capturing multiple states of dynamic protein targets, docking against multiple related structures and collating results to identify structural trends to guide compound design[133]. Typically used with MD-derived simulated protein structures or multiple conformers determined by NMR[134], ensemble docking intends to sample and dock against a number of conformations of the same protein, *e.g.*, several NMR determined structures capturing the dynamics of a protein in solution, and collate results to guide molecular design.

Aurora-A, however, is a highly dynamic kinase, to the point that full structural assignment by NMR has so far proven unattainable. It is a well-studied protein by XRD, however, with >170 distinct structures present in the Protein Data Bank (PDB). These structures are highly diverse, including apo, ADP-bound, inhibitor-bound, bound to various peptides, proteins and affimers, and in various states of phosphorylation. These Aurora-A structures are also in various states of activation, with the Y-pocket architecture related to the position of the αC-helix and therefore the Lys-Glu salt bridge critical for kinase activity. X-Ray crystallography, however,

inherently captures a static conformation of the protein in question, meaning ensemble docking is impossible.

It was envisaged that exploring several different Y-pocket conformations found in a range of Aurora-A crystal structures in different states of activation *via* docking may enable the identification of improved allosteric binders to this pocket. Similarly, the 2 distinct binding poses of 2-hetaryl phenol ligands in this pocket, see Fig. **3.2**, suggests docking a focused library that exploit multiple vectors may be productive for compound design. A small virtual library would be designed and docked against selected Aurora-A structures. Collation and analysis of the highest docking scored compounds from each Aurora-A structure would then be scrutinised to determine the most common positions of substitution around the core scaffold and subsequently the most common structural motifs found in these positions. These results would then be used to guide design and synthesis of a small library of functionalised 2-hetaryl phenol compounds for biological evaluation though focusing on the structural features in the enriched top 10% of docked compounds.

3.2.4.1 Design of 2-hetaryl Phenol Virtual Library

A virtual library was designed based around the 2-hetaryl phenol series of Aurora-A inhibitors, described in Section **3.2.2**. Library design was undertaken based on availability of structural diversity, availability of starting materials, synthetic tractability of products, and explored four different positions around the bicyclic scaffold, see Fig. **3.7**. Library design was split in to four distinct areas of variation: substitution of phenolic OH, substitution from the 3-position of the 5-membered ring, the 5-membered heterocycle, and substitution around the phenol ring.
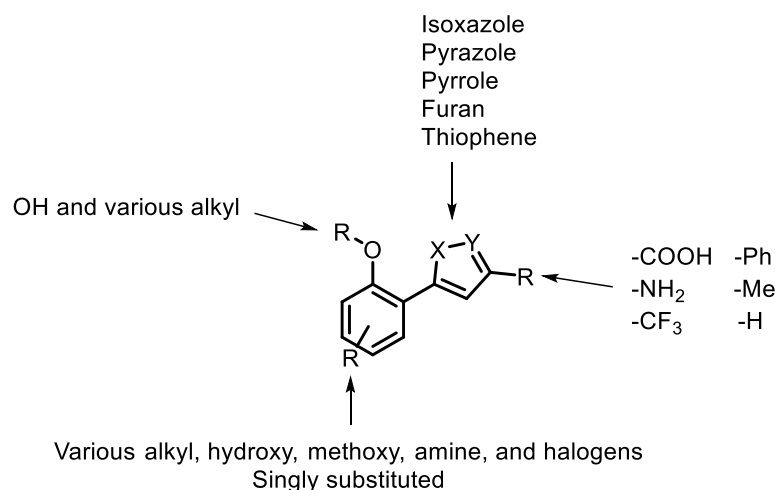
Figure **3.7**. General Design of *in silico* library of 2-hetaryl phenol-based inhibitors.

The phenol OH was substituted with alkyl substituents of varying length and cyclic aliphatic substituents, to permit molecular understanding of the effect of substitution at this position from previous experimentally determined results. Substitution from the 3-position of the 5-membered ring enabled the effect of H-bond acceptors and donors, hydrophobic groups and electron withdrawing effects to be explored. The 4-position of the heterocycle was left unsubstituted as previous results indicated this to be an unfavourable position for functionalisation, see Section **3.2.2**. Substitution around the 6-membered ring had a significant impact on the IC$_{50}$ value, as previously discussed, therefore the library contained the largest variety of substituents around the ring. Finally, the 5-membered ring was explored to determine its impact on docking score. Prior crystal structures compared in Fig. **3.2** indicated the pyrazole and isoxazole did not make important interactions due to the flipped poses between the compounds, therefore this position was explored with a range of 5-membered rings to determine if substitution at this position would inform further design and synthesis. Full design of the 2726-membered virtual library can be seen in the Appendix.

3.2.4.1.1   Analysis and Comparison of Aurora-A Crystal Structures

To obtain a reliable and accurate set of potentially improved compounds from the docking experiments, careful selection of relevant Aurora-A structures in which to dock was considered important. Prior work in the Bayliss group by Mathilde Suarez, under my supervision, performed an analysis of Aurora-A structures from the PDB, identifying the activation state of each kinase through determination of Lys-Glu salt bridge distances and DFG motif location[135]. Y-pocket volume and druggability were also assessed, providing a metric by which to determine

the suitability of each crystal structure for inhibitor binding. This analysis was initially utilised to select crystal growth conditions amenable for Y-pocket allosteric inhibitor binding for ongoing structural determination of inhibitor binding.

It was envisaged that a docking study could be performed across several suitable Aurora-A structures, identified from this prior analysis, to identify potentially improved binders for the Y-pocket. These structures would form the ensemble from which the docking results would be collated and analysed for further inhibitor design. This would be performed through enrichment of the library to focus on only the highest scoring docked compounds, followed by analysis of the structural motifs found within this enriched set.

3.2.4.1.2   Selection of Aurora-A Structures for *in silico* docking

Selection of Aurora-A structures for the docking study was based on calculated druggability of the Y-pocket, kinase activation state, and presence of ligands in Y-pocket. The 10 PDBs are shown in Table **3.3** and sample a variety of activation states of the kinase (active and intermediate) with desirable Y-pocket druggability scores. Druggability scores >0.8 are usually considered the minimum by which to consider a site druggable[136], considered a difficult target, while values >1 indicate a druggable site, with the larger the value the more amenable the pocket considered to drug development. Four of the 10 crystal structures selected have Y-pocket druggability values <0.8 but were included in the set due to similarity to a fully inactive kinase (3EFW and 3P9J)[135], archetypal active Aurora-A structure (4CEG), and the presence of an existing inhibitor (5DN3).

The remaining structures have druggability scores (DScores) >0.8 to a maximum of 0.92 (3W16), considered sites that may still be difficult to drug.[136] This is unsurprising considering the target is a pocket distant to the active site that is shallower, more exposed to solvent, and lacking a deep hydrophobic region typical in well defined, druggable, binding sites. It was envisaged that by sampling and collating docking data from several so-called undruggable and difficult Y-pocket structures a clearer picture of potentially beneficial substitutions of the 2-hetaryl phenol fragment series may be formed for further compound synthesis.

PDB ID/Crystal Structure	Y-pocket Druggability (DScore)	Activation State	Active Site Ligand	Y-pocket Ligand
5L8L	0.85	Intermediate	No	No
3EFW	0.75	Intermediate	Yes	No
3LAU	0.85	Intermediate	Yes	No
3P9J	0.75	Intermediate	Yes	No
3W16	0.92	Intermediate	Yes	No
4CEG	0.78	Active	No	No
4JBQ	0.80	Intermediate	Yes	No
5DN3	0.77	Active	No	Yes
5ORY	0.87	Active	No	Yes
O-Chloro	0.86	Intermediate	No	Yes

Table **3.3**. Druggability and Y-Pocket Volume of Selected Aurora-A Structures. Druggability determined in Schrodinger Maestro using the SiteMap module. Activation state determined through analysis of DFG-motif position and Lys-Glu salt bridge distance.[135] Active Site Ligand refers to the presence or absence of a small molecule bound to the ATP-binding site. Y-Pocket Ligand refers to presence or absence of a small molecule bound to the Y-pocket.

3.2.5 *In silico* docking of 2-hetaryl phenol-based library against Aurora-A Structure Ensemble

3.2.5.1 Analysis of Docking Results

Schrödinger Maestro[137] was used to dock the focused library of *ca.* 2700 2-hetaryl phenol analogues against the ten selected Aurora-A structures using the Glide module[138] (for experimental details, see: Chapter **4.X**). Only the top 200 scoring compounds from each data set were selected for further analysis, enriching the structural motifs to only those with higher docking scores, therefore guiding future compound design and synthesis toward compounds with potentially improved binding characteristics. These results can be seen in Fig. **3.8**, with the top 200 compounds from two example docked kinase structures highlighted in red on a plot of HA count against docking score.
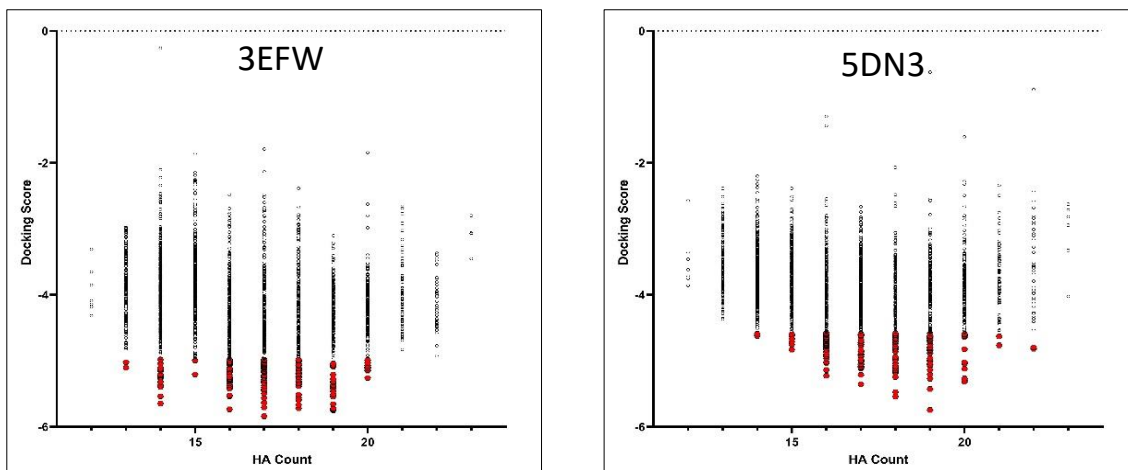
PDB ID/Crystal Structure	Average Docking Score	Average Enriched Docking Score
3EFW	-4.11	-5.25
3LAU	-3.30	-4.30
3P9J	-3.37	-4.45
3W16	-3.33	-4.47
4CEG	-3.12	-3.92
4JBQ	-3.87	-5.05
5DN3	-3.84	-4.84
5L8L	-3.46	-4.67
5ORY	-3.82	-4.80
O-chloro	-3.30	-4.35

Figure **3.8**. *In silico* docking results against Aurora-A ensemble. Average Enriched Docking Score refers to Top 200 docking scored compounds from each data set.

The enriched data were then analysed to determine the structural motifs present in each of the top 200 docked compounds for each kinase. This analysis was performed sequentially, first identifying enriched structural motifs at the 3-position the 5-membered heterocycle. These enriched moieties were then fixed as part of the central scaffold and substitution around the remainder of the analogue was determined.

The results of the initial analysis are shown in Fig. **3.9**, organised by the different 5-membered ring substitutions. Each kinase is shown as a circular plot, where the area of the circle represents the enrichment factor of the associated substitution compared to the entire virtual library. *E.g.*, Fig. **3.9**-**A** shows 3-COOH substitution from the heterocycle, where PDB 3P9J has a 3.6 fold enrichment of 3-COOH in the top 200 docking scored compounds compared to the

library as a whole. This enrichment value is simply the factor by which the highlighted structural feature is found in the top 200 docked compounds against each kinase compared to the entire virtual library and shown only when the value is >1. This analysis was intended to enable easy, visual, identification of enriched structural features that may lead to improved inhibitors when validated experimentally.

Carboxylic acid and trifluoromethyl substitution at the 3-position of these varying ring systems were the most enriched structural features, shown in Fig. **3.9**-**A** and **3.9**-**C**. 3-carboxylic acids were enriched by 1.4- to 3.6-fold in all of the docked data sets, while 3-trifluoromethyl groups were enriched by 1.2- to 3.6-fold across the majority of data sets. Phenyl, methyl and amine groups seen in Fig. **3.9**-**B**, -**D** and -**F**, conversely, were only enriched in a maximum of two data sets, while an unsubstituted 3-position was not enriched at all. This data suggests that substituting the 3-position of the 5-membered heterocycle with a carboxylic acid or trifluoromethyl group has a positive impact on the docking score across the majority of docked kinase structures, therefore may have a beneficial effect on binding and inhibition of Aurora-A. Only compounds containing 3-COOH and 3-CF_3 were therefore taken forward in the docking analysis workflow to determine functionalisation at other positions.

Analysis of the phenolic OH position showed that substitutions from this position other than H were detrimental to the docking score, highlighting the importance of this as the free phenolic OH. This docking result correlates well with the experimentally determined effect of methylation at this position, see Section **3.2.2** and compounds **3.8** and **3.25**. While only the OH was considered for further synthesis, substitutions from this position were permitted and subsequently ignored during onward analysis of docking data to ensure all substitution was considered at the remaining positions around the scaffold. Similarly, the 5-membered ring system made little difference to the overall docking score. When combined with 3-COOH and 3-CF_3 substitutions no single 5-membered ring system was enriched over the whole library, indicating that changing this had very little effect on the docking efficacy of the compounds and were therefore permitted but deprioritised for further analysis.
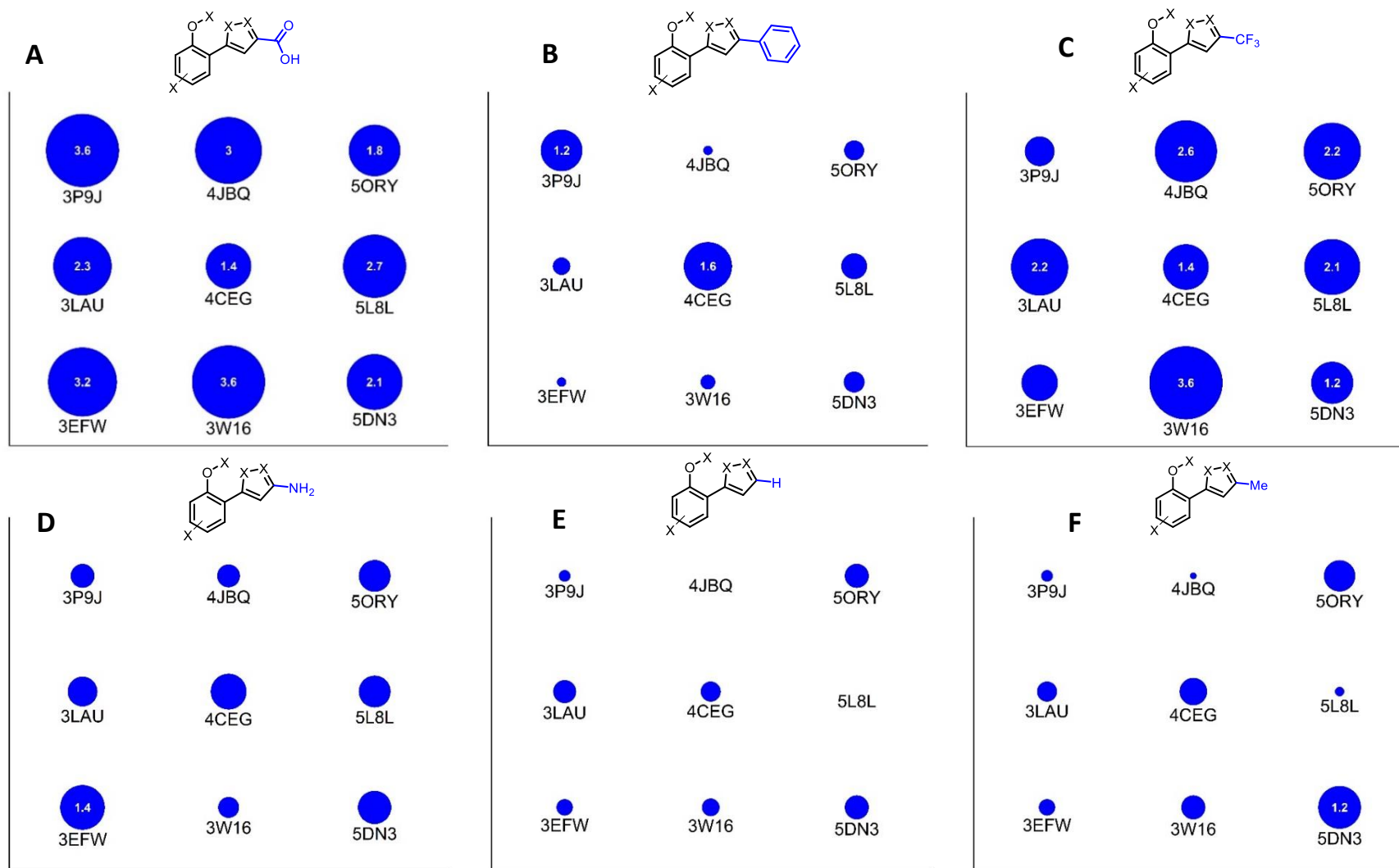
Figure **3.9**. Docking Analysis of 5-membered heterocycle substitution. Enrichment factor corresponds to the factor by which the highlighted structural feature is found in the top 200 docked compounds against each kinase, compared to the entire virtual library and shown only when the value is >1. Numerical value and circle area correspond to enrichment factor of each substitution, highlighted in blue.

94

When fixed with 3-COOH or 3-CF$_3$ substitutions from the 5-membered heterocycle, and with all substitutions permitted at the phenolic OH and 5-membered heterocycles, analysis of the 6-membered ring substitution pattern was performed. This showed the 4- and 6-positions of the phenol ring to be the most frequently substituted with a 3-COOH substituent from the 5-membered ring, and the 4-, 5- and 6-positions most substituted with a 3-CF$_3$ on the 5-membered ring.

The most frequent substitutions at these positions were plotted, shown in Fig. **3.10**. The frequency each substituent is represented by the colour of the heat map, with the darker colour representing more compounds in the data set that contain the structural motif shown on the Y-axis, as a proportion of the total. White areas indicate the structural feature from that row is not found in the docked data set for that kinase. At this stage, substitutions of H at each position are omitted for clarity.

When the 5-membered ring has a 3-COOH substitution, ten different substituents are found at the 6-position across the docked data set, Fig. **3.10**-**A**. Of these ten, CF$_3$ and CF$_2$H are the most common with CF$_3$ found in all docked data sets and CF$_2$H found in all but one. These substitutions also form a high proportion of the different groups find in this position, indicated by the darker colour on the heatmaps. Next most common are *i*Pr and OH groups, with seven of the ten docked data sets containing these structural motifs at the 6-position. Substitution at the 4-position (R$_6$) is similar in its structural motifs, Fig. **3.10**-**B**, with eleven different substituents found in this position. Similar to the 6-position, CF$_3$ and CF$_2$H are present in all docked data sets across the kinase structures in high proportions. Substitution at this position with Cl is also common, appearing in eight of the ten data sets.

When the 5-membered heterocycle was substituted with a 3-CF$_3$ group, Fig. **3.11**-**C**-**E**, the 4-, 5-, and 6-positions of the scaffold phenol were frequently substituted with OH groups, represented in ≥80% of the ten kinase structures. While a positive result from the docking, benzenediols are potentially susceptible to oxidative and metabolic instability in downstream drug development, so these were considered unsuitable for further development at this point. Substitution with Br groups at these positions were also common, present in ≥70% of kinase data sets and were therefore considered for further development.

Figure **3.10.** Docking Analysis of 6-membered ring substitution. Heatmap corresponds to kinase structure docked against on X-axis and structural motifs on Y-axis. The darker the colour, the higher proportion of each substitution found at highlighted position. Panel **A** and **B** show fixed 3-COOH from heterocycle, with enriched CF_3 and CF_2H features at the 2- and 4-position highlighted in red. Panel **C-E** show fixed 3-CF_3 from heterocycle, with enriched Br groups highlighted in red.

96

Several interactions across the CF$_3$- and CF$_2$H-containing fragments docked within the Y-pocket may explain the increase in docking score for this series. As shown in Fig. **3.11**, a typical docking pose and binding interaction map of 5-[2-hydroxy-5-(trifluoromethyl)phenyl]-1,2-oxazole-3-carboxylic acid **3.24** shows a flipped pose when compared to the crystal structure, see Fig. **3.2**, picking up an H-bonding interaction between the phenolic OH and Glu175 backbone carbonyl. In this orientation, the CF$_3$ group is partially buried in a hydrophobic region that forms the surface of the pocket while the COO$^-$ group is making a H-bonding interaction with Lys166 in a solvent exposed region.
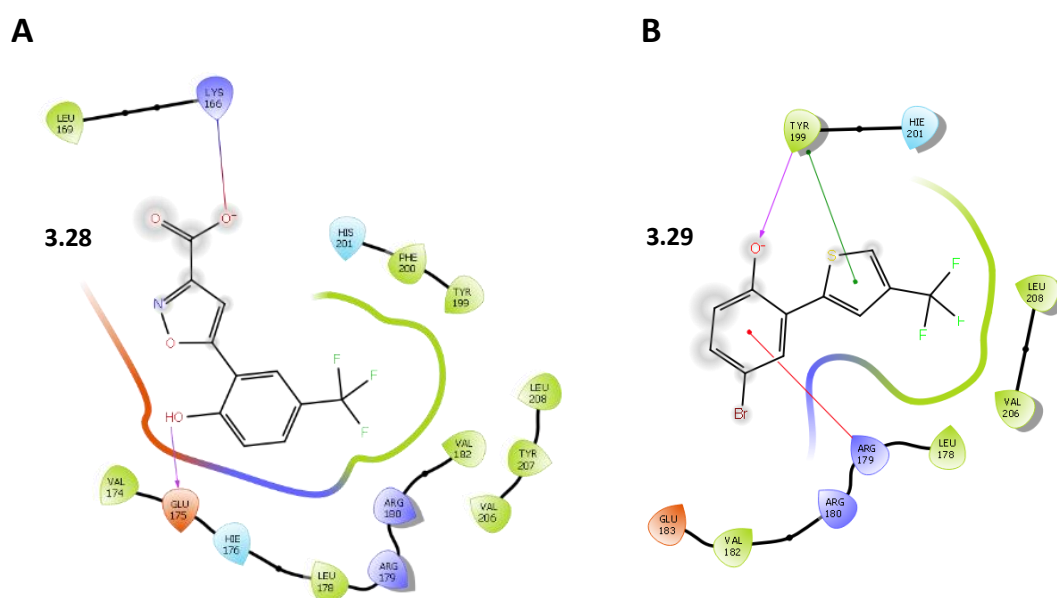
Figure **3.11**. Ligand Interaction Diagrams of Exemplar Docking Results. Red/blue line indicates ionic interaction, pink arrow indicates H-bond, green line indicates π-π stacking, red line indicates cation-π interaction. Panel **A**: Example of 5-[2-hydroxy-5-(trifluoromethyl)phenyl]-1,2-oxazole-3-carboxylic acid **3.28** interactions with docked PDB 3LAU. Panel **B**: Example of 4-bromo-2-[4-(trifluoromethyl)thiophen-2-yl]phenol **3.29** interactions with docked PDB 4JBQ.

3-CF$_3$ substituted heterocycles, exemplified by 4-bromo-2-[4-(trifluoromethyl)thiophen-2-yl]phenol **3.28** in Fig. **3.11**-**B**, appear to project the CF$_3$ group toward the hydrophobic region much like the carboxylic acid substituted compounds and gain an additional H-bonding interaction with Tyr199, potentially leading to the increase in docking score. These compounds, however, are enriched to a lesser extent than their 3-COOH counterparts, indicating the quality of these interactions is likely lower, and were therefore considered lower priority for subsequent synthetic efforts.

The outcome of the docking analysis is summarised structurally in Fig. **3.12**. Two product classes were considered for synthesis and biochemical evaluation: a 3-COOH substituted 5-membered heterocycle series with a CF_3 group the 4- or 6-position of the phenol; and a 3-CF_3 substituted 5-membered heterocycle series with a bromo group in the 4-, 5-, or 6-position. The chosen series of compounds maintained the 5-membered heterocycle as an isoxazole-5-yl or pyrazol-5-yl due to the lack of enrichment of any one series in the docking. Finally, the phenolic OH was maintained due to the apparent importance of this group for the docking score. It was envisaged this docking study and subsequent outcome would be combined with the SAR determined in Section **3.2.2** to guide design of further analogues of the 2-hetaryl phenol series. While useful, it is worth noting the docking outcome was meant only to supplement the experimentally determined SAR rather than supplant it, and any potentially detrimental substitutions with existing SAR evidence would not be included in further analogue design, as discussed in Section **3.3.1**.

X = O or NH
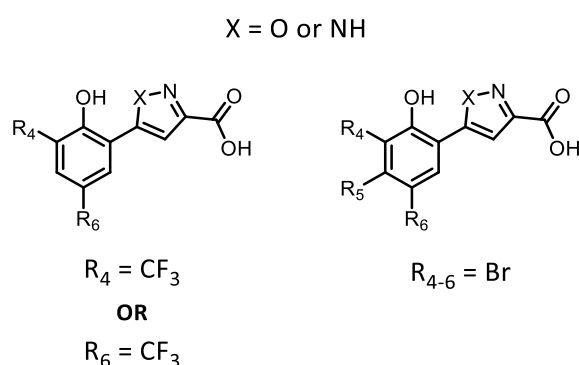
Figure **3.12**. Summary of Prioritised Structures for synthesis identified through docking analysis.

3.2.6 Further SAR of 2-hetaryl Phenol Fragment Series

With the experimentally determined SAR and docking study results in hand, a number of elaborated 2-hetaryl phenol analogues were designed, synthesised and screened against Aurora-A. These compounds were intended to broaden the SAR of the series through substitution from the 5-membered heterocycle suggested by docking combined with the existing SAR of substituted phenols determined in Section **3.2.2** and would serve to both improve biological potency and validate the ensemble docking strategy employed.

3.2.6.1 Docking and SAR guided design of 2-hetaryl phenol analogues

Design of the analogues was informed by prior SAR determination and docking studies, described in Sections **3.2.2** and **3.3.1**, respectively. Docking-guided substitution of the phenolic ring included CF_3 groups at the 4- and 5-positions, while the CF_3 substitution was omitted from the 6-position due to lack of availability of the starting materials and the minimal effect this position had been shown to have on biological potency. Benzenediols suggested by the docking were also omitted as these motifs have potential metabolic liabilities, as previously discussed. 2,4-Dibromo-6-(1,2-oxazol-5-yl)phenol also formed the basis for elaboration from the 5-membered heterocycle due to the observed increase in potency of compound **3.20**, while the singly substituted 4-bromo-2-hetaryl phenol suggested by docking was omitted due to the relatively poor improvement in potency of compound **3.11** in Section **3.2.2**. 2,4-dichloro-6-(1,2-oxazol-5-yl)phenol **1** and 4-chloro-6-(1,2-oxazol-5-yl)phenol **6** were included as previous best-in-class inhibitors from this series to provide a consistent point of reference from which to build further understanding of the SAR. Substitution from the 3-position of the 5-membered heterocycle consisted of carboxylic acids, CF_3, CF_2H, or methyl groups. While the CF_2H was not included in the docking study at this position and the methyl group had performed poorly, these were straightforward to synthesise *via* the same route as the CF_3 substituted analogue. Similarly, facile reduction of the carboxylic acid resulted in inclusion of methylhydroxy compounds. Finally, these analogues contained isoxazole and pyrazole rings, rather than furan, pyrrole or thiophene utilised in the docking study, due to the lack of heterocycle enrichment observed in the docking and to retain synthetic tractability from existing starting materials. The design of the small library can be seen in Fig. **3.13**, consisting of 13 compounds total.
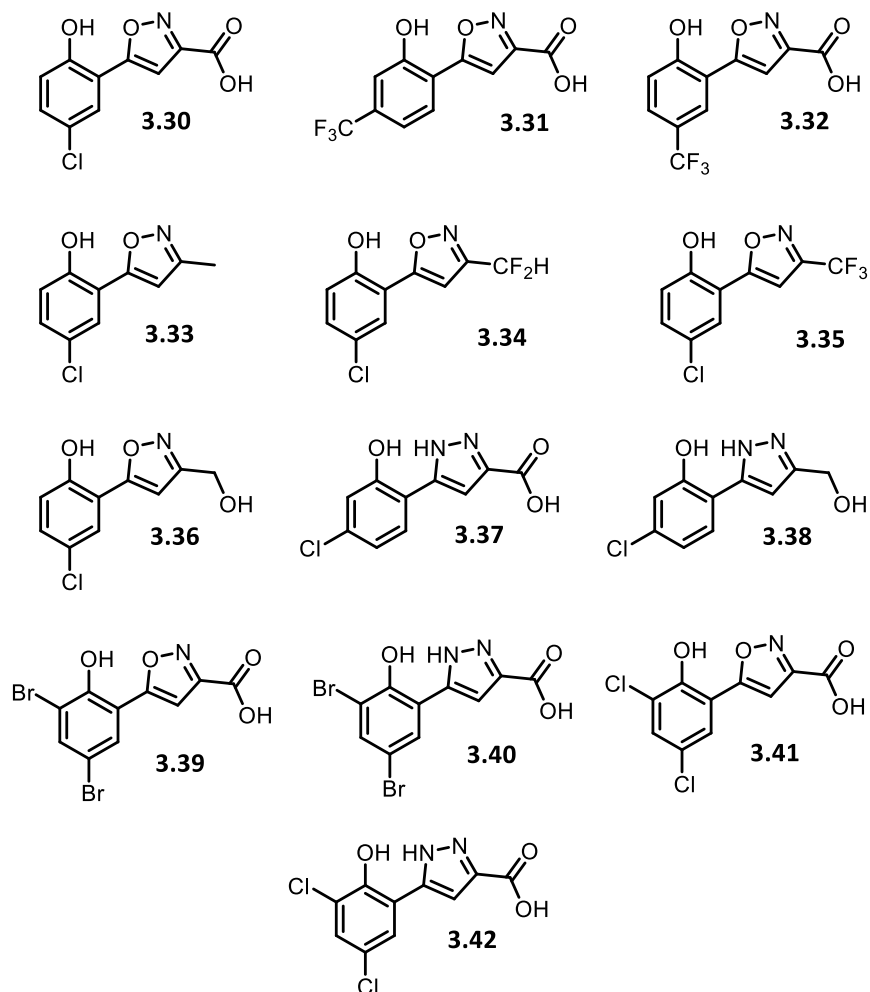
Figure **3.13**. Design of Library for SAR Exploration of 5-membered heterocycle substitution.

3.2.7 Synthesis of Further Analogues

Chromenone intermediates of COOH substituted compounds **3.30-3.32**, **3.37**, and **3.39-3.42** were synthesised prior to cyclisation. Briefly, the associated hydroxyacetophenone was dissolved in diethyl oxalate and added portion-wise to a stirred solution of NaOEt in EtOH (21% w/v) and heated to 70 °C. Following consumption of the starting material observed by TLC and aqueous work-up, the resulting yellow oils were stirred in AcOH with conc. HCl (3:1) at 85 °C overnight, before cooling to room temperature, diluting with H_2O and filtration of the solid precipitate to yield the intermediate chromenones. These were then stirred subject to General Procedure **J** or **K** to yield the substituted isoxazole or pyrazole products, respectively.
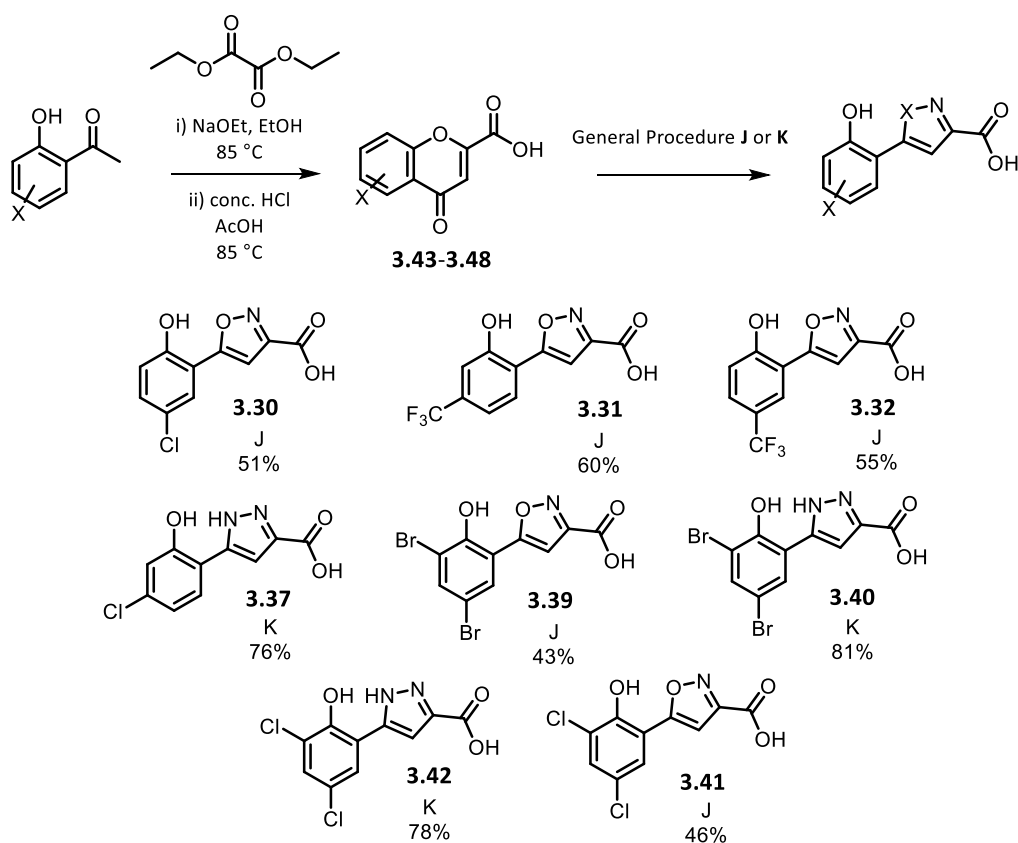
Scheme **3.2**. Synthesis of Carboxylic Acid Substituted Fragments. Yields reported over 2 steps. General Procedure **J**: Chromenone (1 eq.), hydroxylamine hydrochloride (2 eq.), KOH (3 eq.), EtOH, rt. General Procedure **K**: Chromenone (1 eq.), hydrazine monohydrate (2.5 eq.), EtOH, rt.

Fragments **3.33**-**3.35** were also synthesised from the associated hydroxyacetophenones, shown in Scheme **3.3**. Briefly, the hydroxyacetophenone was dissolved in the associated ethyl acetate, added to a stirred solution of NaH in THF (amount) and heated to 80 °C for three hours. The solution was cooled to room temperature and following an aqueous work-up, the organic solvent was removed *in vacuo* and the residual material subjected to purification to afford chromenones **3.49**-**3.51** in good yield. Attempts to cyclise these chromenones under the same conditions as shown in Scheme **3.2** resulted poor conversion of the starting material, with only trace amounts of desired product observed by crude NMR and LC-MS. The mass of **3.52**, however, was observed as the major product, indicating the formation of an oxime was taking place but the desired cyclisation was not.

Reaction conditions were altered to favour the formation of this intermediate, observed in good yield, which was then subject to acidic conditions that promoted the cyclisation to the desired substituted isoxazole **3.33**. Finally, these compounds were considered potentially amenable to telescoping of the intermediate step. The final optimised reaction conditions are

shown in Scheme **3.3**, furnishing substituted isoxazoles **3.50** and **3.51** in moderate but comparable yield following purification.
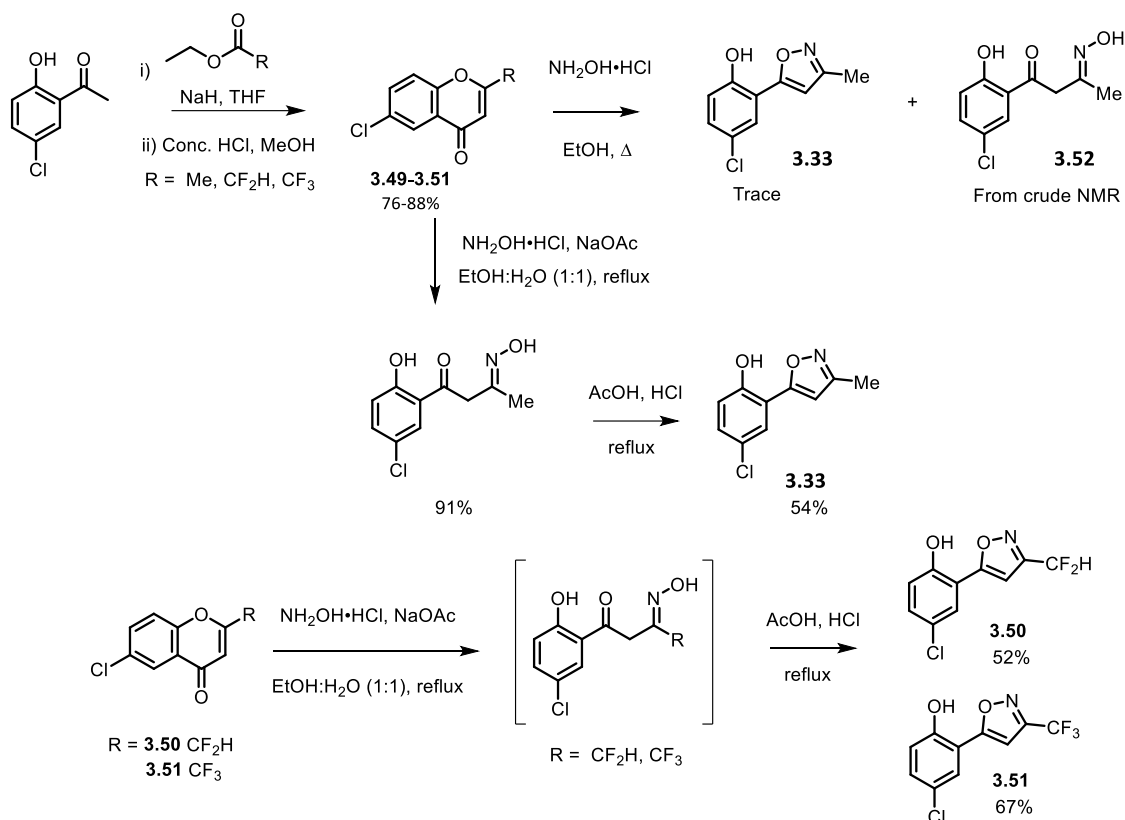
Scheme **3.3**. Synthesis of CH₃, CF₂H, and CF₃ substituted analogues.
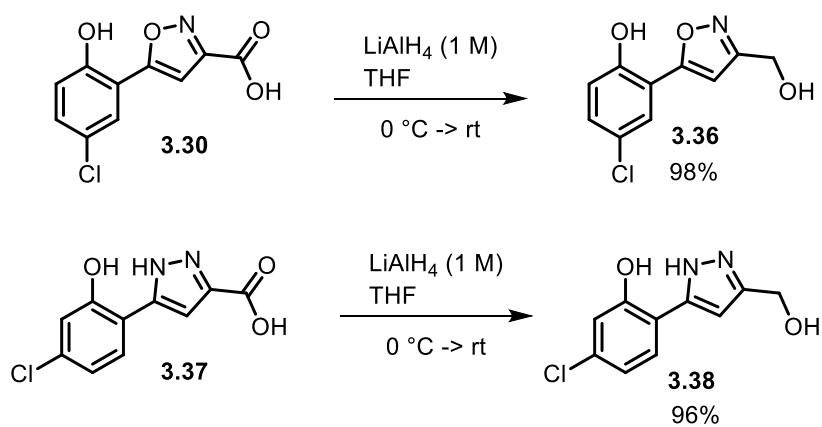
Scheme **3.4**. Synthesis of methylhydroxy substituted analogues.

Synthesis of hydroxymethyl-substituted compounds **3.36** and **3.38** was performed *via* the LiAlH$_4$-mediated reduction of the carboxylic acids **3.30** and **3.37**, shown in Scheme **3.4**. Briefly, the respective carboxylic acid was added dropwise to a stirred solution of LiAlH$_4$ in THF at 0 °C under inert atmosphere, and stirred for 2 h. Following quench and aqueous work-up, the hydroxymethyl-substituted compounds **3.36** and **3.38** were obtained in excellent yield.

3.2.8   Biological Evaluation of 5-membered ring analogues

With the additional library of fragments in hand, biological screening was undertaken against Aurora-A kinase activity to provide biological data for determination of the SAR of the elaborated inhibitor series. A dose-response for each fragment was performed using the Caliper mobility-shift assay in kinetic mode, as discussed in Section **3.2.2**. A 10-point, 3-fold serial dilution of each fragment was utilised, resulting in a range of concentrations (3 mM – 152 nM). Additionally, each compound was assayed *via* DSF, previously described in Section **3.2.2**, at 100 µM. The results of these assays can be seen in Table **3.4** and are summarised in Fig. **3.14**.

Compound	Phenol Substitution	Heterocycle	IC$_{50}$ (uM)	Ligand Efficiency (LE)	ΔTm (°C)
3.30	4-chloro	3-carboxylic acid Isoxazol-5-yl	95 ±19	0.35	1.39
3.31	5-CF$_3$	3-carboxylic acid Isoxazol-5-yl	115 ± 20	0.31	0.62
3.32	4-CF$_3$	3-carboxylic acid Isoxazol-5-yl	106 ± 12	0.31	N/A
3.33	4-chloro	3-methyl Isoxazol-5-yl	121 ± 90	0.39	1.96
3.34	4-chloro	3-difluoromethyl Isoxazol-5-yl	56 ± 12	0.37	2.30
3.35	4-chloro	3-trifluoromethyl Isoxazol-5-yl	970 ± 160	0.25	2.37
3.36	4-chloro	3-hydroxymethyl Isoxazol-5-yl	48 ± 14	0.40	1.49
3.37	5-chloro	3-carboxylic acid Pyrazol-5-yl	23 ± 2	0.41	0.36
3.38	5-chloro	3-hydroxymethyl Pyrazol-5-yl	43 ± 11	0.41	1.81
3.39	2,4-dibromo	3-carboxylic acid Isoxazol-5-yl	19 ± 4	0.39	1.93
3.40	2,4-dibromo	3-carboxylic acid Pyrazol-5-yl	37 ± 13	0.36	3.69
3.41	2,4-dichloro	3-carboxylic acid Isoxazol-5-yl	330 ± 70	0.29	0.63
3.42	2,4-dichloro	3-carboxylic acid Pyrazol-5-yl	140 ± 60	0.32	1.79

Table **3.4**. Biological Screening Results of Elaborated 2-hetaryl phenol fragments. IC$_{50}$ values in green indicate comparable or improved potency compared to **3.20**, previous best-in-class. ΔTm values in green indicate ΔTm ≥1.5 °C, considered significant.

Direct comparison of compound **3.4** in Section **3.2.2** to **3.26** suggests the inclusion of the COOH-substituted isoxazoles has a negative impact on potency for this series, increasing IC$_{50}$

values roughly 2-fold from 42 ± 12 µM to 95 ± 19 µM. When combined with 5-CF$_3$ on the phenol ring (compounds **3.31**), however, the 3-COOH substituted heterocycle improves potency over 10-fold over the unsubstituted analogue **3.26**. Similarly, compound **3.37** displays a nearly 20-fold increase in potency over closest analogue **3.10** with IC$_{50}$ values of 23 ± 2 and $430 \pm$ **X**, respectively. Finally, when combined with 4,6-Dibromo and 4,6-Dichloro phenol, 3-COOH substitution from pyrazole (**3.40** and **3.42**) had a beneficial impact on IC$_{50}$ value of 10-fold and 4-fold, respectively. Close analogues containing an isoxazole (**3.39** and **3.41**) however, showed no significant increase or a 3-fold reduction in potency, respectively.

Compounds **3.33-3.35** with 3-Me, 3-CF$_2$H, and 3-CF$_3$ isoxazol-5-yl showed no beneficial effect when combined with 4-chloro phenol, displaying a up to a 20-fold reduction in potency for compound **3.35** containing the CF$_3$ group. Interestingly, 4-chloro-2-[3-(difluoromethyl)-1,2-oxazol-5-yl]phenol **3.34** was better tolerated than **3.23** and **3.35**, showing only a 1.3-fold reduction in potency from $42 \pm$ **X** µM to 56 ± 12 µM against Aurora-A activity, despite containing a similar group in terms of both structure and electronics. 4-chloro-2-(3-methyl-1,2-oxazol-5-yl)phenol, while showing a roughly 3-fold reduction in potency against kinase activity when compared to the unsubstituted isoxazole compound **3.4**, retained binding efficacy in the thermal shift assay with a ΔTm of 1.96 °C. Finally, the effect of 3-hydroxymethyl was showed no significant benefit or large detriment to biological potency, with comparable IC$_{50}$ values between compounds **3.4** and **3.36**, and a roughly 2-fold reduction observed for **3.38** compared with closest analogue **3.37**. Interestingly, however, **3.38** showed significant thermal shift compared to **3.37**, indicating it is binding more effectively despite the lack of efficacy against kinase activity.
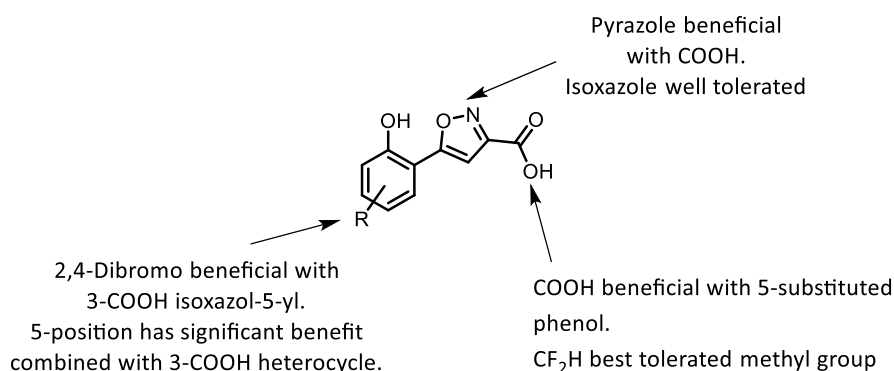
Figure **3.14** Summary of explored SAR with heterocycle substitution.

Productive substitution from the 5-membered heterocycle has been identified, albeit in an unexpected manner. Previous SAR and docking studies determined substitution from the 5-position of the phenol was likely to be unproductive. When combined with 3-COOH substitution from the 5-membered heterocycle, this COOH was found to have a highly beneficial effect on the biological potency compared to an unsubstituted analogue. Additionally, the combination of previous best-in-class fragment **3.20** 2,4-Dibromo substitution with 3-COOH isoxazol-5-yl displayed a minor increase in potency, although not significantly so. Overall, the SAR of this series has been productively explored, resulting in a 2-fold increase (42 µM to 19 µM for **3.4** to **3.39**) in biological potency and increasing molecular complexity without significant decrease in LE. This positions the series well for further elaboration and development against the challenging goal of allosteric inhibitor development.

3.3 Conclusions and Future Perspectives

The SAR landscape of allosteric Aurora-A inhibitors was explored through design, *in silico* docking, synthesis, and biological screening of a 2-hetaryl phenol-based library of small molecules. Initially, known inhibitors of Aurora-A kinase were screened against Aurora-A to determine their mode of inhibition, indicating they attenuate kinase activity in a non-competitive manner. Based on these results, structural evidence, and the small amount of SAR previously determined, this compound series was expanded. Generation of a library exploring various substitutions around the phenol ring resulted in a 2-fold improvement in potency over previous best-in-class compounds following biological screening. *In silico* docking against an ensemble of Aurora-A structures was utilised to guide further design, docking against the allosteric Y-pocket of a judiciously selected range of Aurora-A crystal structures in various conformations and activation states, then collating docking results to identify trends in potentially beneficial structural motifs for onward synthesis. The results of this docking campaign were combined with the previously determined SAR in a rational manner to design a small, targeted library of compounds with additional functionality for synthesis. Following biological screening, these compounds were found to not have a significant increase in biological potency. They did, however, identify trends in the SAR that could be used in the design of further compounds, providing SAR and therefore rationale for further synthetic efforts.

This study represents one of the earliest attempts to elaborate upon allosteric inhibitors of Aurora-A through traditional medicinal chemistry means. In comparison to prior work[63,64], it is

interesting to contrast the methodology employed here against previous studies. Rather than performing a fragment screen against Aurora-A to identify initial fragment hits both structurally and against the Aurora-A/TPX2 PPI, the strategy employed here was intended to expand SAR of an existing hit series through concerted medicinal and computational chemistry efforts, generating a targeted library for biological screening resulting in increased potency within the series. A challenge for this strategy was the selection and expansion of a series of fragments that would retain the allosteric mode of inhibition, targeting the highly dynamic phosphorylated kinase to develop allosteric inhibition from a relatively undefined and shallow binding pocket. Small molecule docking to ensembles of targets for allosteric inhibition is a relatively underexplored field, despite the well-known challenge of intrinsic target flexibility combined with challenging binding sites. Here a targeted ensemble docking strategy was employed to overcome this challenge and provided meaningful results when experimentally validated. Incorporation of a more structure-guided approach, whether determined by crystal structures of existing inhibitors or further *in silico* experiments harnessing both MD and docking, may be a more feasible strategy for future library design of allosteric inhibitors of Aurora-A.

Finally, the efficacy of these inhibitors against the Aurora-A/TPX2 PPI presents an interesting topic for further investigation. Allosteric inhibition of Aurora-A from the Y-pocket , if indeed that is where this series continues to exert influence on kinase activity, is only a small part of the overall picture of Aurora-A function *in vivo*. By probing the perturbation of the Aurora-A/TPX2 interaction by targeting the Y-pocket where crucial residues of TPX2 bind, this series of inhibitors would not only broaden the SAR of specific PPI inhibition, but may provide significant therapeutically relevant effects on the cancer-driving potential of the PPI itself worthwhile of further investigation and development, separate from the *in vitro* potency against kinase activity. With certain compounds from the series exerting significant effect on Aurora-A thermal stability and therefore binding effectively, the series presents itself as an exciting potential avenue of further investigation.

4   Experimental

4.1   General Information and Instrumentation

Commercially available starting materials were obtained from Sigma-Aldrich, Fluorochem, Alfa Aesar, Insight Biotechnology, Strem Chemicals, Enamine BB (EU) or Fisher Scientific with no further purification before use. Water-sensitive reactions were performed in anhydrous solvents obtained from PureSolv MD5 Purification system in oven- or flame-dried glassware cooled under N_2 before use. All other solvents and reagents were analytical grade and used as supplied, with no further purification. Diethyl ether is referred to as ether, and petroleum spirit (b.p. 40-60 °C) is referred to as petrol. An IKA RV 10 or Büchi rotary evaporator with a Vacuubrand PC2001 Vario diaphragm pump was used to remove solvents *in vacuo*.

Thin layer chromatography (TLC) was carried out using pre-coated aluminium plates (Merck silica gel 60 F254) obtained from Merck and visualised with ultraviolet light (λ_{max} = 254 nm) and $KMnO_4$. Flash column chromatography was performed using silica gel 60 (35-70 μm particles) supplied by Merck or on an Isolera Biotage® using Biotage® Sfär 5/10/25 g pre-packed silica cartridges for normal phase chromatography.

Analytical LC-MS was performed on a system comprised of an Ultimate3000 HPLC instrument with a Brucker Amazon Speed MS detector with electrospray ionisation. The system was run with a positive and negative switching mode and a UV diode array detector using a Phenomenex Kinetex C18 (50 mm × 2.1 mm × 2.6 μm) column and a gradient elution with two solvent systems: MeCN/H_2O or MeCN/H_2O with 0.1 % formic acid. Accurate mass spectrometry was performed with electrospray ionisation on a Bruker MaXis Impact spectrometer. Analytical LC-MS of Reaction Arrays was performed using a system comprising a Waters Acquity H-CLASS UPLC with a PDA detector, ELS detector and SQD2 with electrospray ionisation. The system ran with a positive and negative switching mode using a Waters Acquity UPLC BEH C18 (50 mm × 2.1 mm × 1.7 μm) column and gradient elution with a binary solvent system: MeCN plus 0.1% formic acid and H2O plus 0.1% formic acid. Mass directed purification was performed using a Waters Autopurification system comprising a PDA detector, ELS detector and SQD2 with electrospray ionisation. The system ran in positive mode using a Waters XBridge Prep C18 (100 mm × 19 mm × 5 μm) column and gradient elution with a binary solvent system: MeCN plus 0.1% formic acid and H2O plus 0.1% formic acid. Gradients used for purification are shown below:

Column	Run Length (min)	Flow Rate (mL/min)	Gradient	Gradient Start (Min)	Solvent Mix Start		Gradient End (Min)	Solvent Mix End	
					A: H2O (%)	B: MeCN (%)		A: H2O (%)	B: MeCN (%)
100 x 19 mm (5 um)	17.5	25	Generic	0.85	95	5	9.4	5	95
			Early	0.6	95	5	9.6	60	40
			Early-Middle	0.6	80	20	9.6	50	50
			Middle	0.6	65	35	9.6	40	60
			Middle-Late	0.6	55	45	9.6	35	65
			Late	0.6	45	55	9.6	25	75

NMR analysis was conducted using Bruker AV-500(Cryoprobe) (^{1}H = 500 MHz, ^{13}C = 125 MHz), Bruker AV-500 (^{1}H = 500 MHz, ^{13}C = 125 MHz), and Bruker AV-400 (^{1}H = 400 MHz, ^{13}C = 100 MHz) spectrometers using an internal deuterium lock. NMR spectra were obtained at 300 K, unless otherwise specified. Chemical shifts are quoted in parts per million (ppm) down field of trimethylsilane, with coupling constants (*J*) given in Hz. Assignment of NMR spectra was aided by DEPT 135, COSY, HMBC, and HMQC where necessary. Splitting patterns are abbreviated as follows: br (broad), app (apparent), s (singlet), d (doublet), dd (doublet of doublets), t (triplet), q (quartet), m (multiplet). NMR data is reported in the format: ppm (number of protons, splitting pattern, coupling constant). Infra-red (IR) spectra were obtained on a Bruker Alpha ATR FR-IR spectrometer, with absorptions reported in wavenumber (cm^{-1})

Structures included in figures were produced using PyMOL 2.3.4[152] from the referenced PDB unless otherwise stated. PDBs were imported, any unnecessary waters removed, and surfaces generated, followed by overlay and visualisation of associated small molecules or peptides.

4.2 Materials and Methods for Activity-Directed Synthesis

4.2.1 Rhodium Carbenoid Reaction Array Procedure

The reaction array was performed in 750 µl borosilicate glass vials. Fragments were dissolved in DCM to 200 mM. 25 µl of each fragment were added to the appropriate vials and the solvent was evaporated at atmospheric pressure and temperature. Co-substrates were dissolved in DCM to 220 mM, and 25 µl of each was added to the appropriate vials and the solvent evaporated at atmospheric pressure and temperature. The catalysts were dissolved in DCM to 1 mM and sonicated for 15 min before addition to appropriate wells followed by immediate capping, resulting in a final substrate, co-substrate and catalyst concentration of 100 mM, 110 mM, and 1 mM (1 mol%), respectively. Following 48 h of unstirred reaction at room

temperature the vials were scavenged with 30 mg QuadraPure TU resin, incubated for 24 h, followed by filtration, evaporation, and washed five times with the appropriate solvent system used to load the substrate. The resulting reaction solutions were allowed to evaporate, followed by addition of 50 μL DMSO to result in a product mixture with a total product concentration 100 mM which were then assayed against to ascertain activity against Aurora-A. The mock array wells were included in the design of the reaction array, to be screened in advance of the reaction array itself.

4.2.2 Synthesis of Diazo Compounds

4.2.2.1 General Procedure A: Synthesis of α-diazo amides by hydrazone decomposition

Compound **2.15** (1 eq.) was suspended in anhydrous toluene (0.2 m), stirred and cooled to 0 °C using an ice-bath under N_2 atmosphere. Thionyl chloride (2 eq.) was added and the solution heated to 90 °C for 3 hours, then the solvent removed under vacuum to yield an orange solid. This solid was dissolved in anhydrous DCM (0.1 M) and cooled to 0 °C, and a solution of amine (2 eq.) and *N*,*N*-dimethylaniline (1 eq.) in DCM (0.3 m) was slowly added to the stirred solution over 5 minutes. After 1 hour, triethylamine (5 eq.) was added and the reaction allowed to warm to room temperature overnight. The solvent was removed *in vacuo* and the resulting crude material purified by column chromatography.

2-diazo-*N*-methyl-*N*-phenylacetamide, D3
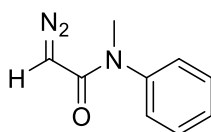
Chemical Formula: $C_9H_9N_3O$

By general procedure **A**, *N*-methylaniline (964 μl, 9.1 mmol) gave crude material as a dark orange oil that was purified by flash column chromatography in 9:1 DCM/Et2O to yield the diazo **CS3** as a light yellow oil (332 mg, 23%). R_F 0.46 (1:1 pentane/Et$_2$O); δ_H (400 MHz, (CD$_3$)$_2$CO) 7.39-7.29 (2H, m, Ar 3–H and 5–H), 7.27 – 7.14 (2H, m, Ar 2–H and 6–H), 4.68 (1H, s, 2–H), 3.12 (3H, s, N–C*H$_3$*); δ_C (101 MHz, Acetone) 164.8, 143.5, 129.6, 127.5, 127.3, 46.5, 36.2. v_{max}/cm^{-1} (film) 3119, 3061, 2936, 2110 (diazo), and 1630. HRMS (ESI): $C_9H_9N_3O$ requires [M-N$_2$+H]$^+$, calculated: 148.0762, found: 148.0757.

2-diazo-*N*-methyl-*N*-(oxan-4-yl)acetamide, D1
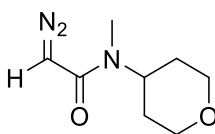
Chemical Formula: $C_8H_{13}N_3O_2$

By general procedure **A**, *N*-methyloxan-4-amine (964 μl, 9.1 mmol) gave crude material as a dark orange oily solid which was purified by column chromatography eluted with Et_2O to yield the diazo as a light yellow oil (257 mg, 17%). R_F 0.26 (Et_2O); δ_H (400 MHz, $(CD_3)_2CO$) 5.62 (1H, s, 2-H), 3.93 (2H, dd, *J* 11.5, 4.7, 2-H_a), 3.41 (2H, td, *J* 11.9, 2.0, 2-H_b), 2.84-2.72 (4H, m, N-C*H₃* and 4-H), 1.78 (2H, qd, *J* 12.3, 4.7, 3-H_a), 1.55-1.45 (2H, m, 3-H_b). ^{13}C spectroscopic properties match prior work in the group. HRMS (ESI): $C_8H_{13}N_3O_2$ requires $[M+Na]^+$, calculated: 206.0905, found: 206.0899.

2-diazo-1-(morpholin-4-yl)ethanone, D6
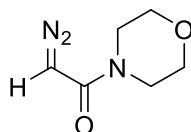
Chemical Formula: $C_6H_9N_3O_2$

By general procedure **A**, morpholine (789 μl, 9.1 mmol) gave a crude product as an orange oil which was purified by column chromatography eluting with Et_2O to yield the diazo as a light yellow oil (231 mg, 23%). R_F 0.2 (Et_2O); δ_H (400 MHz, $(CD_3)_2CO$) 5.34 (1H, s, 2-H), 3.35 (2H, br m, morphlinyl 2-H_a and 6-H_a), 3.27 (2H, br m, morpholinyl 2-H_b and 6-H_b), 1.86 (4h, app s, morpholinyl 3-H_{ab} and 5-H_{ab}). δ_C (101 MHz, $(CD_3)_2CO$) 164.0, 46.0, 26.7, 25.2. ^{13}C spectroscopic properties match prior work in the group. HRMS (ESI): $C_6H_9N_3O_2$ requires $[M+H]^+$, calculated: 156.0773, found 156.0767.

***N*-(4-chlorophenyl)-2-diazo-*N*-methyl-3-oxobutanamide, D4**
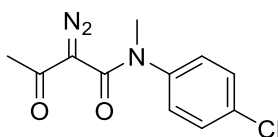
Chemical Formula: $C_{11}H_{10}ClN_3O_2$

4-chloro-*N*-methylaniline (1 eq.) and 2,2,2,6-trimethyl-1,3-dioxin-4-one (1.5 eq.) were added to a 20 mL microwave vial, dissolved in toluene (1.4 M) and heated under microwave irradiation at 110 °C for 30 minutes. The solvent was removed *in vacuo* and the crude material was dissolved in acetonitrile (0.01 M). The solution was cooled to 0 °C and 1,8-Diazabicyclo[5.4.0]undec-7-ene (1.4 eq.) and 4-Acetamidobenzenesulfonyl azide (1.2 eq.) were added sequentially then stirred for 16 hours. During the reaction a white precipitate was formed, which was removed by filtration, and the solvent removed *in vacuo* to give a crude material as a dark red oil. The crude was purified by flash column chromatography eluting with 9:1 DCM/Et_2O to yield diazo **D1** as a yellow oil (0.56 g, 60%), R_F 0.10 (DCM); δ_H (400 MHz, $CDCl_3$) 7.39 (2H, d, *J* 8.7, chlorophenyl-2H and -6H), 7.14 (2H, d, *J* 8.7, chlorophenyl–3H and –5H), 3.34 (3H, s, *N*-methyl) and 2.46 (3H, s, oxobutanamide–H_3). δ_C (100 MHz) 191.4, 161.1, 157.1, 141.7, 133.9, 130.6, 127.5, 38.6 and 28.5. v_{max}/cm^{-1} (film) 2184 (diazo), 1637, 1590, 1491, 1356. HRMS (ESI) found MNa$^+$, 274.0352, $C_{11}H_{10}ClN_3NaO_2$ requires 274.0359.

4.2.3   Synthesis of Fragment Substrates

N-methyl-5-(4-methylphenyl)pyridine-3-carboxamide, F9
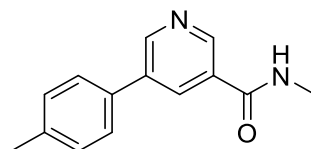
Chemical Formula: $C_{14}H_{14}N_2O$

Following a modified procedure,[139] 5-bromo-*N*-methylnicotinamide **2.9** (300 mg, 1.39 mmol), *p*-tolylboronic acid **2.10** (193 mg, 1.41 mmol), Pd(PPh$_3$)$_4$ (32.3 mg, 0.0278 mmol, 2 mol %), and MeOH-PhMe (1:4, 15.0 ml) were placed under nitrogen atmosphere. Na_2CO_3 (590 µl, 1.18 mmol, 2 M) was added and the reaction heated to 75 °C for 2 h. The reaction was cooled to room temperature and concentrated *in vacuo*. H_2O (15 ml) was added to dissolve the solid crude product and extracted with DCM (3 × 15 ml). Combined organic layers were washed with saturated aqueous NaCl solution (2 × 10 ml), dried over Na_2SO_4 and concentrated *in vacuo* to yield crude product, which was purified *via* flash column chromatography, eluting in 70:30 EtOAc – petrol to yield product **F9** as an amorphous, fluffy, white, solid (165 mg, 52%). R_F 0.1 (DCM); δ_H (300 MHz, $CDCl_3$) 8.93 (1H, d, *J* 2.2, 2–H), 8.87 (1H, d, *J* 2.2, 6–H), 8.29 (1H, t, *J* 2.2, 4–H), 7.52 (2H, d, *J* 8.0, Ph 3–H), 7.30 (2H, d, *J* 8.0, Ph 2–H), 6.24 (1H, s, N–H), 3.07 (3H, d, *J* 4.9, N–CH$_3$), 2.42 (3H, s, Ph 4–Me). δ_C (101 MHz, $CDCl_3$) 166.4, 150.4, 145.8, 138.6, 136.6, 133.8, 133.2, 130.3,

129.9, 127.0, 26.9, 21.2. IR v_{MAX} (neat)/cm^{-1} 3312, 2921, 2167, 1846, 1798, 1637, 1596, 1513. HRMS (ESI): $C_{14}H_{14}N_2O$ requires [M+H]$^+$, calculated: 27.1184, found: 227.1175.

3-[4-(trifluoromethyl)phenyl]-1*H*-pyrazole, F2
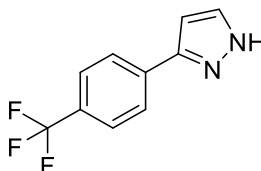
Chemical Formula: $C_{10}H_7F_3N_2$

Following a modified procedure,[140] 4'-(trifluoromethyl)acetophenone **2.11** (941 mg, 5.01 mmol) and anhydrous THF (15.0 ml) were added to a round bottomed flask under nitrogen atmosphere and cooled to 0 °C. NaH (60% in mineral oil, 202 mg, 5.00 mmol) was added in a single portion, with evolution of gas observed. Once gas evolution had ceased, EtOCHO (401 µl, 5.00 mmol) was added and the reaction was warmed to room temperature over 30 min. THF was removed *in vacuo*, followed by addition of MeOH (15.0 ml) and $NH_2NH_2 \cdot H_2O$ (4.02 ml, 50.0 mmol) under nitrogen atmosphere, and stirred overnight. The reaction was concentrated *in vacuo*, dissolved in EtOAc (20.0 ml) organic layer washed with H_2O (3 × 15.0 ml) then saturated aqueous NaCl solution (3 × 15.0 ml), dried over MgSO$_4$, and concentrated *in vacuo* to yield the crude product as an orange oil, which was purified *via* flash column chromatography, eluting in 50:50 EtOAc–petrol to yield product **F2** as a dense, yellow solid (162 mg, 22%). R$_F$ 0.21 (1:1 EtOAc–petrol); δ$_H$ (400 MHz, CDCl3) 7.89 (2H, d, *J* 8.2, Ph–3,5–H), 7.65 (3H, app d, *J* 8.2, 4–H, Ph–2,6–H), 6.69 (1H, d, *J* 2.0, 5–H). ^{13}C spectroscopic properties match reported literature.[140] HRMS (ESI): $C_{10}H_7F_3N_2O$ requires [M+H]$^+$, calculated: 213.0639, found: 213.0631.

(2*E*)-1-(3-chloro-2-hydroxyphenyl)-3-(dimethylamino)prop-2-en-1-one, 2.14
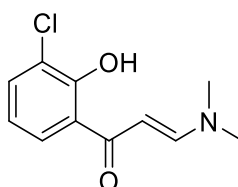
Chemical Formula: $C_{11}H_{12}ClNO_2$

Following a modified procedure,[141] 1-(3-chloro-2-hydroxyphenyl)ethanone **2.13** (400 mg, 2.34 mmol) and DMFDA (4.00 ml, 3.51 mmol) were added to a round bottomed flask equipped with

a condenser and heated to 110 °C for 4 h. The DMFDA was then remove *in vacuo*, and the resulting solid dissolved in hot chloroform and crystallised to yield product **2.14** as a large, hexagonal, yellow crystals (201 mg, 38%). R_F 0.3 (DCM); M.pt: 136-141 °C; δ_H (400 MHz, CDCl3) 14.88 (1H, s, O-H), 7.91 (1H, d, *J* 12.1, 3-H), 7.60 (1H, dd, *J* 7.9, 1.3, Ph-4-H), 7.44 (1H, dd, *J* 7.9, 1.3, Ph-6-H), 6.75 (1H, t, *J* 7.9, Ph-5-H), 5.74 (1H, d, *J* 12.1, 2-H), 3.20 (3H, s, Methyl-H), 2.98 (3H, s, Methyl-H). δ_C (101 MHz, CDCl3) 190.8, 159.0, 155.5, 134.0, 126.7, 122.6, 121.4, 118.0, 89.9, 45.7, 37.6. HRMS (ESI): $C_{11}H_{13}ClNO_2$ requires $[M+H]^+$, calculated: 226.0634, found: 226.0630.

2-chloro-6-(1,2-oxazol-5-yl)phenol, F4
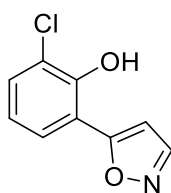
Chemical Formula: $C_9H_6ClNO_2$

Following a modified procedure,[142] (2*E*)-1-(3-chloro-2-hydroxyphenyl)-3-(dimethylamino)prop-2-en-1-one **2.14** (203 mg, 0.89 mmol), hydroxylamine hydrochloride (92.0 mg, 1.33 mmol), and EtOH (15 ml) were added to a round bottomed flask equipped with a condenser and heated to 85 °C for 45 min, until a colourless solution was formed. The solvent was removed *in vacuo*, and ice-cold H_2O (10 ml) was added to the crude reaction mixture, resulting the formation of white precipitate which was filtered by vacuum filtration, washed with ice-cold H_2O, dried, and purified by precipitation in EtOAc-petrol (50:50) to yield **F4** as a fine, off-white, amorphous, solid (118 mg, 68%). R_F 0.31 (DCM); δ_H (501 MHz, CDCl$_3$) 8.34 (1H, d, *J* 1.8, Isoxazolyl 3–H), 7.88 (1H, dd, *J* 8.0, 1.5, 3–H), 7.42 (1H, dd, *J* 8.0, 1.5, 5–H), 7.02 (1H, t, *J* 8.0, 4–H), 6.89 (1H, d, *J* 1.8, Isoxazolyl 5–H), 6.32 (1H, s, O–H). δ_C (101 MHz, CDCl3) 164.5, 151.0, 148.3, 130.3, 126.5, 121.4, 121.1, 115.7, 103.2; IR v_{MAX} (neat)/cm^{-1} 3119, 1925, 1795, 1607, 1567, 1461, 1444, 1317. HRMS (ESI): $C_9H_6ClNO_2$ requires $[M+H]^+$, calculated: 196.0165, found: 196.0159.

4-(2-phenylethyl)phenol, **F12**
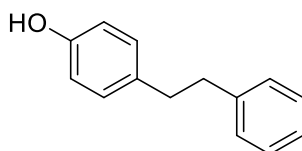
Chemical Formula: $C_{14}H_{14}O$

Trans-4-Hydroxystilbene **2.20** (500 mg, 2.54 mmol) and Pd/C (106 mg, 5% Pd basis) were added to a round-bottomed flask and placed under N_2. 5 mL of EtOH was added, followed by flushing RBF with H_2 atmosphere (balloon). The solution was stirred vigorously under H_2 atmosphere for 24 hours and following complete consumption of starting material by TLC, the solvent was flushed through a celite plug eluting with EtOAc. Solvent was removed *in vacuo* to yield **F12** as a crystalline white solid requiring no further purification (501 mg, >98% yield). R_f 0.29 (4:1 petrol/EtOAc); M.pt 99-102 °C; IR ν_{MAX} (neat)/cm^{-1} 3411, 3026, 2934, 1720, 1599, 1514, 1449, 1369, 1287, 1138, 1079 and 823; δ_H (400 MHz, MeOD) 7.25-7.19 (2H, m, phenyl 1–H), 7.16-7.10 (3H, m, phenyl 1–H and 3–H), 6.96 (2H, d, J 8.5, phenol 3–H), 6.69-6.63 (2H, m, phenol 2–H), 2.89-2.72 (4H, m, ethyl). δ_C (100 MHz, MeOD) 153.9, 142.0, 134.3, 129.8 (2C), 128.4 (2C), 126.1, 115.1 (2C), 38.4, 37.3. HRMS (ESI) found MH$^+$, 199.1125, $C_{14}H_{15}O$ requires 199.1123.

4-[(4-methoxyphenyl)methyl]benzonitrile, 2.19
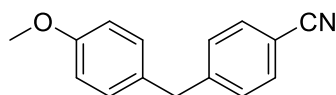
Chemical Formula: $C_{15}H_{13}NO$

4-chloromethyl benzonitrile **2.17** (600 mg, 3.95 mmol), (4-methoxyphenyl)boronic acid **2.18** (721 mg, 4.75 mmol), K_2CO_3 (1.09 g, 7.9 mmol), and palldium dichloride (28 mg, 0.16 mmol) were added to a round-bottomed flask and stirred in 7 mL DMF:H_2O (4:1) at 90 °C for 4 hours. Following completion monitored by TLC, the reaction was cooled to room temperature and diluted with ether (10 mL), H_2O (10 mL), and extracted with ether (3 x 10 mL). The organic layer was washed with 10% w/v aq. LiCl solution (3 x 10 mL), brine (10 mL), dried over $MgSO_4$, and filtered. The solvent was removed *in vacuo* to yield crude material as a yellow solid which was purified by flash column chromatography to yield **2.19** as a light yellow solid (553 mg, 82 %). R_f 0.27 (9:1 petrol/EtOAc); δ_H (501 MHz, CDCl$_3$) 7.56 (2H, d, J 8.3, benzonitrile 3–H), 7.27 (2H, br. d, J 7.3, benzonitrile 2–H), 7.07 (2H, d, J 8.7, phenyl 3–H), 6.85 (2H, d, J 8.7, phenyl 2–H), 3.97 (2H, s, methylene CH$_2$), 3.79 (3H, s, O-Me). δ_C (125 MHz, CDCl$_3$) 158.4, 147.3, 132.3, 131.4, 130.0, 129.5, 119.1, 114.2, 110.0, 55.3, 41.1. LC-MS found M, 223.8, $C_{15}H_{13}NO$ requires 223.3.

114

4-[(4-hydroxyphenyl)methyl]benzonitrile, F13
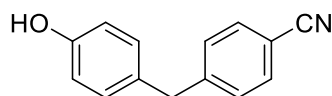
Chemical Formula: $C_{14}H_{11}NO$

Compound **2.19** (407 mg, 1.83 mmol) was added to a round-bottomed flask and placed under N_2. 6 mL of anhydrous DCM was added and the solution cooled to 0 °C in an ice-bath. 1 M BBr$_3$ in DCM (4.2 mL, 4.2 mmol) was added dropwise and following addition the solution was stirred for 18 hours while warming to room temperature. 7 mL H_2O was added and stirred vigorously for 1 hour, then the solution was extracted with ether (35 mL). The organic layer was washed with H_2O (10 mL), brine (10 mL), and dried over Mg_2SO_4 then filtered. The solvent was removed *in vacuo* to yield material **F13** as an off-white, crystalline solid that required no further purification (387 mg, 98%). R_f 0.2 (9:1 petrol/EtOAc); M.pt 162-164 °C; δ_H (501 MHz, CDCl$_3$) 7.56 (2H, d, *J* 8.4, benzonitrile 3–H), 7.26 (2H, d, *J* 8.4, benzonitrile 3–H), 7.06-6.98 (2H, m, phenyl 3–H), 6.81-6.75 (2H, m, phenyl 3–H), 4.64 (1H, s, O–H), 3.96 (2H, s, methylene CH$_2$); δ_C (125 MHz, CDCl$_3$) 154.3, 147.2, 132.3, 131.6, 130.2, 129.5, 119.0, 115.6, 110.0, 41.1; HRMS (ESI) found MNa$^+$, 232.0731, $C_{14}H_{11}NNaO$ requires 232.0733.

2-chloro-6-(1H-pyrazol-5-yl)phenol, F11
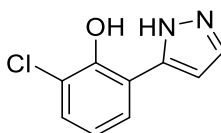
Chemical Formula: $C_9H_7ClN_2O$

Compound **2.14** (579 mg, 2.57 mmol) and EtOH (10 mL) were added to a round-bottomed flask, to which hydrazine monohydrate (1.03 mL, 12.9 mmol) was added portion-wise. The solution was stirred for 1 hour at 85 °C and following completion of the reaction, monitored by TLC, the solution was cooled to room temperature and solvent removed *in vacuo*. 20 mL H_2O was added to the resulting crude material and the fine, white precipitate that formed was filtered and washed with H_2O (15 mL) to yield product as an off-white solid with no further purification necessary (462 mg, 92%). R_f 0.44 (9:1 petrol/EtOAc); δ_H (500 MHz, CDCl$_3$) 11.54 (1H, br. s, 2–pyr N–H), 10.33 (1H, br. s, 1–pyr N–H), 7.68 (1H, d, *J* 2.6, pyr 3–H), 7.52 (1H, dd, *J* 7.8, 1.5, phe 5–H), 7.32 (1H, dd, *J* 7.8, 1.5, phe 3–H), 6.88, (1H, t, *J* 7.8, phe 4–H), 6.73 (1H, d, *J*

2.6, pyr 4–H); δ_C (125 MHz, CDCl$_3$) 151.7, 151.1, 129.6, 129.5, 125.0 ,121.8, 119.7, 117.9, 102.4; HRMS (ESI) found MH$^+$, 195.0315, C$_9$H$_8$ClN$_2$O requires 195.0320.

4.2.4 Synthesis of Amide Array Substrates and Products

4.2.4.1 General Procedure B: Array format amide bond formation

Acetic acid **2.23** or **2.24** (1 eq.), 1-[Bis(dimethylamino)methylene]-1H-1,2,3-triazolo[4,5-b]pyridinium 3-oxide hexafluorophosphate (HATU) (1.2 eq.), and *N,N*-Diisopropylethylamine (DIPEA) (1.1) in 300 μL DMF (0.1 M) were added to borosilicate glass vials and stirred for 30 minutes. The respective secondary amine or aniline (1.25 eq.) and DIPEA (2.5 eq.) in 300 μL DMF was added portion wise to each relevant glass vial. The reaction mixtures were stirred for 16 hours, the solvent removed *in vacuo* and the crude material was redissolved in 0.5 mL DMSO for UPLC analysis and purification by mass-directed HPLC to afford the desired product.

Ethyl 2-(4-benzylphenoxy)acetate, 2.21
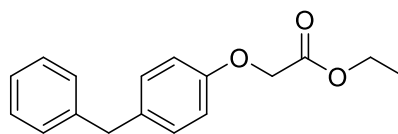
Chemical Formula: C$_{17}$H$_{18}$O$_3$

Benzylphenol **F7** (1 g, 5.42 mmol), K$_2$CO$_3$ (1.8 g, 13.5 mmol) and 15 mL DMF were added to a round-bottomed flask and stirred. Ethylbromoacetate **2.20** (718 μL, 6.5 mmol) was added and the solution was heated to 60 °C for 6 hours. Following complete consumption of starting material by TLC, the solution was cooled to room temperature and 15 mL H$_2$O was added and extracted with EtOAc (3 x 15 mL). The organic layer was washed with 10% w/v aq. LiCl solution (3 x 15 mL), brine (15 mL), dried over MgSO$_4$, filtered, and the solvent removed *in vacuo* to yield crude material. Purification by flash column chromatography eluting with 1% MeOH in DCM afforded the ester (1.38 g, 94%). R_f 0.31 (30:1 DCM/MeOH); δ_H (500 MHz, acetone-d^6) 7.29-7.25 (2H, m, benzyl-3H), 7.23 – 7.19 (2H, m, benzyl-2H), 7.18 – 7.16 (1H, m, benzyl-4H), 7.16 – 7.13 (2H, m, phenoxy-3H), 6.87 – 6.83 (2H, m, phenoxy-2H), 4.66 (2H, s, acetyl-CH$_2$), 4.19 (2H, q, *J* 7.1, ethyl-CH$_2$), 3.91 (2H, s, methylene-CH$_2$), 1.24 (3H, t, *J* 7.1, ethyl-CH$_3$); LC-MS found M, 270.4, C$_{17}$H$_{18}$O$_3$ requires 270.3.

Ethyl 2-(4-phenoxyphenoxy)acetate, 2.22
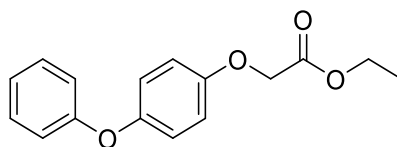
Chemical Formula: $C_{16}H_{16}O_4$

Phenoxyphenol **F8** (1 g, 5.37 mmol), K_2CO_3 (1.8 g, 13.5 mmol) and 15 mL DMF were added to a round-bottomed flask and stirred. Ethylbromoacetate **2.20** (718 µL, 6.5 mmol) was added and the solution was heated to 60 °C for 6 hours. Following complete consumption of starting material by TLC, the solution was cooled to room temperature and 15 mL H_2O was added and extracted with EtOAc (3 x 15 mL). The organic layer was washed with 10% w/v aq. LiCl solution (3 x 15 mL), brine (15 mL), dried over $MgSO_4$, filtered, and the solvent removed *in vacuo* to yield crude material. Purification by flash column chromatography eluting with 1% MeOH in DCM afforded the ester (1.33 g, 91%). R_f 0.29 (30:1 DCM/MeOH); δ_H (500 MHz, acetone-d^6) 7.36 – 7.31 (2H, m, phenoxy-3H), 7.07 (1H, tt, *J* 7.6, 1.1, phenoxy-4H), 7.01 – 6.96 (4H, app br. m, phenoxy-2H and phenoxyacetate-3H), 6.96 – 6.92 (2H, m, phenoxyacetate-2H), 4.70 (2H, s, acetyl-CH_2), 4.21 (2H, q, *J* 7.1, ethyl-CH_2), 1.25 (3H, t, *J* 7.1, ethyl-CH_3); δ_C (125 MHz, acetone-d^6) 168.6, 158.4, 154.5, 150.8, 129.8, 122.7, 120.6, 117.7, 115.9, 65.4, 60.6, 13.7; LC-MS found M, 272.6, $C_{16}H_{16}O_4$ requires 272.3.

2-(4-benzylphenoxy)acetic acid, 2.23
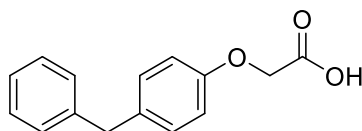
Chemical Formula: $C_{15}H_{14}O_3$

Ethyl 2-(4-benzylphenoxy)acetate **2.21** (1.1 g, 4.54 mmol) in 10 mL 1:1 H_2O/THF was stirred and LiOH (545 mg, 22.7 mmol) was added portionwise and the solution was stirred for 16 hours. The volatile solvents were removed *in vacuo* and the residue diluted with H_2O, acidified to pH 1 with 1 M aq. HCl, and redissolved in EtOH. The solid was filtered, washed with EtOH and aq. HCl and dried *in vacuo* to yield the acid product (977 mg, 89%) without requiring further purification. δ_H (500 MHz, acetone-d^6) 7.29 – 7.25 (2H, m, benzyl-3H), 7.23 – 7.20 (2H, m, benzyl-2H), 7.19 – 7.13 (3H, m, benzyl-4H and phenoxy-3H), 6.89 – 6.85 (2H, m, phenoxy-2H), 4.67 (2H, s, acetyl-CH_2), 3.91 (2H, s, methylene-CH_2); δ_C (125 MHz, acetone-d^6) 169.4, 156.6, 141.8, 134.3, 129.7, 128.7,

128.3, 125.9, 114.5, 64.5, 40.6; HRMS (ESI) found MNa⁺, 265.0828, $C_{15}H_{14}NaO_3$ requires 265.0835.

2-(4-phenoxyphenoxy)acetic acid, 2.24
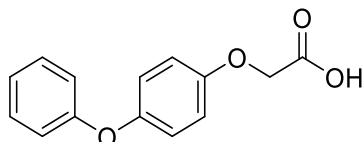
Chemical Formula: $C_{14}H_{12}O_4$

Ethyl 2-(4-phenoxyphenoxy)acetate **2.22** (1.01 g, 3.7 mmol) in 10 mL 1:1 H_2O/THF was stirred and LiOH (545 mg, 22.7 mmol) was added portionwise and the solution was stirred for 16 hours. The volatile solvents were removed *in vacuo* and the residue diluted with H_2O, acidified to pH 1 with 1 M aq. HCl, and redissolved in EtOH. The solid was filtered, washed with EtOH and aq. HCl, and dried *in vacuo* to yield the acid product (812 mg, 90%) without requiring further purification. δ_H (500 MHz, acetone-d^6) 7.36 – 7.31 (2H, m, phenoxy-3H), 7.07 (1H, t, *J* 7.4, phenoxy-4H), 6.99 (4H, app. s, phenoxy-2H and phenoxyacetate-3H), 4.72 (2H, s, acetyl-CH₂); δ_C (125 MHz, acetone-d^6) 169.3, 158.4, 154.6, 150.8, 129.7, 122.6, 120.5, 117.6, 115.8, 64.9; HRMS (ESI) found MNa⁺, 267.0622, $C_{14}H_{12}NaO_4$ requires 267.0628.

2-(4-benzylphenoxy)-*N*-[3-(trifluoromethyl)phenyl]acetamide, 2.17
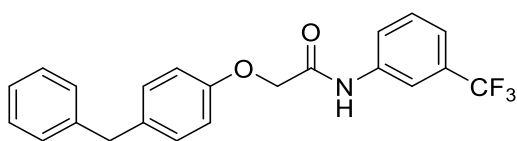
Chemical Formula: $C_{22}H_{18}F_3NO_2$

2-(4-benzylphenoxy)acetic acid **2.23** (26 mg, 0.1 mmol), 1-[Bis(dimethylamino)methylene]-1H-1,2,3-triazolo[4,5-b]pyridinium 3-oxide hexafluorophosphate (HATU) (45 mg, 0.12 mmol), and *N,N*-Diisopropylethylamine (DIPEA) (19 µL, 0.11 mmol) were stirred in DMF (0.1 M) for 30 minutes at room temperature, to which 3-trifluoromethyl aniline (15.6 µL, 0.125 mmol) and DIPEA (44 µL, 0.25 mmol) in DMF (0.5 mL) was added portionwise. The reaction mixture was stirred for 16 hours, the solvent removed *in vacuo* and the crude material was redissolved in 1 mL DMSO for purification by mass-directed HPLC (385.4, mid) to afford product (33 mg, 88%). δ_H (400 MHz, acetone-d^6) 9.60 (1H, s, N-H), 8.22 (1H, br s, aniline-2H), 7.98 (1H, br d, *J* 8.0, aniline-

6H), 7.56 (1H, t, *J* 8.0, aniline-5H), 7.44 (1H, d, *J* 8.0, aniline-4H), 7.31 – 7.24 (2H, m, phenyl-2H), 7.24 – 7.15 (5H, m, phenyl-4H and phenoxy-3H), 7.02 – 6.95 (2H, m, phenoxy-2H), 4.67 (2H, s, acetyl-CH$_2$), 3.93 (2H, s, methylene-CH$_2$); δ_C (100 MHz, acetone-*d^6*) 167.1, 156.2, 141.8, 139.2, 134.9, 129.9, 129.7, 128.7, 128.4, 125.9, 123.3, 123.2, 120.2, 116.3, 114.9, 67.6, 40.6 (CF$_3$ carbon not observed due to splitting); HRMS (ESI) found MH$^+$, 386.1372, C$_{22}$H$_{19}$F$_3$NO$_2$ requires 386.1368.

2-(4-phenoxyphenoxy)-*N*-[3-(trifluoromethyl)phenyl]acetamide, 2.18
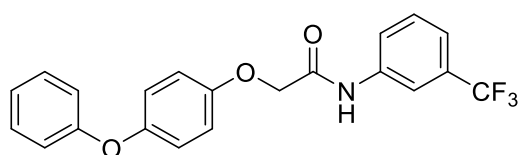
Chemical Formula: C$_{21}$H$_{16}$F$_3$NO$_3$

2-(4-phenoxyphenoxy)acetic acid **2.24** (107 mg, 0.44 mmol), 1-[Bis(dimethylamino)methylene]-1H-1,2,3-triazolo[4,5-b]pyridinium 3-oxide hexafluorophosphate (HATU) (202 mg, 0.53 mmol), and *N*,*N*-Diisopropylethylamine (DIPEA) (84 μL, 0.48 mmol) were stirred in DMF (0.1 M) for 30 minutes at room temperature, to which 3-trifluoromethyl aniline (69 μL, 0.55 mmol) and DIPEA (192 μL, 1.1 mmol) in DMF (0.5 mL) was added portionwise. The reaction mixture was stirred for 16 hours, the solvent removed *in vacuo* and the crude material was redissolved in 1 mL DMSO for purification by mass-directed HPLC (387.4, mid) to afford product (143 mg, 84%). δ_H (500 MHz, acetone-*d^6*) 9.65 (1H, br s, N-H), 8.23 (1H, s, aniline-2H), 8.00 (1H, br d, *J* 8.0, aniline-6H), 7.58 (1H, t, *J* 8.0, aniline-5H), 7.45 (1H, br d, *J* 8.0, aniline-4H), 7.35 (2H, m, phenoxyacetate-2H), 7.14 – 7.10 (2H, m, phenoxy-3H), 7.10 – 7.06 (1H, m, phenoxy-4H), 7.04 – 7.00 (2H, m, phenoxy-2H), 6.97 – 6.93 (2H, m, phenoxyacetate-3H), 4.71 (2H, s, acetyl-CH$_2$); δ_C (125 MHz, acetone-*d^6*) 167.0, 158.3, 154.0, 151.3, 139.1, 130.6, 129.8, 127.5 – 121.0 (br q), 123.4, 123.3, 122.7, 120.55, 120.3, 117.7, 116.4, 116.2, 68.0; HRMS (ESI) found MNa$^+$, 410.0980, C$_{21}$H$_{16}$F$_3$NNaO$_3$ requires 410.0975.

2-(4-benzylphenoxy)-1-(3-phenylpyrrolidin-1-yl)ethan-1-one, 2.18
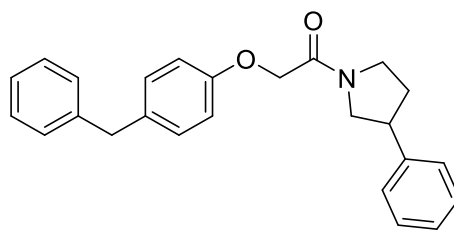
Chemical Formula: $C_{25}H_{25}NO_2$

Benzylphenol **F7** (44 mg, 0.24 mmol) and 2-Diazo-1-(3-phenylpyrrolidin-1-yl)ethan-1-one (258 mg, 1.2 mmol) were dissolved in DCM (0.2 M) and 100 µL each added to 10 individual borosilicate glass vials. The solvent was allowed to evaporate under atmospheric conditions prior to the addition of a solution of **C3** [Rh$_2$((S)-DOSP)$_4$] (200 µL, 1 mM). The vials were sealed and left for 48 hours, after which the solvent was removed *in vacuo* and the resulting crude solids dissolved in 100 µL DMSO-d^6 per vial and combined, prior to purification by mass-directed HPLC to yield product **2.18** as a white solid (69 mg, 78%). δ_H (500 MHz, DMSO-d^6) 7.36 − 7.15 (10H, m), 7.12 (2H, app ddd, J 9.6, 5.8, 2.5), 6.86 − 6.81 (2H, m), 4.76 − 4.64 (2H, m), 3.99 − 3.80 (3H, m), 3.75 − 3.51 (2H, m), 3.48 − 3.19 (2H, m), 2.35 − 2.17 (1H, m), 2.04 − 1.84 (1H, m); δ_C (125 MHz, DMSO-d^6) 166.34, 166.3, 156.9, 156.8, 142.2, 141.9, 141.4, 134.1, 134.0, 130.0, 130.0, 129.0, 128.9, 128.9, 128.8, 127.6, 127.4, 127.2, 127.1, 126.3, 66.7, 52.2, 51.6, 46.1, 45.3, 44.3, 41.9, 40.7, 33.4, 31.3. HRMS (ESI) found MH$^+$, 372.1962, $C_{25}H_{26}NO_2$ requires 372.1964.

2-(4-phenoxyphenoxy)-1-(3-phenylpyrrolidin-1-yl)ethan-1-one, 2.19
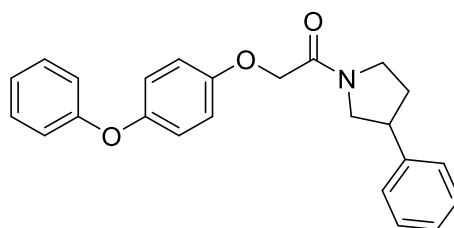
Chemical Formula: $C_{24}H_{23}NO_3$

Phenoxyphenol **F8** (45 mg, 0.24 mmol) and 2-Diazo-1-(3-phenylpyrrolidin-1-yl)ethan-1-one (258 mg, 1.2 mmol) were dissolved in DCM (0.2 M) and 100 µL each added to 10 individual borosilicate glass vials. The solvent was allowed to evaporate under atmospheric conditions prior to the addition of a solution of **C3** [Rh$_2$((S)-DOSP)$_4$] (200 µL, 1 mM). The vials were sealed and left for 48 hours after which the solvent was removed *in vacuo* and the resulting crude solids dissolved in 100 µL DMSO-d^6 per vial and combined, prior to purification by mass-directed HPLC to yield product **2.19** as a white solid (63 mg, 70%). δ_H (500 MHz, DMSO-d^6) 7.38 − 7.28 (6H, m),

7.28 – 7.22 (1H, m), 7.10 – 7.05 (1H, m), 7.02 – 6.95 (4H, m), 6.95 – 6.91 (2H, m), 4.83 – 4.70 (2H, m), 4.04 – 3.84 (1H, m), 3.79 – 3.62 (1H, m), 3.62 – 3.41 (2H, m), 3.41 – 3.22 (3H, m), 2.39 – 2.18 (1H, m), 2.10 – 1.85 (1H, m); δ_C (125 MHz, DMSO-d^6) 166.3, 166.2, 158.4, 155.0, 154.9, 150.1, 150.0, 141.9, 141.4, 130.4, 129.0, 127.7, 127.2, 123.0, 121.0, 117.8, 116.4, 67.0, 52.2, 51.5, 46.1, 45.2, 44.4, 42.0, 33.4, 31.4; HRMS (ESI) found MH$^+$, 374.1759, $C_{23}H_{24}NO_3$ requires 374.1756.

2-(4-benzylphenoxy)-1-(1,2,3,4-tetrahydroisoquinolin-2-yl)ethan-1-one, 2.25
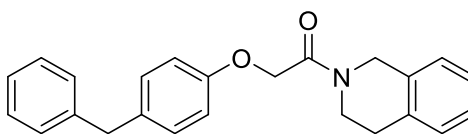
Chemical Formula: $C_{24}H_{23}NO_2$

By general procedure **B**, 2-(4-benzylphenoxy)acetic acid **2.23** and 1,2,3,4-tetrahydroisoquinoline **A1** gave a crude product that was purified by mass-directed HPLC (357.5, mid-late) to yield product **2.25** (2mg, 81%); δ_H (500 MHz, DMSO-d^6) 7.28 – 7.25 (2H, m) 7.20 – 7.14 (7H, m), 7.12 – 7.10 (2H, m), 4.85 (2H, d, J 5.9), 4.68 – 4.60 (2H, br d), 3.85 (2H, s), 3.66 (2H, m), 2.88 – 2.77 (2H, dt); δ_C (125 MHz, DMSO-d^6) 166.5, 156.4, 141.8, 134.6, 133.7, 133.2, 129.6, 129.6, 128.6, 128.5, 128.4, 126.6, 126.5, 126.4, 126.3, 125.9, 114.7, 114.6, 66.3, 45.4, 42.0, 40.3, 28.7; HRMS (ESI) found MH$^+$, 358.1803, $C_{24}H_{24}NO_2$ requires 358.1807.
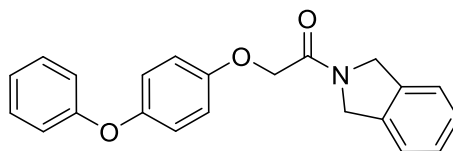
2-(4-phenoxyphenoxy)-1-(1,2,3,4-tetrahydroisoquinolin-2-yl)ethan-1-one, 2.26
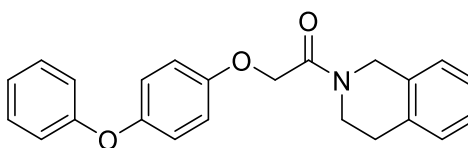
Chemical Formula: $C_{23}H_{21}NO_3$

By general procedure **B**, 2-(4-phenoxyphenoxy)acetic acid **2.24** and 1,2,3,4-tetrahydroisoquinoline **A1** gave a crude product that was purified by mass-directed HPLC (359.4, mid-late) to yield product **2.26** (29 mg, 80%); δ_H (500 MHz, DMSO-d^6) 7.24 (2H, app t), 7.10 (4H, app br s), 6.97 (1H, t, J 7.4), 6.88 (4H, app br d), 6.83 – 6.81 (2H, m), 4.81 (2H, app d), 4.60 – 4.53 (2H, app br d), 3.60 (2H, app q, J 3.6), 2.81 – 2.69 (2H, m); δ_C (125 MHz, DMSO-d^6) 166.9, 158.4, 154.9, 150.1, 135.0, 133.5, 130.4, 129.0, 127.0, 126.7, 123.1, 121.0, 117.8, 116.4, 66.9, 45.8, 44.1, 42.3, 29.1; HRMS (ESI) found MH$^+$, 360.1603, $C_{23}H_{22}NO_3$ requires 360.1600.

2-(4-benzylphenoxy)-1-[4-(furan-2-carbonyl)piperazin-1-yl]ethan-1-one, 2.27
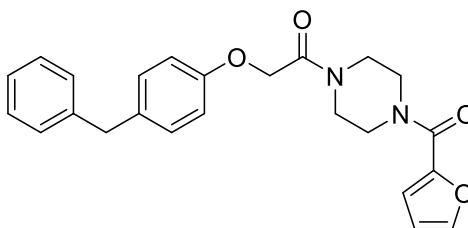
Chemical Formula: $C_{24}H_{24}N_2O_4$

By general procedure **B**, 2-(4-benzylphenoxy)acetic acid **2.23** and 1-(furan-2-carbonyl)piperazine **A2** gave a crude product that was purified by mass-directed HPLC (404.5, mid) to yield product **2.27** (32 mg, 78%); δ_H (500 MHz, DMSO-d^6) 7.84 (1H, dd, J 1.8, 0.8) 7.28 − 7.24 (2H,m), 7.21 − 7.18 (2H, m), 7.18 − 7.14 (1H, m), 7.14 − 7.11 (2H, m), 7.03 (1H, dd, J 3.5, 0.8), 6.86 − 6.84 (2H, m), 6.63 (1H, dd, 3.5, 1.8), 4.80 (2H, s), 3.86 (2H, s)m 3.69 (4H, br d, J 24.2), 3.54 (4H, br s); δ_C (125 MHz, DMSO-d^6) 166.7, 159.0, 156.8, 147.2, 145.4, 142.2, 134.2, 130.0, 129.0, 128.9, 126.3, 116.4, 115.1, 111.9, 66.4, 44.6, 41.7; HRMS (ESI) found MH$^+$, 405.1817, $C_{24}H_{25}N_2O_4$ requires 405.1814.

1-[4-(furan-2-carbonyl)piperazin-1-yl]-2-(4-phenoxyphenoxy)ethan-1-one, 2.28
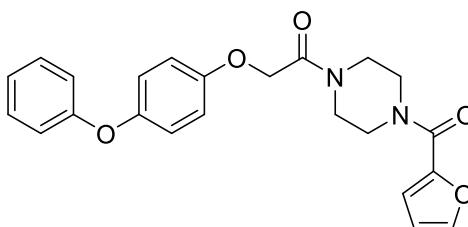
Chemical Formula: $C_{23}H_{22}N_2O_5$

By general procedure **B**, 2-(4-phenoxyphenoxy)acetic acid **2.24** and 1-(furan-2-carbonyl)piperazine **A2** gave a crude product that was purified by mass-directed HPLC (406.4, mid) to yield product **2.28** (31 mg, 78%); δ_H (500 MHz, DMSO-d^6) 7.84 (1H, dd, J 1.8, 0.8), 7.36 − 7.32 (2H, m), 7.06 (1H, tt, 7.5, 1.1), 7.03 (1H, dd, J 3.5, 0.8), 6.97 (4H, app br s), 6.93 − 6.90 (2H, m), 6.63 (1H, dd, J 3.5, 1.8), 4.85 (2H, s), 3.71 (4H, br d, J 23.9), 3.55 (4H, br s); δ_C (125 MHz, DMSO-d^6) 166.7, 159.0, 158.4, 154.8, 150.2, 147.2, 145.4, 130.4, 123.1, 121.0, 117.8, 116.5, 116.4, 111.9, 66.7, 44.5, 41.7; HRMS (ESI) found MNa$^+$, 429.1430, $C_{23}H_{22}N_2NaO_5$ requires 429.1426.

2-(4-benzylphenoxy)-1-(4-benzylpiperidin-1-yl)ethan-1-one, 2.29
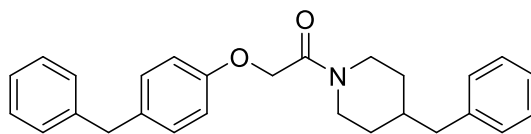
Chemical Formula: $C_{27}H_{29}NO_2$

By general procedure **B**, 2-(4-benzylphenoxy)acetic acid **2.23** and 4-benzylpiperidine **A3** gave a crude product that was purified by mass-directed HPLC (399.5, late) to yield product **2.29** (33 mg, 82%); δ_H (500 MHz, DMSO-d^6) 7.29 – 7.24 (4H, m), 7.22 – 7.14 (6H, m), 7.13 – 7.09 (2H, m), 6.83 – 6.79 (2H, m), 4.73 – 4.70 (2H, m), 4.27 (1H, d, J 12.9), 3.85 (2H, s), 3.79 (1H, d, J 13.4), 2.93 (1H, app t), 2.51 – 2.48 (3H, m), 1.75 (1H, app dddq, J 14.7, 10.9, 7.2, 3.6), 1.57 (2H, app t, J 8.6), 1.14 (1H, qd, J 12.6, 4.0), 0.98 (1H, qd, J 12.6, 4.0); δ_C (125 MHz, DMSO-d^6) 166.0, 156.8, 142.2, 140.4, 134.1, 130.0, 129.5, 129.0, 128.8, 128.6, 126.3, 115.0, 66.6, 44.8, 42.5, 41.9, 40.7, 37.7, 32.5, 31.7; HRMS (ESI) found MNa$^+$, 422.2099, $C_{27}H_{29}NNaO_2$ requires 422.2096.

1-(4-benzylpiperidin-1-yl)-2-(4-phenoxyphenoxy)ethan-1-one, 2.30
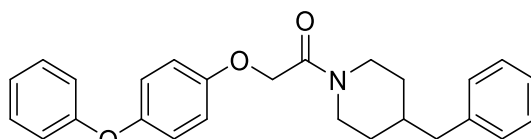
Chemical Formula: $C_{26}H_{27}NO_3$

By general procedure **B**, 2-(4-phenoxyphenoxy)acetic acid **2.24** and 4-benzylpiperidine **A3** gave a crude product that was purified by mass-directed HPLC (401.5, late) to yield product **2.30** (27 mg, 82%); δ_H (500 MHz, DMSO-d^6) 7.27 – 7.23 (2H, m), 7.21 – 7.17 (2H, m), 7.11 – 7.06 (3H, m), 6.98 (1H, tt, J 7.15, 1.1), 6.90 – 6.80 (6H, m), 4.68 – 4.65 (2H, m), 4.21 (1H, br d, J 13.0), 3.72 (1H, br d, J 13.5), 2.87 (1H, app t, J 11.9), 2.50 – 2.56 (3H, m), 1.71 – 1.63 (1H, m), 1.50 (2H, t, J 9.60), 1.07 (1H, m), 0.91 (1H, m); δ_C (125 MHz, DMSO-d^6) 165.9, 158.4, 154.9, 150.1, 140.4, 130.4, 129.5, 128.6, 126.3, 123.1, 121.0, 117.8, 116.3, 66.9, 44.8, 42.5, 41.9, 37.7, 32.5, 31.7; HRMS (ESI) found MH$^+$, 402.2073, $C_{26}H_{28}NO_3$ requires 402.2069.

2-(4-benzylphenoxy)-1-(2,3-dihydro-1*H*-isoindol-2-yl)ethan-1-one, 2.31
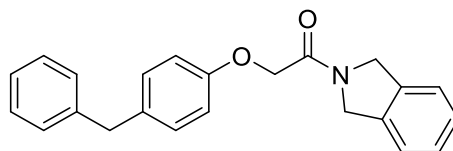
Chemical Formula: C$_{23}$H$_{21}$NO$_2$

By general procedure **B**, 2-(4-benzylphenoxy)acetic acid **2.23** and 2,3-dihydro-1*H*-isoindole **A4** gave a crude product that was purified by mass-directed HPLC (343.4, mid-late) to yield product **2.31** (18 mg, 56%); δ_H (500 MHz, DMSO-*d⁶*) 7.38 – 7.34 (2H, m), 7.35 – 7.24 (4H, m), 7.22 – 7.11 (5H, m), 6.88 (2H, app d, *J* 8.6), 4.90 (2H, s), 4.81 (2H, s), 4.68 (2H, s), 3.86 (2H, s); δ_C (125 MHz, DMSO-*d⁶*) 166.9, 156.8, 142.2, 138.2, 136.1, 134.1, 130.0, 129.0 ,128.9, 127.9, 126.3, 123.5, 123.3, 115.0, 66.4, 52.4, 51.1; HRMS (ESI) found MH⁺, 344.1652, C$_{23}$H$_{22}$NO$_2$ requires 344.1651.

1-(2,3-dihydro-1*H*-isoindol-2-yl)-2-(4-phenoxyphenoxy)ethan-1-one, 2.32

Chemical Formula: C$_{22}$H$_{19}$NO$_3$

By general procedure **B**, 2-(4-phenoxyphenoxy)acetic acid **2.24** and 2,3-dihydro-1*H*-isoindole **A4** gave a crude product that was purified by mass-directed HPLC (345.4, mid) to yield product **2.32** (19 mg, 54%); δ_H (500 MHz, DMSO-*d⁶*) 7.40 – 7.30 (6H, m), 7.07 – 7.05 (1H, m), 7.02 – 6.96 (4H, m), 6.94 – 6.90 (2H, m), 4.91 (2H, s), 4.86 (2H, s), 4.70 (2H, s); δ_C (125 MHz, DMSO-*d⁶*) 166.8, 158.4, 154.9, 150.1, 137.2, 136.1, 130.4, 127.9, 123.5, 123.3, 123.1, 121.0, 117.8, 116.4, 66.7, 52.4, 51.1; HRMS (ESI) found MH⁺, 346.1448, C$_{22}$H$_{20}$NO$_3$ requires 346.1443.

2-(4-benzylphenoxy)-1-(3-phenylpiperidin-1-yl)ethan-1-one, 2.33
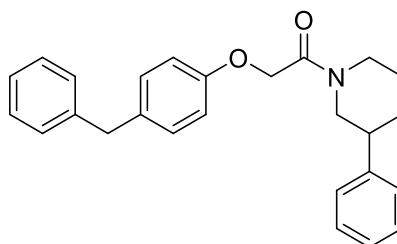
Chemical Formula: C$_{26}$H$_{27}$NO$_2$

By general procedure **B**, 2-(4-benzylphenoxy)acetic acid **2.23** and 3-phenylpiperidine **A5** gave a crude product that was purified by mass-directed HPLC (385.5, late) to yield product **2.33** (31 mg, 80%); δ_H (500 MHz, DMSO-d^6) 7.33 – 7.15 (10H, m), 7.15 – 7.11 (2H, m), 6.86 – 6.82 (2H, m), 4.90 – 4.72 (2H, m), 4.37 (1H, dd, J 26.1, 12.1), 3.87 – 3.83 (3H, m), 3.09 – 3.07 (1H, m), 2.75 – 2.68 (1H, m), 2.64 – 2.54 (1H, m), 1.88 (1H, br s), 1.77 – 1.66 (2H, m), 1.65 – 1.31 (1H, m); δ_C (125 MHz, DMSO-d^6) 166.2, 156.8, 143.9, 143.7, 142.2, 134.1, 130.0, 129.0, 128.9, 128.9, 127.6, 127.4, 127.0, 126.3, 115.0, 66.9, 66.6, 51.5, 48.0, 45.1, 43.2, 42.4, 42.1, 31.9, 26.2, 25.5; HRMS (ESI) found MH$^+$, 386.2117, $C_{26}H_{28}NO_2$ requires 386.2120.

2-(4-phenoxyphenoxy)-1-(3-phenylpiperidin-1-yl)ethan-1-one, 2.34
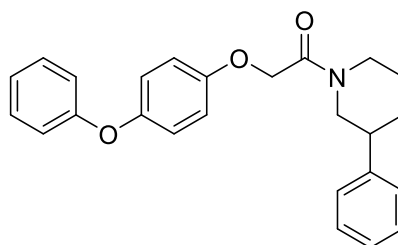
Chemical Formula: $C_{25}H_{25}NO_3$

By general procedure **B**, 2-(4-phenoxyphenoxy)acetic acid **2.24** and 3-phenylpiperidine **A5** gave a crude product that was purified by mass-directed HPLC (387.5, late) to yield product **2.34** (29 mg, 77%); δ_H (500 MHz, DMSO-d^6) 7.44 – 7.16 (7H, br m), 7.13 – 6.85 (7H, br m), 4.92 – 4.67 (2H, m), 4.48 – 4.29 (2H, br m), 3.86 (1H, br s), 3.10 (1H, app br d, J 10.9), 2.80 – 2.67 (1H, m), 2.66 – 2.54 (1H, br m), 1.90 (1H, br s), 1.75 (2H, br s), 1.50 (1H, br app d); δ_C (125 MHz, DMSO-d^6) 166.2, 158.4, 154.9, 150.1, 143.8, 130.4, 128.9, 127.5, 127.0, 123.1, 121.0, 117.8, 116.3, 67.0, 51.4, 45.1, 43.2, 42.5, 31.8, 26.0; HRMS (ESI) found MNa$^+$, 410.1736, $C_{25}H_{25}NNaO_3$ requires 410.1732.

2-(4-benzylphenoxy)-1-(4-phenylpiperidin-1-yl)ethan-1-one, 2.35
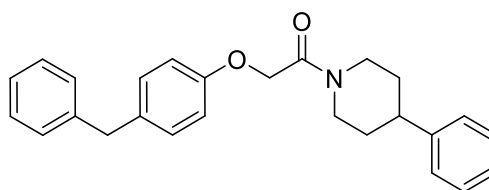
Chemical Formula: $C_{26}H_{27}NO_2$

By general procedure **B**, 2-(4-benzylphenoxy)acetic acid **2.23** and 4-phenylpiperidine **A6** gave a crude product that was purified by mass-directed HPLC (385.5, mid-late) to yield product **2.35** (32 mg, 83%); δ_H (500 MHz, DMSO-d^6) 7.31 – 7.24 (4H, m), 7.23 – 7.14 (6H, m), 7.14 – 7.11 (2H, m), 6.88 – 6.83 (2H, m), 4.84 – 4.71 (2H, m), 4.47 (1H, br d, J 12.9), 3.94 (1H, br d, J 13.4), 3.86 (2H, s), 3.12 (1H, app t, J 12.1), 2.76 (2H, tt, J 12.0, 3.5), 2.65 (1H, app t, 12.0), 1.77 (2H, app br d, J 12.7), 1.62 (1H, qd, J 12.7, 3.8), 1.43 (1H, qd, J 12.7, 3.8); δ_C (125 MHz, DMSO-d^6) 166.2, 156.8, 146.1, 142.2, 134.1, 130.0, 129.0 ,128.9, 128.8, 127.2, 126.7, 126.3, 115.0, 66.7, 45.3, 42.4, 42.1, 40.7, 33.7, 33.1; HRMS (ESI) found MH$^+$, 386.2119, $C_{26}H_{28}NO_2$ requires 386.2120.

2-(4-phenoxyphenoxy)-1-(4-phenylpiperidin-1-yl)ethan-1-one, 2.36
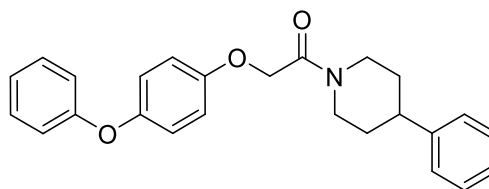
Chemical Formula: $C_{25}H_{25}NO_3$

By general procedure **B**, 2-(4-phenoxyphenoxy)acetic acid **2.24** and 4-phenylpiperidine **A6** gave a crude product that was purified by mass-directed HPLC (387.5, mid-late) to yield product **2.36** (31 mg, 81%); δ_H (500 MHz, DMSO-d^6) 7.28 – 7.23 (1H, m), 7.23 – 7.18 (2H, m), 7.17 – 7.08 (3H, m), 6.98 (1H, tt, J 7.1, 1.1), 6.92 – 6.87 (4H, m), 6.85 – 6.81 (2H, m), 4.81 – 4.68 (2H, m), 4.4 (1H, br d, J 12.9), 3.87 (1H, br d, J 13.4), 3.05 (1H, br t, J 12.0), 2.69 (1H, tt, J 12.0, 3.4), 2.59 (1H, app t, J 12.0), 1.71 (2H, br app d, J 12.5), 1.55 (1H, m), 1.36 (1H, qd, J 12.7, 4.1); δ_C (125 MHz, DMSO-d^6) 166.1, 158.4, 154.9, 150.1, 146.1, 130.4, 128.9, 127.2, 126.7, 123.1, 121.0, 117.8, 116.4, 67.0, 45.3, 42.4, 42.1, 33.5; HRMS (ESI) found MH$^+$, 388.1916, $C_{25}H_{26}NO_3$ requires 388.1913.

2-(4-benzylphenoxy)-1-[4-(pyridin-2-yl)piperazin-1-yl]ethan-1-one, 2.37
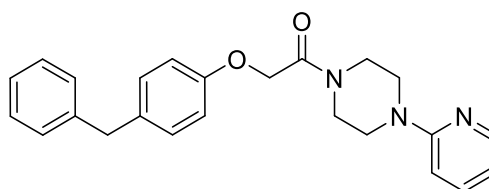
Chemical Formula: $C_{24}H_{25}N_3O_2$

By general procedure **B**, 2-(4-benzylphenoxy)acetic acid **2.23** and 1-(pyridin-2-yl)piperazine **A7** gave a crude product that was purified by mass-directed HPLC (387.5, ear-mid) to yield product **2.37** (19 mg, 51%); δ_H (500 MHz, DMSO-d^6) 8.14 – 8.10 (1H, m), 7.58 – 7.52 (1H, m), 7.26 (2H, app t, *J* 7.6), 7.21 – 7.09 (5H, m), 6.87 – 6.81 (3H, m), 6.66 (1H, dd, *J* 7.1, 4.9), 4.81 (2H, s), 3.85 (2H, s), 3.55 (6H, br s), 3.48 (2H, app br d, *J* 4.6); δ_C (125 MHz, DMSO-d^6) 166.6, 159.2, 156.8, 148.0, 142.2, 138.1, 134.2, 130.0, 129.0, 128.8, 126.3, 115.1, 113.8, 107.8, 66.5, 45.1, 44.8, 44.3, 41.4; HMRS (ESI) found MNa$^+$, 410.1844, $C_{24}H_{25}N_3NaO_2$ requires 410.1845.

2-(4-phenoxyphenoxy)-1-[4-(pyridin-2-yl)piperazin-1-yl]ethan-1-one, 2.38
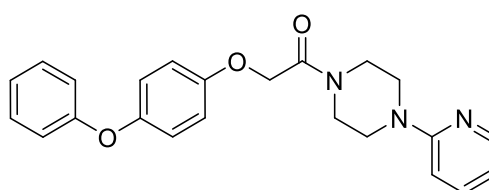
Chemical Formula: $C_{23}H_{23}N_3O_3$

By general procedure **B**, 2-(4-phenoxyphenoxy)acetic acid **2.24** and 1-(pyridin-2-yl)piperazine **A7** gave a crude product that was purified by mass-directed HPLC (389.5, ear-mid) to yield product **2.38** (18 mg, 48%); δ_H (500 MHz, DMSO-d^6) 8.12 (1H, br d, *J* 3.9), 7.55 (1H, br t, *J* 7.0), 7.34 (2H, br t, *J* 7.8), 7.06 (1H, br t, *J* 7.3), 6.98 (4H, br s), 6.91 (2H, br d, *J* 7.9), 6.85 (1H, br d, *J* 8.6), 6.72 – 6.63 (1H, m), 4.86 (2H, s), 3.57 (6H, br s), 3.50 (2H, br s); δ_C (125 MHz, DMSO-d^6) 166.6, 159.2, 154.9, 150.1, 148.0 ,138.2, 130.4, 123.1, 121.0, 117.8, 116.4, 113.8, 107.8, 66.8, 45.0, 44.3, 41.4; HRMS (ESI) found MH$^+$, 390.1821, $C_{23}H_{24}N_3O_3$ requires 390.1818.

4.3 Materials and Methods for Synthesis of 2-hetaryl phenol library

4.3.1 Synthesis of Enaminone Intermediates (En-X)

4.3.1.1 General procedure C: Synthesis of Enaminone Intermediates

Relevant hydroxyacetophenone (1 eq.) was dissolved in *N*,*N*-dimethylformamide dimethyl acetal (DMFDA) as solvent and reactant, and stirred while heating to 90 °C. Following completion of the reaction, monitored by TLC, the solvent was removed *in vacuo* to yield enaminone products that were either purified by column chromatography or pure enough for onward synthesis.

4.3.1.2 General procedure D: Synthesis of Enaminone Intermediates

Relevant hydroxyacetophenone (1 eq.) was dissolved in toluene (0.5 M) and DMFDA (2 eq.) was added portion-wise. Following completion of the reaction, monitored by TLC, the volatile organics were removed *in vacuo* to yield enaminone products that were either purified by column chromatography or pure enough for onward synthesis.

(2*E*)-1-(3,5-dichloro-2-hydroxyphenyl)-3-(dimethylamino)prop-2-en-1-one, En-1
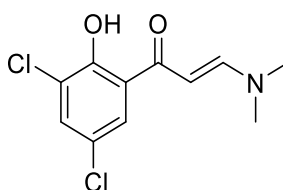
Chemical Formula: $C_{11}H_{11}Cl_2NO_2$

By general procedure **C**, 1-(3,5-dichloro-2-hydroxyphenyl)ethan-1-one (500 mg, 2.44 mmol) gave a crude product as a yellow solid that was used without further purification (522 mg, 82%). R_f 0.18 (DCM); IR v_{MAX} (neat)/cm^{-1} 3081, 2924, 2807, 1629, 1539, 1454, 1420, and 1364; δ_H (400 MHz, acetone-d^6) 8.00 (1H, d, *J* 11.8, propenone-3H), 7.88 (1H, d, *J* 2.4, phenyl-6H), 7.51 (1H, d, *J* 2.4, phenyl-4H), 6.05 (1H, d, *J* 11.8, propenone-2H), 3.34 (3H, s, methyl-CH$_3$), 3.12 (3H, s, methyl-CH$_3$); δ_C (100 MHz, acetone-d^6) 188.7, 156.7, 154.4, 132.6, 126.5, 123.2, 122.1, 121.5, 89.1, 45.0, 37.2; HRMS (ESI) found MH$^+$, 260.0242, $C_{11}H_{12}Cl_2NO_2$ requires 260.0239.

(2*E*)-1-(2-chloro-6-hydroxyphenyl)-3-(dimethylamino)prop-2-en-1-one, En-2
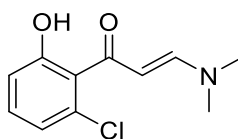
Chemical Formula: $C_{11}H_{12}ClNO_2$

By general procedure **C**, 1-(2-chloro-6-hydroxyphenyl)ethan-1-one (268 mg, 1.6 mmol) gave a crude product as a yellow crystalline solid that was used without further purification (306 mg, 85%). R_f 0.21 (DCM); M.pt 135-138 °C; δ_H (500 MHz, CDCl$_3$) 12.09 (1H, s, O-H), 7.89 (1H, d, *J* 12.0, propenone-3H), 7.14 (1H, t, *J* 8.1, phenyl-4H), 6.87 (1H, dd, *J* 8.1, 1.2, phenyl-3H), 6.84 (1H, dd, *J* 8.1, 1.2, phenyl-5H), 5.98 (1H, dd, *J* 12.0, propenone-2H), 3.19 (3H, s, methyl-CH$_3$), 2.95 (3H, s,

methyl-CH$_3$); δ_C (125 MHz, CDCl$_3$) 189.6, 170.1, 154.1, 131.3, 130.8, 120.5, 115.3, 96.8, 59.4, 44.5, 36.6. HRMS (ESI) found MH$^+$, 226.0629, C$_{11}$H$_{13}$ClNO$_2$ requires 226.0635.

(2*E*)-1-(4-chloro-2-hydroxyphenyl)-3-(dimethylamino)prop-2-en-1-one, En-3
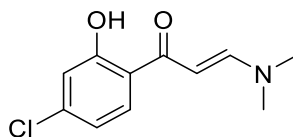
Chemical Formula: C$_{11}$H$_{12}$ClNO$_2$

By general procedure **C**, 1-(4-chloro-2-hydroxyphenyl)ethan-1-one (490 mg, 2.8 mmol) gave a crude product as a yellow crystalline solid that was purified by column chromatography, eluting in 99:1 DCM/MeOH to yield product (594 mg, 94%). R_f 0.19 (DCM); M.pt 138-141 °C; δ_H (400 MHz, acetone-d^6) 7.92 (1H, d, *J* 12.0, propenone-3H), 7.87 (1H, d, *J* 8.6, phenyl-6H), 6.84 (1H, d, *J* 2.1, phenyl-3H), 6.79 (1H, dd, *J* 8.6, 2.1, phenyl-5H), 5.94 (1H, d, *J* 12.0, propenone-2H), 3.28 (3H, s, methyl-CH$_3$), 3.05 (3H, s, methyl-CH$_3$); δ_C (100 MHz, acetone-d^6) 189.9, 164.3, 155.6, 138.3, 129.9, 119.1, 117.9, 117.4, 89.2, 44.7, 36.9; HRMS (ESI) found MNa$^+$, 248.0451, C$_{11}$H$_{12}$ClNNaO$_2$ requires 248.0449.

(2*E*)-3-(dimethylamino)-1-(5-fluoro-2-hydroxyphenyl)prop-2-en-1-one, En-4
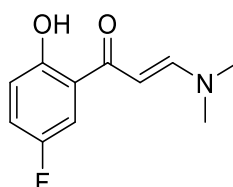
Chemical Formula: C$_{11}$H$_{12}$FNO$_2$

By general procedure **C**, 1-(5-fluoro-2-hydroxyphenyl)ethan-1-one (100 mg, 0.65 mmol) gave a crude product as a yellow crystalline solid that was used without further purification (121 mg, 89%). R_f 0.20 (DCM); M.pt 132-137 °C; δ_H (500 MHz, CDCl$_3$) 13.62 (1H, s, O-H), 7.90 (1H, d, *J* 12.1, propenone-3H), 7.35 (1H, dd, *J* 9.2, 3.1, phenyl-6H), 7.08 (1H, ddd, *J* 9.2, 7.9, 3.1, phenyl-4H), 6.88 (1H, dd, *J* 9.2, 4.8, phenyl-3H), 5.66 (1H, d, *J* 12.1, propenone-2H), 3.21 (3H, s, methyl-CH$_3$), 2.99 (3H, s, methyl-CH$_3$); δ_C (125 MHz, CDCl$_3$) 189.3, 157.9, 154.6, 154.2, 120.1, 119.9, 119.0, 118.1, 112.4, 88.8, 44.5, 36.5; HRMS (ESI) found MH$^+$, 210.0931, C$_{11}$H$_{13}$FNO$_2$ requires 210.0925.

(2*E*)-3-(dimethylamino)-1-(3-fluoro-2-hydroxyphenyl)prop-2-en-1-one, En-5
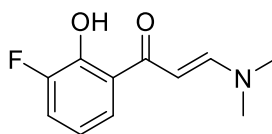
Chemical Formula: $C_{11}H_{12}FNO_2$

By general procedure **D**, 1-(3-fluoro-2-hydroxyphenyl)ethan-1-one (100 mg, 0.65 mmol) gave a crude product that was used without further purification (115 mg, 85%). R_f 0.19 (DCM); IR v_{MAX} (neat)/cm^{-1} 2917, 2810, 2348, 2184, 1843, 1626, 1545, 1279, and 1144; δ_H (500 MHz, CDCl$_3$) 13.62 (1H, s, O-H), 7.91 (1H, d, *J* 12.1, propenone-3H), 7.46 (1H, d, *J* 8.1, phenyl-6H), 7.16 (1H, ddd, *J* 10.6, 8.1, 1.4, phenyl-5H), 6.73 (1H, td, *J* 8.1, 4.8, phenyl-4H), 5.74 (1H, d, *J* 12.1, propenone-2H), 3.22 (3H, s, methyl-CH$_3$), 2.99 (3H, s, methyl-CH$_3$); δ_C (125 MHz, CDCl$_3$) 189.9, 154.2, 150.7, 150.0, 122.1, 121.2, 118.5, 115.8, 89.0, 44.5, 36.5; HRMS (ESI) found MH$^+$, 210.0929, $C_{11}H_{13}FNO_2$ requires 210.0925.

(2*E*)-1-(5-bromo-2-hydroxyphenyl)-3-(dimethylamino)prop-2-en-1-one, En-6
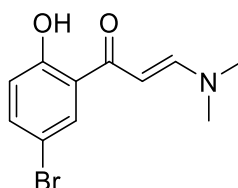
Chemical Formula: $C_{11}H_{12}BrNO_2$

By general procedure **C**, 1-(5-bromo-2-hydroxyphenyl)ethan-1-one (250 mg, 1.16 mmol) gave a crude product that was used without further purification (268 mg, 86%). R_f 0.29 (1:1 petrol/EtOAc); IR v_{MAX} (neat)/cm^{-1} 3065, 2916, 2809, 2233, 1987, 1958, 1569, 1532, and 1494; δ_H (500 MHz, CDCl$_3$) 13.93 (1H, s, O-H), 7.89 (1H, d, *J* 12.0, propenone-3H), 7.76 (1H, d, *J* 2.4, phenyl-6H), 7.41 (1H, dd, *J* 8.8, 2.4, phenyl-4H), 6.83 (1H, d, *J* 8.8, phenyl-3H), 5.67 (1H, d, *J* 12.0, propenone-2H), 3.21 (3H, s, methyl-CH$_3$), 3.00 (3H, s, methyl-CH$_3$);); δ_C (125 MHz, CDCl$_3$) 190.1, 162.0, 155.3, 136.4, 130.6, 121.8, 120.2, 109.6, 89.8, 45.6, 37.6; HRMS (ESI) found MH$^+$, 270.0127, $C_{11}H_{13}{}^{79}BrNO_2$ requires 270.0124.

(2*E*)-1-(4-bromo-2-hydroxyphenyl)-3-(dimethylamino)prop-2-en-1-one, En-7
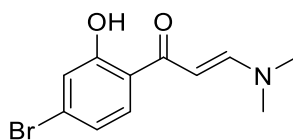
Chemical Formula: $C_{11}H_{12}BrNO_2$

By general procedure **C**, 1-(4-bromo-2-hydroxyphenyl)ethan-1-one (116 mg, 0.53 mmol) gave a crude product that was purified by column chromatography eluting in 5:1 petrol/EtOAc to yield product (121 mg, 84%). R_f 0.36 (1:1 petrol/EtOAc); IR ν_{MAX} (neat)/cm^{-1} 2926, 2915, 2810, 1629, 1571, 1530, 1481, 1421, 1276, 1267, 1225, and 1191; δ_H (400 MHz, acetone-d^6) 7.92 (1H, d, J 12.0, propenone-3H), 7.81 (1H, d, J 8.6, phenyl-6H), 7.01 (1H, d, J 1.8, phenyl-3H), 6.95 (1H, dd, J 8.5, 1.8, phenyl-5H), 5.95 (1H, d, J 12.0, propenone-2H), 3.29 (3H, s, methyl-CH$_3$), 3.06 (3H, s, methyl-CH$_3$); δ_C (100 MHz, acetone-d^6) 190.0, 155.7, 130.0, 126.7, 126.5, 120.8, 120.5, 104.7, 89.2, 44.7, 36.9; HRMS (ESI) found MH$^+$, 270.0126, $C_{11}H_{13}{}^{79}BrNO_2$ requires 270.0124.

(2E)-1-(3-bromo-2-hydroxyphenyl)-3-(dimethylamino)prop-2-en-1-one, En-8
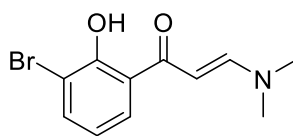
Chemical Formula: $C_{11}H_{12}BrNO_2$

By general procedure **D**, 1-(3-bromo-2-hydroxyphenyl)ethan-1-one (100 mg, 0.46 mmol) gave a crude product that was purified by column chromatography eluting in DCM to yield product (86 mg, 69%). R_f 0.2 (DCM); IR ν_{MAX} (neat)/cm^{-1} 2956, 5919, 2855, 1627, 1543, 1466, 1431, 1368, 1275, 1115, and 1070; δ_H (500 MHz, acetone-d^6) 7.95 (1H, d, J 11.9, propenone-3H), 7.89 (1H, dd, J 8.0, 1.2, phenyl-6H), 7.62 (1H, dd, J 7.9, 1.2, phenyl-4H), 6.75 (1H, t, J 8.0, phenyl-5H), 5.99 (1H, d, J 11.9, propenone-2H), 3.30 (3H, s, methyl-CH$_3$), 3.07 (3H, s, methyl-CH$_3$); δ_C (125 MHz, acetone-d^6) 189.9, 156.0 ,155.9, 136.6, 127.8, 121.5, 118.6, 111.0, 89.1, 44.8, 36.9; HRMS (ESI) found MNa$^+$, 291.9947, $C_{11}H_{12}{}^{79}BrNNaO_2$ requires 291.9943.

(2E)-1-(3,5-dibromo-2-hydroxyphenyl)-3-(dimethylamino)prop-2-en-1-one, En-9
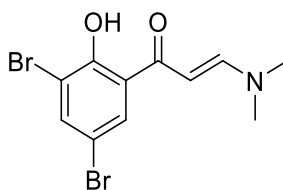
Chemical Formula: $C_{11}H_{11}Br_2NO_2$

By general procedure **D**, 1-(3,5-dibromo-2-hydroxyphenyl)ethan-1-one (433 mg, 1.48 mmol) gave a crude product that was purified by column chromatography eluting in DCM to yield product as a crystalline yellow-orange solid (496 mg, 96%). R_f 0.21 (DCM); M.pt 144-149 °C; IR v_{MAX} (neat)/cm^{-1} 3077, 2929, 2917, 2805, 1626, 1541, 1485, 1442, 1363, 1303, 1271 and 1106; δ_H (500 MHz, acetone-d^6) 8.04 (1H, d, J 2.2, phenyl-6H), 8.00 (1H, d, J 11.8, propenone-3H), 7.76 (1H, d, J 2.2, phenyl-4H), 6.06 (1H, d, J 11.8, propenone-2H), 3.34 (3H, s, methyl-CH$_3$), 3.12 (3H, s, methyl-CH$_3$); δ_C (125 MHz, acetone-d^6) 188.4, 156.7, 138.1, 130.0, 122.4, 112.2, 108.7, 89.0, 44.9, 37.2; HRMS (ESI) found MH$^+$, 347.9230, $C_{11}H_{12}{}^{79}Br_2NO_2$ requires 347.9229.

(2E)-3-(dimethylamino)-1-(5-ethyl-2-hydroxyphenyl)prop-2-en-1-one, En-10
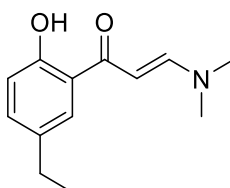
Chemical Formula: $C_{13}H_{17}NO_2$

By general procedure **D**, 1-(5-ethyl-2-hydroxyphenyl)ethan-1-one (100 mg, 0.61 mmol) gave a crude product that was purified by column chromatography eluting in DCM to yield product as a yellow solid (111 mg, 83%). R_f 0.26 (DCM); δ_H (500 MHz, acetone-d^6) 7.87 (1H, d, J 12.0, propenone-3H), 7.70 (1H, d, J 2.0, phenyl-6H), 7.21 (1H, dd, J 8.4, 2.0, phenyl-4H), 6.74 (1H, d, J 8.4, phenyl-3H), 6.00 (1H, d, J 12.0, propenone-2H), 3.26 (3H, s, methyl-CH$_3$), 3.03 (3H, s, methyl-CH$_3$), 2.56 (2H, q, J 7.6, ethyl-CH$_2$), 1.17 (3H, t, J 7.6, ethyl-CH$_3$); δ_C (125 MHz, acetone-d^6) 191.1, 161.4, 155.0, 133.3, 133.2, 127.3, 120.0, 117.6, 89.4, 44.5, 36.8, 27.8, 15.7; HRMS (ESI) found MH$^+$, 220.1341, $C_{13}H_{18}NO_2$ requires 220.1338.

(2E)-1-(5-chloro-2-hydroxy-4-methylphenyl)-3-(dimethylamino)prop-2-en-1-one, En-11
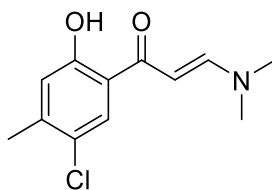
Chemical Formula: C$_{12}$H$_{14}$ClNO$_2$

By general procedure **D**, 1-(5-chloro-2-hydroxy-4-methylphenyl)ethan-1-one (314 mg, 1.71 mmol) gave a crude product that was used without further purification (403 mg, 98%). R_f 0.15 (DCM); δ$_H$ (500 MHz, CDCl$_3$) 13.83 (1H, s, O-H), 7.87 (1H, d, J 12.1, propenone-3H), 7.61 (1H, s, phenyl-6H), 6.80 (1H, s, phenyl-3H), 5.66 (1H, d, J 12.1, propenone-2H), 3.19 (3H, s, N-methyl-CH$_3$), 2.98 (3H, s, N-methyl-CH$_3$), 2.33 (3H, s, methyl-CH$_3$); δ$_C$ (125 MHz, CDCl$_3$) 190.1, 161.4, 155.0, 142.5, 128.0, 123.2, 120.2, 119.3, 89.7, 45.5, 37.6, 20.5; HRMS (ESI) found MNa$^+$, 262.0600, C$_{12}$H$_{14}$ClNNaO$_2$ requires 262.0605.

(2E)-3-(dimethylamino)-1-[2-hydroxy-5-(trifluoromethyl)phenyl]prop-2-en-1-one, En-12
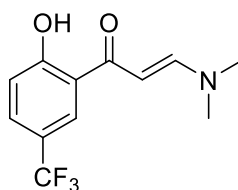
Chemical Formula: C$_{12}$H$_{12}$F$_3$NO$_2$

By general procedure **C**, 1-[2-hydroxy-5-(trifluoromethyl)phenyl]ethan-1-one (206 mg, 1 mmol) gave a crude product that was used without further purification (271 mg, 96%). R_f 0.42 (DCM); IR ν$_{MAX}$ (neat)/cm^{-1} 2927, 2872, 1631, 1542, 1503, 1439, 1320, 1267, 1228, 1188, 1134 and 1106; δ$_H$ (500 MHz, acetone-d^6) 8.18 (1H, d, J 1.8, phenyl-6H), 7.99 (1H, d, J 11.9, propenone-3H), 7.64 (1H, dd, J 8.7, 1.8, phenyl-4H), 6.99 (1H, d, J 8.7, phenyl-3H), 6.11 (1H, d, J 11.9, propenone-2H), 3.32 (3H, s, methyl-CH$_3$), 3.10 (3H, s, methyl-CH$_3$); δ$_C$ (125 MHz, acetone-d^6) 189.6, 166.1, 156.3, 129.9, 125.8, 127.9 – 121.5 (br q), 120.0, 119.7 – 118.9 (q), 118.6, 89.0, 44.8, 37.1; HRMS (ESI) found MNa$^+$, 282.0720, C$_{12}$H$_{12}$F$_3$NNaO$_2$ requires 282.0712.

(2E)-3-(dimethylamino)-1-[2-hydroxy-4-(trifluoromethyl)phenyl]prop-2-en-1-one, En-13
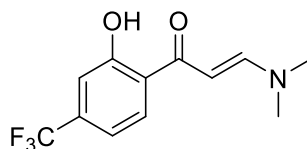
Chemical Formula: $C_{12}H_{12}F_3NO_2$

By general procedure **D**, 1-[2-hydroxy-4-(trifluoromethyl)phenyl]ethan-1-one (200 mg, 0.98 mmol) gave a crude product that was used without further purification (178 mg, 70%). R_f 0.23 (DCM); δ_H (500 MHz, acetone-d^6) 8.09 (1H, d, J 8.2, phenyl-6H), 7.98 (1H, d, J 11.9, propenone-3H), 7.09 (2H, br app d, J 9.5, phenyl-3H and -4H), 6.04 (1H, d, 11.9, propenone-2H), 3.32 (3H, s, methyl-CH$_3$), 3.10 (3H, s, methyl-CH$_3$); δ_C (125 MHz, acetone-d^6) 189.6, 156.2, 133.9, 130.5, 129.5, 124.9, 122.7, 114.5, 113.8, 89.4, 44.8, 37.0; HRMS (ESI) found MH$^+$, 260.0897, $C_{12}H_{13}F_3NO_2$ requires 260.0893.

(2*E*)-3-(dimethylamino)-1-(2-hydroxy-5-nitrophenyl)prop-2-en-1-one, En-14
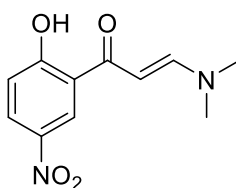
Chemical Formula: $C_{11}H_{12}N_2O_4$

By general procedure **D**, 1-(2-hydroxy-5-nitrophenyl)ethan-1-one (800 mg, 4.42 mmol) gave a crude product that was used without further purification (811 mg, 77%). R_f 0.13 (DCM); IR v_{MAX} (neat)/cm^{-1} 3101, 3077, 3043, 2923, 1918, 1626, 1583, 1519, 1372, 1309, and 1124; δ_H (500 MHz, CDCl$_3$) 8.61 (1H, d, J 2.7, phenyl-6H), 8.20 (1H, dd, J 9.2, 2.7, phenyl-4H), 7.96 (1H, d, J 11.9, propenone-3H), 6.95 (1H, d, J 9.2, phenyl-3H), 5.79 (1H, d, J 11.9, propenone-2H), 3.26 (3H, s, methyl-CH$_3$), 3.06 (3H, s, methyl-CH$_3$); δ_C (125 MHz, acetone-d^6) 189.5, 169.1, 156.0, 138.7, 128.9, 124.8, 119.4, 119.1, 89.4, 45.8, 37.9; HRMS (ESI) found MH$^+$, 237.0875, $C_{11}H_{13}N_2O_4$ requires 237.0870.

4.3.2 Synthesis of Chromenone Intermediates

4.3.2.1 General procedure E: Synthesis of 4-oxo-4*H*-chromene-2-carboxylic acid intermediates

Relevant hydroxyacetophenone (1 eq.) was dissolved or suspended in diethyl oxalate (2.2 eq.) and stirred. NaOEt (3 eq.) in EtOH (21% w/v) was added dropwise over 5 minutes. Following completion of the reaction, monitored by TLC, the solvents were removed *in vacuo* to yield crude material. This crude was dissolved in EtOAc (15 mL), washed with H_2O, (2 x 15 mL) and brine (1 x 15 mL), dried over $MgSO_4$, filtered, and the organic solvent removed *in vacuo*. The resulting material was stirred in glacial acetic acid (5 mL) with 10 drops of conc. HCl at 100 °C for 18 hours. The solution was cooled to room temperature and diluted with H_2O, resulting in precipitate that was filtered off, washed with dilute aq. HCl (20 mL), and dried *in vacuo* to yield 4-oxo-4*H*-chromene-2-carboxylic acid products in sufficient purity for onward synthesis.

4.3.2.2 General procedure F: Synthesis of methyl-4*H*-chromen-4-one intermediates

Relevant hydroxyacetophenone (1 eq.) and associated ethyl acetate (2.5 eq.) were dissolved in dry THF (2.5 mL) under N_2 and added dropwise to a stirred solution of NaH (4 eq.) in dry THF (2.5 mL) under N_2, then stirred for 15 minutes. The reaction solution was poured in to 50 mL ice-water and the aqueous layer adjusted to pH 6 with 2 M HCl then extracted with EtOAc (2 x 25 mL). The organic layer was dried with $MgSO_4$, filtered, and the solvent removed *in vacuo*. The obtained material was suspended in 20 mL MeOH and 0.5 mL conc. HCl was added, and the solution stirred for 16 hours. The organic solvent was removed *in vacuo* and crude material was dissolved in EtOAc (25 mL) then washed with saturated aq. $NaHCO_3$ (25 mL), H_2O (25 mL), and brine (25 mL). The organic layer was dried over $MgSO_4$, filtered, and solvent removed *in vacuo* to yield crude material that was purified by column chromatography to yield methyl-4*H*-chromen-4-one intermediates.
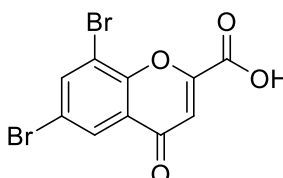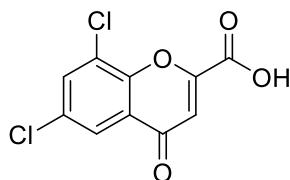
6-chloro-4-oxo-4*H*-chromene-2-carboxylic acid, 3.43
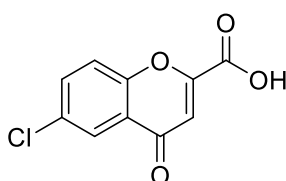
Chemical Formula: $C_{10}H_5ClO_4$

By general procedure **E**, 1-(5-chloro-2-hydroxyphenyl)ethan-1-one (2 g, 11.6 mmol) gave a crude product that was used without further purification (2.02 g, 77%). IR v_{MAX} (neat)/cm^{-1} 3090, 3070, 2637, 1739, 1644, 1614, 1598, 1451, 1418, 1277, 1257, and 1233; δ_H (500 MHz, MeOD) 8.09 (1H, d, J 2.6, phenyl-5H), 7.83 (1H, dd, J 9.0, 2.6, phenyl-7H), 7.72 (1H, d, J 2.6, phenyl-8H), 7.05 (1H, s, chromene-2H); δ_C (125 MHz, MeOD) 178.3, 162.0, 155.4, 154.6, 134.9, 131.5, 124.8, 124.0, 120.8, 112.7; HRMS (ESI) found MNa$_2$-H$^+$, 268.9584, C$_{10}$H$_4$ClNa$_2$O$_4$ requires 268.9588.

4-oxo-7-(trifluoromethyl)-4*H*-chromene-2-carboxylic acid, 3.44
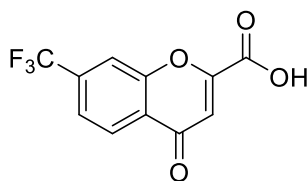
Chemical Formula: C$_{11}$H$_5$F$_3$O$_4$

By general procedure **E**, 1-[2-hydroxy-4-(trifluoromethyl)phenyl]ethan-1-one (538 mg, 2.6 mmol) gave a crude product that was used without further purification (576 mg, 86%). IR v_{MAX} (neat)/cm^{-1} 3435, 3085, 1967, 1905, 1649, 1630, 1571, 1498, 1439, 1352, 1292, and 1208; δ_H (500 MHz, MeOD) 8.33 (1H, d, J 8.3, phenyl-5H), 8.07 (1H, app br s, phenyl-8H), 7.80 (1H, br dd, J 8.3, 1.3, phenyl-6H), 7.12 (1H, s, chromene-2H); δ_C (125 MHz, MeOD) 178.2, 161.1, 155.7, 154.3, 135.8 (q), 126.7, 126.1, 124.22, 121.9, 116.6, 113.9; HRMS (ESI) found MH$^+$, 259.0212, C$_{11}$H$_6$F$_3$O$_4$ requires 259.0213.

4-oxo-6-(trifluoromethyl)-4*H*-chromene-2-carboxylic acid, 3.45
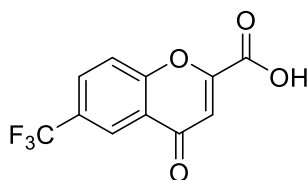
Chemical Formula: C$_{11}$H$_5$F$_3$O$_4$

By general procedure **E**, 1-[2-hydroxy-5-(trifluoromethyl)phenyl]ethan-1-one (224 mg, 1.1 mmol) gave a crude product that was used without further purification (259 mg, 91%). δ_H (500 MHz, MeOD) 8.38 (1H, d, J 1.8, phenyl-5H), 8.09 (1H, dd, J 8.9, 2.3, phenyl-7H), 7.86 (1H, d, J 8.9, phenyl-8H), 7.89 (1H, s, chromene-2H); δ_C (125 MHz, MeOD) 178.1, 173.8, 161.1, 157.7, 154.1,

131.1, 127.8 (q), 124.9 – 122.2 (br q), 122.8, 120.3, 113.9; HRMS (ESI) found MH⁺, 259.0214, $C_{11}H_6F_3O_4$ requires 259.0213.

7-chloro-4-oxo-4H-chromene-2-carboxylic acid, 3.46
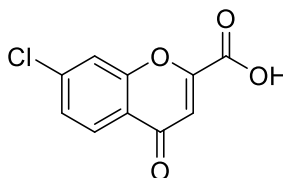
Chemical Formula: $C_{10}H_5ClO_4$

By general procedure **E**, 1-(4-chloro-2-hydroxyphenyl)ethan-1-one (1 g, 5.8 mmol) gave a crude product that was used without further purification (874 mg, 67%). δ_H (500 MHz, MeOD) 8.12 (1H, d, J 8.5, phenyl-5H), 7.79 (1H, d, J 1.8, phenyl-8H), 7.53 (1H, dd, J 8.5, 1.8, phenyl-6H), 7.05 (1H, s, chromene-2H); δ_C (125 MHz, MeOD) 178.4, 161.3, 156.3, 153.9, 140.7, 126.6, 126.5, 122.5, 118.6, 113.7; HRMS (ESI) found MH⁺, 224.9958, $C_{10}H_6ClO_4$ requires 224.9954.

6,8-dibromo-4-oxo-4H-chromene-2-carboxylic acid, 3.47

Chemical Formula: $C_{10}H_4Br_2O_4$

By general procedure **E,** 1-(3,5-dibromo-2-hydroxyphenyl)ethan-1-one (519 mg, 1.77 mmol) gave a crude product that was used without further purification (551 mg, 89%). IR v_{MAX} (neat)/cm⁻¹ 3482, 3102, 3069, 2801, 2414, 1881, 1732, 1646, 1586, 1552, 1452, 1286; δ_H (500 MHz, MeOD) 8.29 (1H, d, J 2.4, phenyl-5H), 8.16 (1H, d, J 2.4, phenyl-7H), 7.06 (1H, s, chromene-2H); δ_C (125 MHz, MeOD) 175.9, 160.3, 153.3, 152.0, 140.0, 127.2, 126.6, 11.8, 114.2, 113.5; HRMS (ESI) found MNa₂-H⁺, 390.8185, $C_{10}H_3{}^{79}Br_2Na_2O_4$ requires 390.8188.

6,8-dichloro-4-oxo-4H-chromene-2-carboxylic acid, 3.48

Chemical Formula: $C_{10}H_4Cl_2O_4$

By general procedure **E**, 1-(3,5-dichloro-2-hydroxyphenyl)ethan-1-one (518 mg, 2.52 mmol) gave a crude product that was used without further purification (555 mg, 85%). IR ν_{MAX} (neat)/cm^{-1} 3218, 3067, 1726, 1632, 1610, 1594, 1562, 1447, 1306, 1264; δ_H (500 MHz, acetone-d^6) 8.04 (1H, d, J 2.5, phenyl-5H), 7.98 (1H, d, J 2.5, phenyl-7H), 7.06 (1H, s, chromene-2H); δ_C (125 MHz, acetone-d^6) 175.9, 160.3, 153.1, 150.7, 134.5, 130.9, 126.3, 124.9, 123.4, 114.3; HRMS (ESI) found MNa$_2$-H$^+$, 302.9195, $C_1H_3Cl_2Na_2O_4$ requires 302.9199.

6-chloro-2-methyl-4H-chromen-4-one, 3.49
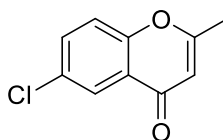
Chemical Formula: $C_{10}H_7ClO_2$

By general procedure **F**, 1-(5-chloro-2-hydroxyphenyl)ethan-1-one (1 g, 5.86 mmol) and ethyl acetate (1.4 mL, 14.6 mmol) gave a crude product that was purified by column chromatography eluting with 9:1 to 6:1 petrol/EtOAc to yield product as a colourless oil (914 mg, 80%). R_f 0.22 (5:1 petrol/EtOAc); IR ν_{MAX} (neat)/cm^{-1} 3088, 1657, 1602, 1568, 1459, 1435, 1384, 1347, 1268; δ_H (500 MHz, acetone-d^6) 7.97 (1H, d, J 2.7, phenyl-5H), 7.74 (1H, dd, J 8.9, 2.7, phenyl-7H), 7.58 (1H, d, J 8.9, phenyl-8H), 6.19 (1H, d, J 0.6, chromene-2H), 2.42 (3H, d, J 0.6, methyl-CH$_3$); δ_C (125 MHz, acetone-d^6) 175.6, 167.0, 154.9, 133.5, 130.1, 124.7, 124.2, 120.3, 110.0, 19.5; HRMS (ESI) found MH$^+$, 195.0217, $C_{10}H_8ClO_2$ requires 195.0212.

6-chloro-2-(difluoromethyl)-4H-chromen-4-one, 3.50
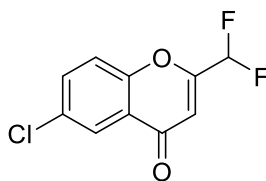
Chemical Formula: $C_{10}H_5ClF_2O_2$

By general procedure **F**, 1-(5-chloro-2-hydroxyphenyl)ethan-1-one (1 g, 5.86 mmol) and ethyl 2,2-difluoroacetate (1.45 mL, 14.6 mmol) gave a crude product that was purified by column chromatography eluting with 20:1 to 3:1 petrol/EtOAc to yield product as a yellow oil (863 mg, 63%). R_f 0.24 (DCM); IR ν_{MAX} (neat)/cm^{-1} 3092, 3065, 2997, 1701, 1659, 1603, 1465, 1447, 1405, 1322, 1276; δ_H (400 MHz, acetone-d^6) 8.03 (1H, d, J 2.6, phenyl-5H), 7.87 (1H, d, J 9.0, 2.6, phenyl-7H), 7.74 (1H, d, J 9.0, phenyl-8H), 6.92 (1H, t, J 53.1, CF$_2$-H), 6.67 (1H, s, chromene-2H); δ_C (100 MHz, acetone-d^6) 175.4, 157.6, 154.5, 134.8, 131.3, 125.2, 124.5, 120.8, 110.2 (t), 110.0 (br t); HRMS (ESI) found MH$^+$, 231.0013, C$_{10}$H$_6$ClF$_2$O$_2$ requires 231.0019.

6-chloro-2-(trifluoromethyl)-4H-chromen-4-one, 3.51
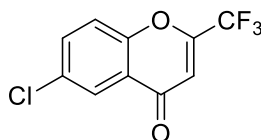
Chemical Formula: C$_{10}$H$_4$ClF$_3$O$_2$

By general procedure **F**, 1-(5-chloro-2-hydroxyphenyl)ethan-1-one (1 g, 5.86 mmol) and ethyl 2,2,2-trifluoroacetate (1.4 mL, 14.6 mmol) gave a crude product that was purified by column chromatography eluting with 20:1 to 3:1 petrol/EtOAc to yield product as a yellow oil (1.1 g, 76%). R_f 0.4 (DCM); δ_H (500 MHz, acetone-d^6) 8.05 (1H, d, J 2.7, phenyl-5H), 7.92 (1H, dd, J 8.9, 2.7, phenyl-7H), 7.79 (1H, d, J 8.9, phenyl-8H), 6.90 (1H, s, chromene-2H); δ_C (125 MHz, acetone-d^6) 175.1, 154.3, 136.3, 135.2, 131.7, 125.2, 124.5, 120.9, 120.3, 110.6; HRMS (ESI) found MH$^+$, 248.9924, C$_{10}$H$_5$ClF$_3$O$_2$ requires 248.9925.

4.3.3 Synthesis of 5-membered heterocycle Fragments

4.3.3.1 General procedure G: Synthesis of Isoxazoles

Associated enaminone (1 eq.) was dissolved in EtOH (0.7 M) and added to a round-bottomed flask equipped with a condenser and stirred. Hydroxylamine hydrochloride (1.5 eq.) was added and the solution heated to 85 °C until complete consumption of starting material was observed by TLC. The solution was cooled to room temperature and the solvent removed *in vacuo* and the resulting material was dissolved in DCM and washed with H$_2$O (1 x 15 mL) and brine (1 x 15 mL). The organic layer was then dried over MgSO$_4$, filtered, and removed *in vacuo* to yield crude material for purification by column chromatography.

4.3.3.2 General procedure H: Synthesis of Pyrazoles

Associated enaminone (1 eq.) was dissolved in EtOH (0.7 M) and added to a round-bottomed flask equipped with a condenser and stirred. Hydrazine monohydrate (5 eq.) was added and the solution heated to 85 °C until complete consumption of starting material was observed by TLC. The solution was cooled to room temperature and the solvent removed *in vacuo* and the resulting material was dissolved in DCM and washed with H_2O (1 x 15 mL) and brine (1 x 15 mL). The organic layer was then dried over $MgSO_4$, filtered, and removed *in vacuo* to yield crude material for purification by column chromatography.

4.3.3.3 General procedure I: Telescoped Synthesis of Isoxazoles or Pyrazoles

Relevant hydroxyacetophenone (1 eq.) was dissolved in toluene (0.5 M) and DMFDA (2 eq.) was added portion-wise. Following completion of the reaction, monitored by TLC, the volatile organics were removed *in vacuo* to yield enaminone crude material. This material was dissolved in EtOH (0.7 M) and added to a round-bottomed flask equipped with a condenser and stirred. Hydroxylamine hydrochloride (1.5 eq.) **or** hydrazine monohydrate (5 eq.) was added and the solution heated to 85 °C until complete consumption of starting material was observed by TLC. The solution was cooled to room temperature and the solvent removed *in vacuo* and the resulting material was dissolved in DCM and washed with H_2O (1 x 15 mL) and brine (1 x 15 mL). The organic layer was then dried over $MgSO_4$, filtered, and removed *in vacuo* to yield crude isoxazole or pyrazole material for purification by column chromatography.

4.3.3.4 General procedure J: Synthesis of 3-COOH Isoxazol-5-yls

Associated chromenone (1 eq.) was dissolved in EtOH (0.7 M) and added to a round-bottomed flask and stirred. Hydroxylamine hydrochloride (1.5 eq.) and KOH (3 eq.) were added and the solution stirred until complete consumption of starting material was observed by TLC or 48 hours had elapsed. The solvent was removed *in vacuo* and the resulting material was dissolved in H_2O and acidified to pH 1 resulting in precipitate. The solid was filtered and washed with 1 M aq. HCl (15 mL) and H_2O (15 mL) to yield either pure product or material for purification by mass directed HPLC.

4.3.3.5 General procedure K: Synthesis of 3-COOH Pyrazol-5-yls

Associated chromenone (1 eq.) was dissolved in EtOH (0.7 M) and added to a round-bottomed flask and stirred. Hydrazine monohydrate (2 eq.) was added and the solution stirred until complete consumption of starting material was observed by TLC or 48 hours had elapsed. The solution was cooled to room temperature and the solvent removed *in vacuo* and the resulting

material was dissolved in DCM and washed with H_2O (1 x 15 mL) and brine (1 x 15 mL). The organic layer was then dried over $MgSO_4$, filtered, and removed *in vacuo* to yield crude material for purification.

4.3.3.6 General procedure L: Telescoped synthesis of 3-methyl Isoxazole series

Associated chromenone (1 eq.), hydroxylamine hydrochloride (2 eq.) and NaOAc (3 eq.) were added to a round-bottom flask with 5 mL 1:1 $EtOH/H_2O$ and stirred at reflux for 1 hour. The solution was cooled to room temperature and diluted with 20 mL H_2O, resulting in a precipitate that was filtered and washed with ice-cold H_2O. This was subsequently added to a stirred solution of glacial acetic acid and conc. HCl and stirred at 130 °C for 15 minutes, then cooled to room temperature and diluted with 20 mL H_2O resulting in precipitate that was filtered, washed with H_2O (15 mL) and dried *in vacuo*. The crude material was purified by column chromatography to yield associated substituted isoxazole.

2,4-dichloro-6-(1,2-oxazol-5-yl)phenol, 3.4
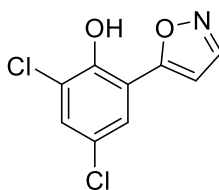
Chemical Formula:
$C_9H_5Cl_2NO_2$
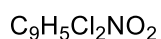
By general procedure **G**, enaminone **En-1** (158 mg, 0.6 mmol) gave a crude product that was purified by column chromatography eluting in 99:1 DCM/MeOH to yield product as a white solid (136 mg, 98%). R_f 0.18 (DCM); δ_H (500 MHz, acetone-d^6) 8.52 (1H, d, *J* 1.8, isox-3H), 7.82 (1H, d, *J* 7.5, phenol-5H), 7.58 (1H, d, *J* 7.5, phenol-3H), 7.02 (1H, d, *J* 1.8, isox-4H); δ_C (125 MHz, acetone-d^6) 163.2, 151.3, 148.7, 130.0, 125.5, 124.9, 122.6, 117.7, 104.1; HRMS (ESI) found MH^+, 229.9767, $C_{19}H_6Cl_2NO_2$ requires 229.9770.

2,4-difluoro-6-(1*H*-pyrazol-5-yl)phenol, 3.1
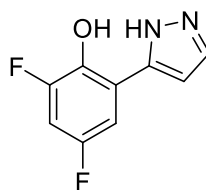
Chemical Formula:
$C_9H_6F_2N_2O$

By general procedure **I**, 1-(3,5-difluoro-2-hydroxyphenyl)ethan-1-one (150 mg, 0.66 mmol) gave a crude product that was purified by filtration through short silica plug to yield product as a white solid (122 mg, 93%). R_f 0.26 (DCM); δ_H (500 MHz, acetone-d^6) 7.98 (1H, d, J 2.5, pyrazole-3H), 7.38 (1H, ddd, J 9.5, 3.0, 1.9, phenol-5H), 7.01 – 6.96 (2H, m, pyrazole-4H and phenol-3H); δ_C (125 MHz, acetone-d^6) 155.7, 153.8, 152.2, 150.3, 140.9, 119.2, 107.6, 103.4, 102.4. HRMS (ESI) found MH$^+$, 197.0514, $C_9H_7F_2N_2O$ requires 197.0521.

3-chloro-2-(1,2-oxazol-5-yl)phenol, 3.7
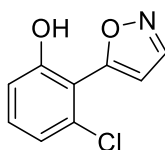
Chemical Formula:
$C_9H_6ClNO_2$

By general procedure **G**, enaminone **En-2** (116 mg, 0.51 mmol) gave a crude product that was purified by column chromatography eluting with 9:1 to 3:1 petrol/EtOAc to yield product as a white solid (96 mg, 97%). R_f 0.11 (9:1 petrol/EtOAc); IR v_{MAX} (neat)/cm^{-1} 2960, 2929, 2672, 1948, 1809, 1746, 1588, 1577, 1463, 1442; δ_H (400 MHz, CDCl$_3$) 8.43 (1H, d, J 1.9, isox-3H), 7.28 (1H, t, J 8.1, phenol-5H), 7.10 (1H, dd, J 8.1, 1.1, phenol-4H), 6.98 (1H, dd, J 8.1, 1.1, phenol-6H), 6.83 (1H, d, J 1.9 isox-4H); δ_C (100 MHz, CDCl$_3$) 155.8, 150.8, 132.0, 122.7, 116.2, 105.5 (weak sample precludes additional peaks); HRMS (ESI) found MH$^+$, 196.0153, $C_9H_7ClNO_2$ requires 196.0160.

**5-(5-chloro-2-methoxyphenyl)-1,2-oxazole, 3.8**
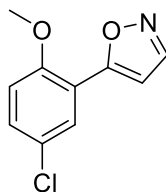
Chemical Formula:
$C_{10}H_8ClNO_2$

By general procedure **I**, 1-(5-chloro-2-methoxyphenyl)ethan-1-one (56 mg, 0.32 mmol) gave a crude product that was purified by column chromatography eluting with 9:1 to 3:1 petrol/EtOAc to yield product as a white solid (96 mg, 97%). R_f 0.24 (DCM); IR ν_{MAX} (neat)/cm^{-1} 3001, 2972, 2939, 2838, 1496, 1467, 1434, 1419, 1321, 1299; δ_H (500 MHz, acetone-d^6) 8.49 (1H, d, J 1.8, isox-3H), 7.88 (1H, d, J 2.7, phenol-6H), 7.48 (1H, dd, J 8.9, 2.7, phenol-4H), 7.25 (1H, d, J 8.9, phenol-3H), 6.93 (1H, d, J 1.8, isox-4H), 4.03 (3H, s, O-CH$_3$); δ_C (125 MHz, acetone-d^6) 163.5, 155.1, 151.2, 130.8, 126.5, 125.3, 117.5, 113.6, 103.6, 55.7; HRMS (ESI) found MH$^+$, 210.0316, $C_{10}H_9ClNO_2$ requires 210.0316.

4-chloro-2-(4-methyl-1,2-oxazol-5-yl)phenol, 3.9
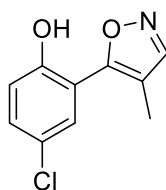
Chemical Formula:
$C_{10}H_8ClNO_2$

By general procedure **I**, 1-(5-chloro-2-hydroxyphenyl)propan-1-one (200 mg, 1.1 mmol) gave a crude product that was purified by column chromatography eluting with DCM to yield product (160 mg, 69%). R_f 0.31 (DCM); IR ν_{MAX} (neat)/cm^{-1} 2926, 2767, 2624, 1631, 1502, 1477, 1412, 1293, 1270, 1120; δ_H (500 MHz, MeOD) 8.27 (1H, s, isox-3H), 7.33 (1H, d, J 2.7, phenol-3H), 7.29 (1H, dd, J 8.7, 2.7, phenol-5H), 6.93 (1H, d, J 8.7, phenol-6H), 2.06 (3H, s, methyl-CH$_3$); δ_C (125 MHz, MeOD) 162.2, 153.9, 152.5, 130.7, 129.2, 123.8, 117.4, 116.6, 112.3, 7.0; HRMS (ESI) found MH$^+$, 210.0315, $C_{10}H_9ClNO_2$ requires 210.0316.

5-chloro-2-(1,2-oxazol-5-yl)phenol, 3.10
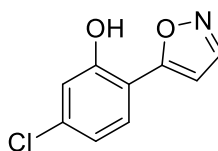
Chemical Formula:
$C_9H_6ClNO_2$
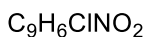
By general procedure **G**, enaminone **En-3** (274 mg, 1.22 mmol) gave a crude product that was purified by column chromatography eluting with 9:1 to 3:1 petrol/EtOAc to yield product as a white solid (198 mg, 81%). R_f 0.23 (DCM); IR v_{MAX} (neat)/cm^{-1} 3102, 1607, 1471, 1417, 11374, 1299, 1226, 1186; δ_H (500 MHz, acetone-d^6) 9.94 (1H, s, O-H), 8.46 (1H, d, J 1.8, isox-3H), 7.88 (1H, d, J 8.5, phenol-3H), 7.13 (1H, d, J 2.0, phenol-6H), 7.09 – 7.05 (1H, m, phenol-4H), 6.92 (1H, d, J 1.8, isox-4H); δ_C (125 MHz, acetone-d^6) 164.4, 155.1, 151.0, 135.7, 128.4, 120.3, 116.3, 113.8, 102.7; HRMS (ESI) found MH$^+$, 196.0155, $C_9H_7ClNO_2$ requires 196.0160.

2,4-dichloro-6-(1H-pyrazol-5-yl)phenol, 3.11
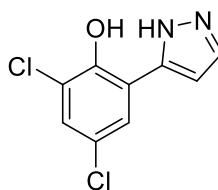
Chemical Formula:
$C_9H_6Cl_2N_2O$
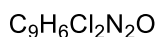
By general procedure **H**, enaminone **En-1** (155 mg, 0.6 mmol) gave a crude product that was purified by filtration through short silica plug eluting with DCM to yield product as a white solid (136 mg, 98%). R_f 0.19 (DCM); δ_H (500 MHz, acetone-d^6) 7.98 (1H, d, J 2.4 pyrazole-3H), 7.42 (1H, d, J 7.4, phenol-5H), 7.01 (1H, d, J 7.4, phenol-3H), 6.96 (1H, d, J 2.4, pyrazole-4H); HRMS (ESI) found MH$^+$, 228.9928, $C_9H_7Cl_2N_2O$ requires 228.9930.

**3-fluoro-2-(1,2-oxazol-5-yl)phenol, 3.12**
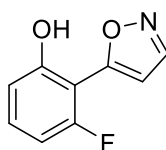
Chemical Formula: $C_9H_6FNO_2$

By general procedure **I,** 1-(2-fluoro-6-hydroxyphenyl)ethan-1-one (150 mg, 1 mmol) gave a crude product that was purified by column chromatography eluting in 99:1 to 4:1 hexane/EtOAc, to yield product (86 mg, 48%). R_f 0.45 (4:1 hexane/EtOAc); IR v_{MAX} (neat)/cm^{-1} 2920, 2852, 2692, 2590, 1620 ,1594, 1566, 1458, 1354, 1305, 1287; δ_H (500 MHz, CDCl$_3$) 8.40 (1H, d, J 2.0, isox-3H), 7.75 (1H, s, O-H), 7.30 (1H, td, J 8.4, 6.5, phenol-4H), 6.88 (1H, dt, J 8.4, 1.0, phenol-5H), 6.80 – 6.75 (1H, m, phenol-6H), 6.74 (1H, d, J 2.0, isox-4H); δ_C (125 MHz, CDCl$_3$) 163.1, 160.8, 158.8, 155.6, 150.7, 132.1, 113.8, 107.6, 103.5; HRMS (ESI) found MH$^+$, 180.0456, C$_9$H$_7$FNO$_2$ requires 180.0455.

5-fluoro-2-(1,2-oxazol-5-yl)phenol, 3.14
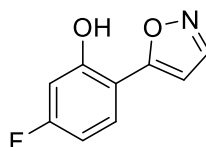
Chemical Formula:
C$_9$H$_6$FNO$_2$

By general procedure **I,** 1-(4-fluoro-2-hydroxyphenyl)ethan-1-one (306 mg, 2 mmol) gave a crude product that was purified by column chromatography eluting in 99:1 to 4:1 hexane/EtOAc, to yield product (242 mg, 79%). R_f 0.23 (DCM); IR v_{MAX} (neat)/cm^{-1} 3465, 3113, 2924, 2792, 2726, 2438, 1573, 1513, 1474, 1420, 1369, 1307, 1254; δ_H (500 MHz, CDCl$_3$) 8.33 (1H, d, J 1.8, isox-3H), 7.66 (1H, dd, J 8.6, 6.4, phenyl-6H), 6.91 (1H, app s, phenyl-5H), 6.79 – 6.75 (1H, m, phenyl-3H), 6.58 (1H, d, J 1.8, isox-4H);); δ_C (125 MHz, CDCl$_3$) 158.6, 150.7, 130.7, 129.4, 110.2, 108.7, 104.9, 100.1; HRMS (ESI) found MH$^+$, 180.0451, C$_9$H$_7$FNO$_2$ requires 180.0455.

2-fluoro-6-(1,2-oxazol-5-yl)phenol, 3.15
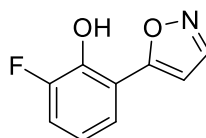
Chemical Formula:
C$_9$H$_6$FNO$_2$

By general procedure **G**, enaminone **En-5** (100 mg, 0.47 mmol) gave a crude product that was purified by filtration through a short silica plug eluting with DCM to yield product (68 mg, 94%). R_f 0.24 (DCM); IR v_{MAX} (neat)/cm^{-1} 2164, 2031, 1976, 1501, 1476, 1456, 1359, 1270, 1223; δ_H (500

MHz, CDCl$_3$) 8.35 (1H, d, *J* 1.8, isox-3H), 7.70 (1H, d, *J* 8.1, phenol-5H), 7.17 (1H, ddd, *J* 9.9, 8.1, 1.4, phenol-4H), 6.98 (1H, app m, phenol-3H), 6.88 (1H, d, *J* 1.8, isox-4H), 6.11 (1H, s, O-H); δ$_C$ (125 MHz, CDCl$_3$) 164.5, 152.4, 151.0, 141.3, 122.8, 120.7, 120.6, 116.6, 102.8; HRMS (ESI) found MH$^+$, 180.0452, C$_9$H$_7$FNO$_2$ requires 180.0455.

2,4-difluoro-6-(1,2-oxazol-5-yl)phenol, 316
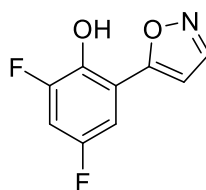
Chemical Formula:
C$_9$H$_5$F$_2$NO$_2$

By general procedure **I**, 1-(3,5-difluoro-2-hydroxyphenyl)ethan-1-one (200 mg, 1.16 mmol) gave a crude product that was purified by column chromatography eluting with DCM to yield product (199 mg, 88%); IR v$_{MAX}$ (neat)/cm^{-1} 2923, 2852, 2744, 1703, 1680, 1613, 1580, 1507, 1433, 1371, 1277; δ$_H$ (500 MHz, MeOD) 8.46 (1H, d *J* 1.8, isox-3H), 7.41 (1H, ddd, 9.3, 3.0, 2.0, phenyl-5H), 7.10 (1H, ddd, *J* 11.0, 8.2, 3.0, phenyl-3H), 7.02 (1H, d, *J* 1.8, isox-4H); δ$_C$ (125 MHz, MeOD) 163.8, 155.8, 152.7, 150.9, 150.8, 116.7, 107.8, 104.9, 103.4; HRMS (ESI) found MH$^+$, 198.0363, C$_9$H$_6$F$_2$NO$_2$ requires 198.0361.

4-bromo-2-(1,2-oxazol-5-yl)phenol, 3.17
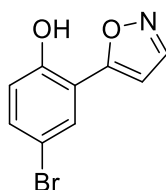
Chemical Formula:
C$_9$H$_6$BrNO$_2$

By general procedure **G**, enaminone **En-6** (100 mg, 0.37 mmol) gave a crude product that was purified by column chromatography eluting in 17:1 petrol/EtOAc to yield product as an off-white solid (77 mg, 86%); *R*$_f$ 0.28 (17:1 petrol/EtOAc); IR v$_{MAX}$ (neat)/cm^{-1} 2770, 1886, 1826, 1759, 1604, 1563, 1495, 1370; δ$_H$ (500 MHz, acetone-*d*^{6}) 9.68 (1H, s, O-H), 8.35 (1H, d, *J* 1.8, isox-3H), 7.84 (1H, d, *J* 2.5, phenol-3H), 7.33 (1H, dd, *J* 8.7, 2.5, phenol-5H), 6.94 (1H, d, *J* 8.7, phenol-6H), 6.83

(1H, d, J 1.8, isox-4H); δ_C (125 MHz, acetone-d^6) 163.9, 153.6, 151.1, 133.6, 129.3, 118.5, 116.5, 111.4, 103.2; HRMS (ESI) found MH⁺, 239.9649, $C_9H_7{}^{79}BrNO_2$ requires 239.9655.
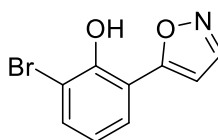
5-bromo-2-(1,2-oxazol-5-yl)phenol, 3.18
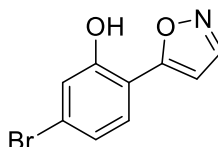
Chemical Formula:
$C_9H_6BrNO_2$

By general procedure **G**, enaminone **En-7** (101 mg, 0.38 mmol) gave a crude product that was purified by column chromatography eluting in 17:1 petrol/EtOAc to yield product as an off-white solid (81 mg, 89%); R_f 0.26 (17:1 petrol/EtOAc); IR ν_{MAX} (neat)/cm⁻¹ 2783, 2593, 1591, 1566, 1468, 1411, 1368, 1329, 1257, 1241, 1126; δ_H (500 MHz, acetone-d^6) 9.95 (1H, s, O-H), 8.46 (1H, d, J 1.8, isox-3H), 7.81 (1H, d, J 8.4, phenol-3H), 7.29 (1H, d, J 1.7, phenol-6H), 7.22 (1H, dd, J 8.4, 1.7, phenol-4H), 6.93 (1H, d, J 1.8, isox-4H); δ_C (125 MHz, acetone-d^6) 164.4, 155.1, 151.0, 128.6, 123.8, 123.2, 119.3, 114.1, 102.8; HRMS (ESI) found MH⁺, 239.9650, $C_9H_7{}^{79}BrNO_2$ requires 239.9655.
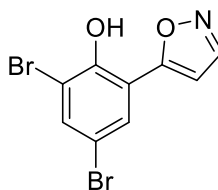
2-bromo-6-(1,2-oxazol-5-yl)phenol, 3.19

Chemical Formula:
$C_9H_6BrNO_2$

By general procedure **G**, enaminone **En-8** (40 mg, 0.14 mmol) gave a crude product that was purified by column chromatography eluting in 17:1 petrol/EtOAc to yield product as a white solid (32 mg, 95%); R_f 0.19 (17:1 petrol/EtOAc); δ_H (500 MHz, acetone-d^6) 8.49 (1H, d, J 1.8, isox-3H), 7.89 (1H, dd, J 8.0, 1.6, phenol-5H), 7.67 (1H, dd, J 8.0, 1.6, phenol-3H), 7.03 (1H, t, J 8.0, phenol-4H), 6.96 (1H, d, J 1.8, isox-4H); δ_C (125 MHz, acetone-d^6) 164.5, 151.1, 150.4, 134.2, 126.9, 121.8, 116.8, 116.5, 103.3; HRMS (ESI) found MNa⁺, 261.9470, $C_9H_6{}^{79}BrNNaO_2$ requires 261.9474.
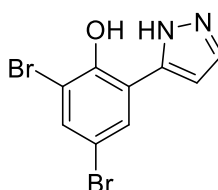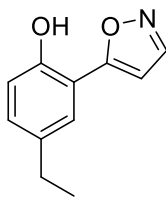
2,4-dibromo-6-(1,2-oxazol-5-yl)phenol, 3.20

Chemical Formula:
$C_9H_5Br_2NO_2$

By general procedure **G**, enaminone **En-9** (170 mg, 0.49 mmol) gave a crude product that was purified by column chromatography eluting in DCM to yield product as a white solid (131 mg, 83%); R_f 0.21 (DCM); δ_H (500 MHz, CDCl$_3$) 8.35 (1H, d, J 1.8, isox-3H), 8.04 (1H, d, J 2.3, phenol-5H), 7.68 (1H, d, J 2.3, phenol-3H), 6.90 (1H, d, J 1.8, isox-4H), 6.32 (1H, s, O-H); δ_C (125 MHz, CDCl$_3$) 163.2, 151.1, 148.2, 135.2, 129.9, 116.7, 113.2, 112.2, 103.9; HRMS (ESI) found MH$^+$, 317.8755, $C_9H_6{}^{79}Br_2NO_2$ requires 317.8760.

2,4-dibromo-6-(1H-pyrazol-5-yl)phenol, 3.21

Chemical Formula:
$C_9H_6Br_2N_2O$

By general procedure **H**, enaminone **En-9** (150 mg, 0.43 mmol) gave a crude product that was purified by column chromatography eluting in DCM to yield product as a white solid (117 mg, 85%); R_f 0.19 (DCM); δ_H (500 MHz, CDCl$_3$) 7.97 (1H, d, J 2.5, pyrazole-3H), 7.63 (1H, d, J 2.4, phenol-5H), 7.19 (1H, d, J 2.4, phenol-3H), 6.83 (1H, d, J 2.5, pyrazole-4H); HRMS (ESI) found MH$^+$, 316.8918, $C_9H_7{}^{79}Br_2N_2O$ requires 316.8920
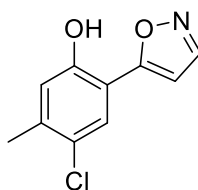
4-ethyl-2-(1,2-oxazol-5-yl)phenol, 3.22

Chemical Formula: $C_{11}H_{11}NO_2$

By general procedure **G**, enaminone **En-10** (149 mg, 0.68 mmol) gave a crude product that was purified by column chromatography eluting in DCM to yield product as a fluffy white solid (124 mg, 96%); IR v_{MAX} (neat)/cm^{-1} 3028, 2961, 2929, 2870, 2797, 2738, 2602, 1619, 1572, 1513, 1475, 1420; $δ_H$ (500 MHz, acetone-d^6) 9.22 (1H, s, O-H), 8.43 (1H, d, J 1.8, isox-3H), 7.72 (1H, d, J 2.2, phenol-3H), 7.17 (1H, dd, J 8.3, 2.2, phenol-5H), 7.00 (1H, d, J 8.3, phenol-6H), 6.91 (1H, d, J 1.8, isox-4H), 2.64 (2H, q, J 7.6, ethyl-CH$_2$), 1.22 (3H, t, J 7.6, ethyl-CH$_3$); $δ_C$ (125 MHz, acetone-d^6) 165.6, 152.5, 150.9, 135.7, 130.6, 126.1, 116.4, 114.3, 102.2, 27.6, 15.4; HRMS (ESI) found MH$^+$, 190.0865, $C_{11}H_{12}NO_2$ requires 190.0863.
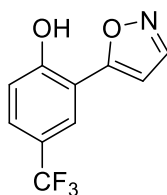
4-chloro-5-methyl-2-(1,2-oxazol-5-yl)phenol, 3.23

Chemical Formula: $C_{10}H_8ClNO_2$

By general procedure **G**, enaminone **En-11** (400 mg, 1.67 mmol) gave a crude product that was purified by column chromatography eluting in DCM to yield product as an off-white crystalline solid (320 mg, 91%); R_f 0.29 (DCM); M.pt 230-236 °C; IR v_{MAX} (neat)/cm^{-1} 3053, 2958, 2925, 2759, 2587, 1611, 1574, 1472, 1404, 1325, 1293; $δ_H$ (500 MHz, MeOD) 8.40 (1H, d, J 1.9, isox-3H), 7.76 (1H, s, phenol-3H), 6.88 (1H, s, phenol-6H), 6.88 (1H, d, J 1.9, isox-4H), 2.34 (3H, s, methyl-CH$_3$); $δ_C$ (125 MHz, MeOD) 164.7, 153.4, 150.8, 138.9, 126.4, 124.4, 118.1, 113.5, 102.1, 18.8; HRMS (ESI) found MH$^+$, 210.0321, $C_{10}H_9ClNO_2$ requires 210.0316.
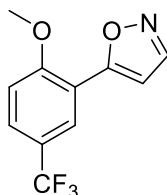
2-(1,2-oxazol-5-yl)-4-(trifluoromethyl)phenol, 3.24

Chemical Formula: $C_{10}H_6F_3NO_2$

By general procedure **G**, enaminone **En-12** (235 mg, 0.91 mmol) gave a crude product that was purified by filtration through short silica plug eluting with DCM to yield product (168 mg, 81%). R_f 0.24 (DCM); δ_H (500 MHz, acetone-d^6) 10.37 (1H, s, O-H), 8.51 (1H, d, J 1.8, isox-3H), 8.16 (1H, d, J 2.2, phenol-3H), 7.66 (1H, dd, J 2.3, 8.6, phenol-5H), 7.28 (1H, d, J 8.6, phenol-6H), 7.01 (1H, d, J 1.8, isox-4H); δ_C (125 MHz, acetone-d^6) 163.8, 157.1, 151.2, 127.9, 125.5 (q), 124.3, 121.8 (q), 117.1, 115.0, 103.4; HRMS (ESI) found MH$^+$, 230.0419, $C_{10}H_7F_3NO_2$ requires 230.0423.

5-[2-methoxy-5-(trifluoromethyl)phenyl]-1,2-oxazole, 3.25

Chemical Formula: $C_{11}H_8F_3NO_2$

By general procedure **I**, 1-[2-methoxy-5-(trifluoromethyl)phenyl]ethan-1-one (422 mg, 1.9 mmol) gave a crude product that was purified by column chromatography eluting in 9:1 to 3:1 petrol/EtOAc to yield product (186 mg, 40%). R_f 0.28 (3:1 petrol/EtOAc); IR v_{MAX} (neat)/cm^{-1} 3189, 2975, 2845, 1623, 1593, 1509, 1476, 1458, 1444, 1327, 1278; δ_H (500 MHz, acetone-d^6) 8.52 (1H, d, J 1.8, isox-3H), 8.18 (1H, d, J 2.3, phenol-6H), 7.81 (1H, ddd, J 8.8, 2.3, 0.6, phenol-4H), 7.42 (1H, d, J 2.3, phenol-3H), 6.97 (1H, d, J 1.8, isox-4H), 4.12 (3H, s, methoxy-CH$_3$); δ_C (125 MHz, acetone-d^6) 163.4, 158.7, 151.2, 128.3, 125.4 (q), 124.2, 122.4 (q), 116.6, 112.5, 103.8, 55.9; HRMS (ESI) found MH$^+$, 244.0578, $C_{11}H_9F_3NO_2$ requires 244.0580.
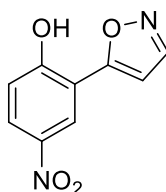
2-(1,2-oxazol-5-yl)-5-(trifluoromethyl)phenol, 3.26
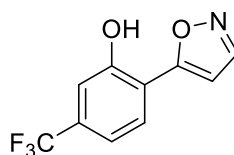
Chemical Formula: $C_{10}H_6F_3NO_2$

By general procedure **G**, enaminone **En-13** (234 mg, 0.9 mmol) gave a crude product that was purified by column chromatography eluting in DCM to yield product (155 mg, 75%). R_f 0.3 (DCM); IR v_{MAX} (neat)/cm^{-1} 2620, 2312, 1625, 1579, 1473, 1432, 1328, 1244, 1173; δ_H (500 MHz, acetone-d^6) 10.15 (1H, s, O-H), 8.53 (1H, d, J 1.8, isox-3H), 8.10 (1H, d, J 8.1, phenol-3H), 7.39 (1H, app s, phenol-4H), 7.37 (1H, app m, phenol-6H), 7.06 (1H, d, J 1.8, isox-4H); δ_C (125 MHz, acetone-d^6) 163.9, 154.4, 151.2, 131.9 (q), 128.2, 124.9 (q), 118.1, 116.6, 113.0, 104.0; HRMS (ESI) found MH$^+$, 230.0423, $C_{10}H_7F_3NO_2$ requires 230.0423.
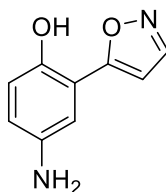
4-nitro-2-(1,2-oxazol-5-yl)phenol, 3.27

Chemical Formula: $C_9H_6N_2O_4$

By general procedure **G**, enaminone **En-14** (365 mg, 1.54 mmol) gave a crude product that was purified by filtration through short silica plug eluting with DCM to yield product (311 mg, 98%). R_f 0.15 (DCM); δ_H (500 MHz, MeOD) 8.72 (1H, d, J 2.8, phenol-3H), 8.48 (1H, d, J 1.9, isox-3H), 8.20 (1H, dd, J 9.1, 2.8, phenol-5H), 7.11 (1H, d, J 9.1, phenol-6H), 7.01 (1H, d, J 1.9, isox-4H); δ_C (125 MHz, MeOD) 163.5, 160.1, 151.1, 140.5, 126.2, 122.8, 116.2, 114.6, 103.5; HRMS (ESI) found MH$^+$, 207.0407, $C_9H_7N_2O_4$ requires 207.0406.

4-amino-2-(1,2-oxazol-5-yl)phenol, 3.28

Chemical Formula: $C_9H_8N_2O_2$

151

4-nitro-2-(1,2-oxazol-5-yl)phenol **3.27** (153 mg, 0.74 mmol), $SnCl_2 \cdot H_2O$ (501 mg, 2.23 mmol), conc. HCl (2 mL) and EtOH (0.5 m) was added to a round-bottomed flask and stirred at 70 °C for 1 hour. The reaction was cooled to room temperature and filtered through celite/KF, washed with EtOAc, and the organic solvent removed *in vacuo* to yield crude product that was purified by column chromatography eluting with 20:1 DCM/MeOH·NH₄ to yield product (64 mg, 49%). R_f 0.15 (20:1 DCM/MeOH·NH₄); IR ν_{MAX} (neat)/cm⁻¹ 3383, 3304, 2930, 2715, 2657, 2562, 1610, 1573, 1515, 1441, 1229, 1204, 1187; δ_H (500 MHz, MeOD) 8.38 (1H, d, *J* 1.8, isox-3H), 7.30 (1H, dd, *J* 2.4, 0.7, phenol-3H), 6.88 (1H, d, *J* 1.9, isox-4H), 6.80 – 6.73 (2H, m, phenol-5H and -6H); δ_C (125 MHz, MeOD) 166.3, 150.7, 147.9, 139.4, 119.4, 116.6, 114.2, 113.5, 101.9; HRMS (ESI) found MH⁺, 177.0657, $C_9H_9N_2O_2$ requires 177.0659.

5-(5-chloro-2-hydroxyphenyl)-1,2-oxazole-3-carboxylic acid, 3.30
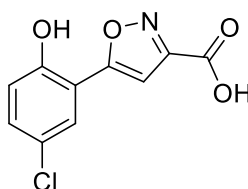
Chemical Formula: $C_{10}H_6ClNO_4$

By general procedure **J**, chromenone **3.43** (200 mg, 0.9 mmol) gave product as a pure, off-white solid (211 mg, 98%). R_f 0.13 (3:1 petrol/EtOAc + 0.2% formic acid); δ_H (500 MHz, MeOD) 7.82 (1H, d, *J* 2.6, phenol-6H), 7.31 (1H, dd, *J* 8.8, 2.6, phenol-4H), 7.22 (1H, s, isox-4H), 6.97 (1H, d, *J* 8.8, phenol-3H); δ_C (125 MHz, MeOD) 167.0, 161.3, 157.5, 153.8, 131.1, 125.9, 124.2, 117.4, 114.9, 103.6; HRMS (ESI) found MNa⁺, 261.9876, $C_{10}H_6ClNNaO_4$ requires 261.9878.

### 5-[2-hydroxy-4-(trifluoromethyl)phenyl]-1,2-oxazole-3-carboxylic acid, 3.31
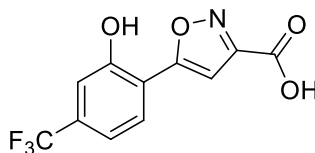
Chemical Formula: $C_{11}H_6F_3NO_4$

By general procedure **J**, chromenone **3.44** (209 mg, 0.81 mmol) gave crude product as an off-white solid that was purified by mass-directed HPLC (273.2, mid-gradient) to yield product (176 mg, 80%); IR ν_{MAX} (neat)/cm⁻¹ 3182, 2918, 2743, 2600, 1710, 1577, 1452, 1427, 1333; δ_H (500

MHz, acetone-d^6) 8.14 (1H, d, J 8.2, phenol-6H), 7.43 (1H, app s, phenol-5H), 7.40 (1H, d, J 8.2, phenol-3H), 7.34 (1H, s, isox-3H); δ_C (125 MHz, acetone-d^6) 166.5, 160.3, 157.5, 154.7, 132.5 (q), 128.1, 124.9 (q), 117.4, 116.6, 113.1, 104.9; HRMS (ESI) found MNa$^+$, 296.0149, $C_{11}H_6F_3NNaO_4$ requires 296.0146.

5-[2-hydroxy-5-(trifluoromethyl)phenyl]-1,2-oxazole-3-carboxylic acid, 3.32
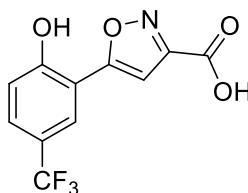
Chemical Formula: $C_{11}H_6F_3NO_4$

By general procedure **J**, chromenone **3.45** (88 mg, 0.34 mmol) gave crude product as an off-white solid that was purified by mass-directed HPLC (273.2, mid-gradient) to yield product (46 mg, 49%); δ_H (500 MHz, acetone-d^6) 8.19 (1H, br d, J 2.1, phenol-6H), 7.72 (1H, br dd, 8.6, 2.1, phenol-4H), 7.35 (1H, d, J 8.6, phenol-3H), 7.32 (1H, s, isox-4H); δ_C (125 MHz, acetone-d^6) 166.4, 160.4, 157.7, 157.4, 128.6, 125.5 (q),124.3, 121.9 (q), 117.3, 114.3, 104.4; HRMS (ESI) found MNa$^+$, 296.0150, $C_{11}H_6F_3NNaO_4$ requires 296.0146.
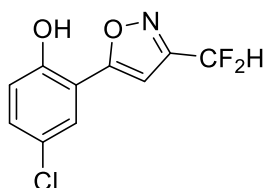
4-chloro-2-(3-methyl-1,2-oxazol-5-yl)phenol, 3.33
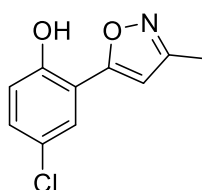
Chemical Formula: $C_{10}H_8ClNO_2$

By general procedure **L**, chromenone **3.46** (196 mg, 1.01 mmol) gave a crude product that was purified by filtration through a short silica plug eluting with DCM to yield product (157 mg, 74%); R_f 0.31 (DCM); IR ν_{MAX} (neat)/cm^{-1} 3083, 2960, 2769, 2634, 2462, 1748, 1608, 1578, 1406; δ_H (500 MHz, acetone-d^6) 9.72 (1H, s, O-H), 7.78 (1H, d, J 2.7, phenol-3H), 7.31 (1H, dd, J 8.7, 2.7, phenol-5H), 7.09 (1H, d, J 8.7, phenol-6H), 6.82 (1H, s, isox-4H), 2.31 (3H, s, methyl-CH$_3$); δ_C (125 MHz, acetone-d^6) 164.2, 160.3, 153.1, 130.4, 129.2, 124.3, 118.0, 116.3, 104.7, 10.5; HRMS (ESI) found MH$^+$, 210.0310, $C_{10}H_9ClNO_2$ requires 210.0316.

4-chloro-2-[3-(difluoromethyl)-1,2-oxazol-5-yl]phenol, 3.34

Chemical Formula: $C_{10}H_6ClF_2NO_2$

By general procedure **L**, chromenone **3.47** (190 mg, 0.82 mmol) gave a crude product that was purified by filtration through a short silica plug eluting with DCM to yield product (196 mg, 97%); R_f 0.26 (DCM);); IR v_{MAX} (neat)/cm^{-1} 3171, 2963, 2926, 2623, 1611, 1575, 1486, 1452, 1400, 1270; δ_H (500 MHz, acetone-d^6) 7.86 (1H, d, J 2.6, phenol-3H), 7.39 (1H, dd, J 8.8, 2.6, phenol-5H), 7.17 (1H, s, isox-4H), 7.14 (1H, d, 8.8, phenol-6h), 7.14 (1H, t, J 53.5, CF$_2$-H); δ_C (125 MHz, acetone-d^6) 166.7, 159.6, 153.5, 131.6, 126.3, 124.5, 118.2, 115.1, 109.7 (t), 100.4; HRMS (ESI) found MH$^+$, 246.0125, $C_{10}H_7ClF_2NO_2$ requires 246.0128.

4-chloro-2-[3-(trifluoromethyl)-1,2-oxazol-5-yl]phenol, 3.35
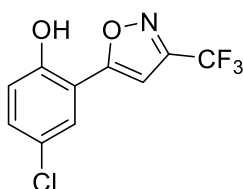
Chemical Formula: $C_{10}H_5ClF_3NO_2$

By general procedure **L**, chromenone **3.48** (200 mg, 0.81 mmol) gave a crude product that was purified by filtration through a short silica plug eluting with DCM to yield product (183 mg, 86%); R_f 0.26 (DCM); δ_H (500 MHz, acetone-d^6) 7.87 (1H, d, J 2.6, phenol-3H), 7.41 (1H, dd, J 8.8, 2.6, phenol-5H), 7.30 (1H, s, isox-4H), 7.16 (1H, d, J 8.8, phenol-6H); δ_C (125 MHz, acetone-d^6) 167.9, 155.8 (q), 153.7, 132.1, 126.4, 124.6, 121.2 (q), 118.3, 114.5, 100.8; HRMS (ESI) found MH$^+$, 264.0024, $C_{10}H_6ClF_3NO_2$ requires 264.0033.

4-chloro-2-[3-(hydroxymethyl)-1,2-oxazol-5-yl]phenol, 3.36
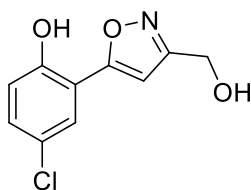
Chemical Formula: $C_{10}H_8ClNO_3$

Carboxylic acid **3.30** (1 g, 4.2 mmol) was placed in a round-bottomed flask in anhydrous THF (5 mL) under N_2 and cooled to -78 °C with an acetone-dry ice bath. 1 M $LiAlH_4$ in anhydrous THF (16.2 mmol) was added dropwise, taking care to control vigorous evolution of gas. The solution was allowed to slowly warm to room temperature over 16 hours, and following completion of the reaction by monitoring with TLC, the solution was diluted with diethyl ether (20 mL) and cooled to 0 °C. 10 mL H_2O and 10 mL 1 M aq. NaOH were slowly added sequentially and after 15 minutes of stirring $MgSO_4$ was added and the solution stirred for an additional 15 minutes. The resulting salts were filtered off and the aqueous layer was extracted with EtOAc (3 x 15 mL). The organic layer was washed with brine (15 mL), dried over $MgSO_4$, filtered, and removed *in vacuo* to yield pure product (929 mg, 98%). R_f 0.14 (DCM); δ_H (500 MHz, acetone-d^6) 7.81 (1H, d, J 2.7, phenol-3H), 7.33 (1H, dd, J 8.7, 2.7, phenol-5H), 7.11 (1H, d, J 8.7, phenol-6H), 7.01 (1H, s, isox-4H), 4.69 (2H, s, hydroxymethyl-CH_2); δ_C (125 MHz, acetone-d^6) 165.2, 164.4, 153.1, 130.6, 126.2, 124.3, 118.0, 116.2, 103.1, 55.8; HRMS (ESI) found MH^+, 226.0263, $C_{10}H_9ClNO_3$ requires 226.0265.

5-(4-chloro-2-hydroxyphenyl)-1*H*-pyrazole-3-carboxylic acid, 3.37
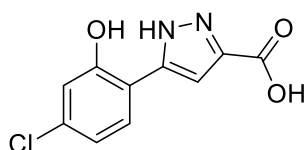
Chemical Formula: $C_{10}H_7ClN_2O_3$

By general procedure **K**, chromenone **3.46** (360 mg, 1.6 mmol) gave pure product as a brown solid (371 mg, 98%). IR ν_{MAX} (neat)/cm^{-1} 2915, 2643, 1894, 1730, 1627, 1583, 1500, 1438, 1402, 1239; δ_H (500 MHz, MeOD) 7.65 (1H, d, J 8.4, phenol-6H), 7.23 (1H, s, pyrazole-4H), 6.95 (1H, d, J 2.0, phenol-6H), 6.92 (1H, dd, J 8.4, 2.0, phenol-4H); δ_C (125 MHz, MeOD) 178.6, 162.1, 155.8, 134.1, 128.0, 119.4, 116.1, 115.2, 105.6; HRMS (ESI) found MNa^+, 261.0045, $C_{10}H_7ClN_2NaO_3$ requires 261.0043.

5-chloro-2-[3-(hydroxymethyl)-1*H*-pyrazol-5-yl]phenol, 3.38
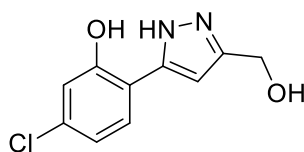
Chemical Formula: $C_{10}H_9ClN_2O_2$

Carboxylic acid **3.37** (156 g, 0.66 mmol) was placed in a round-bottomed flask in anhydrous THF (2 mL) under N_2 and cooled to -78 °C with an acetone-dry ice bath. 2.4 M LiAlH₄ in anhydrous THF (1.1 mL, 2.6 mmol) was added dropwise, taking care to control vigorous evolution of gas. The solution was allowed to slowly warm to room temperature over 16 hours, and following completion of the reaction by monitoring with TLC, the solution was diluted with diethyl ether (10 mL) and cooled to 0 °C. 10 mL H_2O and 10 mL 1 M aq. NaOH were slowly added sequentially and after 15 minutes of stirring MgSO₄ was added and the solution stirred for an additional 15 minutes. The resulting salts were filtered off and the aqueous layer was extracted with EtOAc (3 x 15 mL). The organic layer was washed with brine (15 mL), dried over MgSO₄, filtered, and removed *in vacuo* to yield pure product (141 mg, 95%). R_f 0.1 (DCM); δ_H (500 MHz, acetone-d^6) 7.67 (1H, d, *J* 8.3, phenol-3H), 6.94 (1H, d, *J* 2.1, phenol-6H), 6.91 (1H, dd, *J* 8.3, 2.1, phenol-4H), 6.73 (1H, s, pyrazole-4H), 4.78 (2H, s, hydroxymethyl-CH₂); δ_C (125 MHz, acetone-d^6) 157.1, 150.9, 145.4, 133.2, 127.6, 119.1, 116.5, 116.2, 99.4, 55.3; HRMS (ESI) found MNa⁺, 247.0244, $C_{10}H_9ClN_2NaO_2$ requires 247.0245.
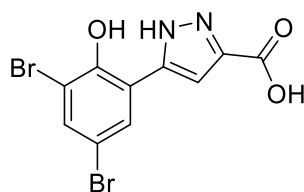
5-(3,5-dibromo-2-hydroxyphenyl)-1,2-oxazole-3-carboxylic acid, 3.39
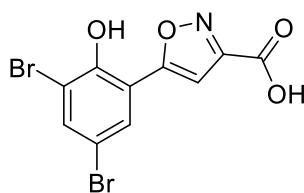
Chemical Formula: $C_{10}H_5Br_2NO_4$

By general procedure **J**, chromenone **3.47** (101 mg, 0.29 mmol) gave crude product as an off-white solid that was purified by mass-directed HPLC (362.9, mid-gradient) to give product (61 mg, 58%). δ_H (500 MHz, acetone-d^6) 8.02 (1H, d, *J* 2.3, phenol-6H), 7.76 (1H, d, *J* 2.3, phenol-4H), 7.46 (1H, s, isox-4H); 164.7, 160.3, 156.6, 148.7, 131.1, 126.5, 126.0, 122.4, 116.0, 106.8; HRMS (ESI) found MNa⁺, 383.8486, $C_{10}H_5{}^{79}Br_2NNaO_4$ requires 383.8483.
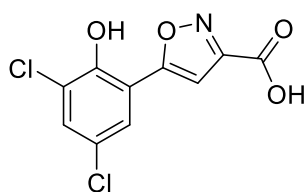
5-(3,5-dibromo-2-hydroxyphenyl)-1*H*-pyrazole-3-carboxylic acid, 3.40

Chemical Formula: $C_{10}H_6Br_2N_2O_3$

By general procedure **K**, chromenone **3.47** (96 mg, 0.28 mmol) gave crude product as a brown solid that was purified by mass directed HPLC (362.0, mid-gradient) to give product (79 mg, 78%). δ_H (500 MHz, acetone-d^6) 8.04 (1H, d, *J* 2.3, phenol-6H), 7.68 (1H, d, *J* 2.3, phenol-4H), 7.59 (1H, s, pyrazole-4H); δ_C (125 MHz, acetone-d^6) 159.2, 152.1, 150.3, 136.1, 128.6, 119.1, 111.5, 110.9, 106.1; HMRS (ESI) found MNa$^+$, 382.8646, $C_{10}H_6{}^{79}Br_2N_2NaO_3$ requires 382.8643.

5-(3,5-dichloro-2-hydroxyphenyl)-1,2-oxazole-3-carboxylic acid, 3.41

Chemical Formula: $C_{10}H_5Cl_2NO_4$

By general procedure **J**, chromenone **3.48** (249 mg, 0.96 mmol) gave crude product as an off-white solid that was purified by mass-directed HPLC (274.1, mid-gradient) to give product (196 mg, 75%). δ_H (500 MHz, acetone-d^6) 7.88 (1H, d, *J* 2.5, phenol-6H), 7.65 (1H, d, *J* 2.5, phenol-4H), 7.31 (1H, s, isox-4H); δ_C (125 MHz, acetone-d^6) 165.7, 160.2, 157.6, 148.9, 130.7, 125.5, 125.0, 122.7, 117.0, 105.0; HRMS (ES) found MH$^+$, 273.9667, $C_{10}H_6Cl_2NO_4$ requires 273.9668.

5-(3,5-dichloro-2-hydroxyphenyl)-1*H*-pyrazole-3-carboxylic acid, 3.42
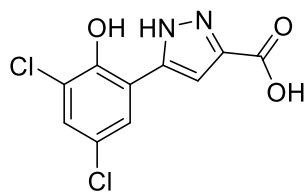
Chemical Formula: $C_{10}H_6Cl_2N_2O_3$

By general procedure **K**, chromenone **3.48** (100 mg, 0.39 mmol) gave crude product as a brown solid that was purified by mass directed HPLC (273.1, mid-gradient) to give product (78 mg, 74%). δ_H (500 MHz, acetone-d^6) 7.87 (1H, d, J 2.5, phenol-6H), 7.58 (1H, s, isox-4H), 7.42 (1H, d, J 2.5, phenol-4H); δ_C (125 MHz, acetone-d^6) 159.3, 150.7, 150.3, 136.2, 128.9, 125.1, 123.8, 122.2, 118.8, 106.2; HRMS (ESI) found MH$^+$, 272.9836, $C_{10}H_7Cl_2N_2O_3$ requires 272.9828.

4.4 Materials and Methods for Biological Assays

4.4.1 Mobility-Shift Assay

4.4.1.1 General Experimental

Aurora-A kinase assays were performed with a Labchip EZ Reader II system (PerkinElmer) at room temperature using separation buffer (760367, PerkinElmer) containing Coating Reagent 8 (500 nM, 760278, PerkinElmer). The assays were performed in 384-well low-volume (30 µl) plates (Corning). The kinase substrate was a fluorescein-labelled peptide [5-FAM-LRRASLG-CONH$_2$] dissolved in 20 mM Tris (pH 7.0), 200 mM NaCl, 5 mM MgCl2, 5 mM 2-mercaptoethanol, and 10% w/v glycerol. Measurements of substrate phosphorylation were made every two minutes for 30 cycles unless otherwise stated. Assays were carried out in duplicate using a 12-sipper chip (760404 PerkinElmer) with a 2.5% final DMSO concentration unless otherwise stated.

4.4.1.1.1 Ideal Kinase concentration

The ideal Aurora-A concentration for use in the assay was determined by measuring substrate conversion over time at varying concentration of enzyme. Aurora-A at 400 nM was subjected to a six-point, two-fold serial dilution in Aurora-A buffer (20 mM Tris (pH 7.0), 200 mM NaCl, 5 mM MgCl2, 5 mM 2-mercaptoethanol, and 10% w/v glycerol), resulting in 2 × Aurora-A stock solutions. 14 µl of this stock was added to the appropriate wells of the 384-well plate. A 2 × stock solution of the substrate (3 µM) and ATP (from prior work,[143] 118 µM) in Aurora-A buffer was prepared and 14 µl added to the wells containing enzyme, resulting in six final Aurora-A concentrations of 200 – 6.25 nM, and final substrate and ATP concentrations of 1.5 µM and 59 µM, respectively. The percentage conversion of substrate at each enzyme concentration was generated by the EZ Reader software and plotted against time in GraphPad Prism 7. A WT Aurora-A concentration of 50 nM was selected for future assays.

The ideal concentration for Aurora-A^{CM} was performed in the same manner, aside from the range of enzyme concentration was 500 – 31.25 nM.

4.4.1.1.2   Ideal ATP concentration

The WT Aurora-A and Aurora-A^{CM} K_M ATP values were determined by performing a 12-point, 3-fold serial dilution of 12 mM ATP in Aurora-A buffer to result in 4 × stock solutions of ATP. A 4 × substrate solution (6 µM) and a 2 × enzyme solution (100 and 62.5 nM for WT and Aurora A^{CM}, respectively) were prepared. Each of the 4 × ATP stock solutions were diluted two-fold in the 4 × substrate solution and 14 µl of the produced solutions were added to the appropriate wells on the 384-well plate, followed by the 2 × enzyme solution, resulting in 12 final ATP concentrations (3 mM – 17 nM) and final substrate and enzyme concentrations of 1.5 µM, 50, and 31.25 nM concentrations, respectively. The percentage conversion of substrate at each ATP concentration was generated by the EZ Reader software and plotted against time in GraphPad Prism 7. The initial rate at each ATP concentration was plotted against the corresponding ATP concentration to generate a Michaelis-Menten plot.   An ATP K_M for WT Aurora-A and Aurora-A^{CM} were determined as 63 ± 12 µM and 80 ± 3 µM, respectively.

4.4.1.1.3   DMSO Tolerance

The WT Aurora-A and pseudo-WT Aurora-A DMSO tolerance values were determined by performing an 11-point, 2-fold serial dilution of 40% DMSO in Aurora-A buffer to result in 4 × stock solutions of DMSO. A 4 × substrate and ATP solution (6 µM and 320 µM, respectively) and a 2 × enzyme solution (100 and 62.5 nM for WT and pseudo-WT Aurora A, respectively) were prepared. Each of the 4 × DMSO stock solutions were diluted two-fold in the 4 × substrate and ATP solution and 14 µl of the produced solutions were added to the appropriate wells on the 384-well plate, followed by the 2 × enzyme solution, resulting in 12 final DMSO concentrations (10 – 0.02 % v/v) and final substrate, ATP and enzyme concentrations of 1.5 µM, 80 µM, 50 nM, and 31.25 nM, respectively. The percentage conversion of substrate at each DMSO concentration was generated by the EZ Reader software and plotted against time in GraphPad Prism 7. The initial rate at each DMSO concentration was plotted against the corresponding concentration. An ideal DMSO % for WT Aurora-A and pseudo-WT Aurora-A was determined as 2.5%.

4.4.1.1.4   IC$_{50}$ determination of Aurora-A chemical matter

The bioactivity of fragments against WT Aurora-A and Aurora-A^{CM} were determined by performing a 10-point, 3-fold serial dilution of fragment in DMSO (120 mM, 100% DMSO), followed by dilution in Aurora-A buffer to result in 4 × fragment stock solution (12 mM, 10% DMSO v/v). A 4 × substrate and ATP solution (6 µM and 320 µM, respectively) and a 2 × enzyme solution (100 and 62.5 nM for WT and Aurora A^{CM}, respectively) were prepared. Each of the 4 × fragment stock solutions were diluted two-fold in the 4 × substrate and ATP solution and 14 µl of the produced solutions were added to the appropriate wells on the 384-well plate, followed by the 2 × enzyme solution, resulting in 12 final fragment concentrations (3 mM – 152 nM) and final substrate, ATP and enzyme concentrations of 1.5 µM, 80 µM, 50 nM, and 31.25 nM, respectively, in 2.5% final DMSO. The percentage conversion of substrate at each fragment concentration was generated by the EZ Reader software and plotted against time in GraphPad Prism 7. The initial rate at each fragment concentration was plotted against the corresponding concentration to yield a dose-response curve.

4.4.1.1.5   Rhodium catalyst scavenging study

Tolerance of the assay and Aurora-A to trace metal was assessed, screening the products described in section 4.2.1. Each product solution was diluted in DMSO to 12 mM followed by dilution in Aurora-A buffer, resulting in a 4 × stock solution of each product mixture (1.2 mM, 10% DMSO). A 4 × substrate and ATP solution (6 µM and 320 µM, respectively) and a 2 × WT Aurora-A solution (100 nM) were prepared. Each of the 4 × product mixtures were diluted two-fold in the 4 × substrate and ATP solution and 14 µl of the produced solutions were added to the appropriate wells on the 384-well plate, followed by the 2 × enzyme solution, resulting in a final product mixture concentration of 300 µM, 2.5% DMSO, and final substrate, ATP and enzyme concentrations of 1.5 µM, 80 µM, and 50 nM, respectively. The percentage conversion of substrate at each fragment concentration was generated by the EZ Reader software and plotted against time in GraphPad Prism 7. The initial rate of each product mixture was plotted against the constituents contained in each vial.

4.4.1.1.6   Mock Array

Each product mixture relevant to the mock array described in section 2.2.4.2 was diluted to 5 mM in DMSO, assuming a total product concentration of 100 mM, followed by dilution in Aurora-A buffer, resulting in 4 × product mixture stock solutions at 400 µM, 10 % DMSO. A 4 × substrate and ATP solution (6 µM and 320 µM, respectively) and a 2 × Aurora-A^{CM} solution (100

nM) were prepared. Each of the 4 × product mixtures were diluted two-fold in the 4 × substrate and ATP solution and 14 µl of the produced solutions were added to the appropriate wells on the 384-well plate, followed by the 2 × enzyme solution, resulting in a final product mixture concentration of 100 µM, 2.5% DMSO, and final substrate, ATP and enzyme concentrations of 1.5 µM, 80 µM, and 50 nM, respectively. The percentage conversion of substrate for each product mixture was generated by the EZ Reader software and plotted against time in GraphPad Prism 7. The initial rate of each product mixture was plotted against the constituents contained in each mock array vial.

4.4.1.1.7   Reaction Array

Each product mixture within the reaction array described in section 2.2.4.2 was diluted to 5 mM in DMSO, assuming a total product concentration of 100 mM, followed by dilution in Aurora-A buffer, resulting in 4 × product mixture stock solutions at 400 µM, 10 % DMSO. A 4 × substrate and ATP solution (6 µM and 320 µM, respectively) and a 2 × Aurora-A^{CM} solution (50 nM) were prepared. Each of the 4 × product mixtures were diluted two-fold in the 4 × substrate and ATP solution and 14 µl of the produced solutions were added to the appropriate wells on the 384-well plate, followed by the 2 × enzyme solution, resulting in a final product mixture concentration of 100 µM, 2.5% DMSO, and final substrate, ATP and enzyme concentrations of 1.5 µM, 80 µM, and 25 nM, respectively. The percentage conversion of substrate for each product mixture was generated by the EZ Reader software and plotted against time in GraphPad Prism 7. The initial rate of each product mixture was plotted against the constituents contained in each reaction array vial.

4.4.2   Thermal Shift Assay

Thermal shift/stability assays were performed on a StepOnePlus Real-Time PCR machine (LifeTechnologies) and using SYPRO-Orange dye (emission maximum 570 nm, Invitrogen) with thermal ramping between 20 and 95°C in 0.3°C step intervals per data point to induce denaturation of purified, folded Aurora-A^{CM} in the presence or absence of fragments at a final concentration of 100 µM and 2.5% DMSO. The melting temperature (Tm) corresponding to the midpoint for the protein unfolding transition was calculated by fitting the sigmoidal melt curve to the Boltzmann equation using GraphPad Prism, with R^2 values of ≥0.99. Data points after the fluorescence intensity maximum were excluded from the fitting. Changes in the unfolding

transition temperature compared with the control curve (ΔTm) were calculated for each ligand. A positive ΔTm value indicates that the ligand stabilises the protein from thermal denaturation and confirms binding to the protein. All TSA experiments were conducted using a final protein concentration of 5 μM in 100 mM BTP, pH 7.0, and 150 mM NaCl, supplemented with the appropriate ligand concentration. Three independent assays were performed for each protein and protein-ligand combination.

4.5   Molecular Docking

The virtual library of 2-hetaryl phenol analogues was docked using Schrödinger Maestro[137] user interface and the Glide[138] module to the X-ray crystal structures listed below. X-ray structures had dimers, binding partners and ligands removed, and were then pre-processed to assign bond orders, add missing hydrogens, create zero-order bonds to metals, create disulfide bonds, fill in missing side chains with Prime[144,145], and generate het states at pH 7.0 ± 2.0 using Epik[146,147]. H-bonds were then assigned and optimised, sampling water orientations at pH 7.0, waters >3.0 Å removed, and the structure minimised. Virtual library ligands were prepared in LigPrep, generating possible states at physiological pH, retaining specified chirality, and docked to the respective crystal structure using Glide at standard precision (SP) with flexible ligands, sampling nitrogen inversion, ring conformations, adding state penalties to docking scores, sampling 5000 initial poses per ligand, keeping 400 best poses per ligand for energy minimisation, and outputting 1 docked pose per ligand. Top ranked docked compounds were then manually evaluated for the quality of the docked pose. The top 200 docked compounds against each X-ray crystal structure were selected for onward analysis. R-group analysis was initially performed with R-group analysis tool in Maestro to determine frequently substituted positions and motifs. Onward analysis was performed in Excel.

PDB ID	Grid Space (Å)			Size (Å)		
	X	Y	Z	X	Y	Z
3EFW	47.35	77.77	13.81	12	12	11
3LAU	-9.53	-4.8	-0.4	12	12	12
3P9J	-11.31	13.7	-16.18	12	12	12
3W16	-11.73	15.48	-17.34	12	12	12
4CEG	-10.67	14.11	-17.5	12	12	12
4JBQ	9.16	13.76	16.57	12	11	11
5DN3	Ligand-centered			12	12	12
5L8L	18.47	-6.62	-2.94	12	12	12
5ORY	Ligand-centered			12	12	12
O-chloro	Ligand-centered			12	12	12

5 List of References

1 Y. L. Deribe, T. Pawson and I. Dikic, *Nat. Struct. Mol. Biol.*, 2010, **17**, 666–672.

2 R. Zahedi and A. Sickmann, *Proteomics*, 2013, **13**, 901–903.

3 G. A. Khoury, R. C. Baliban and C. A. Floudas, *Sci. Rep.*, 2014, **1**, 1–5.

4 S. S. C. Manning, D.B. Whyte, R. Martinez, T. Hunter, *Sciencemag.Org*, 2002, **298**, 1912–1934.

5 S. S. S. Taylor and A. A. P. Kornev, *Trends Biochem. Sci.*, 2011, **36**, 65–77.

6 M. Huse and J. Kuriyan, *Cell*, 2002, **109**, 275–282.

7 R. Bayliss, A. Fry, T. Haq and S. Yeoh, *Open Biol.*, 2012, **2**, 120136–120136.

8 A. P. Kornev, N. M. Haste, S. S. Taylor and L. F. Ten Eyck, *Proc. Natl. Acad. Sci.*, 2006, **103**, 17783–17788.

9 N. Kannan and A. F. Neuwald, *J. Mol. Biol.*, 2005, **351**, 956–972.

10 A. Krupa, G. Preethi and N. Srinivasan, *J. Mol. Biol.*, 2004, **339**, 1025–1039.

11 C. S. Gibbs and M. J. Zoller, *J. Biol. Chem.*, 1991, **266**, 8923–8931.

12 E. A. Nigg, *Nat. Rev. Mol. Cell Biol.*, 2001, **2**, 21–32.

13 L. Trinkle-Mulcahy and A. I. Lamond, *Curr. Opin. Cell Biol.*, 2006, **18**, 623–631.

14 G. Combes, I. Alharbi, L. G. Braga and S. Elowe, *Oncogene*, 2017, **36**, 4819–4827.

15 A. Molla, *Biomol. Concepts*, 2010, **1**, 147–155.

16 L. S. Penna, J. A. P. Henriques and D. Bonatto, *Pharmacol. Ther.*, 2017, **173**, 67–82.

17 C. Roghi, R. Giet, R. Uzbekov, N. Morin, I. Chartrain, R. Le Guellec, a Couturier, M. Dorée, M. Philippe and C. Prigent, *J. Cell Sci.*, 1998, **111 (Pt 5)**, 557–72.

18 C. S. M. Chan and D. Botstein, *Genetics*, 1993, **135**, 677–691.

19 T. Sardon, R. A. Pache, A. Stein, H. Molina, I. Vernos and P. Aloy, *EMBO Rep.*, 2010, **11**, 977–984.

20 A. R. Barr and F. Gergely, *J. Cell Sci.*, 2007, **120**, 2987–2996.

21 M. Carmena and W. C. Earnshaw, *Nat. Rev. Mol. Cell Biol.*, 2003, **4**, 842–854.

22 R. Bayliss, T. Sardon, I. Vernos and E. Conti, *Mol. Cell*, 2003, **12**, 851–862.

23 C. Lindon, R. Grant and M. Min, *Front. Oncol.*, 2016, **5**, 1–13.

24 M. Giubettini, I. A. Asteriti, J. Scrofani, M. De Luca, C. Lindon, P. Lavia and G. Guarguaglini, *J. Cell Sci.*, 2011, **124**, 113–122.

25 P. A. Eyers and J. L. Maller, *J. Biol. Chem.*, 2004, **279**, 9008–9015.

26 D. Sabino, N. H. Brown and R. Basto, *J. Cell Sci.*, 2011, **124**, 1156–1166.

27 V. Joukov, A. De Nicolo, A. Rodriguez, J. C. Walter and D. M. Livingston, *Proc. Natl. Acad. Sci.*, 2010, **107**, 21022–21027.

28 Z. S. Zhao, J. P. Lim, Y. W. Ng, L. Lim and E. Manser, *Mol. Cell*, 2005, **20**, 237–249.

29 D. L. Satinover, C. a Leach, P. T. Stukenberg and D. L. Brautigan, *Proc. Natl. Acad. Sci. U. S. A.*, 2004, **101**, 8625–8630.

30 P. R. Molli, D. Q. Li, R. Bagheri-Yarmand, S. B. Pakala, H. Katayama, S. Sen, J. Iyer, J. Chernoff, M. Y. Tsai, S. S. Nair and R. Kumar, *J. Cell Biol.*, 2010, **190**, 101–114.

31 M. Toya, M. Terasawa, K. Nagata, Y. Iida and A. Sugimoto, *Nat. Cell Biol.*, 2011, **13**, 708–715.

32 J. A. C. M. Goos, V. M. H. Coupe, B. Diosdado, P. M. Delis-Van Diemen, C. Karga, J. A. M. Beliën, B. Carvalho, M. P. van den Tol, H. M. W. Verheul, A. A. Geldof, G. A. Meijer, O. S. Hoekstra and R. J. A. Fijneman, *Br. J. Cancer*, 2013, **109**, 2445–2452.

33 W. Siggelkow, D. Boehm, S. Gebhard, M. Battista, I. Sicking, A. Lebrecht, C. Solbach, B. Hellwig, J. Rahnenführer, H. Koelbl, M. Gehrmann, R. Marchan, C. Cadenas, J. G. Hengstler and M. Schmidt, *BMC Cancer*, 2012, **12**, 562.

34 R. Reiter, P. Gais, U. Jutting, M. K. Steuer-Vogt, A. Pickhard, K. Bink, S. Rauser, S. Lassmann, H. Höfler, M. Werner and A. Walch, *Clin. Cancer Res.*, 2006, **12**, 5136–5141.

35 J. Den Hollander, S. Rimpi, J. R. Doherty, M. Rudelius, A. Buck, A. Hoellein, M. Kremer, N. Graf, M. Scheerer, M. A. Hall, A. Goga, N. Von Bubnoff, J. Duyster, C. Peschel, J. L. Cleveland, J. A. Nilsson and U. Keller, *Blood*, 2010, **116**, 1498–1505.

36 L. I. Marco, M. Valentina and S. Silvia, *J Transl Med*, 2011, **9**, 1–6.

37 J. Zhu, J. L. Abbruzzese, J. Izzo, W. N. Hittelman and D. Li, *Cancer Genet. Cytogenet.*, 2005, **159**, 10–17.

38 M. Malumbres and I. Pérez de Castro, *Expert Opin. Ther. Targets*, 2014, **18**, 1377–1393.

39 C. Aguirre-Portolés, A. W. Bird, A. Hyman, M. Cañamero, I. Pérez De Castro and M. Malumbres, *Cancer Res.*, 2012, **72**, 1518–1528.

40 I. A. Asteriti, W. M. Rensen, C. Lindon, P. Lavia and G. Guarguaglini, *Biochim. Biophys. Acta - Rev. Cancer*, 2010, **1806**, 230–239.

41 G. J. P. L. Kops, B. A. A. Weaver and D. W. Cleveland, *Nat. Rev. Cancer*, 2005, **5**, 773–785.

42 P. Yaish, A. Gazit, C. Gilon and A. Levitzki, *Science*, 1988, **242**, 933–935.

43 P. Cohen, *Curr. Opin. Chem. Biol.*, 1999, **3**, 459–465.

44 D. L. Nelson and M. M. Cox, *Principles of Biochemistry*, Freeman, Fifth Edit., 2008.

45 M. J. Mauro and B. J. Druker, *Oncologist*, 2001, **6**, 233–238.

46 K. S. Bhullar, N. O. Lagarón, E. M. McGowan, I. Parmar, A. Jha, B. P. Hubbard and H. P. V. Rupasinghe, *Mol. Cancer*, 2018, **17**, 1–20.

47 MRC, List of Clinically Approved Kinase Inhibitors, https://www.kinase-screen.mrc.ac.uk/phosphorylation-ubiquitylation-drug-discovery, (accessed 14 October 2021).

48 R. Roskoski, *Pharmacol. Res.*, 2016, **103**, 26–48.

49   J. Schoepfer, W. Jahnke, G. Berellini, S. Buonamici, S. Cotesta, S. W. Cowan-Jacob, S. Dodd, P. Drueckes, D. Fabbro, T. Gabriel, J. M. Groell, R. M. Grotzfeld, A. Q. Hassan, C. Henry, V. Iyer, D. Jones, F. Lombardo, A. Loo, P. W. Manley, X. Pellé, G. Rummel, B. Salem, M. Warmuth, A. A. Wylie, T. Zoller, A. L. Marzinzik and P. Furet, *J. Med. Chem.*, 2018, **61**, 8120–8135.

50   Novartis, FDA approves Novartis Scemblix® (asciminib), with novel mechanism of action for the treatment of chronic myeloid leukemia, https://www.novartis.com/news/media-releases/fda-approves-novartis-scemblix-asciminib-novel-mechanism-action-treatment-chronic-myeloid-leukemia, (accessed 1 November 2021).

51   FDA, FDA approves asciminib for Philadelphia chromosome-positive chronic myeloid leukemia, https://www.fda.gov/drugs/resources-information-approved-drugs/fda-approves-asciminib-philadelphia-chromosome-positive-chronic-myeloid-leukemia, (accessed 15 November 2021).

52   F. J. Adrián, Q. Ding, T. Sim, A. Velentza, C. Sloan, Y. Liu, G. Zhang, W. Hur, S. Ding, P. Manley, J. Mestan, D. Fabbro and N. S. Gray, *Nat. Chem. Biol.*, 2006, **2**, 95–102.

53   D. Fabbro, P. W. Manley, W. Jahnke, J. Liebetanz, A. Szyttenholm, G. Fendrich, A. Strauss, J. Zhang, N. S. Gray, F. Adrian, M. Warmuth, X. Pelle, R. Grotzfeld, F. Berst, A. Marzinzik, S. W. Cowan-Jacob, P. Furet and J. Mestan, *Biochim. Biophys. Acta - Proteins Proteomics*, 2010, **1804**, 454–462.

54   W. Jahnke, R. M. Grotzfeld, X. Pellé, A. Strauss, G. Fendrich, S. W. Cowan-Jacob, S. Cotesta, D. Fabbro, P. Furet, J. Mestan and A. L. Marzinzik, *J. Am. Chem. Soc.*, 2010, **132**, 7043–7048.

55   A. A. Wylie, J. Schoepfer, W. Jahnke, S. W. Cowan-Jacob, A. Loo, P. Furet, A. L. Marzinzik, X. Pelle, J. Donovan, W. Zhu, S. Buonamici, A. Q. Hassan, F. Lombardo, V. Iyer, M. Palmer, G. Berellini, S. Dodd, S. Thohan, H. Bitter, S. Branford, D. M. Ross, T. P. Hughes, L. Petruzzelli, K. G. Vanasse, M. Warmuth, F. Hofmann, N. J. Keen and W. R. Sellers, *Nature*, 2017, **543**, 733–737.

56   NIH, Asciminib and ABL001 clinicaltrials.gov search result, https://clinicaltrials.gov/ct2/results?cond=&term=asciminib&cntry=&state=&city=&dist=, (accessed 20 November 2021).

57   A. Mora, D. Komander, D. M. F. Van Aalten and D. R. Alessi, *Semin. Cell Dev. Biol.*, 2004, **15**, 161–170.

58   L. A. Lopez-Garcia, J. O. Schulze, W. Fröhner, H. Zhang, E. Süß, N. Weber, J. Navratil, S. Amon, V. Hindie, S. Zeuzem, T. J. D. Jørgensen, P. M. Alzari, S. Neimanis, M. Engel and R. M. Biondi, *Chem. Biol.*, 2011, **18**, 1463–1473.

59   T. J. Rettenmaier, H. Fan, J. Karpiak, A. Doak, A. Sali, B. K. Shoichet and J. A. Wells, *J. Med. Chem.*, 2015, **58**, 8285–8291.

60   L. Palmieri and G. Rastelli, *Drug Discov. Today*, 2013, **18**, 407–414.

61   M. Abdel-Halim, B. Diesel, A. K. Kiemer, A. H. Abadi, R. W. Hartmann and M. Engel, *J. Med. Chem.*, 2014, **57**, 6513–6530.

62   J. M. Arencibia, W. Fröhner, M. Krupa, D. Pastor-Flores, P. Merker, T. Oellerich, S. Neimanis, C. Schmithals, V. Köberle, E. Süß, S. Zeuzem, H. Stark, A. Piiper, D. Odadzic, J. O. Schulze and R. M. Biondi, *ACS Chem. Biol.*, 2017, **12**, 564–573.

63   M. Janeček, M. Rossmann, P. Sharma, A. Emery, D. J. Huggins, S. R. Stockwell, J. E. Stokes, Y. S. Tan, E. G. Almeida, B. Hardwick, A. J. Narvaez, M. Hyvönen, D. R. Spring, G. J. McKenzie and A. R. Venkitaraman, *Sci. Rep.*, 2016, **6**, 1–12.

64   P. J. McIntyre, P. M. Collins, L. Vrzal, K. Birchall, L. H. Arnold, C. Mpamhanga, P. J. Coombs, S. G. Burgess, M. W. Richards, A. Winter, V. Veverka, F. Von Delft, A. Merritt and R. Bayliss, *ACS Chem. Biol.*, 2017, **12**, 2906–2914.

65   J. O. Schulze, G. Saladino, K. Busschots, S. Neimanis, E. Süß, D. Odadzic, S. Zeuzem, V. Hindie, A. K. Herbrand, M. N. Lisa, P. M. Alzari, F. L. Gervasio and R. M. Biondi, *Cell Chem. Biol.*, 2016, **23**, 1193–1205.

66   E. W. Lake, J. M. Muretta, A. R. Thompson, D. M. Rasmussen, A. Majumdar, E. B. Faber, E. F. Ruff, D. D. Thomas and N. M. Levinson, *Proc. Natl. Acad. Sci. U. S. A.*, 2018, **115**, E11894–E11903.

67   V. Bavetsias and S. Linardopoulos, *Front. Oncol.*, 2015, **5**, 1–10.

68   M. Payton, T. L. Bush, G. Chung, B. Ziegler, P. Eden, P. McElroy, S. Ross, V. J. Cee, H. L. Deak, B. L. Hodous, H. N. Nguyen, P. R. Olivieri, K. Romero, L. B. Schenkel, A. Bak, M. Stanton, I. Dussault, V. F. Patel, S. Geuns-Meyer, R. Radinsky and R. L. Kendall, *Cancer Res.*, 2010, **70**, 9846–9854.

69   D. Fancelli, J. Moll, M. Varasi, R. Bravo, R. Artico, D. Berta, S. Bindi, A. Cameron, I. Candiani, P. Cappella, P. Carpinelli, W. Croci, B. Forte, M. L. Giorgini, J. Klapwijk, A. Marsiglio, E. Pesenti, M. Rocchetti, F. Roletto, D. Severino, C. Soncini, P. Storici, R. Tonani, P. Zugnoni and P. Vianello, *J. Med. Chem.*, 2006, **49**, 7247–7251.

70   E. A. Harrington, D. Bebbington, J. Moore, R. K. Rasmussen, A. O. Ajose-Adeogun, T. Nakayama, J. A. Graham, C. Demur, T. Hercend, A. Diu-Hercend, M. Su, J. M. C. Golec and K. M. Miller, *Nat. Med.*, 2004, **10**, 262.

71   X. Wang, A. L. Sinn, K. Pollok, G. Sandusky, S. Zhang, L. Chen, J. Liang, C. D. Crean, A. Suvannasankha, R. Abonour, C. Sidor, M. R. Bray and S. S. Farag, *Br. J. Haematol.*, 2010, **150**, 313–325.

72   J. P. Jani, J. Arcari, V. Bernardo, S. K. Bhattacharya, D. Briere, B. D. Cohen, K. Coleman, J. G. Christensen, E. O. Emerson, A. Jakowski, K. Hook, G. Los, J. D. Moyer, I. Pruimboom-Brees, L. Pustilnik, A. M. Rossi, S. J. Steyn, C. Su, K. Tsaparikos, D. Wishka, K. Yoon and J. L. Jakubczak, *Mol. Cancer Ther.*, 2010, **9**, 883–894.

73   S. Howard, V. Berdini, J. A. Boulstridge, M. G. Carr, D. M. Cross, J. Curry, L. A. Devine, T. R. Early, L. Fazal, A. L. Gill, M. Heathcote, S. Maman, J. E. Matthews, R. L. McMenamin, E. F. Navarro, M. A. O'Brien, M. O'Reilly, D. C. Rees, M. Reule, D. Tisi, G. Williams, M. Vinković and P. G. Wyatt, *J. Med. Chem.*, 2009, **52**, 379–388.

74   C. A. Dodson, M. Kosmopoulou, M. W. Richards, B. Atrash, V. Bavetsias, J. Blagg and R. Bayliss, *Biochem. J.*, 2010, **427**, 19–28.

75   M. G. Manfredi, J. A. Ecsedy, A. Chakravarty, L. Silverman, M. Zhang, K. M. Hoar, S. G. Stroud, W. Chen, V. Shinde, J. J. Huck, D. R. Wysong, D. A. Janowick, M. L. Hyer, P. J. LeRoy, R. E. Gershman, M. D. Silva, M. S. Germanos, J. B. Bolen, C. F. Claiborne and T. B. Sells, *Clin. Cancer Res.*, 2011, **17**, 7614–7624.

76   T. Shimomura, S. Hasako, Y. Nakatsuru, T. Mita, K. Ichikawa, T. Kodera, T. Sakai, T. Nambu, M. Miyamoto, I. Takahashi, S. Miki, N. Kawanishi, M. Ohkubo, H. Kotani and Y. Iwasawa, *Mol. Cancer Ther.*, 2010, **9**, 157–166.

77   R. Ando, H. Ikegami, M. Sakiyama, S. Ooike, M. Hayashi, Y. Fujino, D. Abe, H. Nakamura, T. Mishina, H. Kato, Y. Iwase, H. Tomozane and M. Morioka, *Bioorganic Med. Chem. Lett.*, 2010, **20**, 4709–4711.

78   Aliagas-Martin, I., Burdick, D.J., Corson, L.B., Dotson, J., Drummond, J., Fields, C., Huang, O.W., Hunsaker, T.L., Kleinheinz, T., Krueger, E.B., Liang, J., Moffat, J.G., Phillips, G.D., Pulk, R.A., Rawson, T.E., Ultsch, M., Walker, L.R., Wiesmann, C., Zhang, B., Zhu, B., & Cochran, A.G., *J. Med. Chem.,* 2009, **52 10**, 3300-3307.

79   T. A. Kufer, H. H. W. Silljé, R. Körner, O. J. Gruss, P. Meraldi and E. A. Nigg, *J. Cell Biol.*, 2002, **158**, 617–623.

80   C. A. Dodson and R. Bayliss, *J. Biol. Chem.*, 2012, **287**, 1150–1157.

81   J. A. H. Gilburt, H. Sarkar, P. Sheldrake, J. Blagg, L. Ying and C. A. Dodson, *Angew. Chemie - Int. Ed.*, 2017, **56**, 11409–11414.

82   E. F. Ruff, J. M. Muretta, A. R. Thompson, E. W. Lake, S. Cyphers, S. K. Albanese, S. M. Hanson, J. M. Behr, D. D. Thomas, J. D. Chodera and N. M. Levinson, *Elife*, 2018, **7**, 1–22.

83   J. P. Hughes, S. S. Rees, S. B. Kalindjian and K. L. Philpott, *Br. J. Pharmacol.*, 2011, **162**, 1239–1249.

84   R. Macarron, M. N. Banks, D. Bojanic, D. J. Burns, D. A. Cirovic, T. Garyantes, D. V. S. Green, R. P. Hertzberg, W. P. Janzen, J. W. Paslay, U. Schopfer and G. S. Sittampalam, *Nat. Rev. Drug Discov.*, 2011, **10**, 188.

85   C. A. Lipinski, F. Lombardo, B. W. Dominy and P. J. Feeney, *Adv. Drug Deliv. Rev.*, 1997, **23**, 3–25.

86   P. G. Polishchuk, T. I. Madzhidov and A. Varnek, *J. Comput. Aided. Mol. Des.*, 2013, **27**, 675–679.

87   R. J. Hall, P. N. Mortenson and C. W. Murray, *Prog. Biophys. Mol. Biol.*, 2014, **116**, 82–91.

88   F. Wang and S. W. Fesik, *Fragment-based Drug Discovery: Lessons and Outlook*, WILEY-VCH, 67th edn., 2016.

89   C. W. Murray and D. C. Rees, *Angew. Chemie - Int. Ed.*, 2016, **55**, 488–492.

90   A. Agrawal, S. L. Johnson, J. A. Jacobsen, M. T. Miller, L. H. Chen, M. Pellecchia and S. M. Cohen, *ChemMedChem*, 2010, **5**, 195–199.

91   J. A. Erickson, M. M. Mader, I. A. Watson, Y. W. Webster, R. E. Higgs, M. A. Bell and M. Vieth, *Biochim. Biophys. Acta - Proteins Proteomics*, 2010, **1804**, 642–652.

92   C. John Harris, R. D. Hill, D. W. Sheppard, M. J. Slater and P. F.W. Stouten, *Comb. Chem. High Throughput Screen.*, 2011, **14**, 521–531.

93   S. Akhter, B. A. Lund, A. Ismael, M. Langer, J. Isaksson, T. Christopeit, H. K. S. Leiros and A. Bayer, *Eur. J. Med. Chem.*, 2018, **145**, 634–648.

94   G. M. Keseru, D. A. Erlanson, G. G. Ferenczy, M. M. Hann, C. W. Murray and S. D. Pickett, *J. Med. Chem.*, 2016, **59**, 8189–8206.

95   A. L. Hopkins, C. R. Groom and A. Alex, *Drug Discov. Today*, 2004, **9**, 430–431.

96   D. A. Erlanson, S. W. Fesik, R. E. Hubbard, W. Jahnke and H. Jhoti, *Nat. Rev. Drug Discov.*, 2016, **15**, 605.

97   S. B. Shuker, P. J. Hajduk, R. P. Meadows and S. W. Fesik, *Science*, 1996, **274**, 1531–1534.

98   J. Tsai, J. T. Lee, W. Wang, J. Zhang, H. Cho, S. Mamo, R. Bremer, S. Gillette, J. Kong, N. K. Haass, K. Sproesser, L. Li, K. S. M. Smalley, D. Fong, Y.-L. Zhu, A. Marimuthu, H. Nguyen, B. Lam, J. Liu, I. Cheung, J. Rice, Y. Suzuki, C. Luu, C. Settachatgul, R. Shellooe, J. Cantwell, S.-H. Kim, J. Schlessinger, K. Y. J. Zhang, B. L. West, B. Powell, G. Habets, C. Zhang, P. N. Ibrahim, P. Hirth, D. R. Artis, M. Herlyn and G. Bollag, *Proc. Natl. Acad. Sci. U.S.A.*, 2008, **105**, 3041–3046.

99   G. Bollag, P. Hirth, J. Tsai, J. Zhang, P. N. Ibrahim, H. Cho, W. Spevak, C. Zhang, Y. Zhang, G. Habets, E. A. Burton, B. Wong, G. Tsang, B. L. West, B. Powell, R. Shellooe, A. Marimuthu, H. Nguyen, K. Y. J. Zhang, D. R. Artis, J. Schlessinger, F. Su, B. Higgins, R. Iyer, K. Dandrea, A. Koehler, M. Stumm, P. S. Lin, R. J. Lee, J. Grippo, I. Puzanov, K. B. Kim, A. Ribas, G. A. McArthur, J. A. Sosman, P. B. Chapman, K. T. Flaherty, X. Xu, K. L. Nathanson and K. Nolop, *Nature*, 2010, **467**, 596–599.

100   M. Itzstein, G. B. Kok, M. S. Pegg, J. Dyason, B. Jin, T. Van Phan, M. L. Smythe, H. F. White, S. Oliver, P. M. Colman, J. N. Varghese, D. M. Ryan, J. M. Woods, R. C. Bethell, V. Hotham, J. M. Cameron and C. R. Penn, *Nature*, 1993, **363**, 418–423.

101   S. W. Kaldor, V. J. Kalish, J. F. Davies, B. V. Shetty, J. E. Fritz, K. Appelt, J. A. Burgess, K. M. Campanale, N. Y. Chirgadze, D. K. Clawson, B. A. Dressman, S. D. Hatch, D. A. Khalil, M. B. Kosa, P. P. Lubbehusen, M. A. Muesing, A. K. Patick, S. H. Reich, K. S. Su and J. H. Tatlock, *J. Med. Chem.*, 1997, **40**, 3979–3985.

102   D. . Cheirdaris, *Artificial Neural Networks in Computer-Aided Drug Design: An Overview of Recent Advances*, Springer International Publishing, 2020.

103   E. H. B. Maia, L. C. Assis, T. A. de Oliveira, A. M. da Silva and A. G. Taranto, *Front. Chem.*, 2020, **8**.

104   A. Scarpino, G. G. Ferenczy and G. M. Keseru, *Curr. Pharm. Deisng*, 2020, **26**, 5684–5699.

105   F. D. Prieto-Martínez, E. López-López, K. Eurídice Juárez-Mercado and J. L. Medina-Franco, ed. K. B. T.-I. S. D. D. Roy, Academic Press, 2019, pp. 19–44.

106   H. A. Carlson, K. M. Masukawa and J. A. McCammon, *J. Phys. Chem. A*, 1999, **103**, 10213–10219.

107   H. A. Carlson, K. M. Masukawa, K. Rubins, F. D. Bushman, W. L. Jorgensen, R. D. Lins, J. M. Briggs and J. A. McCammon, *J. Med. Chem.*, 2000, **43**, 2100–2114.

108   J. Ricci-Lopez, S. A. Aguila, M. K. Gilson and C. A. Brizuela, *J. Chem. Inf. Model.*, 2021, **61**, 5362–5376.

109   R. E. Amaro, J. Baudry, J. Chodera, Ö. Demir, J. A. McCammon, Y. Miao and J. C. Smith, *Biophys. J.*, 2018, **114**, 2271–2278.

110   R. A. Goodnow, C. E. Dumelin and A. D. Keefe, *Nat. Rev. Drug Discov.*, 2017, **16**, 131–147.

111   N. J. Gesmundo, B. Sauvagnat, P. J. Curran, M. P. Richards, C. L. Andrews, P. J. Dandliker and T. Cernak, *Nature*, 2018, **557**, 228–232.

112   A. Leggott, J. E. Clarke, S. Chow, S. L. Warriner, A. J. O'Neill and A. Nelson, *Chem. Commun.*, 2020, **56**, 8047–8050.

113   A. I. Green, F. Hobor, C. P. Tinworth, S. Warriner, A. J. Wilson and A. Nelson, *Chem. - A Eur. J.*, 2020, **26**, 10682–10689.

114 G. Karageorgis, S. Warriner and A. Nelson, *Nat. Chem.*, 2014, **6**, 872.

115 G. Karageorgis, M. Dow, A. Aimon, S. Warriner and A. Nelson, *Angew. Chemie - Int. Ed.*, 2015, **54**, 13538–13544.

116 P. A. Harris, B. W. King, D. Bandyopadhyay, S. B. Berger, N. Campobasso, C. A. Capriotti, J. A. Cox, L. Dare, X. Dong, J. N. Finger, L. S. C. Grady, S. J. Hoffman, J. U. Jeong, J. Kang, V. Kasparcova, A. S. Lakdawala, R. Lehr, D. E. McNulty, R. Nagilla, M. T. Ouellette, C. S. Pao, A. R. Rendina, M. C. Schaeffer, J. D. Summerfield, B. A. Swift, R. D. Totoritis, P. Ward, A. Zhang, D. Zhang, R. W. Marquis, J. Bertin and P. J. Gough, *J. Med. Chem.*, 2016, **59**, 2163–2178.

117 N. Favalli, G. Bassi, J. Scheuermann and D. Neri, *FEBS Lett.*, 2018, **592**, 2168–2180.

118 A. B. Santanilla, E. L. Regalado, T. Pereira, M. Shevlin, K. Bateman, L. C. Campeau, J. Schneeweis, S. Berritt, Z. C. Shi, P. Nantermet, Y. Liu, R. Helmy, C. J. Welch, P. Vachal, I. W. Davies, T. Cernak and S. D. Dreher, *Science*, 2015, **347**, 49–53.

119 S. Chow, S. Liver and A. Nelson, *Nat. Rev. Chem.*, 2018, **2**, 174–183.

120 M. Shevlin, *ACS Med. Chem. Lett.*, 2017, **8**, 601–607.

121 S. M. Pant, A. Mukonoweshuro, B. Desai, M. K. Ramjee, C. N. Selway, G. J. Tarver, A. G. Wright, K. Birchall, T. M. Chapman, T. A. Tervonen and J. Klefström, *J. Med. Chem.*, 2018, **61**, 4335–4347.

122 S. W. Krska, D. A. DiRocco, S. D. Dreher and M. Shevlin, *Acc. Chem. Res.*, 2017, **50**, 2976–2985.

123 S. Lin, S. Dikler, W. D. Blincoe, R. D. Ferguson, R. P. Sheridan, Z. Peng, D. V. Conway, K. Zawatzky, H. Wang, T. Cernak, I. W. Davies, D. A. DiRocco, H. Sheng, C. J. Welch and S. D. Dreher, *Science*, 2018, **361**, 569-576.

124 A. Baranczak, N. P. Tu, J. Marjanovic, P. A. Searle, A. Vasudevan and S. W. Djuric, *ACS Med. Chem. Lett.*, 2017, **8**, 461–465.

125 F. Sutanto, S. Shaabani, R. Oerlemans, D. Eris, P. Patil, M. Hadian, M. Wang, M. E. Sharpe, M. R. Groves and A. Dömling, *Angew. Chemie - Int. Ed.*, 2021, **60**, 18231–18239.

126 S. D. Roughley and A. M. Jordan, *J. Med. Chem.*, 2011, **54**, 3451–3479.

127 D. G. Brown and J. Boström, *J. Med. Chem.*, 2016, **59**, 4443–4458.

128 D. J. Newman and G. M. Cragg, *J. Nat. Prod.*, 2016, **79**, 629–661.

129 P. J. McIntyre, *Targeting the Aurora-A/TPX2 Interaction*, Ph.D. thesis University of Leicester, 2017.

130 G. J. Fan, Z. Wang and A. G. H. Wee, *Chem. Commun.*, 2006, **12**, 3732–3734.

131 H. Lei and J. Atkinson, *J. Org. Chem.*, 2000, **65**, 2560–2567.

132 R. A. Copeland, *Evaluation of Enzyme Inhibitors in Drug Discovery*, WILEY-VCH, Second Ed., 2013.

133 Y. Li, D. M. Wu, L. M. Kong, S. Zhang, H. Du, W. Sun, L. Zhang, Y. Li and Z. Zuo, *Future Med. Chem.*, 2019, **11**, 1889–1906.

134 S.-Y. Huang and X. Zou, *Protein Sci.*, 2006, **16**, 43–51.

135   M. Suarez, *Assistant-researcher Internship Report - Aurora-A Kinases: Which are the best crystals for allosteric inhibitor soaking experiments?*, Placement report, University of Leeds/Sigma-Clermont Engineering Graduate School, 2019.

136   T. A. Halgren, *J. Chem. Inf. Model.*, 2009, **49**, 377–389.

137   Schrödinger, LLC, 2020, *Schrödinger Release 2020-1: Maestro, Glide*, [Software], [First accessed April 2020].

138   T. A. Halgren, R. B. Murphy, R. A. Friesner, H. S. Beard, L. L. Frye, W. T. Pollard and J. L. Banks, *J. Med. Chem.*, 2004, **47**, 1750–1759.

139   J. C. D. Hartwieg, J. W. Priess, H. Schütz, D. Rufle, C. Valente, C. Bury, L. La Vecchia and E. Francotte, *Org. Process Res. Dev.*, 2014, **18**, 1120–1127.

140   I. Abdiaj, C. Bottecchia, J. Alcazar and T. Noël, *Synth.*, 2017, **49**, 4978–4985.

141   M. C. Bryan, K. Biswas, T. A. N. Peterkin, R. M. Rzasa, L. Arik, S. G. Lehto, H. Sun, F. Y. Hsieh, C. Xu, R. T. Fremeau and J. R. Allen, *Bioorganic Med. Chem. Lett.*, 2012, **22**, 619–622.

142   T. Ghosh, S. Saha and C. Bandyopadhyay, *Synthesis (Stuttg).*, 2005, **35**, 1845–1849.

143   F. C. Rowan, M. Richards, R. A. Bibby, A. Thompson, R. Bayliss and J. Blagg, *ACS Chem. Biol.*, 2013, **8**, 2184–2191.

144   M. P. Jacobson, D. L. Pincus, C. S. Rapp, T. J. F. Day, B. Honig, D. E. Shaw and R. A. Friesner, *Proteins Struct. Funct. Genet.*, 2004, **55**, 351–367.

145   M. P. Jacobson, R. A. Friesner, Z. Xiang and B. Honig, *J. Mol. Biol.*, 2002, **320**, 597–608.

146   J. C. Shelley, A. Cholleti, L. L. Frye, J. R. Greenwood, M. R. Timlin and M. Uchimaya, *J. Comput. Aided. Mol. Des.*, 2007, **21**, 681–691.

147   J. R. Greenwood, D. Calkins, A. P. Sullivan and J. C. Shelley, *J. Comput. Aided. Mol. Des.*, 2010, **24**, 591–604.

148   A. Card, C. Caldwell, H. Min, B. Lokchander, H. Xi, S. Sciabola, A. V. Kamath, S. L. Clugston, W. R. Tschantz, Leyu Wang and D. J. Moshinsky, *J. Biomol. Screen.*, 2009, **14**, 31–42.

149   D. Perrin, C. Frémaux and A. Scheer, *J. Biomol. Screen.*, 2006, **11**, 359–368.

150   S. Park and R. T. Raines, *Methods Mol. Biol.*, **261**, 155–160.

151   P. Del Valle, F. Busto, D. De Arriaga and J. Soler, *J. Enzyme Inhib. Med. Chem.*, 1990, **3**, 219–228.

152   Schrödinger, LLC, 2020, *PyMOL, Version 2.3.4*, [Software], [First accessed April 2020]

6   Appendix

6.1 Establishing the Mobility-Shift Assay for Biological Screening and Results

In mobility-shift assays, modified products are distinguished from un-modified substrates by their relative mobilities.[148–150] While several different modifications can be used as the basis for this distinction, in the context of kinase activity phosphorylation is the transformation leading to differentiation of product from substrate due to the highly charged phosphate group altering the product mobility. The kinase catalyses the transfer of the phosphate to an appropriate peptide substrate. These are separated by a charge potential difference drawn across pressure-driven microfluidic channels, whereby the fluorescently-labelled peptide substrate and phosphorylated product are drawn through the channels, across a viewing window, excited *via* LED and detected by CCD. The relative intensities of the substrate and product allow for the determination of percentage substrate converted, and taking these measurements over time allows for the kinetics of the reaction to be obtained based on the measured initial rate of the reaction. Advantages of mobility-shift assays include high quality of data and high sensitivity, low protein loading, low interference from compounds, no
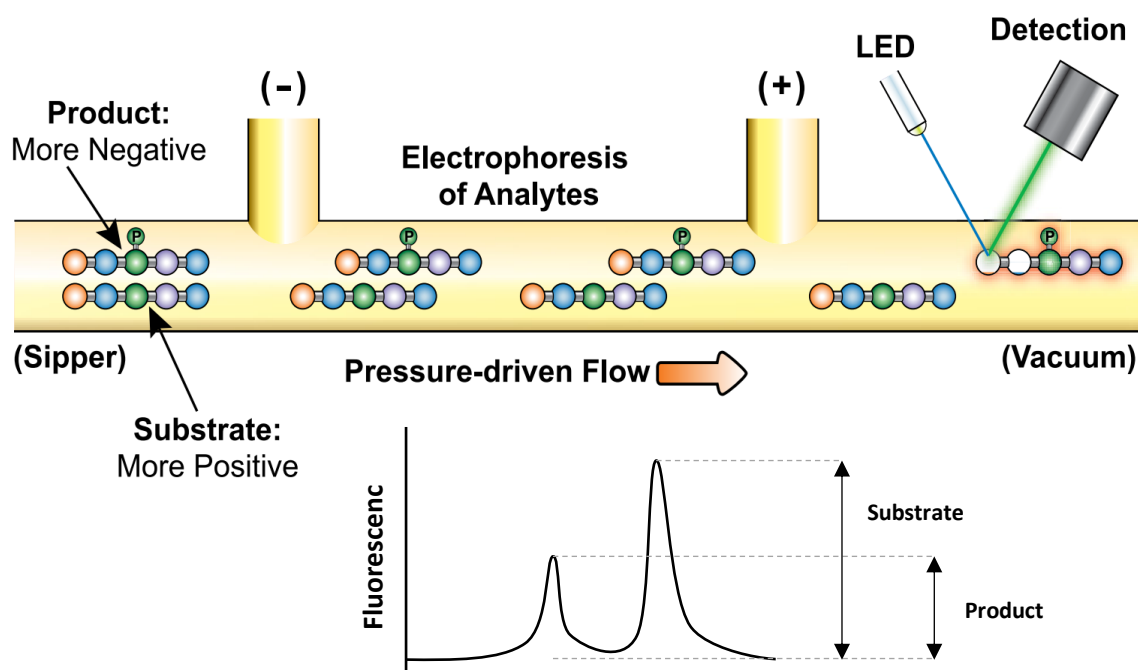
Figure **A.1**. Graphical representation of mobility-shift electrophoresis. **Top:** Principle of electrophoresis, separation occurs in microfluidic channels due to the electrical charge drawn across them. **Bottom**: Example output data from assay. Fluorescence output is measured and % conversion calculated as % conversion = 100 x (product/product + substrate).

requirement for radioactive substrates, and ease of maintenance. Fig. **A.1** shows an example setup and output for the assay.

6.1.1 Enzyme Titration

Utilising the literature K_M value for ATP of 83 µM[143] for the Aurora-A 122-403 complex, an enzyme titration experiment was performed to determine the ideal concentration of Aurora-A^{CM} in future screens. A six point, two-fold serial dilution was performed from an upper concentration of 1 mM and a final peptide substrate concentration of 1.5 µM. Following thirty plate cycles over forty minutes, the data was plotted as shown in Fig. **A.2**.
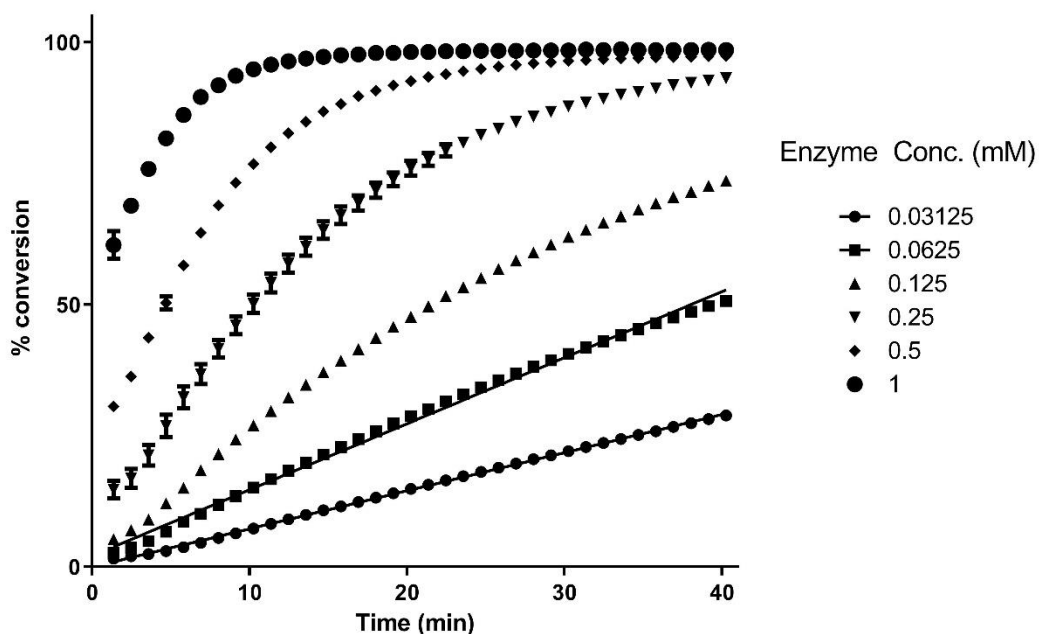
Figure **A.2** Enzyme titration assay. Linear response observed at 31.25 nM was considered suitable.

6.1.2 Determination of ATP K_M

For the maximum sensitivity of the assay in the determination of fragment IC_{50} values and reaction array screening, the K_M for ATP was determined to experimentally find the optimal concentration. At a final enzyme and peptide substrate concentration of 25 nM and 1.5 µM respectively, a twelve-point 3-fold serial dilution of ATP from 3 mM was performed. As shown in Fig. **A.3**, the K_M of ATP for Aurora-A 122-403 was experimentally determined as 81 µM, which is in accordance with the literature value of 83 µM.

172
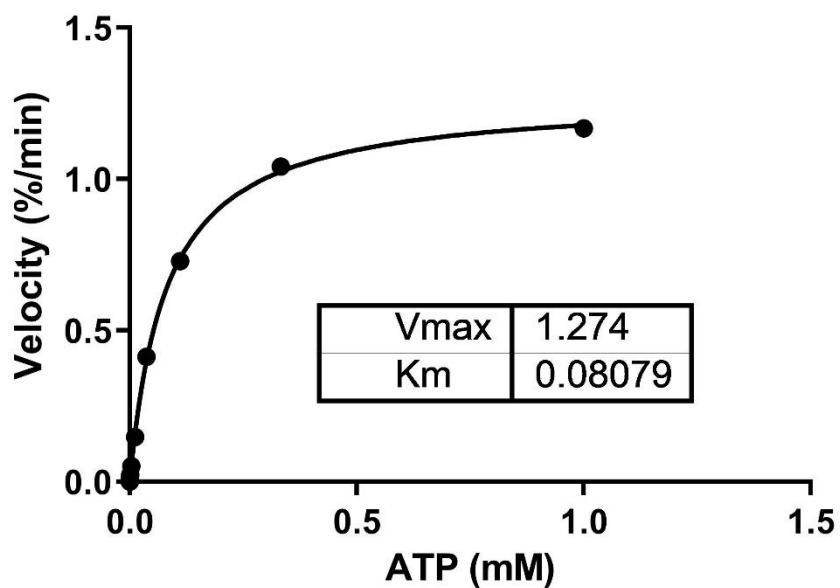
Figure **A.3** ATP K_m determination

While the titration was from 3 mM, this final data point wasn't included due to potential substrate inhibition effect on the enzyme displaying a lower initial rate than at 1 mM. Substrate-feedback inhibition has been characterised previously, providing a potential explanation for this observation.[151]

6.1.3 DMSO Tolerance assay

DMSO was utilised in the screening studies as the solvent for both fragments and stock solutions of the reaction array products. To ensure the DMSO content wouldn't interfere with the expected assay output, a tolerance screen was performed. An eleven point, 2-fold serial dilution of DMSO was performed from 10%, including a negative control (0% DMSO), as shown in Fig. **A.4**
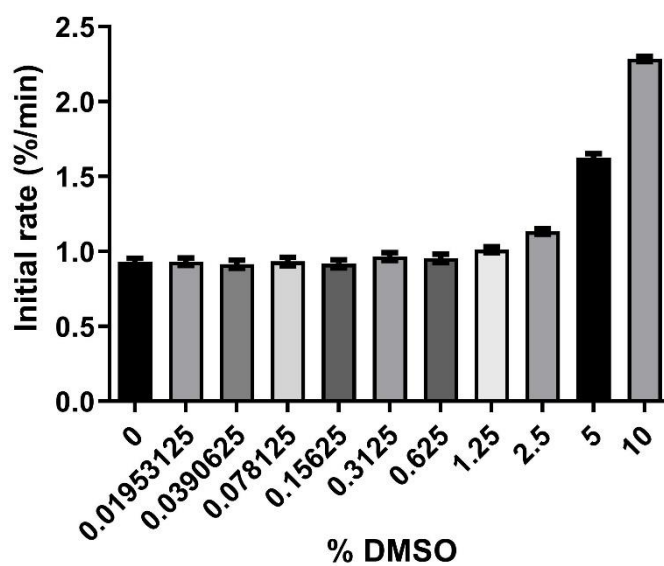
Figure **A.4**. DMSO Tolerance assay of Aurora-A^{CM}

A final DMSO concentration of 2.5% was chosen moving forward in the IC$_{50}$ and reaction array screening. However, increasing this to 5% to account for fragment solubility during screening wouldn't present any significant issues providing suitable controls were run.

6.2 ATP-Competition Assay Results
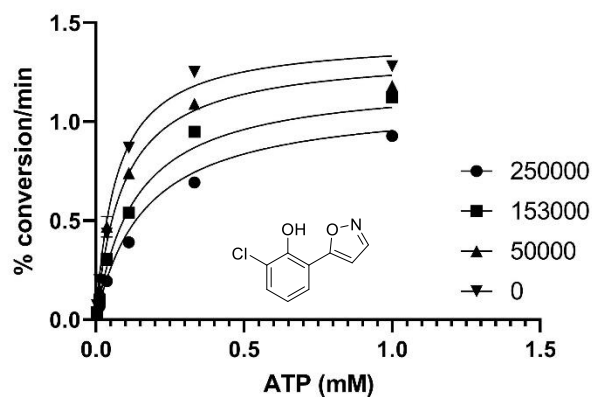
| Comparison of Fits		
Null hypothesis	Competitive inhibition	Uncompetitive inhibition
Alternative hypothesis	Mixed model inhibition	Mixed model inhibition
P value	0.0009	<0.0001
Conclusion (alpha = 0.05)	Reject null hypothesis	Reject null hypothesis
Preferred model	Mixed model inhibition	Mixed model inhibition
F (DFn, DFd)	15.19 (1, 20)	44.39 (1, 20)
K_{iC}	85294 (49880 to 120709)	
K_{iU}		212997 (130797 to 295197)
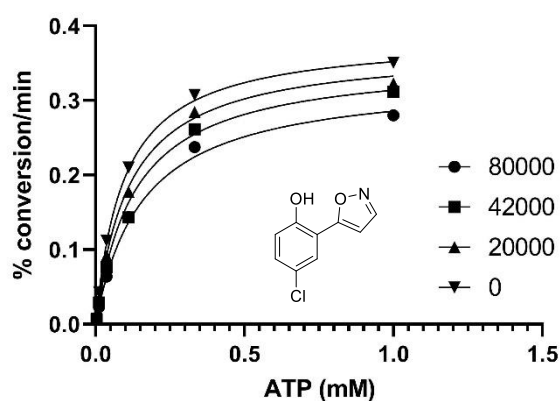
Comparison of Fits		
Null hypothesis	Competitive inhibition	Uncompetitive inhibition
Alternative hypothesis	Mixed model inhibition	Mixed model inhibition
P value	0.0007	<0.0001
Conclusion (alpha = 0.05)	Reject null hypothesis	Reject null hypothesis
Preferred model	Mixed model inhibition	Mixed model inhibition
F (DFn, DFd)	16.11 (1, 20)	53.97 (1, 20)
K_{iC}	121289 (64178 to 178401)	
K_{iU}		363387 (207125 to 519649)
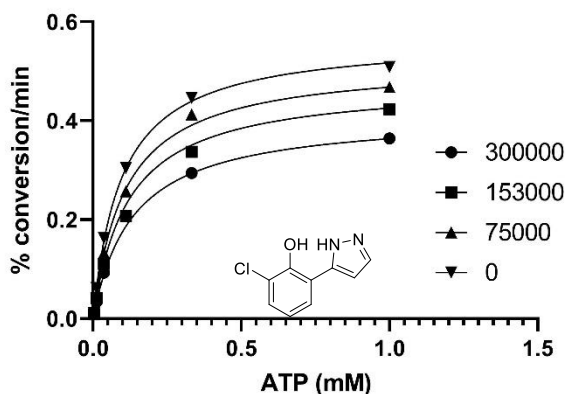
Comparison of Fits		
Null hypothesis	Competitive inhibition	Uncompetitive inhibition
Alternative hypothesis	Mixed model inhibition	Mixed model inhibition
P value	<0.0001	<0.0001
Conclusion (alpha = 0.05)	Reject null hypothesis	Reject null hypothesis
Preferred model	Mixed model inhibition	Mixed model inhibition
F (DFn, DFd)	65.87 (1, 20)	40.84 (1, 20)
K_{iC}	135950 (78050 to 193850)	
K_{iU}		495924 (363295 to 628553)
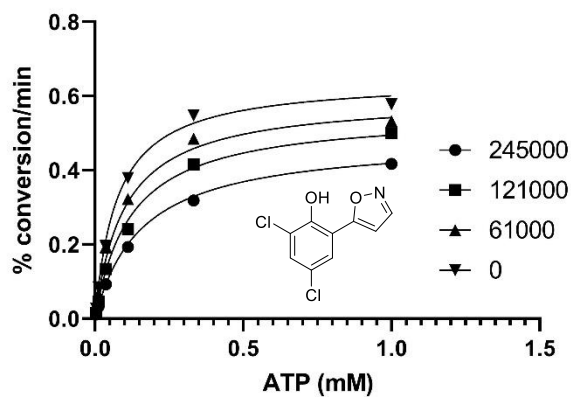
Comparison of Fits		
Null hypothesis	Competitive inhibition	Uncompetitive inhibition
Alternative hypothesis	Mixed model inhibition	Mixed model inhibition
P value	<0.0001	<0.0001
Conclusion (alpha = 0.05)	Reject null hypothesis	Reject null hypothesis
Preferred model	Mixed model inhibition	Mixed model inhibition
F (DFn, DFd)	35.29 (1, 20)	72.52 (1, 20)
K_{iC}	76356 (47199 to 105512)	
K_{iU}		344715 (217199 to 472231)
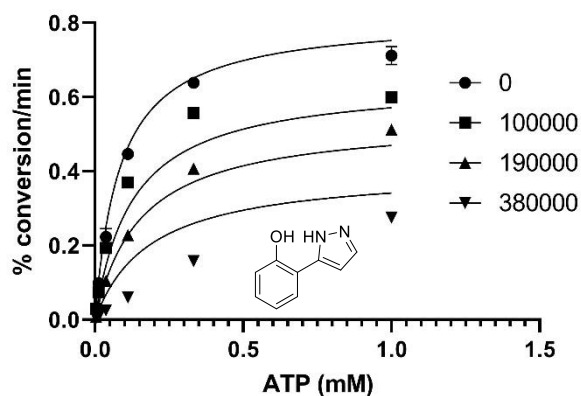
Comparison of Fits		
Null hypothesis	Competitive inhibition	Uncompetitive inhibition
Alternative hypothesis	Mixed model inhibition	Mixed model inhibition
P value	0.0005	0.0004
Conclusion (alpha = 0.05)	Reject null hypothesis	Reject null hypothesis
Preferred model	Mixed model inhibition	Mixed model inhibition
F (DFn, DFd)	16.90 (1, 20)	17.83 (1, 20)
KiC	41512 (12925 to 70099)	
KiU		194542 (105761 to 283323)

6.3   IC$_{50}$ Curves of best performing fragments

IC$_{50}$ values were determined using a 10-point, 3-fold serial dilution from 3 mM as described in Experimental Section **4.4.1.1.4**. In cases of insolubility, 3 mM data point was removed.
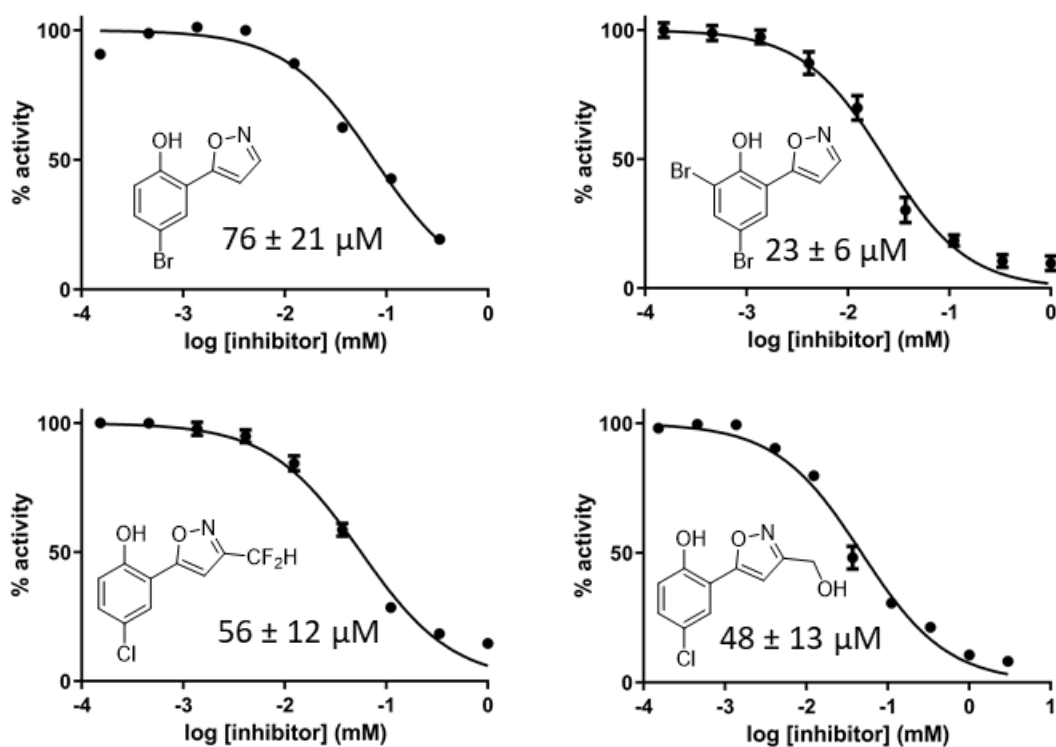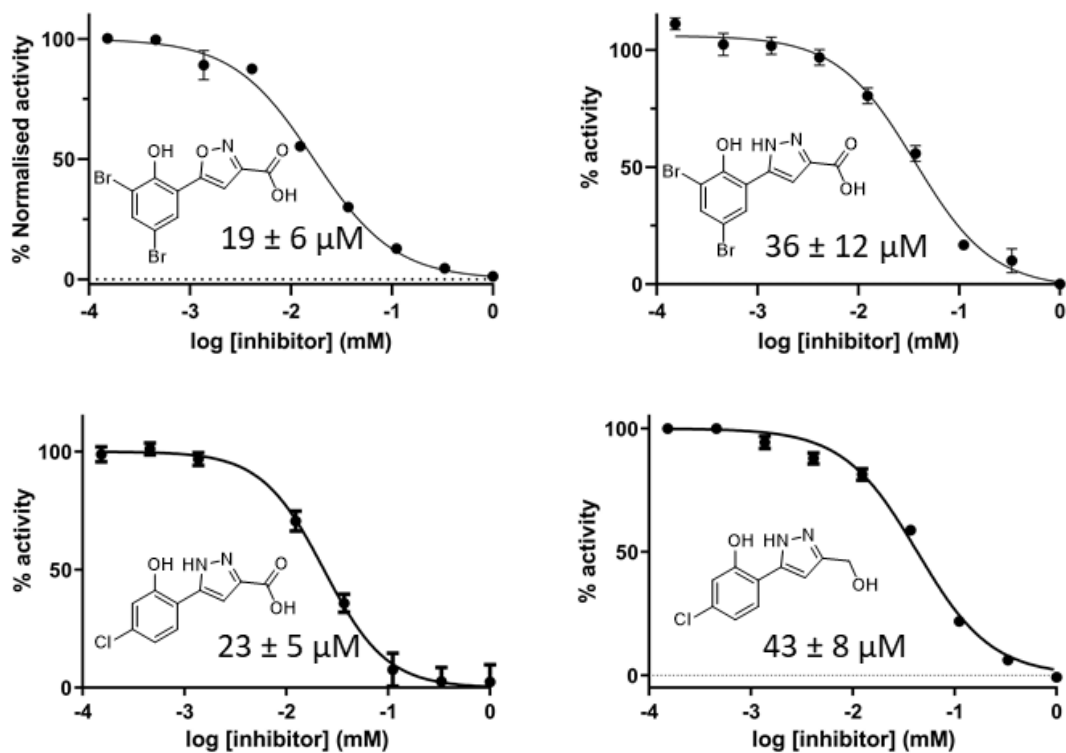
Figure **A.5**. IC$_{50}$ curves of the best performing inhibitors from Chapter 3.

6.4 Thermal Shift Assay Data

6.4.1 TSA Data for Chapter 2 – Amide bond Array

As described in Experimental Section **4.4.2**, compounds from the Amide Bond Array were screened in a Thermal Shift Assay against Aurora-A^{CM}. Each compound was screened at a final concentration of 100 µM in 2.5% DMSO to determine the effect, if any, on protein thermal stability and therefore indicating if binding was able to be observed at this concentration. Results were plotted and normalised to a DMSO control, with ΔTm compared to this control.

Figure **B.1**. TSA Plot of Saturated Amine Products from Amide Bond Array.

Figure **B.2**. TSA Plot of Anilines and Indole products from Amide Bond Array. The anilines and indole used in this array are shown in Appendix C.
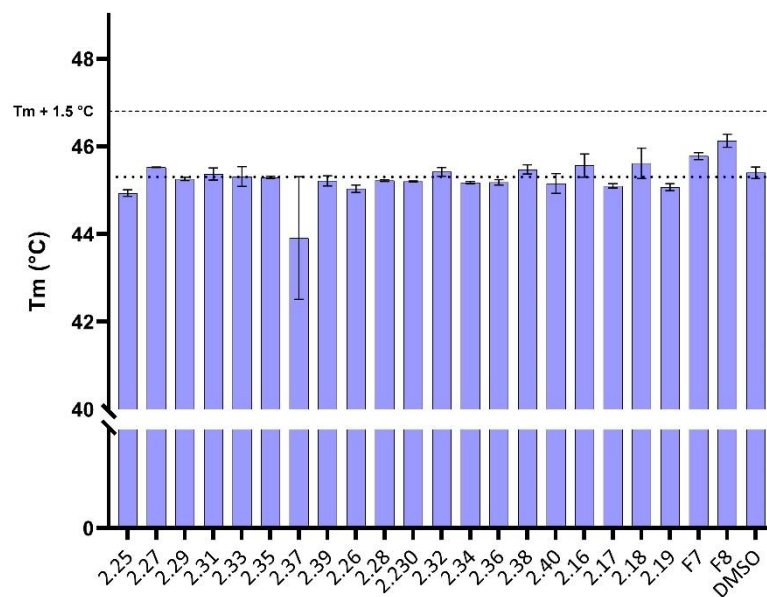
6.4.2 TSA Data for Chapter 3 – 2-Hetaryl phenol library.
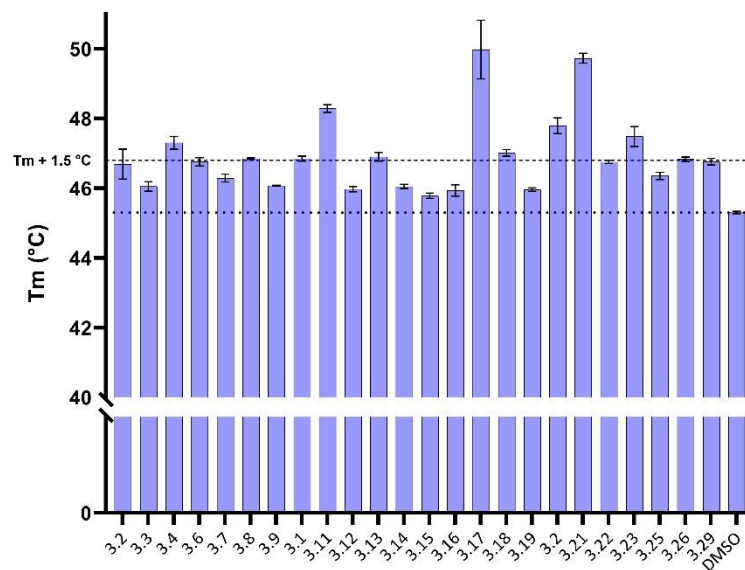
Figure **B.3**. TSA Plot of 2-Hetaryl phenol analogues from Section **3.2.2**. Compounds **3.1**, **3.24**, and **3.5** were not analysed by this method. Compound **3.28** was darkly coloured and interfered with assay output, therefore was omitted.
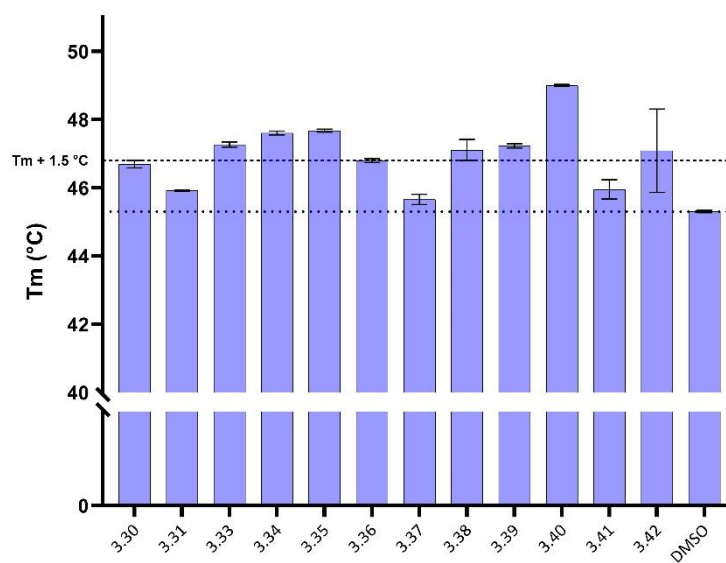
Figure **B.4**. TSA Plot of 3-functionalised 5-membered heterocycle analogues from Section **3.3.3**. Compound **3.32** was not analysed by this method.

6.5   Virtual Library Design and *in silico* docking results

6.5.1   Virtual Library Design
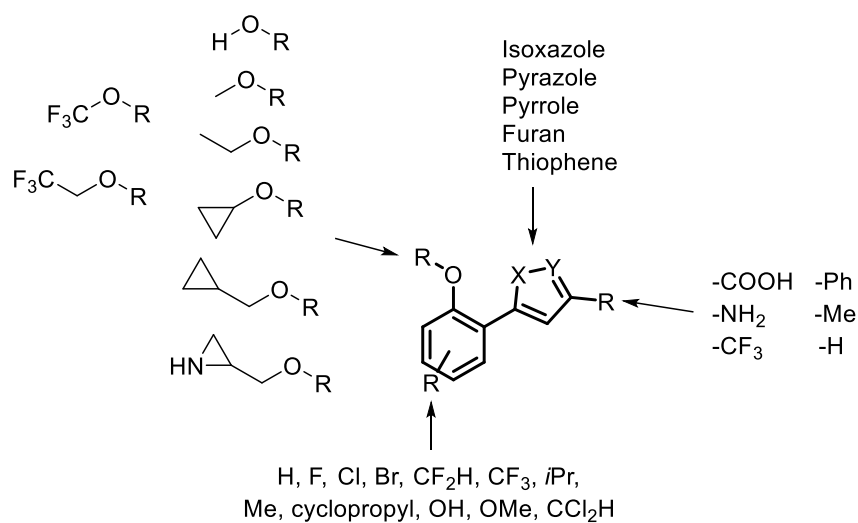
Figure **B.1**. Design of Virtual Library for *in silico* ensemble docking

The design of the virtual library that was docked against Aurora-A X-ray structures is shown in full in Fig. **B.1**. All possible combinations of substituents were exploited, resulting in a library of 2640 small molecules, and docked using Schrödinger Maestro and Glide using standard precision docking.

6.5.2   Heavy Atom (HA) count vs Docking Score

In silico docking results were plotted to show HA count against docking score, with the top 200 docked compounds against each kinase highlighted in red.
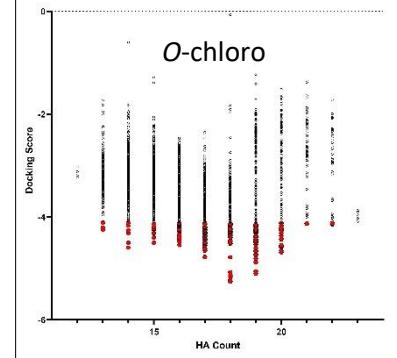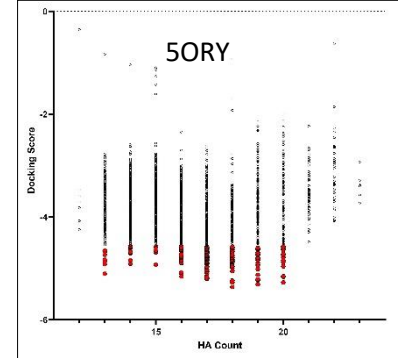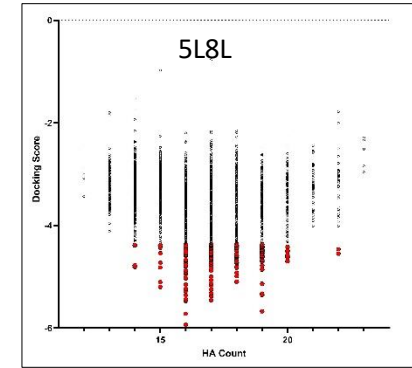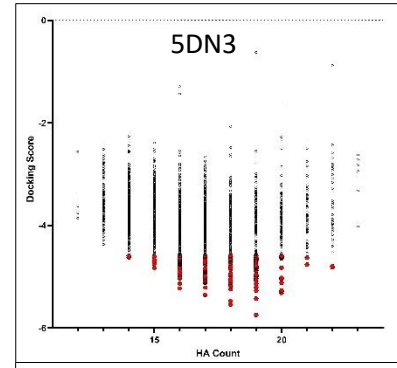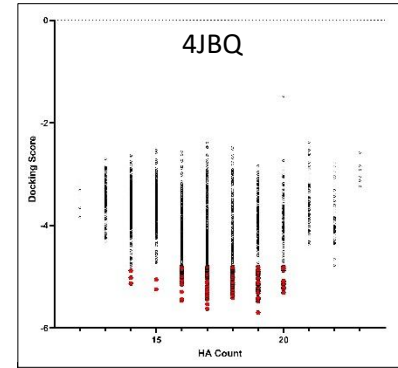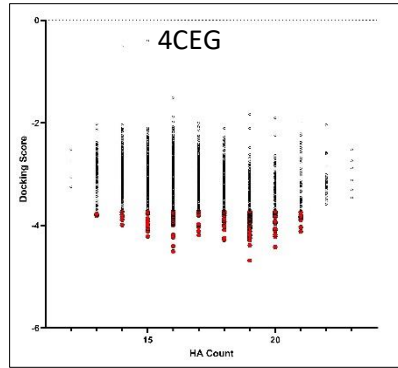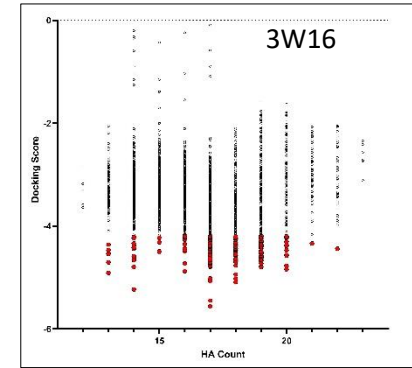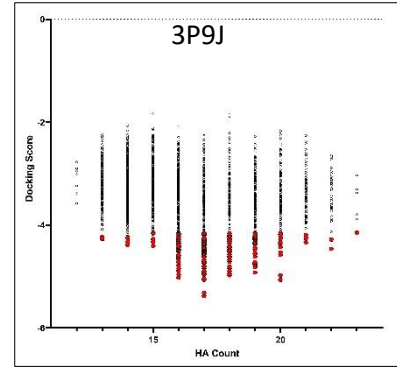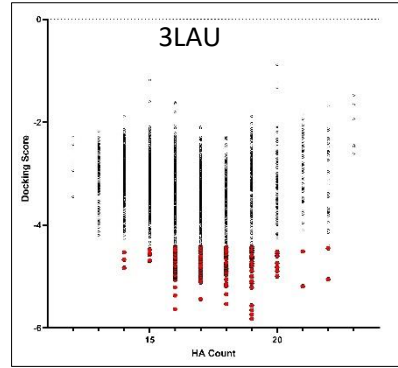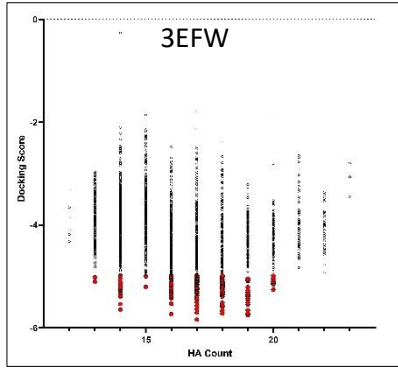
6.6 Amide Bond Array Aniline Results

6.6.1 Anilines used in Amide Bond Array and Biological Screening Results

Prior to the scale-up and full characterisation of purified reaction array products, described in Section **3.2.7.4.2**, the amide bond array was performed and included 13 anilines and one indole as coupling partners. These underwent the same workflow as described for the saturated N-heterocycles shown in the main body of the text including biological screening against Aurora-A activity. 4-chloropyrimidin-2-amine **A18** showed no conversion of starting materials, likely due to lack of nucleophilicity of this aniline.
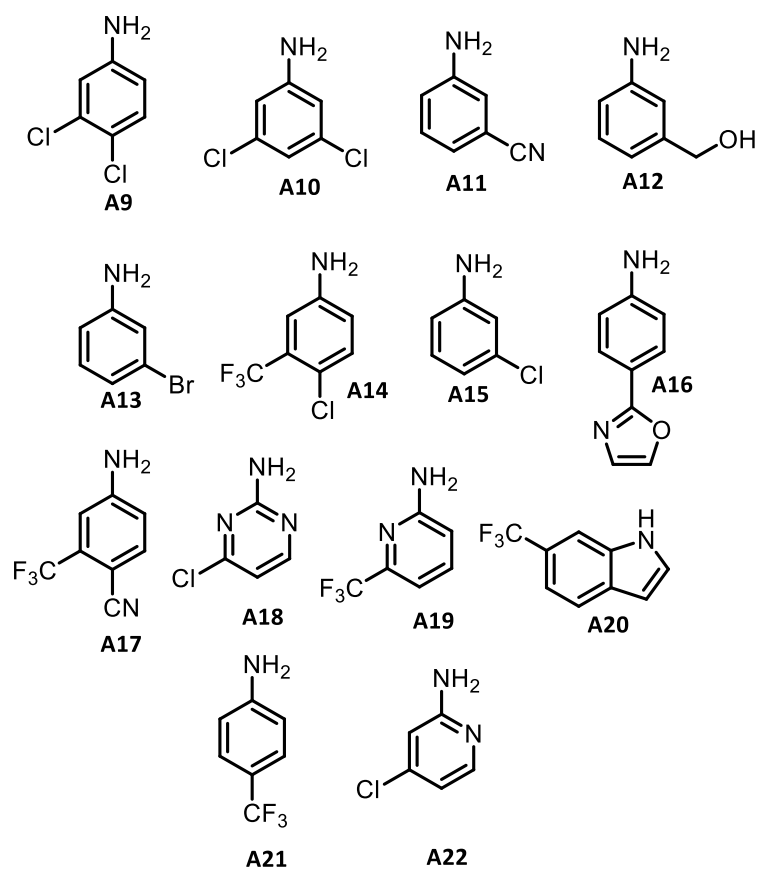
Figure **C.1**. Anilines and indole used in Amide Bond Array

Amine	Acid	Prep gradient	Yield (%)	Aurora-A Inhibition (%)	ΔTm (°C)
A9	7	Late	76	-1	0.42 (0.41)
	8	Late	75	-9	0.68 (0.23)
A10	7	Late	66	4	0.21 (0.09)
	8	Late	66	-4	0.42 (0.38)
A11	7	Mid-late	75	0	0.71 (0.41)
	8	Mid	73	-8	0.24 (0.03)
A12	7	Mid	66	5	0.11 (0.06)
	8	Mid	68	15	-0.01 (0.12)
A13	7	Late	75	14	0.16 (0.03)
	8	Late	77	-1	0.13 (0.18)
A14	7	Late	70	12	0.92 (0.11)
	8	Late	66	15	0.31 (0.25)
A15	7	Late	80	-9	0.63 (0.34)
	8	Mid-late	78	12	0.42 (0.14)
A16	7	Mid-late	66	1	-0.02 (0.13)
	8	Mid	64	7	0.16 (0.05)
A17	7	Late	38	14	0.62 (0.67)
	8	Mid-late	34	8	0.65 (0.16)
A18	7	N/A	0	N/A	N/A
	8	N/A	0	N/A	N/A
A19	7	Late	36	-9	0.04 (0.01)
	8	Late	65	3	-0.05 (0.14)
A20	7	Late	46	3	0.39 (0.27)
	8	Late	56	3	0.27 (0.16)
0.07A21	7	Late	62	2	0.20 (0.01)
	8	Late	82	3	0.07 (0.05)
A22	7	Mid-late	40	-6	0.66 (0.07)
	8	Mid-late	35	8	0.02 (0.04)

Table **C.1**. Amide Array Results A9-A22. ΔTm (°C) refers to ΔTm compared to DMSO control (Tm 45.30 (0.165) °C), with s.d. of triplicate measurements for each fragment shift in parentheses.